Technical Report Documentation Page

1. Report No. FHWA/TX-11/0-6094-1	2. Government Accession No.	3. Recipient's Catalog No.

4. Title and Subtitle MITIGATION METHODS FOR TEMPORARY CONCRETE TRAFFIC BARRIER EFFECTS ON FLOOD WATER FLOWS	5. Report Date Published July 2011 6. Performing Organization Code
7. Author(s) S. Bin-Shafique, M. Barrett, H. Sharif, R. Charbeneau, K. Ali, and C. Hudson	8. Performing Organization Report No. Report 0-6094-1
9. Performing Organization Name and Address The University of Texas at San Antonio One UTSA Circle San Antonio, TX 78249	10. Work Unit No. (TRAIS) 11. Contract or Grant No. Project 0-6094
12. Sponsoring Agency Name and Address Texas Department of Transportation Research and Technology Implementation Office P.O. Box 5080 Austin, TX 78763-5080	13. Type of Report and Period Covered Technical Report September 2008–August 2010 14. Sponsoring Agency Code

15. Supplementary Notes

Project performed in cooperation with the Texas Department of Transportation and the Federal Highway Administration.
Project Title: Mitigation Methods for Temporary Concrete Traffic Barrier Effects on Flood Water Flows
URL: http://tti.tamu.edu/documents/0-6094-1.pdf

16. Abstract

A combined experimental and analytical approach was put together to evaluate the hydraulic performance and stability of TxDOT standard and modified temporary concrete traffic barriers (TCTBs) in extreme flood. Rating curves are developed for different TCTBs from the laboratory experiments and methods are developed to model TCTBs using HEC-RAS during extreme flood condition. In addition, the effect of clogging of the openings of the TCTBs is also evaluated. A parametric study was conducted with important field parameters to evaluate the effect on stability of TCTBs against sliding and overturning during extreme flood. Based on the study of hydraulic performance, stability analysis, and parametric study, it can be seen that the modified single slope barrier is the most efficient TCTB from the perspective of hydraulic performance and the low speed concrete barrier is the most efficient TCTB from the perspective of stability. A guideline is prepared to use TCTBs in flood prone zones so that the use of TCTBs will not be detrimental in extreme flood.

17. Key Words Hydraulic Performance, Traffic Barrier, Concrete Barrier, Stability Analysis, Stability During Flood	18. Distribution Statement No restrictions. This document is available to the public through NTIS: National Technical Information Service Alexandria, Virginia 22312 http://www.ntis.gov

19. Security Classif. (of report) Unclassified	20. Security Classif. (of this page) Unclassified	21. No. of pages 190	22. Price

Form DOT F 1700.7 (8-72) **Reproduction of completed page authorized**

Mitigation Methods for Temporary Concrete Traffic Barrier Effects on Flood Water Flows

Research Supervisor: **Sazzad Bin-Shafique**

Principal Investigators: **Hatim Sharif**
Michael Barrett
Randall Charbeneau

Student Researchers: **Kausar Ali**
Cody Hudson

Project Director: **Jack Kayser**

PMC Members: **Amy Ronnfeldt**
Evan Roberts
Rob Fanning
Tom Beck

RTI Research Engineer: **Wade Odell**

RTI Contract Specialist: **Sandra Kaderka**

Published July 2011

DISCLAIMER

ACKNOWLEDGMENTS

This work was funded by the Texas Department of Transportation (TxDOT) under Project 0-6094, Mitigation Methods for Temporary Concrete Traffic Barrier Effects on Flood Water Flows. We thank Dr. Jack Kayser for his guidance and input. The authors would also like to acknowledge the cooperation from Mr. Wade Odell and the PMC members.

TABLE OF CONTENTS

LIST OF FIGURES

LIST OF TABLES

LIST OF SYMBOLS AND ACRONYMS

Acronyms

AASHTO – American Association of State Highway and Transportation Officials
ASTM – American Society for Testing and Materials
CRWR – Center for Research in Water Resources
CSB – F-shaped Concrete Safety Barrier
DOT – Department of Transportation
EI – Engineering Index
FDOT – Florida Department of Transportation
FHWA – Federal Highway Administration
FS – Factor of safety
HEC-RAS – Hydrologic Engineering Centers River Analysis System
HMA – Hot Mixed Asphalt
LPCB – Low Speed Concrete Barriers
MSSCB – Modified Single Slope Concrete Barrier
NCHRP – National Cooperative Highway Research Program
NTIS – National Transportation Information Service
RIP – Research in Progress
SSCB – Single Slope Concrete Barrier
SSCB-SPL – Modified Traffic Barrier
TCTB – Temporary Concrete Traffic Barrier
TRB – Transportation Research Board
TxDOT – Texas Department of Transportation

Symbols

A_o = cross-sectional area of the orifice
A_r = total area of the rail
b_{rl} = width of the opening of the barrier
C = discharge coefficient
E = specific energy
E_c = critical energy
E_u= specific energy at upstream
F_o = fraction of open space
F_r = Froude number
g = acceleration due to gravity
h_c = critical head
h_r = height of the barrier
h_{rl} = height of the opening of the barrier
h_u = height of water above the base of the barrier
N = number of observed data points
Q = volumetric flow rate
S.E. = standard error
S_0 = longitudinal slope

S_c = cross slope
v_c = critical velocity
ΣF_d = Sum of horizontal driving forces
ΣF_R = Sum of horizontal resisting forces
ΣM_0 = Sum of the moments of forces tending to overturning.
ΣM_R = Sum of the moments of forces tending to resist overturning
μ = coefficient of static friction

CHAPTER 1: INTRODUCTION

1.1 INTRODUCTION

Temporary traffic barriers are installed in the work zone with the purpose of shielding motorists from hazards, and separating and protecting work crews from traffic (Figure 1.1). In 1986, the Federal Highway Administration (FHWA) specified that all temporary concrete traffic barriers qualify the specified crash test (NCHRP Report 350). In general, crash tested concrete traffic barriers have greater height and less open space when compared to concrete traffic barriers that have failed crash testing. The requirements for crash test pose concerns with respect to hydraulic performance for concrete traffic barriers because the additional height and less open space may adversely impact the surrounding floodplain elevation. The fraction of open space in the two standard (F-shaped and single-slope) temporary concrete traffic barriers (TCTBs) of TxDOT is insignificant. In the event of extreme flooding, these barriers obstruct water flow and magnify the flooding by increasing the head water elevation. The issue of hydraulic performance of concrete traffic barriers came into the limelight when a number of major arterial highways in Texas were shut down due to widespread flooding last year.

Figure 1.1. Temporary Concrete Traffic Barrier in Construction Zone.

Ocelot (an endangered cat with less than 120 individuals remaining in the US) roadkills are an important problem potentially threatening ocelot survival in south Texas. Thus, in recent years, the single-slope temporary concrete traffic barrier has been modified by accommodating larger openings as an option for the resolution of traffic-ocelot conflicts, which have been used in selected projects in south Texas. While this larger opening is expected to have a positive impact on the flow of water and the accumulation of flood debris, the lower weight and upward shifting of the centroid due to adding the opening at the bottom of the barrier is expected to have a negative impact on stability during extreme situations. A lower stability, in terms of sliding and overturning, can cause traffic hazards during extreme flooding as shown in Figure 1.2. The hydraulic performance and stability of the standard and modified TCTB are not known yet. If the modified

TCTBs are better in terms of hydraulic performance and have adequate factor of safety for sliding and overturning, then the modified TCTB might be the choice for the future to achieve the objectives without considerably hindering water flow during any flood event.

In accordance with NCHRP Report 350, there are three types of devices, such as temporary traffic barriers, shadow vehicles, and arrestor nets that are used to redirect vehicles from the workspace. The factors that affect the choice of a particular device are the traffic speed and volume, project/task duration, geometry, and vehicle mix. The use of temporary traffic barriers is based on engineering judgment. However, TCTBs are required on bridge-rehabilitation jobs with bridge rail replacement and/or full depth repair and are to be considered for any other type of long-term repair work. The TCTB is very efficient for high traffic speed and volume and for a project with relatively longer duration. However, TCTBs are expensive and require more setup and removal time. Moreover, the TCTBs have some adverse effects during flooding because they obstruct water flow.

Figure 1.2. Sliding and Overturning of TCTBs during a Flood Event.

1.2 OBJECTIVES

The primary objectives of this project are to determine the hydraulic performance and stability analysis of standard and modified TCTBs in extreme flood condition. The additional objectives include: evaluation of susceptibility to clogging, development of a method to model standard and modified TCTBs in HEC-RAS to make guidelines for the mitigation of TCTB aggravated roadway flooding, and conducting parametric study to identify flood situations in which installation of TCTBs may be detrimental.

Based on the hydraulic performance, stability analysis and parametric study, a guideline to use TCTBs in flood prone zone has been developed, which is shown in Appendix A.

1.3 ORGANIZATION OF THE REPORT

This study of hydraulic performance and stability of TCTBs in extreme flood has been organized in seven chapters in this report. Chapter 1 describes introduction and objectives of the study. Chapter 2 describes the literature review that includes all relevant literature concerning hydraulic performance and the stability analysis of TCTBs or similar structures. Chapter 3 includes the hydraulic performances of TCTBs. All the model derivation, laboratory test methods, results and interpretations of the laboratory results have been included in Chapter 3. Chapter 4 describes the stability of the TCTBs against sliding and overturning in different flood settings. Chapter 5 describes how the rating curves developed from the laboratory tests for different TCTBs can be used to model TCTBs in extreme flood using HEC-RAS (two examples of analysis is added). All the parametric studies have been included in Chapter 6. Chapter 7 describes the conclusions of this study.

CHAPTER 2: LITERATURE REVIEW

Literature review has been performed to assess all relevant studies concerning hydraulic performance and the stability analysis of TCTBs or similar structures. This literature search included studies by TxDOT, other state DOTs, FHWA, and all other reliable sources. Moreover, different databases for relevant articles was searched, which include the National Transportation Information Service (NTIS), the Engineering Index (EI Compendex), and the Transportation Research Board's (TRB) Research in Progress (RIP) database.

2.1 TXDOT TCTBS

2.1.1 Type of TCTBs

TxDOT has two standard types of TCTBs, such as single slope concrete barrier (SSCB) and F-shaped concrete safety barrier (CSB), which have been used quite often throughout Texas. In addition to that, the SSCB has been modified by accommodating larger openings as to protect ocelots from traffic hazards, which have been used in selected projects in south Texas in recent years. This modified special type of single slope concrete barrier (SSCB-SPL) is often called as "modified traffic barrier."

Low speed concrete barriers (LPCB) were developed more than a decade ago for use in low-speed urban work zones where it is required to have frequent cross-traffic entrances. The reduced height of the low speed barrier greatly enhances the ability of drivers who are traversing the work zone to maintain visual contact with the local traffic situation. Since its introduction, the low speed barrier has demonstrated that it is extremely useful in increasing safety in such situations.

2.1.2 Geometry of the TCTBs

The cross-sections of the TxDOT TCTBs are shown in Figure 2.1. The standard drawings of the TxDOT TCTBs are attached in Appendix B. Since the SSCB-SPL is originated from the SSCB only by incorporating bigger openings, both types of TCTBs have the same height and base with of 42 in. and 24 in., respectively. The base width of the CSB is also 24 in., but the height is 33 in. The height of the LPCB is only 24 in and the base width is 26 in. All the TCTBs are 30 ft long except the LPCB (20 ft long) and they have two slots at the bottom.

The size of the slots and the percent of area of openings are different for each type of TCTB. The SSCB has the lowest opening ratio of 0.63%, while the SSCB-SPL has the highest opening ratio of 9.52%.

2.1.3 Construction of TxDOT TCTBs

The TCTBs are constructed by casting concrete in a still mold. Figure 2.2 shows the still mold and the construction of the TCTBs. The contact surface of the TCTBs with the base such as asphalt pavement, concrete pavement, and base or subbase courses might have significant impact on the stability of the TCTB against sliding.

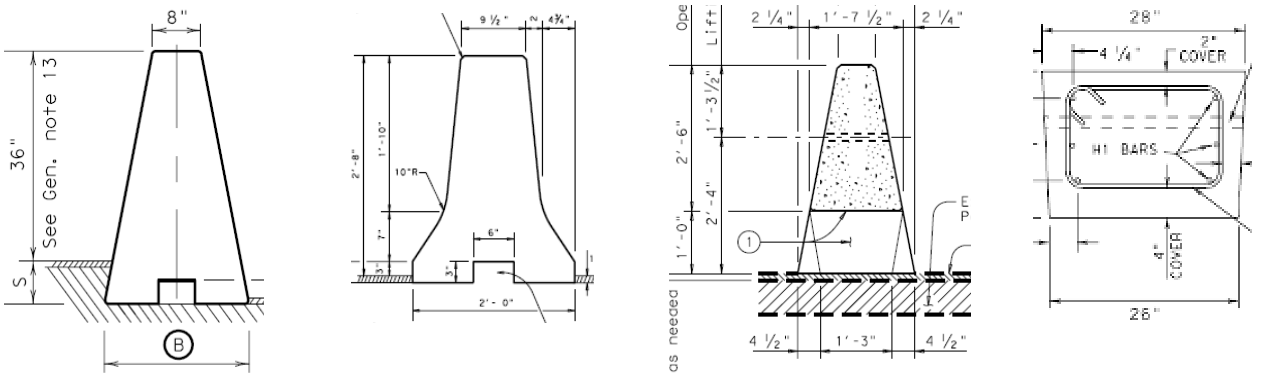

(a) (b) (c) (d)

Figure 2.1. Cross Section of the TCTBs: (a) SSCB, (b) CSB, (c) SSCB-SPL, and (d) LPCB.

Based on the method of casting, the contact surface of the TCTB will have different frictional properties. If the Bottom surface of the TCTB is:

- Inside the mold, then the surface will be relatively smooth.
- Is exposed, then the surface will be relatively rough and will vary from person to person who are casting the TCTBs.

(a) (b)

Figure 2.2. Construction of TCTBs: (a) TCTB Mold and (b) Construction and Movement of TCTBs.

2.2 HYDRAULIC PERFORMANCES TCTBS

A very few studies have been conducted to understand the hydraulic performance of TCTB so far. The only study that was found to be directly related to the hydraulic performance of TCTB was conducted by Kranc et al. (2005) for a FDOT research project. Kranc et al. (2005) investigated and analyzed the flow under TCTB to establish the hydraulic performance of barrier wall inlets, as a first step to evaluating the capacity of the barrier wall drainage system. To accomplish this goal, experimental measurements of the discharge characteristics of various aperture configurations were conducted both under sump and transverse flow conditions. Discharge rates (non-dimensional) of individual inlets have been measured as a function of approach flow rate and as a function of the depth of water at wall.

Similarly, the other study that is quite similar to evaluating the hydraulic performance TCTB was conducted by Charbeneau et al. (2008) in order to determine the hydraulic performance and the impact of different bridge rails on the surrounding floodplains during different flood events. One of the bridge rails is very similar to single slope TCTB and two of the rails are similar with a small scupper drain at the bottom but have different cross sectional geometries. Both of these studies were reviewed carefully.

2.2.1 Kranc Model

During a rainstorm, the runoff flows along the longitudinal slope as well as transverse slope. Thus, a continuous array of TCTB along the edge of a pavement forms a configuration similar to a curb and gutter system with close spaced inlets for drainage, which was assumed to have a similar hydraulic characteristics of channels fitted with side weirs for irrigation (Robinson and McGhee, 1993; Sing and Satyanarayana, 1994) as shown in Figure 2.3. Based on that assumption, various full scale configurations for drainage apertures of the FDOT standard TCTB were tested in a tilting flume experimental facility (Kranc et al., 2005). Both the cross and longitudinal slope of the flume was varied to mimic the roadway. The longitudinal slope was considered zero for the sump conditions when the flow velocity along the longitudinal direction was assumed zero.

The flow conditions on grade as shown in Figure 2.3 suggest that, as the runoff is accumulated along the channel, a simple approach of gradually varied flow is not adequate to describe flow conditions encountered with barrier inlets. For supercritical flow, the depth at the start of each reach (at the downstream edge of an inlet) will be less than normal depth, due to the drawdown caused by inlets discharge. As the flow progresses downstream the depth will increase. As the slope is reduced, detailed computations over the reach between inlets indicates that the flow depth grows rapidly and may actually achieve critical depth somewhat downstream of the inlet. Just as in the case of gradually varied flow with no addition, a variety of flow conditions are possible for the case with addition. Depending on flow rate, it can be expected that the approach to a depression will eventually include a region of mild slope as an initially steep slope is reduced. The flow approaching the next inlet will be subcritical so that the entrance to the next inlet will be with slight drawdown in the water level just before the inlet. The critical depth can be estimated from the equilibrium flow rate in the channel, and although this value appears to depend on the cross slope, the normal depth has an inverse relation to cross slope so that critical depth is not actually dependent on this factor (but does depend on runoff).

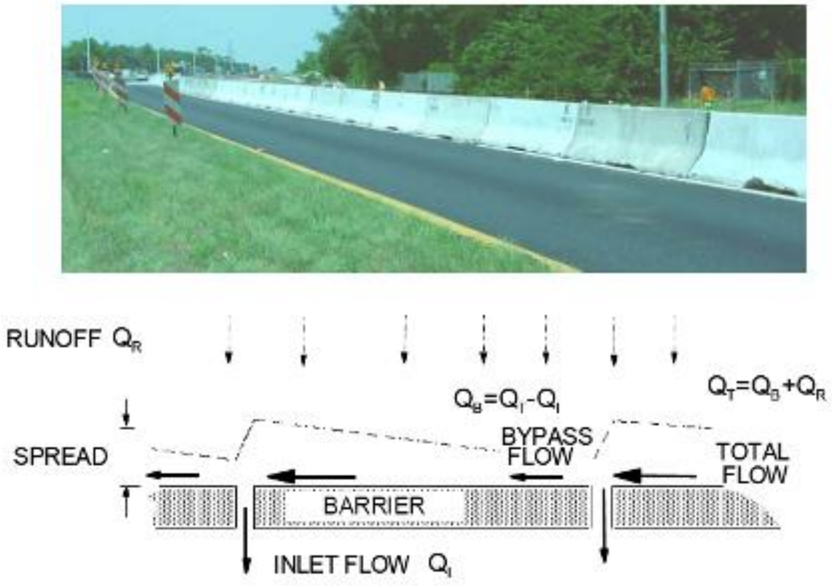

The bottom sketch shows plan view of flow path. Spread is maximum just upstream of inlet entrance (Kranc et al., 2005).

Figure 2.3. Drainage through TCTB Inlets.

As shown in Figure 2.3, continuity for the flows (Q) at each inlet gives:

$$Q_B = Q_T - Q_I \tag{2.1}$$

Where the subscripts T, B, and I refer to total, bypass, and inlet, respectively. The total flow just upstream of an inlet is the combination of carryover from the previous inlet and the accumulated runoff between inlet stations, Q_R.

$$Q_T = Q_B + Q_R \tag{2.2}$$

The total flow in the channel may increase or decrease along the roadway depending on how much of the runoff is captured at each inlet. If all runoff accumulated between inlets is captured, a steady state is reached where Q_T is constant just upstream of each inlet. It is likely that under storm conditions, the accumulation due to runoff is much smaller than bypass flow, and that the total flow is much larger than the capacity of any single inlet.

2.2.1.1 Experimental Facility and Observational Methods

Capacity measurements for single inlets were made using full size models set in a flume over a large fiberglass reservoir tank (Kranc et al., 2005). The flume bed was arranged to tilt at cross slope S_C and longitudinal slope S_0, simulating pavement geometry. The cross slope is small so that the spread is approximately the same as the length across the measurement y, along the wall to the same point. Thus, the spread is related simply to the cross slope ($T \approx y/S_C$) and comparable relations apply for the area and hydraulic radius. The Froude number for the channel flow may be estimated (based on the average depth of flow),

$$F_r \approx \left(\frac{H}{g}\right)^{\frac{1}{2}}\left(\frac{QTSC}{y^{5/2}}\right) \tag{2.3}$$

where *g* is the acceleration of gravity.

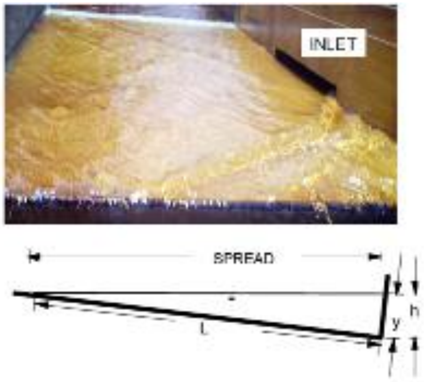

Figure 2.4. Bed Configuration for Flow.

2.2.1.2 Measurement of Inlet Capacity

Experiments to measure inlet capture were performed for the following slope ranges: longitudinal slope $S_o = 0, 0.5, 1, 2, 4, 5, 6\%$ and cross slope $S_c = 1, 2, 4,$ and 6% (Kranc et al., 2005). These tests were made for single inlets with an extended upstream reach, no upstream inlet and no runoff flow added to the bed (Figure 2.4). Typical measurements of hydraulic performance of the barrier wall inlet (capture as a function of approach flow) are presented in Figure 2.6a. Flow rate has been reported as the non dimensional parameter $Q/(g^{1/2} H^{5/2})$, where H is the height of the Inlet (0.167 ft). It was observed that total captures occurs for only a very small range of approach flow (Figure 2.5) and that the efficiency of the inlet was relatively low, as expected. The second approach was to examine the correlation between depths in the gutter just upstream of the inlet with the inlet capture. Figure 2.6b represents the results of this correlation. No substantial correlation with cross slope or longitudinal slope was found for the range examined. This observation indicates water enters the inlet much like a sill flow, probably due to the lack of entrance development.

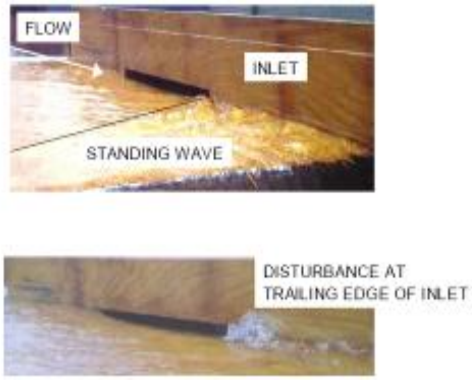

Figure 2.5. Flow at Inlets.

A correlation between inlet flow and the depth just upstream of the inlet has been developed from the data with a simple linear model with intercept as shown below.

$$\frac{Q_1}{g^{1/2}H^{5/2}} = 4.16\,\frac{y}{H} - 0.92 \tag{2.4}$$

To apply this correlation, the normal depth immediately upstream of the inlet was calculated for the total flow (assuming that Manning's *n* and the slope of the pavement is known), then the inlet flow, the spread, and the bypass flow can be obtained directly. This procedure was continued as required along a line of inlets on grade to evaluate system performance.

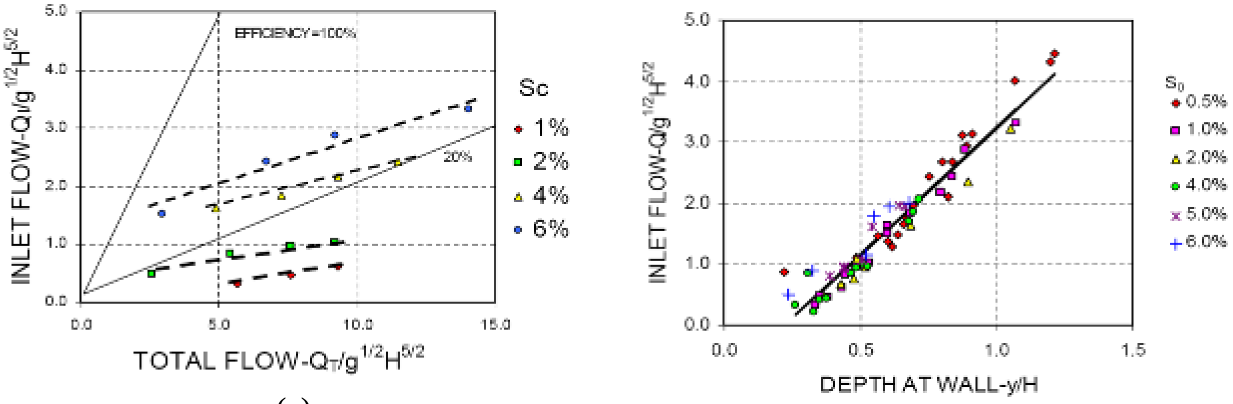

(a)

(b)

Figure 2.6. Inlet Drainage Performance: (a) Inlet Flow vs. Total Flow and (b) Inlet Flow vs. Depth of Water (Kranc et al., 2005).

The study also evaluates the flow through the inlet from pond formation at the bottom of the grade, which shows similar results as described in Kranc et al. (1997). Supplemental experiments to evaluate performance under sump conditions (S_0 =0%, variable cross slope) were conducted. The inlet flow as a function of upstream water depth at wall is shown in Figure 2.7. For the range of depths Y/H<1.4, the flow was within a weir regime and a correlation with a conventional capacity equation is possible.

$$Q = C_{DW}L\,\sqrt{2g}\;Y^{3/2} \tag{2.5}$$

A value for C_{DW} of 0.25 provided an optimal fit to the data. It should be noted that the depth parameter for the sump cannot be interpreted in the same manner as that for the inlet with transverse flow, which is supercritical. Here Y is interpreted as the pond depth. Similarly, for orifice flow, a correlation of C_{DO} was obtained for use in:

$$Q = C_{DO}LH\,\sqrt{2g}\;Y^{1/2} \tag{2.6}$$

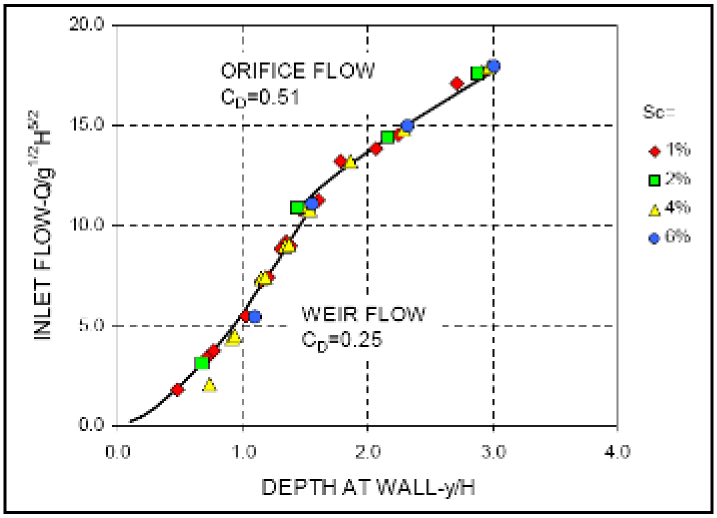

Both Weir and Orifice Correlations are shown with translation at Y/H≈1.4 (Kranc et al., 2005).

Figure 2.7. Sump Performance for Inlet.

2.2.2 Charbeneau Model

The hydraulic performance of various bridge rail types was studied by Charbeneau et al. (2008) in order to determine the hydraulic performance and the impact of different rails on the surrounding floodplains during different flood events. One of the bridge rails (T501) is very similar to single slope TCTB (Figure 2.8). The SSTR and T221 rails are similar to the T501 rail in that they are solid rails with a small scupper drain at the bottom but have different cross sectional geometries.

(a) (b) (c)

Figure 2.8. Bridge Rail and Standard TCTB (a) Bridge Rail T501, (b) Single Slope TCTB, and (c) F-Shaped TCTB.

A three-parameter model is proposed which can be used to accurately predict the free-flow rail-rating curve (Charbeneau et al., 2008). Similar to Kranc et al. (2005) model, three-parameter model estimates flow through the inlets as a function of upstream water depth. The free-flow rating curve model derivation follows the ideas presented by Charbeneau et al. (2006). The Charbeneau et al. (2006) model is a two-parameter model used to describe the hydraulic performance of highway culverts under inlet control. The addition of a third parameter was used to fully define the hydraulic performance of bridge rails. Three flow types occur as water flows through a typical bridge rail. These are depicted in Figure 2.9 which shows the experimental setup for this testing (Klenzendorf et al., 2008). The T203 rail shown here has a continuous concrete beam along the top with concrete posts supporting the beam. Type 1 flow occurs under unsubmerged conditions through the lower open areas of the rail ($h_u < h_{rL}$), where h_u is the upstream water depth as measured from the top of the support base (bridge deck). Type 2 flow occurs when a submerged condition occurs through this same open area ($h_{rL} < h_u < h_r$). Type 3 flow occurs both as submerged orifice flow and weir flow over the top of the rail ($h_u > h_r$). These three flow types can be used to derive the rating curve model for defining the hydraulic performance of a bridge rail. The model also accurately predicts which flow type will govern the flow as well as transition points between each flow type.

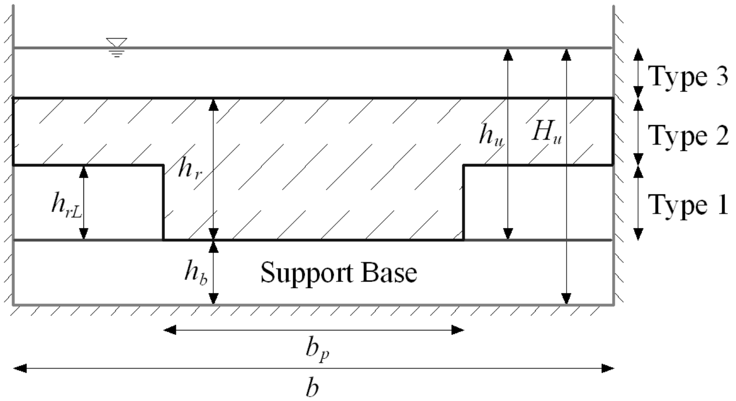

Figure 2.9. Three Types of Flows that Are Considered for Experimental Protocol.

2.2.2.1 Type 1 Flow

The model derivation for Type 1 flow assumes that critical depth occurs at or near the location of the bridge rail due to the choke produced by the rail (Henderson, 1966). In order to determine the hydraulics of bridge rails independent from the entire bridge, a datum is taken at the base of the rail (or top of the support base in Figure 2.9). Therefore, the depth h_u is used in determining the specific energy, as opposed to the actual depth, H_u. The continuity equation defines the flow rate passing over the bridge rail.

$$Q = Av_c = C_b(b - b_p)h_c\sqrt{gh_c} \tag{2.7}$$

In Equation 2.7, Q is the volumetric flow rate; A is the effective flow area through the rail; v_c is the assumed critical velocity at the rail, which, based on a Froude number equal to unity, is equal to $\sqrt{gh_c}$ (King and Brater, 1963); g is the gravitational constant; and h_c is the critical water depth which occurs at the rail. For critical flow within the rectangular-shaped opening $h_c = 2/3\ E_c$, where E_c is the critical specific energy, assumed to be approximately equal to the upstream specific energy, E_u (Rouse, 1950). b is the width of the test channel, equal to 150 cm (5 ft) for this experimental setup; b_p is the width of the bridge rail posts. Therefore, $(b\text{-}b_p)$ is the width available for flow. C_b is a coefficient representing the effective width contraction associated with the bridge rail post entrance edge conditions. Therefore, the effective width available for flow is $C_b\ (b\text{-}b_p)$. The magnitude of C_b also accounts for energy losses between the upstream station and the model rail (Charbeneau et al., 2006).

Rearranging Equation 2.7 in the form of a rating curve based on the dimensionless flow rate and making the substitution for critical depth leads to the following:

$$\frac{Q}{A_r\sqrt{gh_r}} = C_b F_o \left(\frac{h_r}{h_{rL}}\right)\left(\frac{2E_u}{3h_r}\right)^{1.5} \tag{2.8}$$

In Equation 2.8, A_r is the total area of the rail ($A_r = h_r b$), and F_o is the fraction of open space for the rail defined as the ratio of open area in the rail, A_o to the total rail area, A_r. F_o is considered an important design parameter.

$$F_o = \frac{A_o}{A_r} = \frac{(b-b_p)h_{rL}}{bh_r} \tag{2.9}$$

2.2.2.2 Type 2 Flow

Type 2 flow is modeled as orifice or sluice gate flow (Charbeneau et al., 2006). The energy equation can be used to determine the velocity at the rail.

$$E_u \approx h_m + \frac{v_m^{\,2}}{2g} = C_c h_{rL} + \frac{v_m^{\,2}}{2g} \tag{2.10}$$

In Equation 2.10, v_m is the velocity at the rail, and h_m is the water depth at the vena contracta of the rail, which is equal to $C_c h_{rL}$. C_c is a coefficient representing the effective vertical contraction associated with water being forced under the bridge rail beam. C_c also accounts for energy losses between the upstream station and the rail (Charbeneau et al., 2006).

Rearranging Equation 2.10 to solve for velocity and using the continuity equation to determine the dimensionless rating curve leads to the following equation defining Type 2 flow:

$$\frac{Q}{A_r\sqrt{gh_r}} = C_b C_c F_o \sqrt{2\left(\frac{E_u}{h_r} - C_c\frac{h_{rL}}{h_r}\right)} \tag{2.11}$$

In order to determine the transition point between Type 1 flow and Type 2 flow, Equation 2.8 and Equation 2.11 can be set equal to each other and solved for E_u. This leads to a cubic equation with three roots which are equal to −3 and 3/2 (the latter of which is a double root). Since the negative root has no physical meaning, the transition point occurs at the following specific energy, which has been normalized to the height of the rail.

$$\frac{E_u}{h_r} = \frac{3}{2} C_c \frac{h_{rL}}{h_r} \tag{2.12}$$

At the transition point, both the rating curve and its slope are continuous, resulting in a smooth transition.

2.2.2.3 Type 3 Flow

Type 3 flow occurs as a combination of orifice and weir type flows. The principle of superposition is assumed to apply here. For weir flow, the bridge rail is modeled using a broad-crested or short-crested weir equation based on the ratio of the upstream specific energy above the height of the rail to the thickness of the rail (Bos, 1989):

$$Q = C_d \frac{2}{3} b \sqrt{\frac{2}{3} g} (E_u - h_r)^{1.5} \tag{2.13}$$

In Equation 2.13, C_d is a weir discharge coefficient. The significant difference between the broad-crested and short-crested weir equations is that C_d is larger for a short-crested weir (Bos, 1989). Rearranging Equation 2.13 to the dimensionless rating curve form and adding it to the rating curve equation for Type 2 flow results in the rating curve for Type 3 flow as follows:

$$\frac{Q}{A_r \sqrt{g h_r}} = C_b C_c F_o \sqrt{2\left(\frac{E_u}{h_r} - C_c \frac{h_{rL}}{h_r}\right)} + C_d \left(\frac{2}{3}\right)^{1.5} \left(\frac{E_u}{h_r} - 1\right)^{1.5} \tag{2.14}$$

The transition to Type 3 flow occurs when the upstream specific energy is greater than the height of the rail.

$$\frac{E_u}{h_r} \geq 1 \tag{2.15}$$

Therefore, the free-flow rating curve for a bridge rail can be determined based on the three flow types defined in Equations 2.8, 2.11, and 2.14 with transition points defined in Equations 2.12 and 2.15.

2.2.2.4 Submergence Characteristics

Increases in the downstream water depth can result in the submergence of a bridge rail or traffic barrier during a flood event. Downstream submergence will cause further increases in the upstream water surface elevation. This change will cause the free-flow rating curve equations to underestimate the upstream specific energy predicted for a given flow rate. Therefore, the submergence characteristics were analyzed through two independent mathematical models based on a theoretical approach and an empirical approach, respectively.

2.2.2.5 Villemonte Submergence Model

The theoretical model is an alteration of a model presented by Villemonte (1947) for the submergence of weirs. The principle of superposition is used to define the actual flow rate, Q, equal to the hypothetical flow rate produced by the upstream head on the weir, Q_1, minus the hypothetical flow rate produced by the downstream head on the weir, Q_2, i.e., $Q=Q_1-Q_2$. Q_1 and Q_2 are assumed to flow independent from each other in opposite directions and are determined based on a general weir equation using the upstream and downstream weir heads, respectively. The results of Villemonte's experiments give the following equation:

$$\frac{Q}{Q_1}=\left[1-\left(\frac{h_2}{h_1}\right)^n\right]^m \tag{2.16}$$

where h_1 and h_2 are the upstream and downstream weir heads respectively, measured relative to the weir crest, n is a power term based on the weir geometry and determined from the weir equation (n=1.5 for rectangular weirs), and m is an empirical parameter that takes into account the interactions between the hypothetical upstream and downstream flow rates (m=0.385 from Villemonte's experiments). The modification to this model that applies to bridge rails is to use the upstream and downstream specific energy above the support base (instead of above the top of the rail), which leads to the following:

$$\frac{Q}{Q_1}=\left[1-\left(\frac{E_d}{E_u}\right)^{1.5}\right]^m \tag{2.17}$$

where E_u and E_d are the upstream and downstream specific energies. The change from the head on the top of the rail (h_1 and h_2) to the specific energy (E_u and E_d) is necessary because flow can pass through the rail open space without overtopping it and the use of specific energy will match the derivation used for the rating curve equations. Therefore, submergence effects can occur prior to the water overtopping the rail. Although this alteration may add additional error, the model proves to be fairly accurate as shown in the following sections. m is determined experimentally for each rail in order to determine how the upstream and downstream flow rates interact based on different rail geometries.

2.2.2.6 Empirical Submergence Model

Application of the Villemonte model with experimental data showed a bias in the results based on the magnitude of flow rate used during experimental testing. Such a bias is created in part due to the alteration to the original Villemonte model and also due to the additional interactions between the upstream and downstream flows through the rail open space. This bias will be shown in more detail in a later section. Therefore, due to the inaccuracies of the Villemonte model, an empirical model was developed that is implicit with respect to the flow rate in order to attempt to remove this bias. The empirical model is defined as follows:

$$\frac{Q}{Q_1}=\left(\frac{\Delta E}{AE_u}\right)^{A_r\sqrt{gh_r}/BQ} \tag{2.18}$$

In Equation 2.18, Q_1 is the hypothetical flow rate that would occur for the given upstream specific energy, E_u, if there were no submergence and can be determined from the previously defined free-flow rating curve model. ΔE is the difference between the upstream and downstream specific energy, i.e. $\Delta E = E_u - E_d$. The parameter A serves as a lower bound on the magnitude of ΔE for which submergence is not an issue. If $\Delta E > AE_u$, then the downstream specific energy is so small that submergence effects will be negligible and the approximation can be made that $Q = Q_1$. The value of A=2/3 gave the best results to experimental data (Klenzendorf, 2007). The parameter B is a fitting parameter determined experimentally for each rail.

2.2.3 Experimental Methods for Charbeneau Model

The major downfall to this model is that the coefficient values must be obtained experimentally (Klenzendorf et al., 2008). Experimental testing was conducted independently for multiple model bridge rails in a 150 cm (5 ft) rectangular channel with zero slope (Figure 2.10). The collected data consist of the upstream water depth and downstream water depth (when conducting submergence tests) measured from Pitot tubes connected to an inclined manometer board. All model bridge rails were constructed at half-size of the standard dimensions. In some cases, the rail geometry did not allow for exact reduction in size while maintaining the same percent open space due to the channel dimensions. In these cases, slight changes to the horizontal or vertical dimensions are made because the fraction of open space is considered an important design criterion and needed to be maintained. Wood is used as the primary construction material for most rails, with the T101 rail and Wyoming rail being constructed out of metal. All wood is coated with waterproof primer, and no noticeable swelling or warping occurred during testing. A support base made out of wood and concrete is anchored to the channel bottom and prevents the rails from being swept downstream.

Figure 2.10. Rail in the Rectangular Channel.

For the free-flow rating curve testing, a flow rate was set and allowed to reach steady state. The upstream depth and flow rate was measured. The flow rate was then changed and allowed to stabilize before the next set of measurements was taken. For submergence testing, a constant flow rate is used. The downstream depth is increased incrementally through the use of a tailwater gate located downstream from the model bridge rail. As the tailwater gate is lowered into the water, it produces a hydraulic jump that creates an increase in depth downstream of the bridge rail barrier system. The upstream depth, downstream depth, and flow rate are measured six separate times for each level of downstream depth.

The unknown parameter values in the mathematical models (C_b, C_c, C_d, m, and B) are used in the model equations and compared to the observed data in non-dimensional form. The standard error between the observed data and the predicted model results is minimized using the following equation in order to determine the appropriate values for each parameter.

$$S.E. = \sqrt{\frac{1}{N}\sum_{i=1}^{N}\left[\left(\frac{E_u}{h_r}\right)_d - \left(\frac{E_u}{h_r}\right)_m\right]_i^2} \tag{2.19}$$

In Equation 2.19, $S.E.$ is the standard error for N observed data points. The subscript d corresponds to the measured data for the dimensionless flow rate, and the subscript m is for the mathematical model results. Minimizing the standard error is accomplished by changing the model parameter values so that the model results closely match the observed data. The obtained model parameter values are reported in the following sections.

2.2.4 Results from Charbeneau Model

2.2.4.1 Rating Curve Model Results

For the free-flow rating curves, the dimensionless upstream specific energy (E_u/h_r) is determined as a function of the dimensionless flow rate (as described in Equations 2.8, 2.11, and 2.14). The proposed rating curve model proves to be very accurate in predicting the observed data once the coefficient values have been determined. Figure 2.11a shows the observed data and rating curve model for the T203 model bridge rail. In addition, the individual model flow type equations are graphed to show that the model accurately predicts which flow type will govern the overall rating curve. Similar results were obtained for the other rail rating curves. Figure 2.11b shows the results of all nine rail configurations. However, these rating curves are all non-dimensionalized to the rail height for the T203 rail ($h_{r,T203}$ = 36.2 cm [14.25 in.]) as opposed to their respective rail heights. The reason for this change is so that the differences in height can be depicted. For example, the SSTR, T501, and T221 rails have virtually overlapping rating curves when non-dimensionalized to their respective rail heights. When compared to the T203 rail, it is clear that the SSTR rail produces the greatest upstream specific energy due to its greater rail height.

2.2.4.2 Submergence Model Results

Submergence tests are conducted by incrementally increasing the downstream water depth for a given constant flow rate. The submergence model parameters for both the Villemonte model and empirical model were determined by minimizing the standard error between the mathematical model results and the observed data.

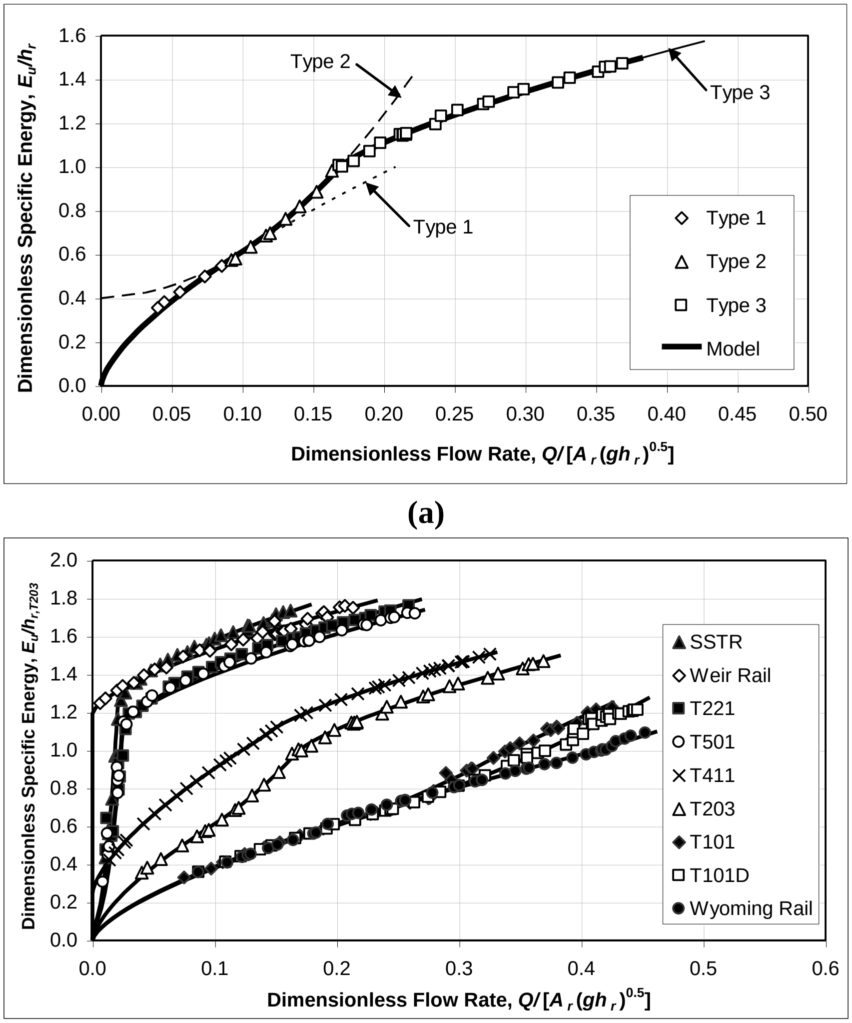

(a)

(b)

Figure 2.11. Free Flow Rating Curves: (a) Rail T203 with Model Curve and (b) All Nine Rails.

2.3 FLOODPLAIN MODELING USING RATING CURVES

Charbeneau et al. (2008) also describes a method for incorporating the hydraulics of various bridge railing systems on a bridge structure to determine the impacts on the surrounding floodplain during extreme flood events. Similar study was also conducted by Konieczki et al. (2007). Typically the geometry of the bridge rails is not considered when conducting floodplain analysis. The use of certain bridge rails with large height or minimal open space may adversely impact the surrounding floodplain. Therefore, a mathematical model used to characterize the hydraulic performance of bridge rails has been developed, and the use of this model in floodplain mapping software such as HEC-RAS is outlined. A second mathematical model is used to approximate and characterize the effects of rail submergence. Finally, an iterative method for incorporating the hydraulics of various bridge railing systems into floodplain analysis software is described together with a simple single bridge example.

The information for the rating curve and submergence models (Charbeneau et al., 2008; Klenzendorf et al., 2008) can be used in HEC-RAS by simply changing the dimensional weir coefficient for flow over a bridge structure (Klenzendorf et al., 2010). This results in an iterative process since the weir coefficient will change with the flow rate passing over the bridge. Analysis of three standard TxDOT bridge rails were investigated in a simple single bridge HEC-RAS model. From this analysis, the T101 results in the smallest impact to the surrounding floodplain. Both the T101 and T203 rails are not expected to increase the upstream headwater by more than 1 ft, thereby avoiding the required floodplain map revision. However, the T221 rail drastically reduces the amount of flow across the bridge roadway. Although this rail will adversely impact the surrounding floodplain, the T221 rail will provide safer driving conditions across the bridge deck. Therefore, when determining which rail to install, a balance between the impact to the floodplain and the driving conditions must be considered together.

2.4 STABILITY OF CONCRETE TRAFFIC BARRIER

Stability of the TCTBs during extreme flood event is an important parameter. Generally, the TCTBs can fail either by sliding or by overturning due to hydrodynamic pressure resulting from any flood event (Coduto, 2001). Since the TCTBs are placed on rigid platform failure due to bearing capacity or settlement is quite uncommon (Das, 2006).

Based on the principle of mechanics (Hibbeler, 2008), the factor of safety (FS) against overturning about point C in Figure 2.12 may be expressed as:

$$\text{FS (overturning)} = \Sigma M_R / \Sigma M_0 \qquad (2.20)$$

where,

ΣM_R = Sum of the moments of forces tending to resist overturning.

ΣM_0 = Sum of the moments of forces tending to overturn about point C.

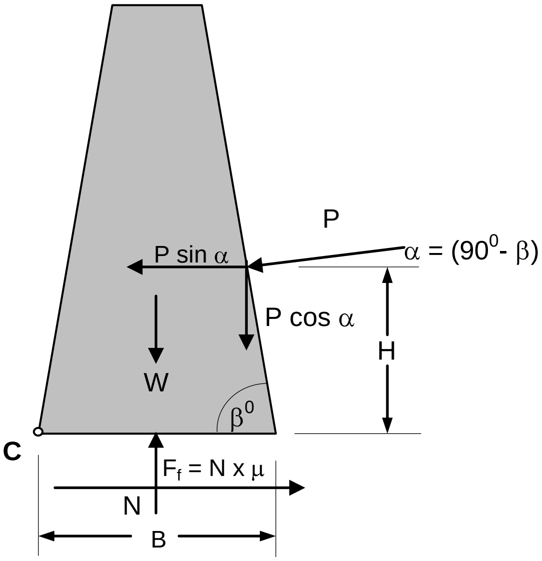

Figure 2.12. Free Body Diagram of a TCTB against Hydrodynamic Force.

In Figure 2.12,

$$\Sigma M_R = W \times 0.5B + (P \text{ cosine } \alpha) \times (B - H \cot \beta) \tag{2.21}$$

where,

W = weight of the TCTB.

B = width of the TCTB at base.

P = hydrodynamic force per unit length of the TCTB, which acts perpendicular to the surface and can be calculated from the specific energy.

H = vertical distance of the resultant force, which can be determined from the pressure diagram.

and:

$$\Sigma M_0 = P \text{ sine } \alpha \times H \tag{2.22}$$

Similarly, the factor of safety against sliding may be expressed as:

$$FS_{\text{(sliding)}} = \Sigma F_R / \Sigma F_d \tag{2.23}$$

where,

ΣF_R = Sum of horizontal resisting forces.

ΣF_d = Sum of horizontal driving forces.

In Figure 2.12,

$$\Sigma F_R = N \text{ x } \mu = (W + P \text{ cosine } \alpha) \text{ x } \mu \tag{2.24}$$

where,

μ = coefficient of static friction, which is a function of two friction surface.

and:

$$\Sigma F_d = P \text{ sine } \alpha \tag{2.25}$$

To increase the factor of safety for overturning, the usual procedure is either to increase the weight of the TCTB or to use anchors to hold it tightly with the base of the TCTB. The anchor would also increase the factor of safety against sliding. The coefficient of static friction changes if the surfaces are wet. During the submerged condition, the weight of the TCTB will decrease due to buoyancy.

All the parameters for the calculation of FS can be obtained from the geometry and unit weight of concrete except the coefficient of static friction. Thus, the literature review has also been focused on “coefficient of static friction” between concrete surface of the TCTBs and the surface on which the TCTBs stand, such as HMA surface, concrete pavement surface, compacted subgrade, subbase, or base surface.

2.4.1 Friction

At the microscopic level the surface of any solid, no matter how polished, looks like Figure 2.13. Two mating surfaces are in contact only on the tips of the asperities (Blau, 1996). When two solid surfaces are brought together the area of contact area is actually extremely small compared to the apparent area of contact.

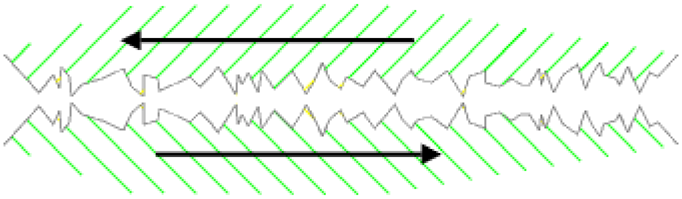

Figure 2.13. Two Contacting Solid Surface.

Friction is the resistive force acting between bodies that tends to oppose and damp out motion. Friction is usually distinguished as being either static friction (the frictional force opposing placing a body at rest into motion) or kinetic friction (the frictional force tending to slow a body in motion). In general, static friction is greater than kinetic friction.

2.4.2 Coefficient of Friction

When the applied force overcomes the frictional force between two surfaces then the surfaces begins to slide relative to each other (Figure 2.14). The static frictional resistance is normally different to the dynamic frictional resistance. The coefficient of static friction and the coefficient of dynamic friction can be expressed using the same formula. However, the coefficient of static friction is always higher than the coefficient of dynamic friction.

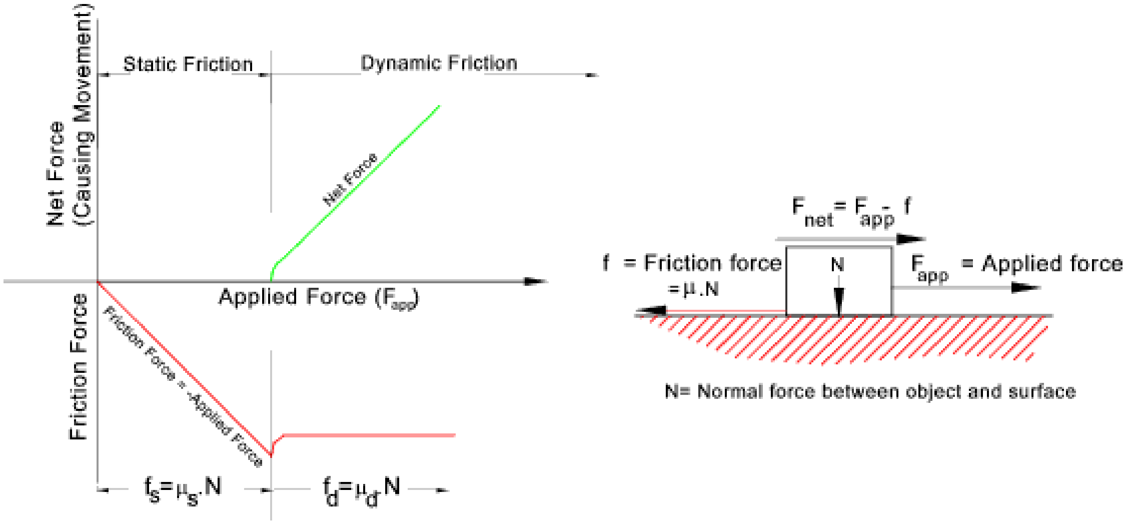

Figure 2.14. Coefficient of Static and Dynamic Friction.

2.4.3 Coefficient of Static Friction

An enormous number of studies (Stinson et al., 1934; Henry et al., 2000; Jackson, 2008) have been conducted to estimate the coefficient of dynamic friction between the tire and the road surfaces using Circular Track Meter (ASTM E 2157), Dynamic Friction Tester (ASTM E 1911), Sand Patch Test (ASTM E 965), Locked Wheel Tester (AASHTO M 261 or ASTM E 501). However, a very few studies have been done to estimate the coefficient of static friction between concrete (TCTB) and different road surfaces. The coefficients of static friction for surfaces that are related to our study are available in different literatures are listed in Table 2.1.

Table 2.1. The Coefficient of Static Friction of Concrete and Different Road Surfaces.

Material 1	Material 2	Coefficient of Static Friction
Cement Concrete	Cement Concrete (wet)	0.5-0.6[a]
Cement Concrete	Cement Concrete (dry)	0.6-0.7[a]
Cement Concrete	Clay (wet)	0.2[b]
Cement Concrete	Clay (dry)	0.4[b]
Cement Concrete	Sand (wet)	0.4[b]
Cement Concrete	Sand (dry)	0.5-0.6[b]
Cement Concrete	Rock (wet)	0.5[b]
Cement Concrete	Rock (dry)	0.6-0.7[b]
Cement Block	Cement Blocks	0.65[b]
Cement Concrete	Rubber (dry)	0.6-0.85[c]
Cement Concrete	Rubber (wet)	0.45-0.75[c]
Asphalt Concrete	Rubber (dry)	0.5-0.8[c]
Asphalt Concrete	Rubber (wet)	0.25-0.75[c]

[a] ACI 318R-89 Manual of Concrete Practice
[b] http://www.supercivilcd.com/friction.htm
[c] EngineersHandbook.com

The coefficient of friction is sensitive to atmospheric dust and humidity, oxide films, surface finish, velocity of sliding, temperature, vibration, and extent of contamination (Bowden and Tabor 1973). Moreover, presence of moisture and different types of liquids, such as oil, surfactants, lubricants etc, could decrease the coefficient of static friction significantly. In many cases the degree of contamination is perhaps the most important single variable. Thus, the only way to determine the accurate coefficient of friction between two surfaces is to conduct experiments.

2.4.4 Effect of the Presence of Sand Particles in between Two Smooth Surfaces

Sand is not normally regarded as a lubricant. Sands are often used in icy road to enhance friction. However, in many cases, the presence of sand dry particles in between two smooth surfaces might cause a reduction in friction. Cross (2006) conducted experiments to evaluate the effect of the presence of dry sand on tennis court to understand the friction between the rubber of the tennis shoe and the smooth court and found that the presence of dry rounded river sand decreased the coefficient of static friction from 0.39 to 0.14.

2.4.5 Determination of Coefficient of Static Friction

The procedure to determine the coefficient of static friction is described in ASTM C 1028-07 for different floor materials using horizontal Dynamometer Pull-Meter (Figure 2.15). The dynamometer pull-meter assembly consists of 3/4 in. × 8 in. square block of the material that needs to be tested for a particular surface, 50-lb weight, and a dynamometer. Using the dynamometer, the force required to cause the test assembly to slip continuously is determined. Four pulls perpendicular to the previous pull on each of three surface areas or three test specimens constitute the 12 reading required to calculate the coefficient of friction. The coefficient of friction is calculated by dividing the average of the 12 readings by the total weight of the base and 50 lb surcharge.

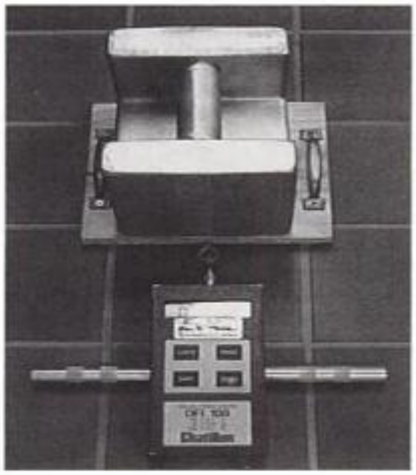

Figure 2.15. Dynamometer Pull-Meter.

The TCTBs are often placed in construction sites on different types of construction materials, such as compacted clay, sand, gravel, etc. The TCTBs are also placed on top of finished road surfaces. The coefficient of static friction usually decreases due to aging of the surfaces. The stability analysis based on the coefficient of static friction of a newly constructed road surface may lead to serious error. Thus, the coefficient of static friction of different pavement surface must be measured for pavements with different ages and pavements with both wet and dry conditions.

2.5 TXDOT HYDRAULIC DESIGN GUIDANCE

The Texas Department of Transportation's Hydraulic Design Manual (2009) provides guidance and recommendations for the design, analysis and construction of hydraulic facilities. Hydrologic and hydraulic analyses are required to determine the need and size of a hydraulic facility. Table 2.2 summarizes recommended design floods and check floods for various structures.

The design frequency or design flood is the maximum severity of flood the structure will pass without inundation. The design flood is intended to establish conditions under which the highway facility will provide uninterrupted service with minimal damage to the highway and must not overtop the highway. The magnitude of flow associated with each frequency is determined based on historic hydrologic data specific to the area where the structure is located. Based on TxDOT policy, the recommended design storm for a freeway bridge is a 50-year storm, which has a 2% probability of occurring in any given year. The check flood is applied on proposed highway or stream crossing facilities to determine whether a proposed crossing will cause significant damage to the highway or to any other property. For TxDOT design, the 100-year event is the primary check condition, which has a 1% probability of occurring in any given year. In the event of a 100-year storm, a freeway bridge would most likely be overtopped by floodwaters, which would force water to flow over the temporary barrier or bridge rails and bridge deck. If it does not overtop, an additional check flood that reaches highway overtopping would be checked. When overtopping occurs, the type of temporary barrier or bridge rail would play a key factor in the impact of the 100-year floodplain and may raise compliance issues with the Federal Emergency Management Agency (FEMA). According to FEMA, an increase of water surface elevation by more than 1 ft for the 100-year flood event requires a FEMA detailed floodplain map revision.

Table 2.2. TxDOT Design and Check Frequencies.

	Design Flood					**Check Flood**
Functional Classification and Structure Type	**2**	**5**	**10**	**25**	**50**	**100**
Freeways (main lanes):						
♦ Culverts					X	X
♦ Bridges					X	X
Principal arterials:						
♦ Culverts			X	(X)	X	X
♦ small bridges			X	(X)	X	X
♦ major river crossings					(X)	X
Minor arterials and collectors (including frontage roads):						
♦ Culverts		X	(X)	X		X
♦ small bridges			X	(X)	X	X
♦ major river crossings				X	(X)	X
Local roads and streets (off-system projects):						
♦ Culverts	X	X	X			X
♦ small bridges	X	X	X			X
Storm drain systems on interstate and controlled access highways (main lanes):						
♦ Inlets and drain pipe			X			X
♦ Inlets for depressed roadways*					X	X
Storm drain systems on other highways and frontage:						
♦ Inlets and drain pipe	X	(X)				X
♦ Inlets for depressed roadways*				(X)	X	X

Notes.

* A depressed roadway provides nowhere for water to drain even when the curb height is exceeded.

( ) Parentheses indicate desirable frequency.

(Sources: *TxDOT Hydraulic Design Manual*, 2009)

The recommended design frequency for small bridges on principal arterials and minor arterials and collector roadways is the 25-year storm with a 4% probability of occurrence in any given year. These structures must also be checked for the 100-year storm.

Interstate highways and facilities such as underpasses and depressed roadways must be protected from the 50-year storm. Continued adequate hydraulic performance for highway rehabilitation, modification, or maintenance work including the addition of roadway barrier must be verified for compliance with FEMA. The *TxDOT Hydraulic Design Manual* states whenever "higher or less hydraulic efficient railing" is used and a "safety project involving addition of safety barrier," the floodplains must check consistency with the National Flood Insurance Program (NFIP) requirements.

CHAPTER 3: HYDRAULIC PERFORMANCES OF TCTBS

3.1 INTRODUCTION

Temporary Concrete Traffic Barriers (TCTBs) are essential in order to protect the traveling public and highway construction crews. They are rigid barricades that help prevent accidents due to driver misfortune or negligence. However, for these barriers to maximize crash safety, some properties such as hydraulic capacity become diminished. This is because larger drain openings that would increase the hydraulic capacity result in a decrease in the barrier weight and/or a higher center of gravity, which increases the barrier's susceptibility to overturning when impacted. However, smaller openings can result a higher water elevation upstream of the barrier, which in turn can increase the local floodplain elevation. It is therefore paramount that the balance between barrier stability and hydraulic performance be optimized. The hydraulic performance of four barriers is the focus of this report. In particular, this research focuses on development of a hydraulic rating curve that models the relationship between flow and upstream energy and how downstream submergence and clogging will affect this relationship.

The objectives of the research described in this chapter are as follows:

- Develop rating curves for four standard type TCTBs.
- Model the effect that downstream submergence will have on the rating curves.
- Evaluate the effect of clogging.

In order to accomplish the first objective, a three parameter model developed by Charbeneau et al. (2008) as discussed in Chapter 2 was utilized. To accomplish the second task two models were used. The first, by Villemonte (1947), was developed in order to describe the effects that downstream submergence will have on a weir, but has proven to model barriers with small drainage openings quite well. Also, a model developed by Charbeneau et al. (2008) will be employed by which the Villemonte model was adapted to account for larger drainage openings. For the third task, a procedure was developed during this research by which a model barrier was fitted with a device that allowed for testing the barrier with different amounts of clogging.

3.2 THEORY OF FLOW

The foundation for this study is based on several key principles from fluid mechanics. This section will review principles including the energy equation, specific energy/critical flow, and the equations for flow over a weir and through an orifice, in order to provide a starting point for explaining the models that were developed in this research.

3.2.1 General Energy Equation

In order to understand how phenomenon in the environment work, a study of the energy in a system is generally conducted. This is because the law of conservation of energy allows for the development of equations that can predict future outcomes based on changes in energy states. One such relationship is the General Energy Equation for open channel flow (Equation 3.1). This equation is an adaptation of Bernoulli's Equation that accounts for a non-uniform flow distribution (α) and energy lost to heat (h_L), due to friction, between locations 1 and 2. Other key terms in the equation are as follows: z (vertical distance from constant datum), h (liquid depth), v (velocity), and g (gravitational constant), where the subscript denotes locations 1 and 2.

$$z_1 + h_1 + \alpha_1 \frac{v_1}{2g} - h_L = z_2 + h_2 + \alpha_2 \frac{v_2}{2g} \tag{3.1}$$

However, several simplifying assumptions can be made that greatly reduce the complexity of this equation. The following simplifications to Equation 3.1 were presented by Klenzendorf, 2007. First of all, z_1 and z_2 can be omitted, because the slope in the test channel is approximately zero, which makes these terms equal. Also, if a uniform flow distribution is assumed, due to a negligible effect by the channel walls and bottom, α can also be omitted because it would approximately equal a value of 1. The result of these assumptions is then given by Equation 3.2, given below, in which E is the specific energy.

$$E_1 = h_1 + \frac{{v_1}^2}{2g} = h_2 + \frac{{v_2}^2}{2g} = E_2 \tag{3.2}$$

Next, it is then possible using the volumetric flow rate equation, Q=Av, to solve for the velocity term. In this equation Q (volumetric flow rate) is equal to the v (velocity) of the liquid times the A (area) that the water is flowing through. Since the geometry of the channel is known and the height and flow of the water are being measured, it is then possible to calculate the energy. Equation 3.3, located below, shows this result, where E (energy) is related to the h (liquid depth) and Q (volumetric flow rate).

$$E = h + \frac{Q^2}{2gA^2} \tag{3.3}$$

Lastly, one more change is necessary, which allows for the calculation of flow on a per linear foot basis. This step allows an easy calculation to be performed for determining the flow rate that is associated with varying lengths of barrier. The variable q (unit flow rate) is then defined as Q (volumetric flow rate) divided by b (channel width), or q=Q/b. Substituting this change into Equation 3.3, then results in Equation 3.4 listed below, which is the form of the energy equation used for this research, where some further simplification has also been accomplished given that A (area) equals b (channel width) times h (liquid depth).

$$E = h + \frac{q^2}{2gh^2} \tag{3.4}$$

3.2.2 Specific Energy and Critical Flow

As it was developed in the last section in Equation 3.2, the energy of a fluid in an open channel can be calculated if the height and velocity of a fluid are known. Figure 3.1 below, shows the specific energy associated with a varying water depth. There are several key features in this figure. First, the line E=h corresponds to the potential energy that would occur if the fluid was stagnant. This is important because it means that the horizontal distance from the y axis to this line represents the value of the h term in Equation 3.2, and the remaining distance from the E=h line to the curve is the resulting kinetic energy ($v^2/2g$). Secondly, it can be seen from the graph that two different water depths can result in equivalent quantities of energy. It is then useful to be able to name the type of flow that is associated with each energy condition. A clear breaking point between the potential energy dominated flow regime and the kinetic energy dominated flow regime is the critical point. This point is the minimum specific energy that can be developed for a given channel discharge and is calculated by taking the derivative of the specific energy with respect to depth, dE/dh, and setting the resulting equation equal to zero. Solving this equation for depth results in the value for the critical depth, h_c, and is shown below in Equation 3.5. Points on the graph greater than the critical depth are called subcritical and points less than the critical depth are called supercritical.

$$h_c = \left(\frac{q^2}{g}\right)^{1/3} \tag{3.5}$$

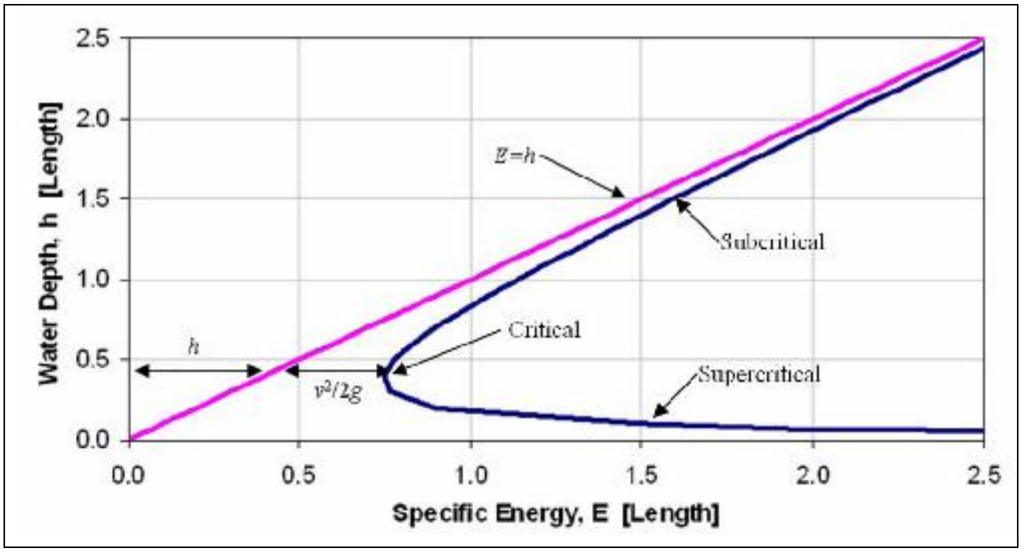

Figure 3.1. Specific Energy Graph.

The critical depth is important for the development of a mathematical model used in developing a rating curve for this research. If it is assumed that water flowing through an obstruction (i.e., a TCTB) causes the water to pass through a critical state at or near the obstruction, a relationship between the critical height and a measured height upstream can be developed using the general energy equation and Equation 3.5. This is illustrated below in Equation 3.6, in which the subscript c indicates the critical location near the TCTB and the subscript u indicates the location upstream where the water level height is being recorded.

$$h_c + \alpha_c \frac{v_c^{\ 2}}{2g} - h_L = h_u + \alpha_u \frac{v_u^{\ 2}}{2g} \tag{3.6}$$

However, additional assumptions can also be made that will further simplify the equation. First, the upstream flow will be subcritical due to the TCTB obstruction. This will cause the upstream kinetic energy part of the equation to be negligible when compared to the potential energy or $\frac{v_u^{\ 2}}{2g} \ll h_u$. Secondly, as previously mentioned, the α and h_L terms can be neglected. Lastly, if v_c is converted into an equivalent expression with q (unit flow) as was done in Section 3.2.1, we obtain Equation 3.7, which is listed below.

$$h_c + \frac{q^2}{2gh_c^{\ 2}} = h_u \tag{3.7}$$

Next, if Equation 3.5 is rearranged and solved for q^2, the result is $q^2 = gh_c^{\ 3}$. If this is then substituted into Equation 3.7 and rearranged to solve for h_c, an equation is developed which gives the critical depth as a function of upstream depth. This equation is given below as Equation 3.8.

$$h_c = \frac{2}{3} h_u \tag{3.8}$$

This equation is especially helpful for the development of a mathematical model, which approximates the rating curve data gathered for each barrier type. Since, the actual value of the critical depth cannot be measured, this relationship allows for the calculation of the transition point, between supercritical to subcritical, with the measured data upstream of the model.

3.2.3 General Flow Equation

3.2.3.1 Weir Flow

Several different methods can be used to measure the flow of a liquid, such as venturi tubes, turbine flowmeters, magnetic flowmeters, pitot tubes, and weirs. The method used in this research is the weir. A weir is a barrier or dam placed in the channel so that the fluid backs up behind it then falls through a notch cut into the face of the weir (Mott, 2000). The weir equation will also be useful when deriving the model equations describing the flow over a barrier, and will be discussed more in Section 3.3.2.

The general equation for weirs with horizontal crests is given by the following equation (King & Brater, 1963):

$$Q = Cbh_w{}^n \tag{3.9}$$

In this equation Q is the volumetric flow rate, C is the weir coefficient derived for each specific weir, b is the width of the weir, h_w is the height of the water above the weir crest, and n is dependent on the weir geometry. The weir equation in this research is used both in the calculation of flow for the development of a rating curve and in deriving the model used to describe the flow over the barrier. For measuring the flow rate during the experiments a more specific form of the weir equation is used, which was developed to model the flow over sharp crested rectangular weirs and is given below in Equation 3.10 (Rouse, 1950). In this equation C_d is an empirically derived weir coefficient that is dependent on the effects of viscosity, the velocity distribution and capillarity (Rouse, 1950), and all other terms have been defined previously.

$$Q = C_d \frac{2}{3} b\sqrt{2g}h_w{}^{1.5} \tag{3.10}$$

3.2.3.2 Orifice Flow

In addition to the weir equation, the orifice flow equation is useful in the development of the model used in this research. According to King & Brater (1963), an orifice is a restricted opening with a closed perimeter through which water flows. The flow rate through a sharp crested orifice (the type of orifice that the barriers possess) is described by Equation 3.11, which is given by Bos (1989).

$$Q = C_d A_o \sqrt{2gh_o} \tag{3.11}$$

In this equation, C_d is a unitless discharge coefficient, A_o is the cross-sectional area of the orifice, h_o is the upstream head acting on the centroid of the orifice area, and Q and g have been defined previously.

Equation 3.11, however, is only valid when h_o is greater than the height of the orifice opening, and the discharge is unrestricted downstream. When the orifice becomes submerged upstream and downstream a slight alteration to this equation is necessary. The equation governing submerged orifice flow is also given by Bos (1989) and is shown below as Equation 3.12, where Δh_o is the difference in upstream and downstream head acting on the centroid of the orifice.

$$Q = C_d A_o \sqrt{2g\Delta h_o} \tag{3.12}$$

3.3 THEORETICAL MODEL DERIVATION

In order to develop the rating curve that will describe the relationship between upstream water energy and flow for a typical TCTB, two different models were developed. The first model, the Rating Curve Model is a model that develops the link between upstream energy and flow, without the presence of a downstream obstruction. This model will demonstrate the ideal condition, where water flowing through the orifice and over the top of the barrier is not affected by backwater. The second model, the Submergence Model, will then describe the effects of an impediment downstream that forces water to back up on the downstream side of the TCTB. This water will then reduce flow through the orifice in the barrier and cause the potential energy (water height) upstream of the barrier to increase.

3.3.1 Rating Curve Model

This research builds upon a previous study conducted by Charbeneau et al. (2006) and the summary of the model used for the evaluation of hydraulic performance of bridge rail has been described in Chapter-2. The same model has been used for the evaluation of hydraulic performance of TCTB. The equations governing each flow type are provided in Equations 2.8, 2.11, and 2.14.

A detailed development of the model for TCTB is described here. Figure 3.2 illustrates the different flow types, which are defined by the water height. Also, in this figure, several key parameters used in the creation of the model are shown. The first parameter of interest is the term H_u, which is the overall height of the water that is measured by the pitot tubes at a location upstream of the barrier. Next, h_b is defined as the height of the support base. Furthermore, h_u is the difference between H_u and h_b, i.e., h_u=H_u-h_b. Furthermore, h_r is the height of the barrier, and h_{rl} is the height of the drain opening. Lastly, b is the width of the channel, and b_p is the support base with, which is the difference between b and b_{rl}, (b_p=b-b_{rl}), where b_{rl} is the width of the drainage opening. These terms describe the physical properties of the barrier being tested and are important in deriving the equations for the different flow types in the subsequent sections.

3.3.1.1 Type 1 Flow

In Type 1 flow, water is allowed to pass through the scupper drain, but the water level is less than the height of the drain opening. For this flow regime, water is forced to go from a subcritical flow upstream of the barrier, to a critical flow at the barrier, and then to supercritical as the water flows through the opening. This is because the barrier acts as an obstruction to the flow, which causes the potential energy to increase and the kinetic energy to decrease upstream of the barrier. Downstream of the barrier, the water is then in a supercritical state, because of the lack of an obstruction. Therefore, it can be surmised that at the barrier, critical flow will be developed. This is extremely helpful information, and serves as the launching point for deriving the mathematical model developed by Charbeneau et al. (2006). It is also important to know that the height of the water upstream of the barrier can be related to the critical height by Equation 3.8, or h_c=2h_u/3, because the critical height cannot be measured, while the height upstream is readily measurable.

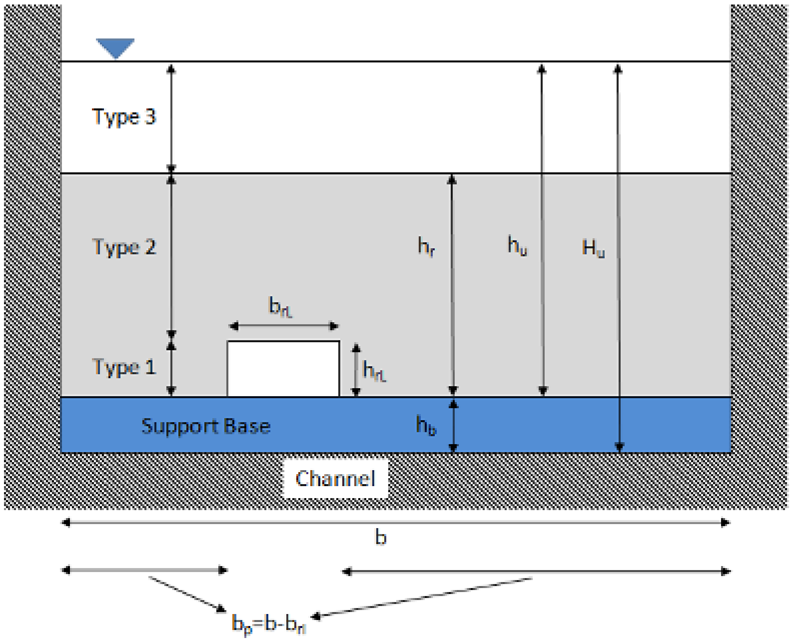

Figure 3.2. Flow Type Schematic for Modified TCTB.

With the critical height related to upstream water depth, it is also helpful to know that at critical flow the Froude number is equal to a value of one. This is because the Froude number is the ratio between inertial forces and gravitational forces, or the ratio between supercritical flow and subcritical flow. Equation 3.13 below, describes this relationship, where v is the velocity, g is the gravitational constant, and D is a characteristic length (water depth).

$$Fr = \frac{v}{\sqrt{gD}} \tag{3.13}$$

If the Froude number (Fr) is then set to one, and Equation 3.13 solved for the velocity term, the results is then presented below in Equation 3.14, where h_c is the critical height.

$$v_c = \sqrt{gh_c} \tag{3.14}$$

This is very helpful, because we now can determine the velocity through the drain opening, which is a function of gravitational forces and the water height upstream, by substituting Equation 3.8 into Equation 3.14 to obtain the following result, Equation 3.15.

$$v_c = \sqrt{g\left(\frac{2}{3}h_u\right)} \tag{3.15}$$

The flow rate through the scupper drain can then be calculated through the use of the continuity equation, Q = vA, where v is the velocity and A is the area of flow. According to Charbeneau et al. (date), the area of flow through a drain is diminished by horizontal contractions that occur as water flows through the opening. To account for the reduction in area, coefficient values can be experimentally determined that account for these losses. Figure 3.3, below, illustrates this phenomenon, where the water entering the drain is contracted. The coefficient C_b is used here to describe the decrease in the effective area by which the water is flowing through the opening. This figure shows the flow being forced to the middle as water passes through the orifice, which then causes a decrease in the effective width as can be seen in Figure 3.4.

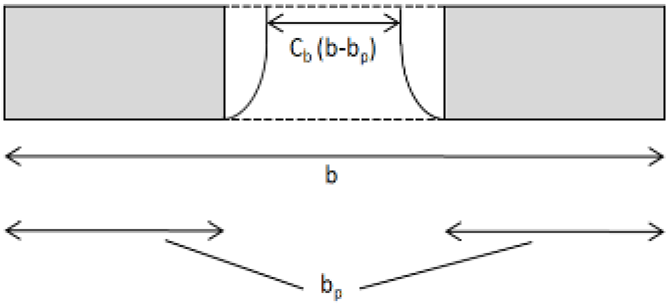

Figure 3.3. Plan View of Type 1 Flow.

Figure 3.4. Type 1 Flow.

What we are left with then is Equation 3.16, which describes the flow rate at the location of critical depth (at the barrier) based on the assumptions described above.

$$Q = Av_c = C_b(b - b_p)\left(\frac{2}{3}h_u\right)\sqrt{g\left(\frac{2}{3}h_u\right)} \tag{3.16}$$

The next step is then to write the equation in a form that will easily allow the comparison of different barriers, and derive it in a way such that it is non-dimensional. Non-dimensionalizing the equation transforms the flow to a per unit basis, so that the equation will be applicable to any length of barrier, and rearranging the terms so that the flow area is based on a fraction of open space facilitates easy comparison between barriers based on the amount of area is allocated to drainage. The fraction of open space is then given below by Equation 3.17, where A_o is the cross-sectional area of the drain perpendicular to the flow and A_r is the cross-sectional area of the barrier perpendicular to the flow, which includes the drain area, and all other terms have been defined previously.

$$F_o = \frac{\mathrm{A_o}}{\mathrm{A_r}} = \frac{(\mathrm{b}-\mathrm{b_p})\mathrm{h_{rL}}}{\mathrm{b\,h_r}} \tag{3.17}$$

Next, by taking Equation 3.15 with 3.16 and employing some algebra, Equation 3.18 (similar to Equation 2.8) can be derived, which is the non-dimensional equation for Type 1 flow.

$$\frac{Q}{A_r\sqrt{g h_r}} = \mathrm{C_b F_o}\frac{\mathrm{h_r}}{\mathrm{h_{rL}}}\left(\frac{2\mathrm{h_u}}{3\mathrm{h_r}}\right)^{1.5} \tag{3.18}$$

3.3.1.2 Type 2 Flow

Type 2 flow occurs when the water level rises above the height of the drainage opening, and is modeled as an orifice flow according to Charbeneau et al. (2006). This flow regime, like Type 1 flow, is also affected by contractions at the opening. Figure 3.5 below, shows the vertical contraction that occurs during orifice flow. For orifice flow both the vertical and horizontal contractions must be considered in calculating the area of flow.

The first step in developing the equation is realizing that the energy upstream of the barrier and at the barrier will be the same. Additionally, like it was with Type 1 flow, it can be assumed that the flow upstream will be subcritical, due to the obstruction of the barrier. This assumption leads to the simplification of the energy equation, because the upstream water velocity (kinetic energy) will negligible when compared to the water depth (potential energy), i.e., $\frac{v_u}{2g} \ll h_u$. Next, it should also be noted that the water depth (potential energy) at the barrier will be related to the height of the drain opening multiplied by the coefficient Cc, because of the contraction that occurs when water flows through the orifice. Finally, it is possible to develop the energy equation, Equation 3.19. In this equation the subscript u refers to the upstream position, the subscript m refers to a location at the model, and all other terms have been defined previously.

$$h_\mathrm{u} = C_c h_\mathrm{rL} + \frac{v_\mathrm{m}^2}{2g} \tag{3.19}$$

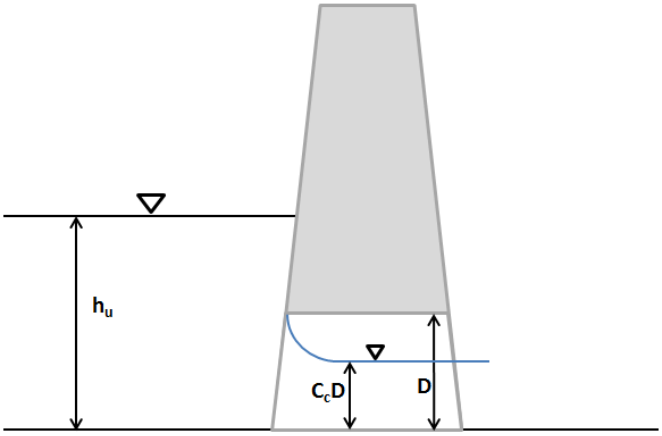

Figure 3.5. Profile View of Type 2 Flow.

The next step is then to use the continuity equation (Q=Av) as we did in evaluating Type 1 flow. By rearranging Equation 3.19 we can solve for v_m. This will give the velocity portion of the continuity equation and is given below as Equation 3.20.

$$v_m = \sqrt{2g(h_u - C_c h_{rL})} \tag{3.20}$$

The area can then be realized as the height of the barrier orifice multiplied by the coefficient C_c times the width of the barrier orifice multiplied by the coefficient C_b. Plugging the values for area and velocity into the continuity equation we are then left with Equation 3.21.

$$Q = Av_m = C_b(b - b_p)C_c h_{rL}\sqrt{2g(h_u - C_c h_{rL})} \tag{3.21}$$

However, as it was done for Type 1 flow, we must also convert the equation to the non-dimensional form. The result of the algebraic conversion is then given by Equation 3.22.

$$\frac{Q}{A_r\sqrt{gh_r}} = C_b C_C F_o\sqrt{2\left(\frac{h_u}{h_r} - C_c\frac{h_{rL}}{h_r}\right)} \tag{3.22}$$

The last step is then to determine the height upstream which will be the transition point between Type 1 and Type 2 flow. To do this we can set the equations for each of the flow types equal to each other. The result is a cubic equation in terms of the upstream water depth, in which there are three roots. The first root is equal to a value of −3 (which has no physical meaning), and the second two roots equals 3/2. The resultant equation with respect to upstream water depth is then given by Equation 3.23.

$$\frac{h_u}{\mathrm{h_r}} = \frac{3}{2}\mathrm{C_c}\frac{\mathrm{h_{rL}}}{\mathrm{h_r}} \qquad (3.23)$$

This equation is non-dimensional with respect to the height of the barrier, as are the equations for Type 1 and 2 flows. Also, it should be noted that this equation is equivalent to Equation 3.8, which was derived earlier. It is at this point that the Type 1 and 2 flow curves intersect and the derivatives of the curves are equal, which creates a smooth transition point between the two flow types.

3.3.1.3 Type 3 Flow

Type 3 flow can be explained through the superposition of orifice and weir flow, in which the orifice flow is described by the equation for Type 2 flow and weir flow is that of a broad crested weir. The equation for broad crested weir flow is then given by Equation 3.24 (Bos, 1989). In this equation an extra term is added, C_v, which accounts for a loss in the velocity head as the water passes over the weir.

$$Q = C_d \mathrm{C_v} \frac{2}{3} b \sqrt{\frac{2}{3} g {h_w}^3} \qquad (3.24)$$

If this equation is then converted into the non-dimensional form, as the equations for Type 1 and Type 2 flows were, the result is Equation 3.25. In this equation, it should be noted that the term C_v is omitted because combining it with C_d will result in a single coefficient, which is more practical for modeling purposes. Also, the term h_w is equivalent to the height of the water above the weir, which is the difference between the water height upstream and the barrier height ($h_w = h_u - h_r$).

$$\frac{Q}{A_r\sqrt{g h_r}} = C_d \left(\frac{2}{3}\right)^{1.5} \left(\frac{\mathrm{h_u}}{\mathrm{h_r}} - 1\right)^{1.5} \qquad (3.25)$$

By combine Equations 3.24 and 3.25, we are then left with a non-dimensional equation for modeling Type 3 flow (Equation 3.26).

$$\frac{Q}{A_r\sqrt{g h_r}} = \mathrm{C_b C_C F_o}\sqrt{2\left(\frac{\mathrm{h_u}}{\mathrm{h_r}} - \mathrm{C_c}\frac{\mathrm{h_{rL}}}{\mathrm{h_r}}\right)} + C_d \left(\frac{2}{3}\right)^{1.5} \left(\frac{\mathrm{h_u}}{\mathrm{h_r}} - 1\right)^{1.5} \qquad (3.26)$$

3.3.2 Submergence Model

The Submergence Model describes the effects of an obstruction that forces water to back up on the downstream side of the TCTB. This water will then hinder flow through the barrier and cause the potential energy (water height) upstream to increase. The increase in the water height will then be a departure from the prediction given in the rating curve model. To describe this departure two methods have been developed. The first is a model developed by Villemonte (1947), which is based on the general weir equation and the principle of superposition. This model, however, tends to overestimate the effects due to low flow rates and underestimate those due to high flow rates (Klenzendorf, 2007). The second is an empirically derived equation developed from the Villemonte model, which is described by Klenzendorf (2007). In this model, the non-dimensional flow rate is included in the equation in order to represent the impact that changing the flow will have on the rating curve.

3.3.2.1 Villemonte Model

As previously noted, the Villemonte Model describes the effect that an increase in downstream water depth (submergence) imparts to upstream water depth. To describe the interaction between upstream and downstream water depth the principle of superposition was used, where the net flow rate (Q) is a function of the upstream and downstream discharges Q_1 and Q_2 that would occur under conditions without submergence.

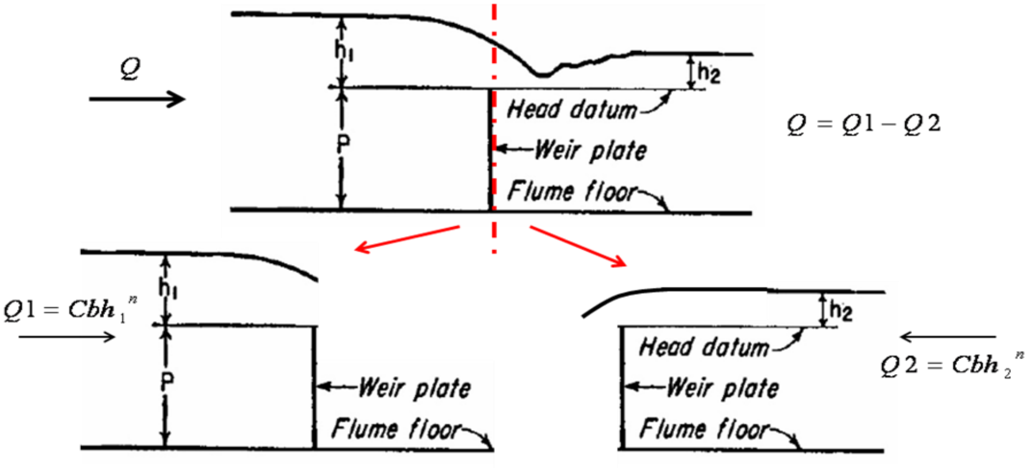

Figure 3.6. Villemonte Model (Villemonte, 1947).

The resulting statement is then given below by Equation 3.27, where the net flow is equal to the difference between flow upstream and downstream ($Q = Q_1 - Q_2$) ,and the equation has been algebraically transformed so that the left hand side represents a submergence coefficient.

$$\frac{Q}{Q_1} = 1 - \frac{Q_2}{Q_1} \tag{3.27}$$

This equation, however, proved to be invalid when compared to the data Villemonte conducted on various weirs. Nevertheless, a relationship was discovered between Equation 3.27 and the data, when a multiplicative and an exponential constant (k, m) were added to the right side of the equation. The result of these additions leads to Equation 3.28, given below, which is the general form of the submergence model.

$$\frac{Q}{Q_1} = k\left(1 - \frac{Q_2}{Q_1}\right)^m \tag{3.28}$$

If we then insert the general form of the weir equation (Equation 3.9) into Equation 3.28 the result is given by Equation 3.29, in which the exponent n is dependent on the particular weir being used.

$$\frac{Q}{Q_1} = k\left(1 - \frac{Cbh_2{}^n}{Cbh_1{}^n}\right)^m \tag{3.29}$$

Furthermore, C and b can be removed from the expression because they are a constant for both the upstream and downstream flows, and the coefficient *k* can be removed, because it was experimentally determined to have a value of 1 for weirs with horizontal crests by Villemonte. This results in Equation 3.30. In this equation energy (e), expressed in ft, has been substituted for the height above the weir, where the head datum is measured from the support base instead of from the top of the weir, as was done in the Villemonte model. Also, because the LPCB has a horizontal crest, a value of 1.5 can be inserted for n.

$$\frac{Q}{Q_1} = \left(1 - \left(\frac{e_d}{e_u}\right)^{1.5}\right)^m \tag{3.30}$$

However, since the LPCB includes orifice flow, the value of 1.5 for n may not be entirely correct. It should be noted though, that this equation is still used, because it has been found to produce reasonable results.

3.3.2.2 Empirical Model

Another model has been developed by which the Villemonte model is adapted to account for changes in the flow rate. In this model proposed by Klenzendorf (2007), the non-dimensional flow rate is included in the power term, and an additional parameter (A) is inserted into the equation to create a lower bound, where the downstream water height has a limited effect on the upstream water elevation. Also, the power term n is assumed to be one. This is because the value of 1.5 used in the Villemonte model is derived from the weir equation, and the addition of orifice flow will alter this term. The result of these changes is given below in Equation 3.31, where F_Q is the non-dimensional flow rate, B is the model coefficient, and all other terms have been defined previously.

$$\frac{Q}{Q_1} = \left(\frac{\Delta e}{Ae_u}\right)^{1/BF_Q} \tag{3.31}$$

Furthermore, the value of A used in this report is taken from an experiment by Klenzendorf. To find a suitable value for A, the type T203 bridge rail submergence test data was compared to Equation 3.31. When different values for A were plugged into the equation a plot of the standard error versus A was developed. This graph is presented in Figure 3.7. In this graph, there appears to be a local minimum when A equals 2/3. Since the flow through the bridge rail is similar to that of a traffic barrier, this value is used as the fitting parameter in this research.

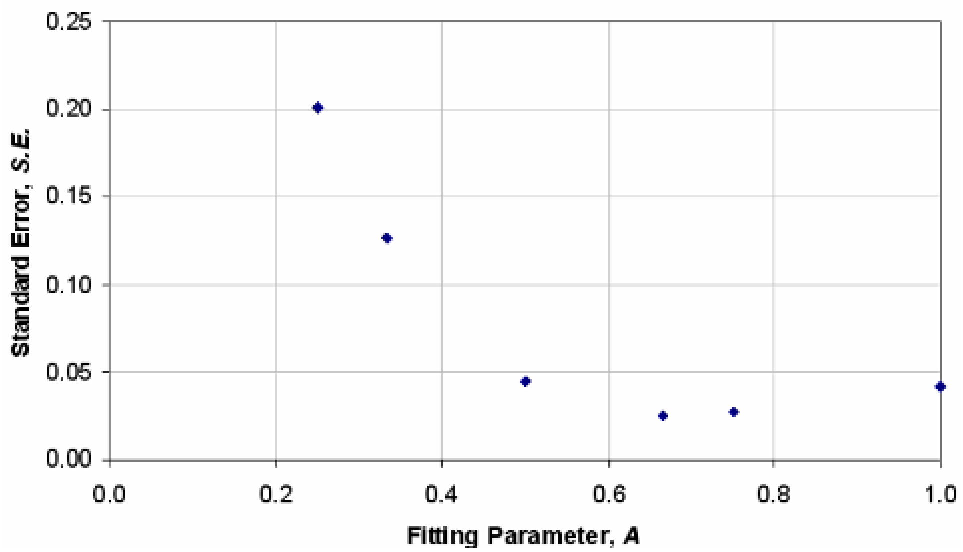

Figure 3.7. Fitting Parameter A (Klenzendorf, 2007).

3.4 PHYSICAL SETUP

3.4.1 Model Barrier Construction

The first step for the laboratory experiment was the construction of the model and model base. This was a key step because the quality of the models being tested will inevitably affect the quality of the results.

The models were constructed using TxDOT standard drawings, which are included in Appendix A. These drawings were obtained from the TxDOT website (TxDOT, 2009) and are available to the public. For the construction of the models, timber was chosen as an alternative to concrete (actual barrier material), because of the relative ease of construction and movement, and because the hydraulic properties being measured are independent of the material, as long as the material is impermeable. In order to make the models as impermeable as possible, all the pieces were coated twice with a water proofing compound and with a final coat of primer paint. This also assured that the models would not warp or disintegrate during multiple tests. As seen in Figures 3.1-3.3, the models were constructed with a hollow interiors and open ends to decrease the effect of buoyancy forces during testing. This, however, will have little effect on the hydraulic properties being tested, because testing is only conducted after the flow has reach steady state, and under these conditions the amount of water flowing into and out of the model is negligible compared to the total amount of flow. Furthermore, in order for the models to conform to the existing test channel at the CRWR, the models were constructed at half scale with only half of a typical barrier section and one scupper drain analyzed. Lastly, only one model barrier was constructed to analyze both the SSCB and SSCB-SPL. This is because both barriers had similar geometries with different sized drainage openings. This model will be referred to as the Modified Single Slope Concrete Barrier (MSSCB). Through adaptations to this model both the SSCB and SSCB-SPL barrier's rating curves were developed.

3.4.2 TCTB Descriptions

Temporary Concrete Traffic Barriers are used in order to prevent traffic from leaving the main driving surface. They are placed in locations where protection from oncoming traffic is needed and to provide safety for work crews in construction areas. The most important factor in determining the hydraulic performance of a TCTB is the drainage opening size. Some of the parameters, which affect this performance, such as height of barrier (h_r), height of drain opening (h_{rl}), width of drain opening (b_{rl}), and F_o (Fraction of open space) for the model barriers are included below in Table 3.1. For a more detailed examination of the actual barrier dimensions, see the standard drawings in Appendix B.

Table 3.1. Key TCTB Model Parameters.

TCTB-Model	h_r (in.)	h_{rl} (in.)	b_{rl} (in.)	F_o (%)
MSSCB	21	6	8	3.81
CSB	16.5	1.5	12	1.82
LPCB	10	1	12	2.00

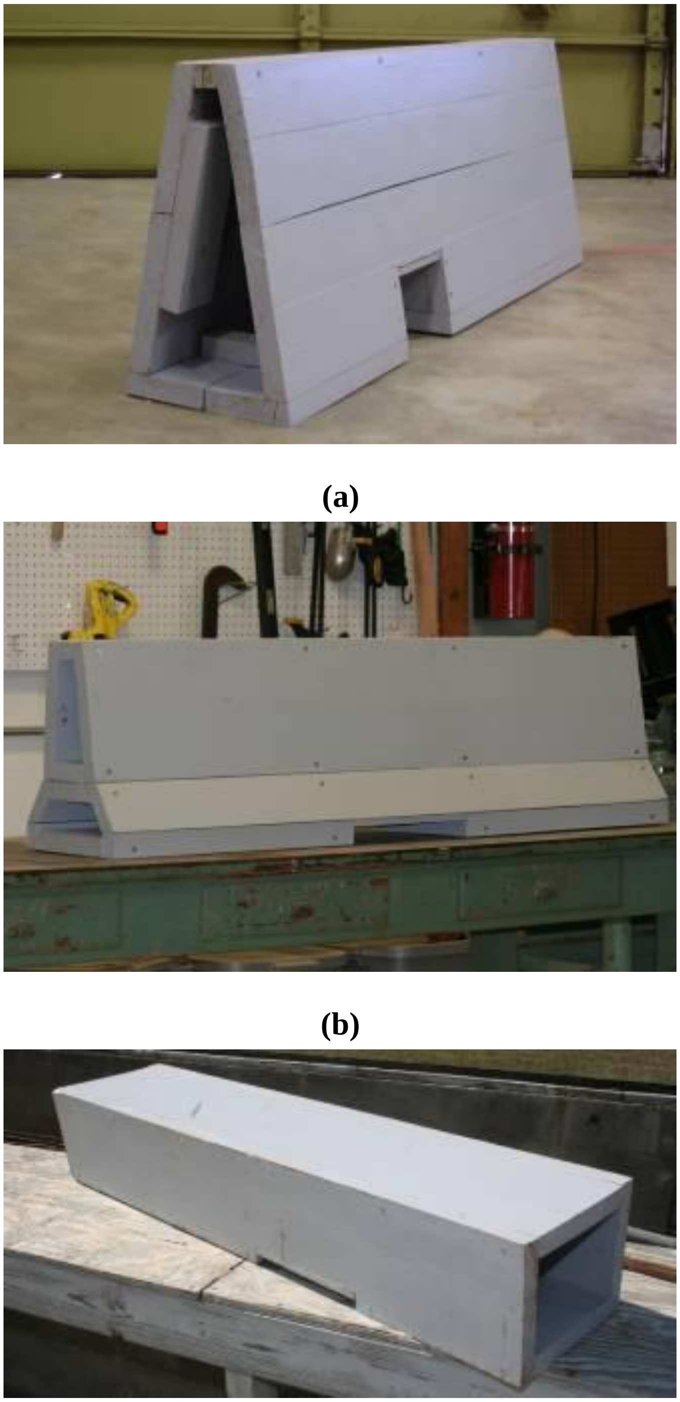

(a)

(b)

(c)

Figure 3.8. Model TCTBs: (a) MSSCB, (b) CSB, and (c) LPCB.

3.4.3 Model Barrier Support Construction

Before construction of the models began, a support base was constructed in the channel to firmly anchor the models during testing. Since previous experiments completed in the channel were successful with a particular base design, it was decided that a similar base should be constructed.

The outside dimensions of the base are as follows: 5 ft (152 cm) along the width of the channel, 4 ft (122 cm) along the length of the channel, and approximately 6 1/2 in. (16.2 cm) in height from the channel bottom. For the construction of the base 2x6 boards, 5/8 in. (1.6 cm) thick plywood, concrete, and sand were utilized. Figure 3.9, looking downstream in the channel, shows the model support base before being sealed with the top plywood piece.

The base was constructed with two sections. The upstream section was filled with concrete and has inside dimensions of 4.5 ft (137 cm) along the width of the channel, 1 ft (31 cm) along the length of the channel, and approximately 5 in. (13 cm) from the channel bottom. The concrete was utilized to provide the rigidity needed for the three support bars, located in the middle of the base and at 9 in. (30 cm) from each side of the channel. The downstream section was filled with sand to give the base more mass, in order to resist the forces experienced during testing. Also, the three boards perpendicular to the direction of flow were each fitted with two brackets that were anchored to the bottom of the channel. Two boards were also added on the outside of the main frame and were not connected to the frame or the channel. Theses boards would allow the release of water upstream of the base after completion of testing, and were held in place with brackets connected to the base and the channel walls on the downstream side of the base.

Figure 3.9. Support Base without Plywood Top.

3.4.4 Testing Facility Layout

The laboratory setup at CRWR consists of: a reservoir, two pumps with valves to regulate flow, a main channel (where the model is located), the return channel, and a sharp crested weir located in the return channel upstream from the reservoir (used to measure flow). A visual diagram, Figure 3.10, is presented below to better explain the layout. In addition to these items, components used in this experiment include: nine pitot tubes connected to an inclined manometer board, which is used for measuring the height of the water upstream and downstream of the model, and a tail water gate located in the main channel that was used to increase the water elevation downstream of the model. Each of the components listed above will be described in more detail in the subsequent sections.

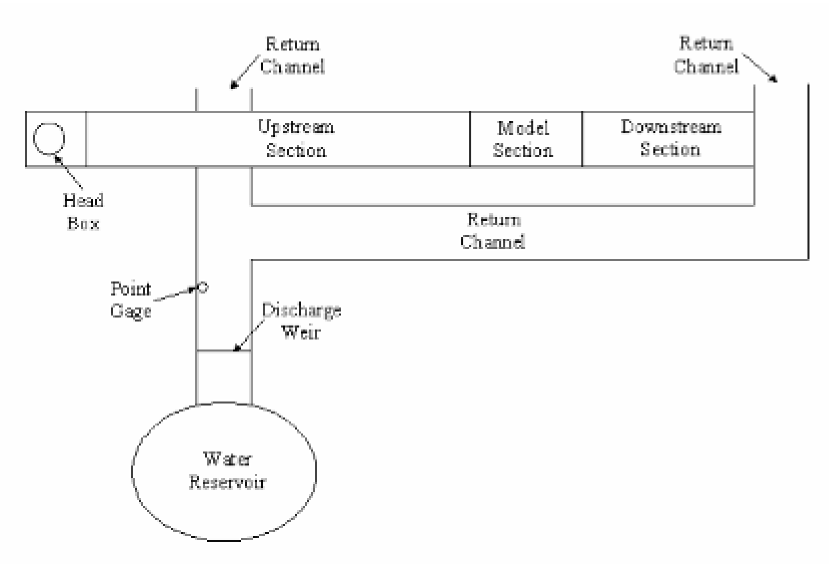

Figure 3.10. Testing Facility Layout (Klenzendorf, 2007).

3.4.4.1 Water Delivery System

The water used in testing is stored in a half million gallon capacity reservoir, which has to be periodically filled due to loss from evaporation and leakage. Two centrifugal pumps are located in the reservoir and are used to move the water to the main testing channel. Each pump can be operated independently and is fitted with a valve which allows the flow in the channel to be adjusted. The water from the pumps enters a head box (see Figure 3.11) which is located at the start of the main channel, and is fitted with several devices that dissipate and distribute the flow of the incoming water, so that the flow upstream of the model is relatively uniform. The first of these devices is a collection of 3.5 in. (9 cm) pall rings used to reduce energy. The pall rings are followed by a partition of concrete cinder blocks, which further decrease the energy. These devices are then finally followed by nine baffle plates that are spaced approximately 6 in. (15 cm) apart and are 5 ft (152 cm) in length, which distribute the flow across the width of the channel.

Figure 3.11. Head Box.

The water then flows down the main channel where the testing equipment and model are located. At the end of the main channel the water then falls into the return channel which is at an elevation of approximately 3 ft (91cm) below that of the test channel. Due to the fact that another testing locale uses the same return channel the water then flows two ways, however, all the water used is routed back to the reservoir, where it must first flow over sharp crested weir. Therefore, no water is lost during testing and flow measurements, using the sharp crested weir, can be recorded once the system has reached steady state conditions.

3.4.4.2 Channel Description

The main channel, where the model is located, is approximately 125 ft (38.1 m) in length, 5 ft (152 cm) in width, and 2 ft 8 in. (81 cm) in height. The slope of the channel is approximately horizontal (zero slope) and the sides are approximately perpendicular to the bottom. The upstream face of the model is located approximately 90 ft (27.4 m) from the start of the channel. The two sets of pitot tubes upstream of the model are at locations 75 ft (22.9 m) and 80 ft (24.4 m) from the start of the channel and the downstream set of pitot tubes are at a location 100 ft (30.5 m) from the start of the channel.

3.4.4.3 Sharp Crested Weir

A sharp crested weir (see Figure 3.12) is located in the return channel approximately 30 ft (9.14 m) upstream of where the water enters the clarifier. The weir covers the whole width of the return channel and is 5 ft (152 cm) wide and 2 ft (61 cm) tall. It is equipped with a small rectangular opening that is 1 ft (30.5 cm) wide and 8 in. (20 cm) tall, which is located in the lower middle portion and is used in order to release the water after testing is complete.

Figure 3.12. Sharp Crested Weir.

The construction of the weir is described in Hydraulic Effects of Safety End Treatments on Culvert Performance by Benson (2004); in this MS thesis the weir coefficient (C_d) was experimentally derived to be 0.618. With the weir coefficient known, it is then possible to calculate a flow rate based on the height of the water above the weir. This is accomplished according to Equation 3.32 (King & Brater, 1963), where b is the width of the weir, g is the gravitational constant (32.2 ft/sec^2), h_w is the height of the water above the weir, and Q is the flow rate in ft^3/sec.

$$Q = C_d \frac{2}{3} b \sqrt{2 g h_w{}^3} \tag{3.32}$$

To determine the height above the weir, a point gage (see Figure 3.13) was used that allowed measurements to be taken to the nearest thousandth of an inch. The gage was located approximately 16 ft (5m) upstream from the weir and was enclosed by a stilling well in order to reduce the effect of waves on the water surface. The gage was placed well upstream of the weir in order to take measurements where the surface profile is undisturbed. Normally, this upstream distance is approximately six times the maximum expected head (distance above the weir) (Mott, 2000). The stilling well was constructed from clear piping that had an inside diameter of 2 in. (5 cm) and was open on both ends. The bottom of the stilling well was located approximately 2 in. (5 cm) from the bottom of the channel and the top was flush with the top of the channel. The gage is also equipped with a level bubble to ensure that readings were not affected by the angle of the gage.

In the MS thesis Hydraulic Performance of Bridge Rails based on Rating Curves and Submergence Effects by Brandon Klenzendorf (2007), the method for calibrating the point gage is discussed. According to Klenzendorf, several measurements were taken with the gage at the point when the water level was at the top of the weir, and the average value using the point gage for the top of the weir was found to be 0.954 ft (Klenzendorf, 2007). This value is then the effective zero point for the amount of head above the weir. In order to calculate the height above the weir, 0.954 ft was subtracted from the gage reading.

Figure 3.13. Weir Point Gage.

3.4.4.4 Pitot Tubes and Manometer Board

Nine pitot tubes connected to an inclined manometer board were utilized to measure the upstream and downstream water level height. Six tubes were used to measure the water depth upstream of the model and three were used to measure the downstream water depth. The pitot tubes were equally spaced across the width of the channel in groups of three and were located a sufficient distance away from the model so that the measurements would not be affected by turbulence or changes to the surface profile near the model. Figure 3.14 demonstrates the location of the pitot tubes in relation to the model.

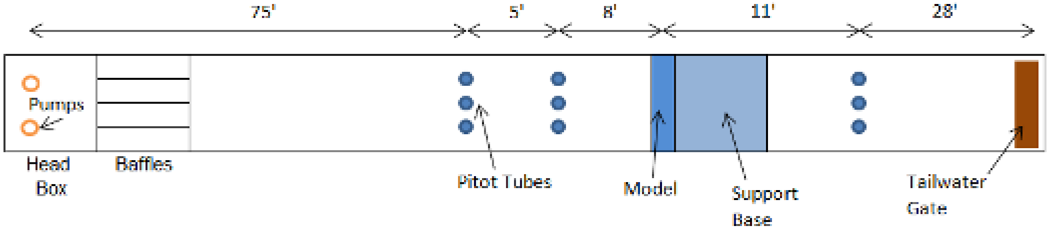

(a)

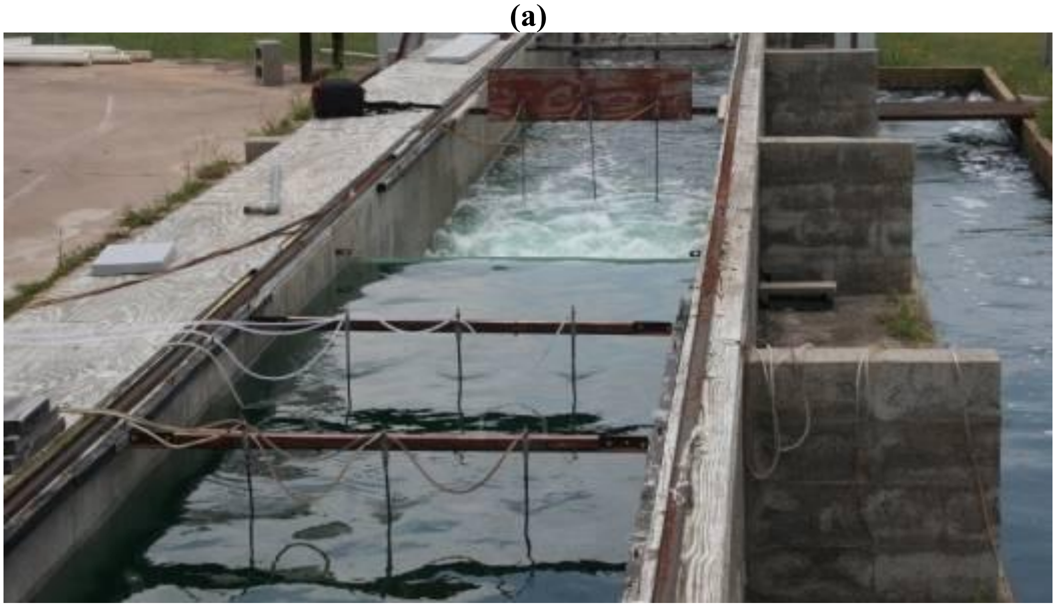

(b)

Figure 3.14. Pitot Tube Locations: (a) the Diagram (NTS) and (b) the Picture.

The pitot tubes used are designed to measure static pressure head (water depth) and total pressure head (static head and velocity head). Two ports are located on the pitot tube for recording each of these heads; however, the port used for static pressure was the only one utilized in this research. A schematic of the pitot tubes that were used is shown below in Figure 3.15.

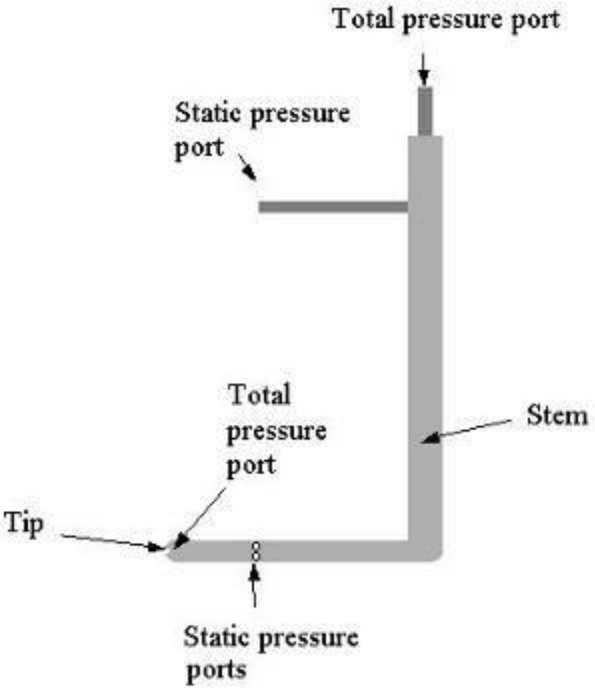

Figure 3.15. Pitot Tube Schematic.

The pitot tubes were then connected to an inclined manometer (see Figure 3.16) board by flexible plastic tubing attached to the static pressure port. An inclined manometer is used in lieu of a vertical one, because of the increased precision that is achieved. This increase in precision is due to the fact that a small vertical change will result in a large change along the incline. The construction of the manometer board and its calibration are described by Brandon Klenzendorf (2007).

Figure 3.16. Inclined Manometer Board.

The manometer board consisted of nine rigid plastic tubes connected on the bottom end to the pitot tubes (via the flexible tubing) and on the upper end to a manifold (via flexible tubing). The manifold was used to flush water through the system in order to remove any air in the lines prior to testing. Also, small holes were drilled into the top of the rigid pipes so that the water in the tubes would be exposed to atmospheric pressure. Since the water in the manometer board and water flowing in the channel are both exposed to atmospheric pressure, the water level in both should be the same.

To gauge the height of water in the channel with the inclined manometer board two pieces of information must be known, which are: the angle of the manometer board and the height of the zero measurement (on the manometer board) above the channel bottom. The angle of inclination of the manometer board used for this research is approximately 25.5° (Klenzendorf, 2007). Therefore, a vertical height can be calculated simply by multiplying the inclined reading by the sine of the angle of inclination. Equation 3.33 is included below to better illustrate how this is accomplished, where h_v is the vertical height, h_i is the height recorded on the incline, and θ is the angle of inclination.

$$h_v = h_i \sin\theta \tag{3.33}$$

In order to determine the height of the water above the channel bottom, however, the height of the zero measurement must also be known. Surveying equipment was used to accurately measure this distance (Klenzendorf, 2007). It was determined that the elevation difference between the channel and the zero measurement is approximately equal to 0.835 ft (25.5 cm). Therefore, to determine the height of the water above the channel bottom this difference must be added to the vertical height calculated in Equation 3.2. This is further illustrated below by Equation 3.34. In this equation, H is the height of the water above the channel, h_v is the vertical height calculated from the inclined manometer board measurement, and h_{mb} is the height of the manometer board zero reading, which is the height of the water above the channel bottom when the manometer board registers a zero value.

$$H(ft) = h_v + h_{mb} = h_i sin(25.5^0) + 0.835 \tag{3.34}$$

3.4.4.5 Tailwater Gate

A gate that is hinged at the top and connected at the bottom with steel cables was installed prior to the main channel discharge into the return channel. The steel cables are connected to a crank that control the height of the gate, which then allows for testing the effects of submergence downstream of the model. This is accomplished by lowering the gate into the water and creating an obstruction that produces a hydraulic jump. The hydraulic jump is the result of the specific energy of the water changing from supercritical to subcritical flow. When this happens the water depth increases, which allows for testing the affects of downstream submergence on the upstream water depth. As the gate is lowered, the obstruction becomes greater and the downstream water depth increases. This affects the upstream water depth by impeding the flow through the orifice, which then causes the upstream water depth to increase.

Figure 3.17. Tailwater Gate.

3.5 METHODOLOGY

As with any experiment, specific methods must be followed to ensure the reliability and accuracy of the data being gathered. This section will discuss the start up procedure, rating curve data gathering and submergence testing data gathering procedures, and shut-down procedures.

3.5.1 Start-Up Procedure

This sub-section will discuss the start-up procedure for both the rating curve and submergence tests. To begin testing, the removable boards were inserted in the model base, and the small rectangular opening in the sharp crested weir was closed. The next step was to make sure that the pitot tubes were working properly. This was done by connecting the manifold on the manometer board to a water faucet located on the exterior of Building 120, which was located next to the channel. With the manifold connected to the water line, the water was then turned on and water allowed to flow into the manometer board and out to the pitot tubes. At this point the flexible tubing connecting the pitot tubes and manometer board and the rigid tubes of the manometer board were both monitored for the presence of air bubbles. Also, the pitot tube's static ports were checked to determine if there was any blockage. The pitot tubes used were equipped with eight ports. If any of the ports were clogged, they were either unclogged via a wire brush or were replaced with a new pitot tube. After the tubes were shown to be in working order and the air in the lines was flushed, the valves on the pumps were then adjusted and the pumps turned on. The water to the manifold was then turned off after the pitot tubes were submerged. This ensured that air would not be allowed to re-enter the lines. The last step was to allow the pumps to run for a minimum of 45 minutes before data was collected. This time was determined during previous research by Klenzendorf (2007), and was set so that enough time was allowed for water to fill up the return channels and steady state conditions could be achieved before flow measurements at the sharp crested weir were recorded.

3.5.2 Rating Curve Testing Procedure

During the development of the rating curves for the TCTBs only the six upstream pitot tubes were used. Three tests were conducted for each flow rate, with a minimum of two minutes between each test. Each test consisted of recording the height readings on the manometer board for each of the pitot tubes, and recording the measurement taken from the point gage for calculating the flow. The precision of the manometer board readings is 0.005 ft and was taken from the bottom of the meniscus. The point gage's precision is 0.001 ft and was recorded when the tip was observed to make contact with the water surface. Due to slight oscillations in the water's surface the arithmetic mean of the values recorded in the three tests are used in the development of the rating curve.

When testing was accomplished for multiple flow rates on the same day, the valves and pump combinations could be changed after one test was complete. Since water had already filled the return channels, 30 minutes was allowed for the flow to stabilize and reach steady state conditions, instead of the 45 minutes that was required for start-up.

3.5.3 Submerged Testing Procedure

For testing the affect of submergence on the water height upstream, all nine pitot tubes were utilized. Six pitot tubes were located upstream of the model and were used to measure the upstream water depth. Three additional pitot tubes were located downstream of the model and were used to measure downstream water depth. During submergence testing six tests were performed for each different position of the tailwater gate. Six tests were performed instead of three, because of the turbulence generate by the hydraulic jump. At lower downstream water elevations, as much as 1.5 in. of change was detected during a test, but as the water level increased the readings became much more stable. However, for the sake of consistency, six tests were performed for all the different tailwater gate positions.

The first test was conducted when the tailwater gate produced a hydraulic jump that brought the downstream water elevation to the top of the model support base. At this point the downstream water depth should have little effect on the upstream water depth and is an appropriate starting point for testing. Also, at this point, the pitot tubes become submerged and the water to the manifold on the manometer board is shut off, so as to prevent any air from entering the lines. As with the rating curve tests, two minutes is allowed in-between each of the tests, in order to detect any fluctuations that might be occurring. A minimum of eight tests were performed at the same flow rate and different tailwater gate positions, and four such series of tests were performed at different flow rates.

Unlike the rating curve tests, the flow rate was not changed between tests. Since the flow rate did not change, the only part of the experiment that required time to stabilize was the downstream water depth. A minimum of 15 minutes was allowed for the water level to stabilize after one test was complete and a new tailwater gate position established. Also, as it was with setting the tailwater gate so that the downstream water level was at the height of the model base, some adjustment was necessary between tests in order to perform experiments where the water elevation was not too similar to the last experiment and did not deviate too much as to create too large a gap between experiments.

3.5.4 Shut-Down Procedure

The shut-down procedure for both the rating curve and submergence tests is the same. The pumps are first shut off and some of the water is allowed to drain. At this time, the tailwater gate is also raised (if performing submergence test). Once the water level in the main channel has dropped it is then possible to remove the boards on the side of the model base and open the gate on the sharp crested weir, so that the remaining water can drain back to the reservoir.

3.6 EXPERIMENTAL RESULTS

3.6.1 Rating Curve Data

Figure 3.18 summarizes the data gathered where the ordinate values are expressed in units of feet and the abscissa is the flow rate. These graphs alone, however, do not constitute a model, as was developed in Section 3.3.1 and 3.3.2 of this report. Furthermore, only three sets of data are given below, because the data for the MSSCB was used in the analysis of both the SSCB and SSCB-SPL.

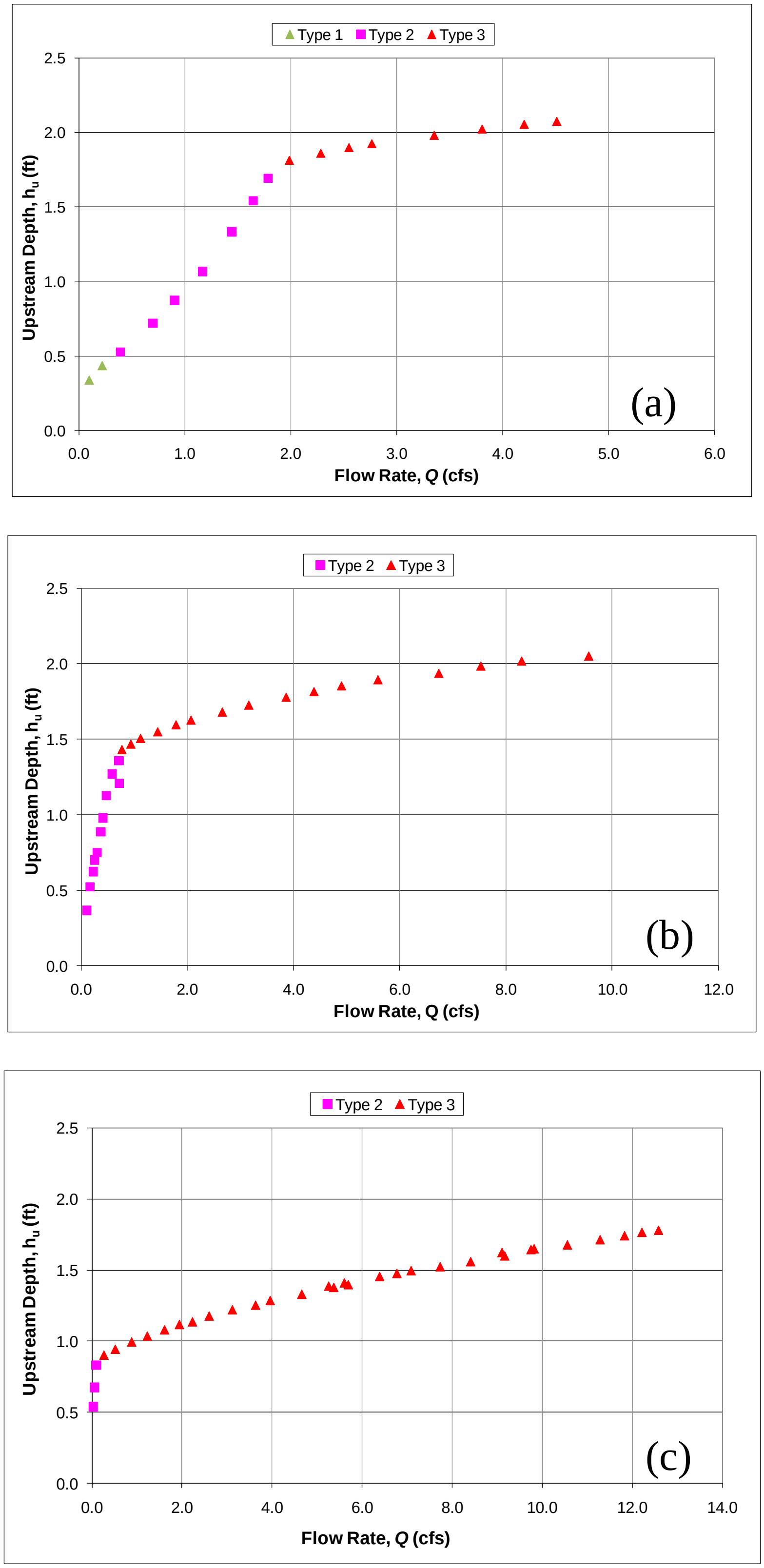

Figure 3.18. Rating Curve Data for (a) MSSCB (b) CSB, and (c) LPCB.

In order to obtain a graph which represents the model equations and the data in Figures 5.1-5.3, the Excel Macro Tool was utilized to create a function that can be used in an Excel spreadsheet. This function, Qnon, calculates the non-dimensional flow rate based on the input variables e (e_u/h_r), fo (fraction of open space), a (h_{rl}/h_r), and the coefficient values C_b, C_c, and C_d.

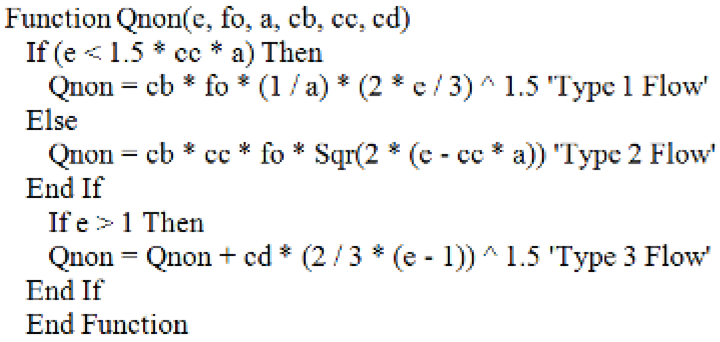

```
Function Qnon(e, fo, a, cb, cc, cd)
  If (e < 1.5 * cc * a) Then
    Qnon = cb * fo * (1 / a) * (2 * e / 3) ^ 1.5 'Type 1 Flow'
  Else
    Qnon = cb * cc * fo * Sqr(2 * (e - cc * a)) 'Type 2 Flow'
  End If
    If e > 1 Then
    Qnon = Qnon + cd * (2 / 3 * (e - 1)) ^ 1.5 'Type 3 Flow'
  End If
  End Function
```

Microsoft Excel Solver and regression was then utilized to fit the model to the data by changing the coefficient values of C_b, C_c, and C_d, where the coefficient values were subject to the following constraints:

$$0.0 < C_b \leq 1.0 \tag{3.35}$$

$$0.0 < C_c \leq 1.0 \tag{3.36}$$

$$0.0 < C_d \tag{3.37}$$

The constraints are necessary because in the developed equations, C_b and C_c describe the contraction that happens when water passes through the orifice, and a zero value would result in no flow in the horizontal or vertical directions, respectively. C_d, on the other hand, has to be greater than zero, because a negative value would produce negative flow after the water overtopped the barrier and a value of zero would result in zero flow over the barrier. The results of this analysis are given below in Figure 3.19, where the abscissa and ordinate are in the non-dimensional form that is given in the model equations developed by Charbeneau et al. (2008). Also, the coefficients that were calculated for each of the barriers are given below in Table 3.2 with the associated standard error between the rating curve and the observed data.

Table 3.2. Rating Curve Coefficient Values.

Coefficient	**MSSCB**	**CSB**	**LPCB**
Cb	0.588	0.477	0.177
Cc	1.000	0.855	0.338
Cd	0.843	1.011	0.900
S.E.	3.20%	8.64%	4.41%

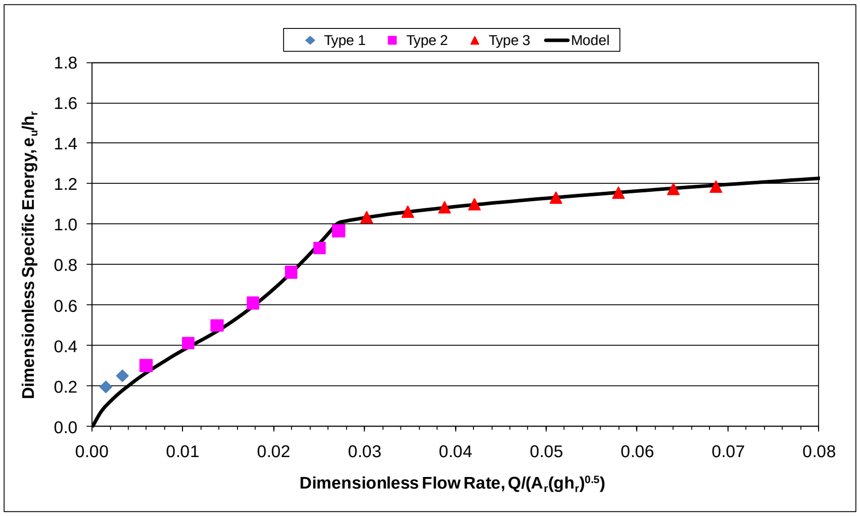

(a)

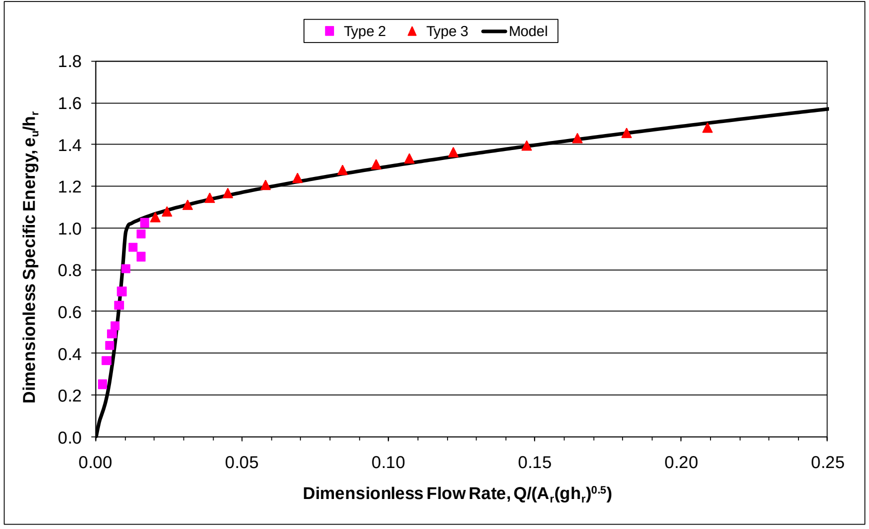

(b)

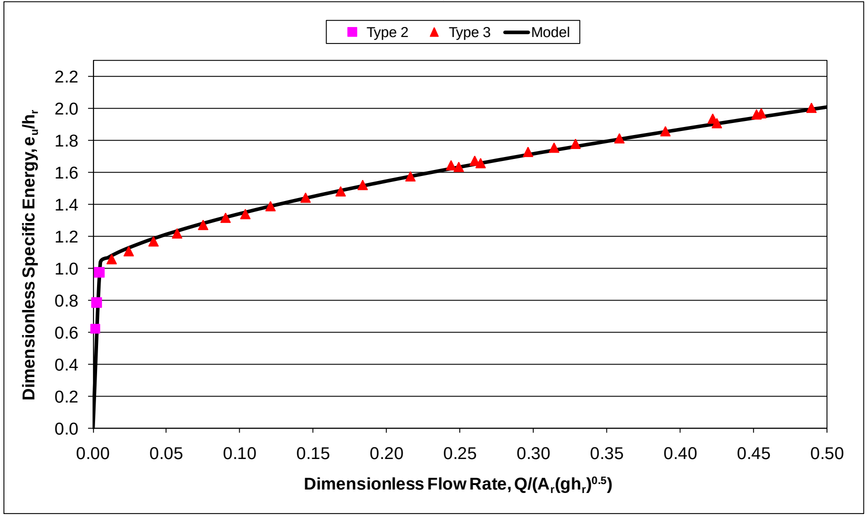

(c)

Figure 3.19. Rating Curves for: (a) MSSCB, (b) CSB, and (c) LPCB.

Furthermore, in order to understand the effects on the actual barrier, we can transform the model output through simple algebra, to get the flow rate and energy upstream. For example, using the function Qnon it is possible to solve for the non-dimensional flow, given the non-dimensional specific energy. If the non-dimensional values are multiplied by the physical parameters of the barrier, the actual flow rate and upstream energy can be calculated. This is shown below by Equations 3.38 and 3.39.

$$Q = \frac{Q}{A_r\sqrt{g h_r}} \times A_r\sqrt{g h_r} = \frac{Q}{A_r\sqrt{g h_r}} \times b_r\sqrt{g h_r{}^3} \tag{3.38}$$

$$e_u = \frac{e_u}{h_r} \times h_r \tag{3.39}$$

Moreover, if the LPCB is analyzed, it is possible to develop a graph similar to Figure 3.20, where the flow is based on a per linear foot of barrier basis (b_r=1).

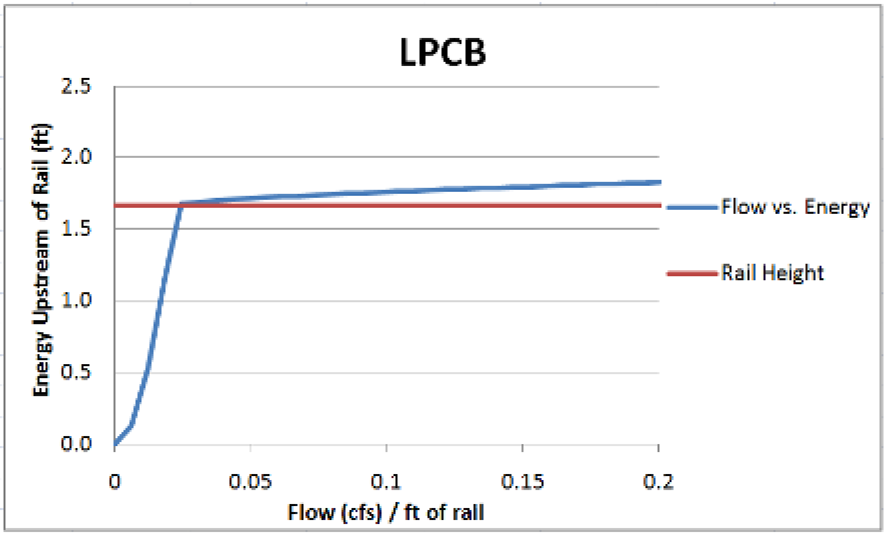

Figure 3.20. LPCB Example Rating Curve.

3.6.2 Submergence Data

The data presented below in Figure 3.21 are the result of testing conducted according to Section 3.3.2. A diagonal line with slope 1.0 has been inserted on the graphs to visualize when an incremental increase in downstream depth will result in the same increase in upstream height. This line is considered the asymptote of the data, because when the data approaches this line the barrier’s effect is negligible and the data will continue to increase and follow this line. Also, it should be noted that the flow rate in the legend is given as the range of values that were recorded during a test. This is because the flow varied slightly during testing.

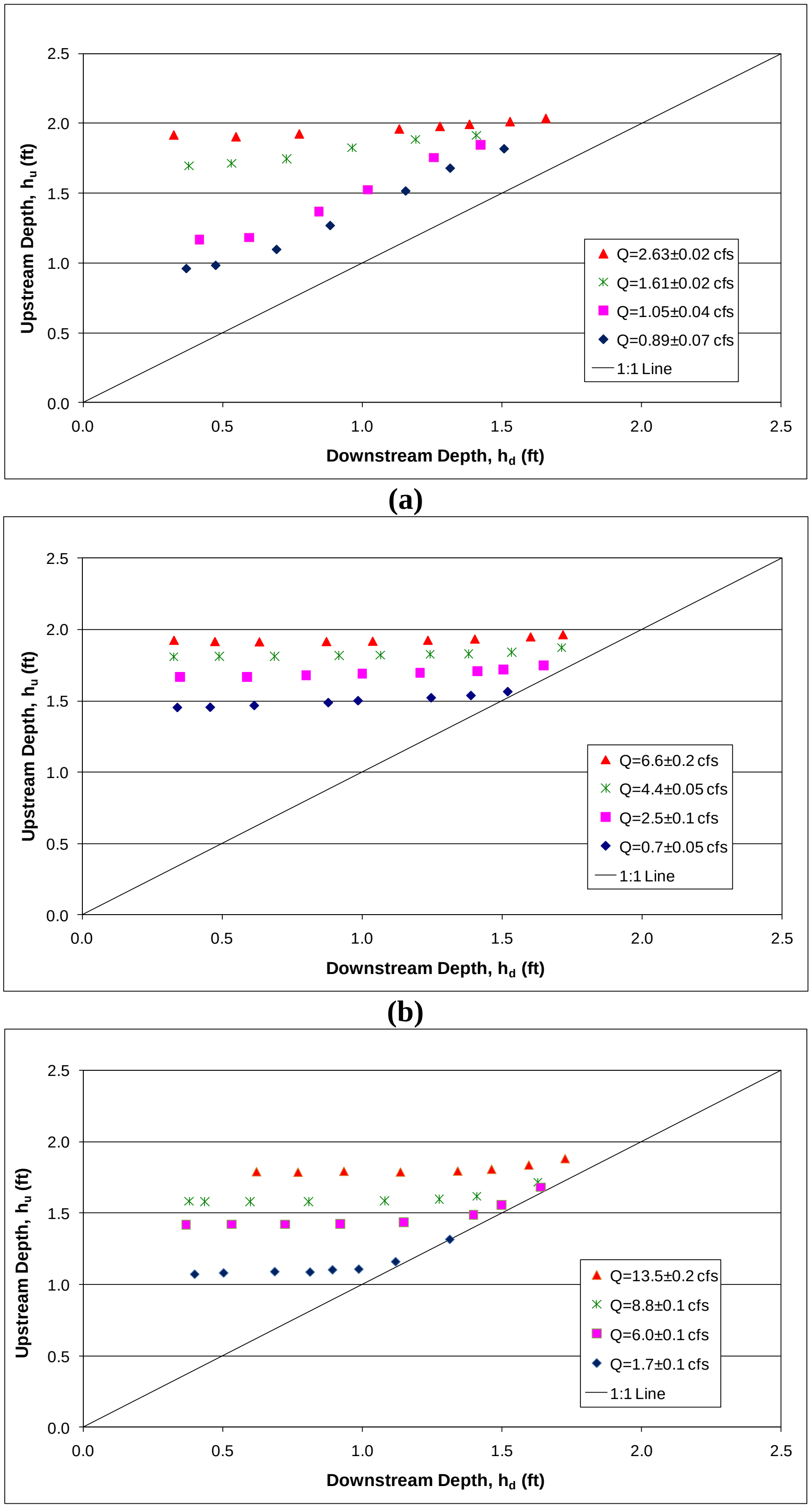

(a)

(b)

(c)

Figure 3.21. Submergence Data for (a) MSSCB, (b) CSB, and (c) LPCB.

Testing was conducted at four different flow rates in order to determine the effect that flow will have on the submergence ratio. In the first model, there will be no effect due to varying the flow, because the Villemonte Model is independent of flow; however, the Empirical model is implicit with respect to flow and a series of curves will be developed to describe the effect of submergence for different values of Q.

3.6.3 Villemonte Model

The resulting Villemonte Models are presented below in Figure 3.22. Also, the coefficient (m) for each of the barriers is listed below in Table 3.3, with the associated standard error. The model provides a reasonable fit to the data, and is more straightforward than the empirical model, which depends on the flow rate being known.

In order to obtain the coefficient value, the actual flow rate (Q) was measured, and the theoretical flow rate upstream (Q_1) was calculated using the rating curve model already developed, with the measured height of water upstream. The only other parameters in the Villemonte model are the energy upstream and downstream, which are also being measured. With these measured values, the Microsoft Excel Solver function was utilized to select values for the coefficient (m) such that the standard error between the measured values of the submergence ratio and the model derived submergence ratio was minimized.

Table 3.3. Villemonte Model Coefficient Values.

Coefficient	MSSB	CSB	LPCB
m	0.485	0.255	0.109
S.E.	6.62%	12.12%	5.89%

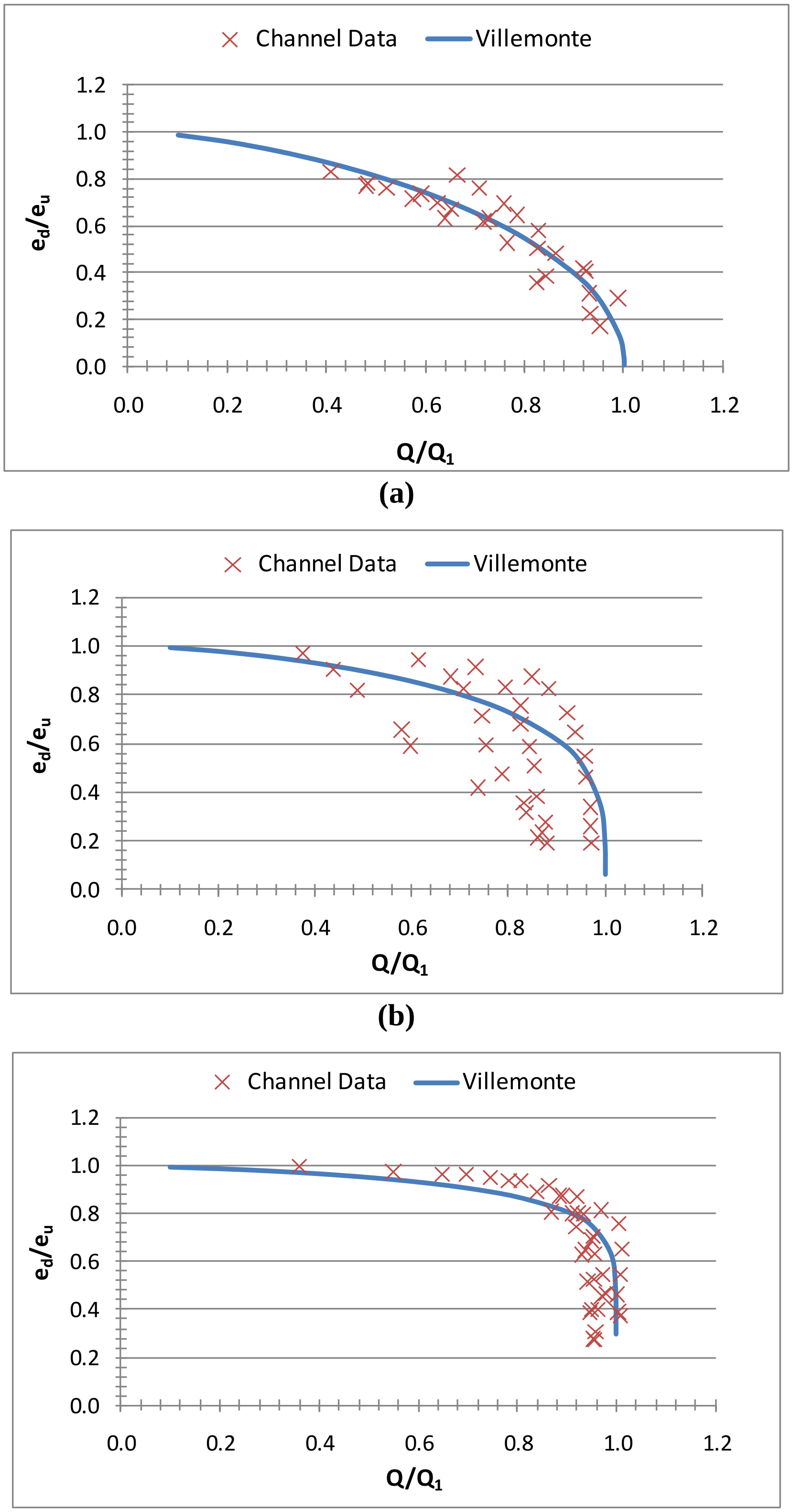

(a)

(b)

(c)

Figure 3.22. Submergence Model (Villemonte) Data for (a) MSSCB, (b) CSB, and (c) LPCB.

Figure 3.23 is the graphical representation of the difference between the predicted submergence ratio and the data. The one to one line inserted on the graph has been inserted so a quick comparison of the difference between the modeled value and measured value can be made. If a data point lies on the line, this means that the modeled and measured values are the same. Conversely, the further away a data point is from the one to one line, the larger the discrepancy between the modeled and measured values. Furthermore, the data points have been separated by flow rate, to present the difference in error for different flow values.

3.6.4 Empirical Model

The resulting Empirical models are given below in Figure 3.24, where a series of curves have been developed using the average of the four different flow rates that were used in the different experiments. The coefficient (B) is also listed below in Table 3.4. The process for obtaining this coefficient is same as used for the Villemonte model, with the exception that the Empirical submergence equation was utilized.

Table 3.4. Empirical Model Coefficient Values.

Coefficient	MSSB	CSB	LPCB
B	100.93	97.690	63.194
S.E.	7.82%	11.87%	7.69%

Figure 3.25 below is the graphical representation of the difference between the Empirical model’s predicted submergence ratio and the data. These graphs are similar to Figure 3.22, which was constructed for the Villemonte model, and are meant to highlight the difference in error for different flow values.

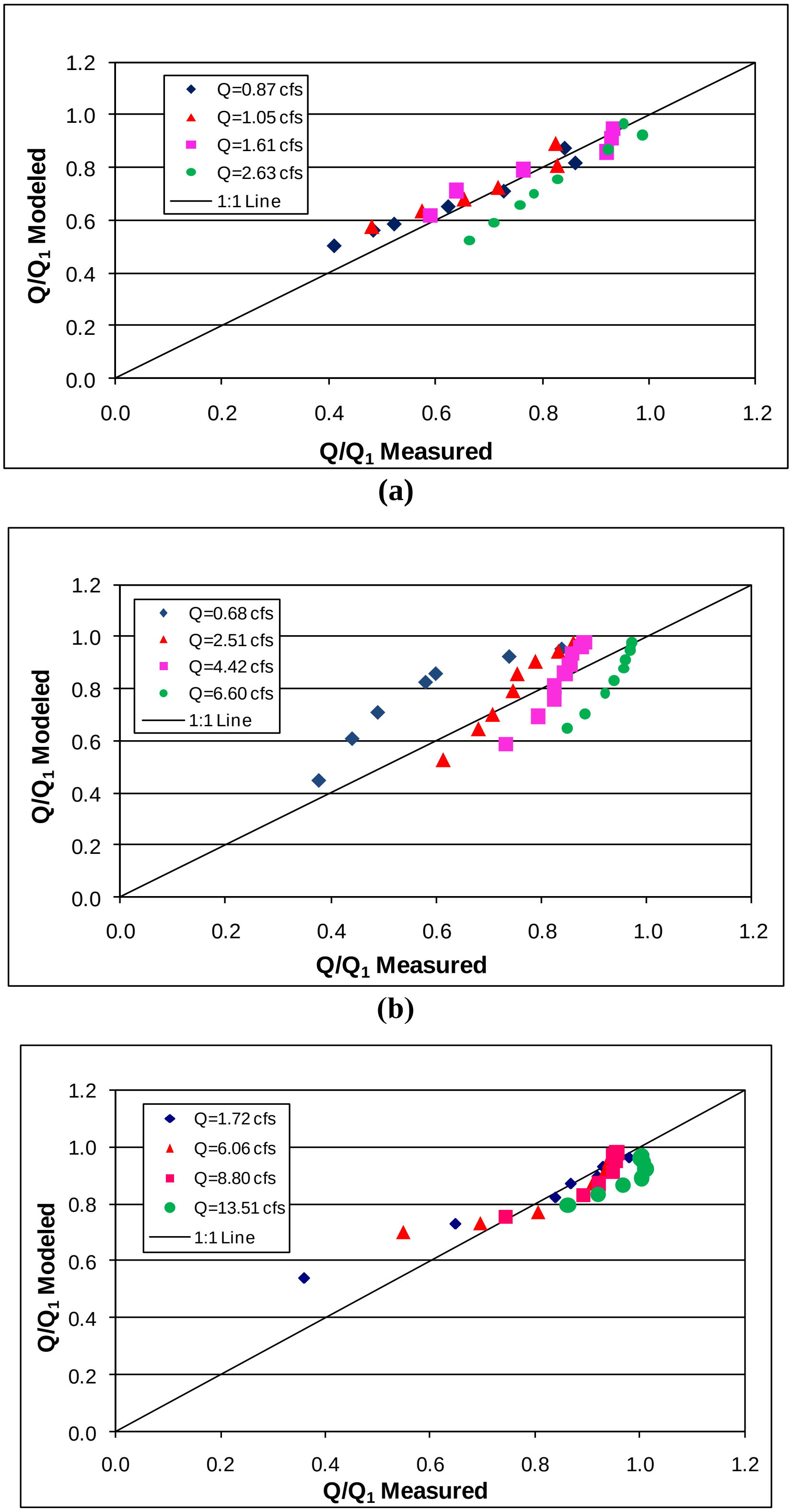

(a)

(b)

(c)

Figure 3.23. Villemonte Model Prediction Variation for (a) MSSCB, (b) CSB, and (c) LPCB.

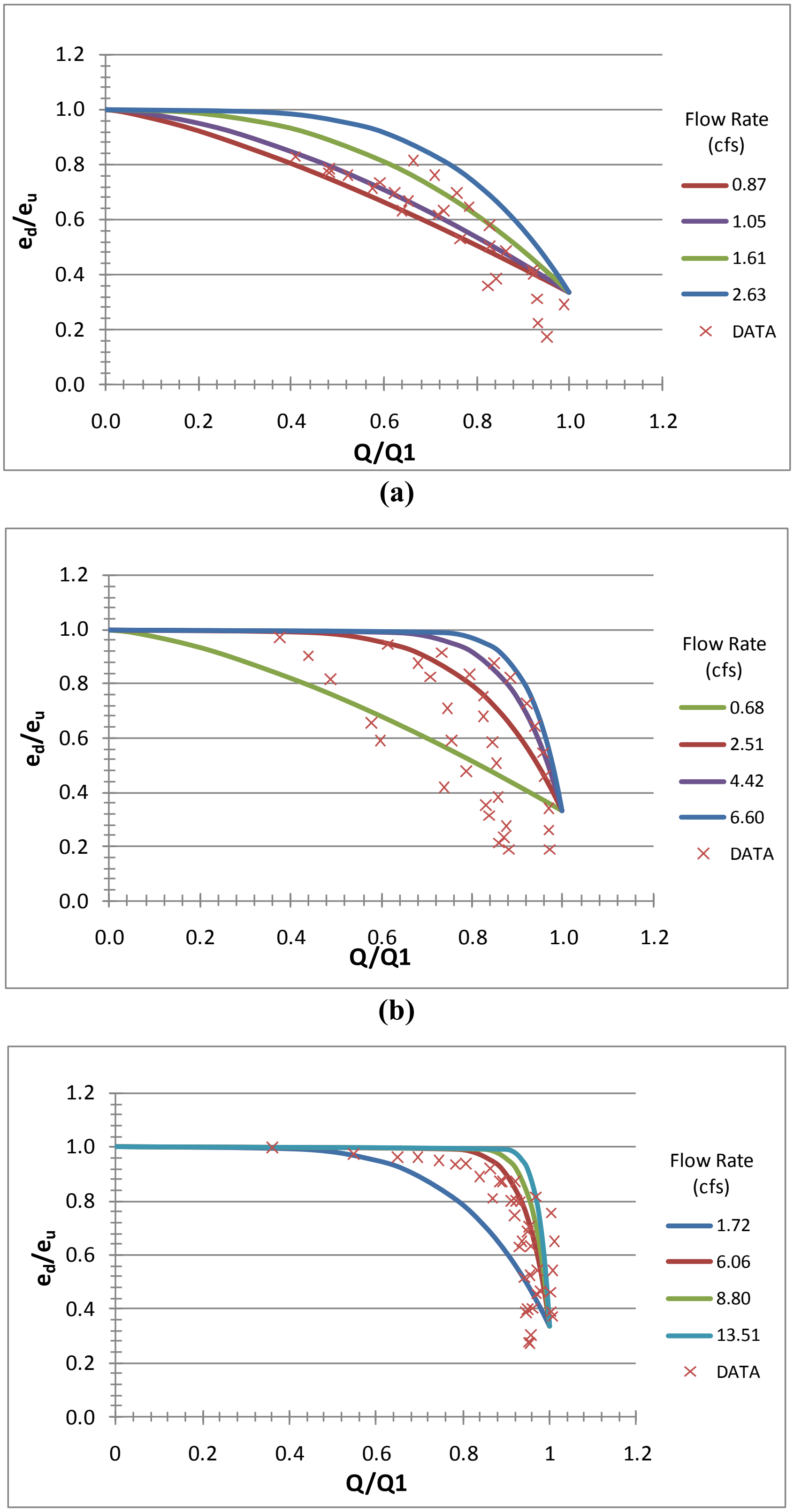

Figure 3.24. Empirical Submergence Model for (a) MSSCB, (b) CSB, and (c) LPCB.

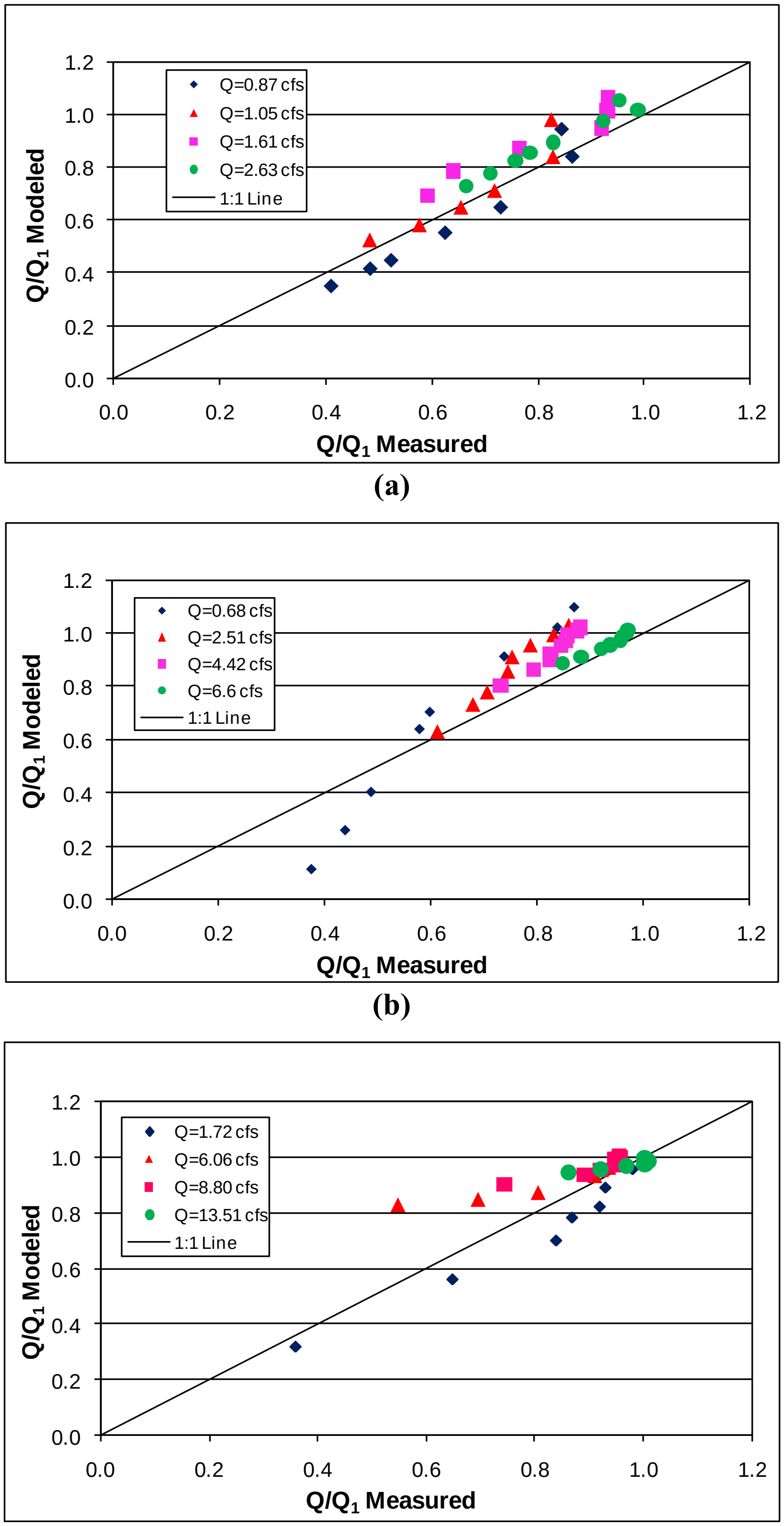

(a)

(b)

(c)

Figure 3.25. Empirical Model Prediction Variation for (a) MSSCB, (b) CSB, and (c) LPCB.

3.6.5 Comparison of Submergence Models

A comparison of the standard errors between the Villemonte and Empirical models reveals that the Villemonte model represents the data more concisely for the MSSCB and LPCB. It can also be seen that the Empirical model represents the CSB more accurately, because of the lower standard error. However, the standard errors between the two models are very similar. Because the errors are comparable and the use of the Villemonte model is more straightforward (not dependent on the flow rate), the use of this model should be the preferred choice when modeling the affect that downstream submergence will have on rating curve. Furthermore, the fact that the Villemonte model describes submergence so well is due to the fact that it was developed for weir structures, which each of the TCTBs approximate with their small orifice sizes. However, the Empirical model did relatively well in its prediction, but is better suited to modeling flow through barriers where the fraction of open space is larger and the flow through the orifice will have more of an impact.

3.7 CLOGGING EVALUATION

3.7.1 Introduction

When considering the hydraulic performance of a TCTB, clogging of the drainage opening should be considered. This is because the small openings in the barriers will make them more susceptible to clogging. If the barrier becomes clogged, the specific energy upstream will increase as a function of the amount of clogging until the drainage opening is completely clogged. After the opening is completely clogged, the barrier will then exhibit flow characteristics similar to a weir.

In order to study the effect that a variable amount of clogging would have on the hydraulic performance of a TCTB, the MSSCB model was tested. This barrier was equipped with a device that closed off part of the open space and allowed testing to be performed at 50% and 75% of the original drainage opening area. The original MSSCB can be seen in Figure 3.26a and the barrier when 50% and 75% clogged can be seen in Figure 3.26b and 3.26c, respectively.

Testing of this barrier in all three conditions was conducted as described in Section 3 of this paper. The next sections will describe the experimental results and the conclusions that can be drawn from those results.

3.7.2 Experimental Results

When clogging occurs, it changes the fraction of open space that is available to the barrier. Since the fraction of open space is a variable in the equations for Type 1, 2, and 3 flow, it should be possible to adjust this parameter to account for a desired amount of clogging. Before the experiments on the MSSB were conducted, the fraction of open space was adjusted to represent the 50% and 75% clogged condition. This was done by simply multiplying the original fraction of open space by the percentage of open space available after clogging, $F_0 * (1 - \%\text{ clogged})$. With this variable changed and all others left the same Figure 3.27 was developed. From this graph it can be seen that as the percentage of clogging increases the equations will shift to closer to the ordinate axis, and that if complete clogging were to occur, weir type flow would be developed.

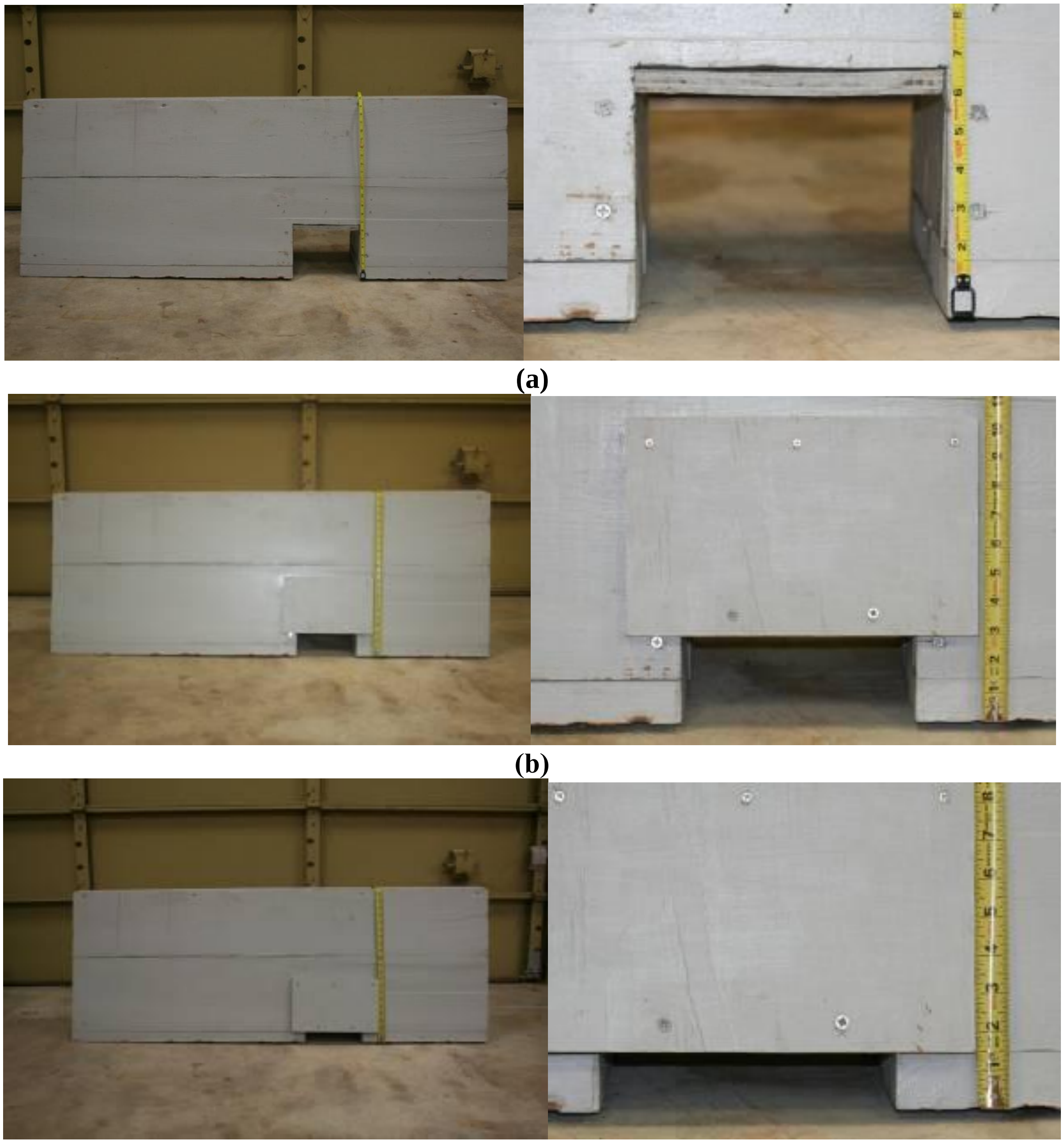

(a)

(b)

(c)

Figure 3.26. MSSCB (a) 0% Clogged, (b) 50% Clogged, and (c) 75% Clogged.

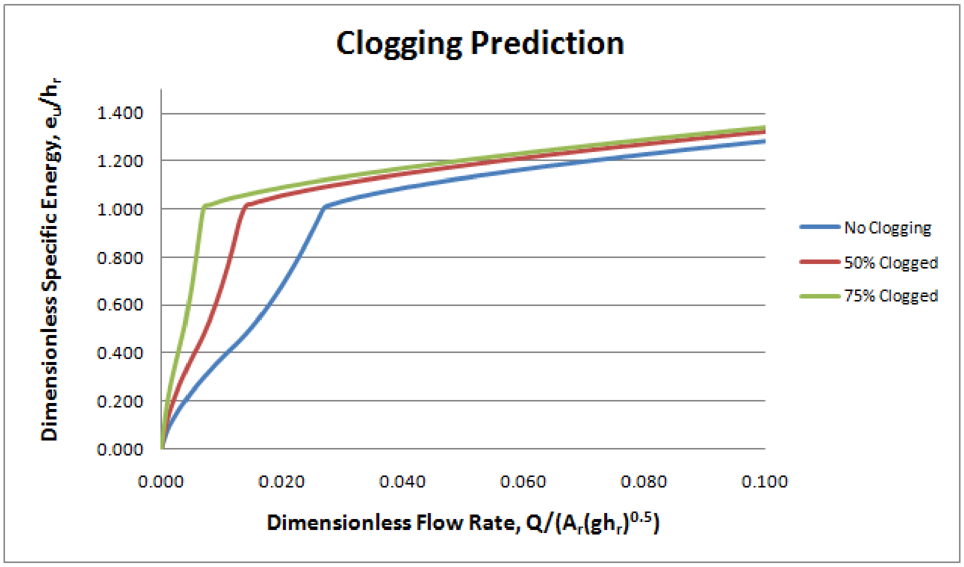

Figure 3.27. MSSCB Clogging Prediction.

Next, in order to determine if this prediction adequately predicts the effects of clogging, the model was compared to the experimental data. This data is displayed below, in Figure 3.28, along with the prediction curves that were displayed in Figure 3.27. It can be seen from the graph that the prediction follows the general trend in the data. The standard error in the prediction is presented in Table 3.5.

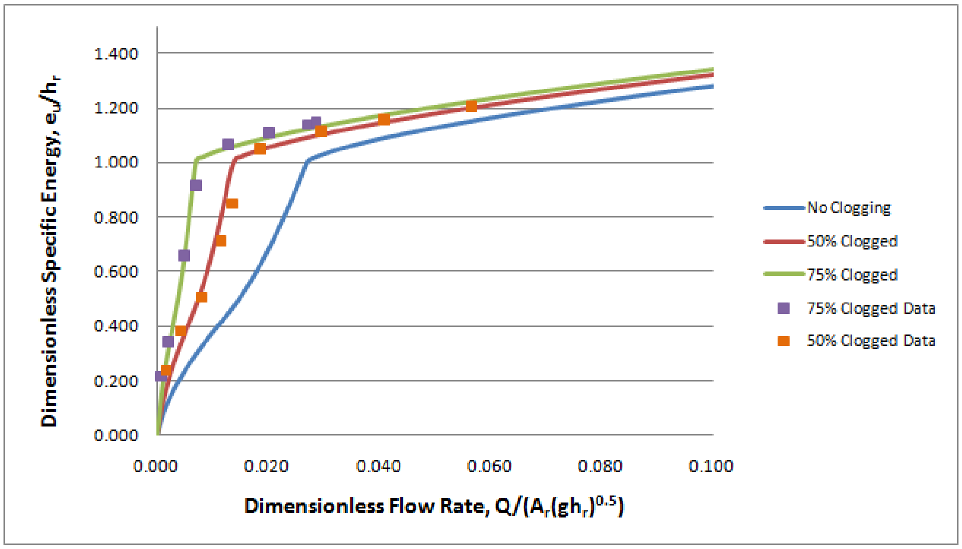

Figure 3.28. MSSCB Clogging Prediction Results.

Table 3.5. Standard Error of Clogging Prediction.

% Clogged	S. E. (%)
50%	6.78
75%	4.20

With these results, it is now possible for designers to determine the effects that various amounts of clogging will have on the hydraulic rating curve of a barrier being considered, by simply changing the fraction of open space to account for the clogged condition. Furthermore, this information can also be used by designers in order to design barriers with different sized openings to meet the hydraulic characteristics in a particular area.

Lastly, this makes possible the creation of a rating curve to describe the SSCB and SSCB-SPL. By using the same coefficients already derived for the MSSCB and changing the fraction of open space to match that of each barrier, a rating curve can be created. These rating curves are presented below in Figure 3.29. The MSSCB barrier has also been included for comparison purposes. Furthermore, the parameters used to create these models are included below in Table 3.6.

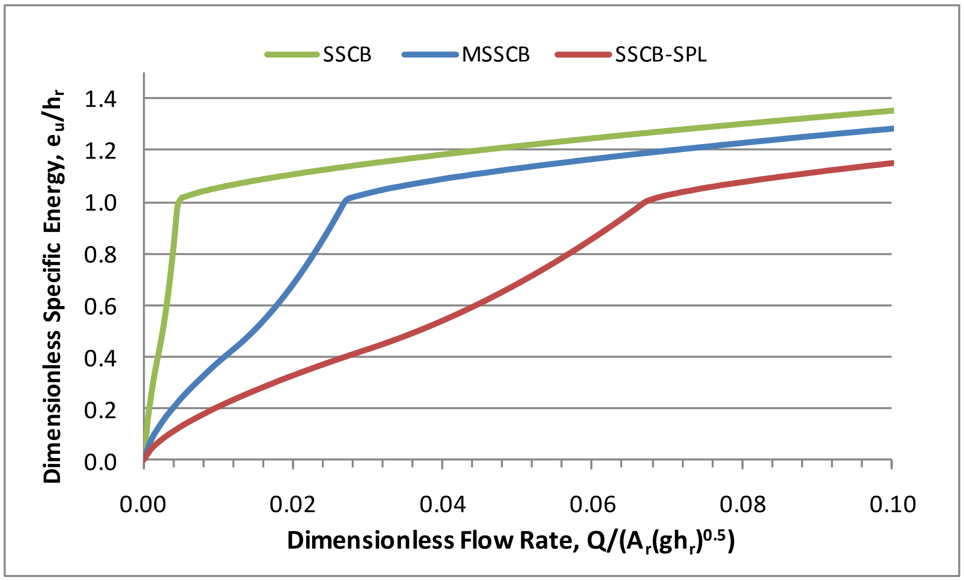

Figure 3.29. SSCB Rating Curve.

Table 3.6. SSCB/SSCB-SPL Rating Curve Parameters.

Type of TCTB	C_b	C_c	C_d	F_o
SSCB	0.588	1.000	0.843	0.635%
SSCB-SPL	0.588	1.000	0.843	9.52%

CHAPTER 4: STABILITY ANALYSIS OF TCTBS IN EXTREME FLOOD

4.1 INTRODUCTION

Stability of the TCTB against sliding or overturning is very important during extreme flood situation for safety. During the extreme flood, most of the TCTBs provide very less amount of flow to the downstream direction compared to the upstream flow and thus magnify the flooding at upstream by increasing the head water elevation. This increased head provides additional water pressure to the barrier which causes the barrier to fail against sliding or overturning. On the other hand, if the opening is increased significantly to provide a larger draining ability, then the weight of the barrier is decreased and also the center of gravity of the barrier becomes higher causing more susceptible to overturning.

The stability against sliding and overturning of the common types of TxDOT traffic barriers has been studied considering different types of scenarios. These scenarios are based on flood condition, geometry of the roadway, and downstream drainage pattern. In order to evaluate the stability against sliding, the coefficient of friction between the barrier surface and different types of pavement surface is also determined for different situations, such as wet and dry, clean and unclean surfaces, and low and high bearing stresses.

4.2 EXPERIMENTAL SETUP AND METHODOLOGY

4.2.1 Determination of Coefficient of Friction

In order to determine the factor of safety against sliding during extreme flooding, the coefficient of friction between the TCTB and the surface on which the TCTBs are placed needs to be known. Thus the coefficient of friction between the TCTB and different surfaces on which the TCTBs could be placed on is measured at field for practical reason. Different surfaces, such as asphalt pavement surface, concrete pavement surface, and compacted subgrade, subbase, and base surfaces are tested to evaluate the frictional coefficient with the concrete surface of the TCTB. The coefficient of friction is determined for a wide range of surfaces with different roughness and ages by field experiments.

To determine the coefficient of friction between the TCTB and the pavement surface, the ASTM standard: ASTM C1028–07 has been used. This standard method is designed primarily to determine the static coefficient of friction of tiles and like materials.

According to the standard, a horizontal dynamometer pull meter and a heel assembly (Figure 4.1) is required to determine the static coefficient of friction. The dynamometer pull meter should be capable of measuring 100 lbf, accurate to 0.1 lbf, and capable of holding the peak value. To fulfill the requirement of the standard, a Chatillon DFE–100 Force Gauge (Figure 4.1) has been used as a horizontal dynamometer pull meter in the field experiments. And a rectangular (6 in. × 8 in.) concrete block is prepared simulating the bottom of TCTB and assembled with weight to apply a weight of 22 kg according to the standard.

Figure 4.1. Horizontal Dynamometer Pull Meter and a Heel Assembly.

To determine the force required to pull the concrete block having a weight of 22 kg, the cable attached to the pull meter was pulled horizontally with an incremental force.

When the block started to move, the peak value from the gauge was recorded. To minimize the variability of the surface, 12 numbers of readings (three in each direction) were taken for each surface and averaged to determine the coefficient of friction. The coefficient of friction was calculated based on the following equation:

Coefficient of friction, f = (F/ W)
Where, f = Coefficient of friction
F = Force (peak value) required to move the assembly, lbf
W = Weight of the heel assembly, lbf

4.2.2 Validation of the Method

For the ASTM C1028–07 standard, the bearing stress caused by the testing block is calculated as $\frac{22\times2.204\ \text{lbf}}{8\times6\ \text{in}^2} = 1.01\approx 1$ psi. But the bearing stresses caused by the TCTBs are different than that of the standard block. For example, the bearing stress caused by a SSCB is calculated as 2.70 psi, which is much higher than the stress comes from the standard heel assembly. The bearing stresses of different TCTBs are shown in Table 4.1. Since the actual bearing stresses are significantly higher than that caused by the heel assembly, the effect of bearing stress on coefficient of friction is determined.

Table 4.1. Actual Field Stress Caused by the Different TCTBs.

Types of TCTB	Height of TCTB (in.)	Field stress caused by the TCTB (psi)
SSCB	42	2.70
	48	3.05
	54	3.38
SCB	33	1.67
SSCB-SPL	42	3.22
	43.5	3.31
LPCB	20	2.26

In order to address the issue of any possible variation of the coefficient of friction with bearing stress, the coefficient of frictions between the bottom of the TCTB and the concrete and asphalt road surfaces were measured first with the standard stress level (1 psi) and then with a bearing stress of 2 psi. Then a statistical analysis was performed to see whether the variation of bearing stress has any significant effect on the coefficient of friction.

Since the statistical analysis showed that the variation of bearing stress has significant effect on the coefficient of friction, four different common pavement surfaces were tested for the coefficient of friction at different stress levels like 1 psi, 1.5 psi, 2 psi, 2.5 psi, and 3 psi to see the trend of change and to develop a curve that could be used to estimate/convert the actual coefficient of friction at any field stress from the test results of the standard testing procedure (ASTM C1028–07).

4.2.3 Determination of Coefficient of Friction for Different Surfaces

The coefficient of friction is determined in the field for five different surfaces, such as asphalt surface, concrete surface, base surface, sub base, and compacted sub grade following the method described in Section 4.2.1. For each type of surface, a number of surfaces were selected based on surface texture and age to get a range of coefficient of friction. The coefficient of friction was determined for both dry and wet condition.

4.2.3.1 Concrete and Asphalt Surfaces

The coefficient of friction between the pavement surfaces and the bottom surface of TCTBs has been determined for different types of concrete and asphalt surfaces (Figure 4.2). Four different types of surfaces were selected for both concrete and asphalt pavement for the determination of the coefficient of friction. The concrete surfaces are: (a) roughly finished, age > 10 yrs, (b) semi-roughly finished, age 5-10 yrs, (c) smoothly finished, age 5-10 yrs, and (d) smoothly finished, age 2-3 yrs. Similarly, the asphalt surfaces are: (a) roughly finished with some crack, age 5 yrs; (b) roughly finished without crack, age 5 yrs; (c) smoothly finished with some crack, age 1-2 yrs; and (d) smoothly finished without crack age 1-2 yrs.

(a) (b)

Figure 4.2. Testing Assembly on a: (a) Concrete Surface and (b) Asphalt Surface.

4.2.3.2 Base, Subbase, and Subgrade Surfaces

The coefficient of friction between the base, subbase, and subgrade surfaces with the bottom surface of TCTBs has also been determined on a variety of surface types (Figure 4.3). The base surface was selected at a TXDOT pavement construction site and the testing for the coefficient of friction was performed just before the asphalt concrete was placed. The surface was compacted with sandy gravel and stone chips. The subbase surface was also at a TXDOT construction site which was compacted with gravel and stone chips mixed with some clayey sand. The subgrade was a black clay soil mixed with some gravel. The testing for the coefficient of friction was performed on a compacted, smooth, and finished subgrade surface before placing the subbase course. Similar to pavement surfaces, the coefficient of friction between the base, subbase, and compacted subgrade and the bottom surface of TCTBs was determined at a number of locations. Based on texture and surface roughness, the coefficient of friction was measured to get a range of data.

(a) (b) (c)

Figure 4.3. Testing Assembly on a: (a) Base, (b) Subbase and (b) Compacted Subgrade Surface.

4.2.4 Effect of Dry or Wet Surface

For many surfaces, the coefficient of friction changes significantly when any of the surfaces is moistened because the thin film of water between the two surfaces acts like a lubricant and decreases the coefficient of friction. A statistical test (pooled t-test) was conducted to understand whether the difference between the mean coefficient of friction for dry surface and wet surface is significant or not for each of the surfaces.

4.2.5 Effect of Dirt on Surfaces

In a construction site where TCTBs are used, the pavement surface might have some dirt on the surface. Similarly, the presence of dirt at the bottom surface of the TCTBs is not uncommon. Since the TxDOT specifications do not require cleaning the TCTBs before installation, the presence of dirt in between two surfaces might have a significant effect on the coefficient of friction. The effect on the coefficient of friction due to the presence of dirt in between the surfaces (concrete and asphalt surfaces) has also been investigated. To simulate the extreme condition, sand particles (d_{50} = 0.62 mm, d_{10} = 0.43 mm) were added at the bottom of the heel assembly before testing. A statistical test (pooled t-test) was conducted for both the surfaces to understand whether the difference between the mean coefficient of friction for the surfaces without and with dirt on the surfaces is significant or not for each of the surfaces.

4.3 STABILITY ANALYSIS OF THE TCTBS DURING EXTREME FLOOD

Stability analysis has been conducted for all four types of TCTBs. The factor of safety against sliding and overturning during extreme flood has been determined for each of TCTBs for four different critical conditions. In order to determine the factor of safety against sliding, a frictional coefficient of 0.62 is assumed, which is basically the lowest field measured coefficient of friction between the asphalt pavement surface (mostly used surface for placing TCTBs) and the bottom surface of the TCTB measured at the field.

4.3.1 Theory of Stability

Generally, the TCTBs can fail either by sliding or by overturning due to hydraulic/hydrodynamic pressure resulting from any flood event. Since the TCTBs are placed on rigid platform, failure is very unlikely due to bearing capacity or settlement. The factor of safety against sliding and overturning has been described in Section 2.4.

4.3.2 Critical Scenarios and Factors Considered for Stability Analysis

Four different scenarios of flooding are considered based on the geometry of the roadway and flooding type to determine the factor of safety against sliding and overturning. These four scenarios are shown in Figure 4.4. Scenario 1 represents a situation when the flood water height is variable only at the upstream of the barrier because of the drainage pattern at the downstream. In this situation, the water in the downstream will be drained quickly and the height of water is assumed to be zero at downstream. Scenario 2 represents a situation when the flood water is equal to the barrier height at the upstream and variable at the downstream because of slow drainage of water. Scenario 3 represents a situation when the water is flowing above the TCTB, which is submerged under flowing flood water. Scenario 4 represents a situation when the TCTBs will face a tidal surge for highways near the coastal area. Two different surge velocities of 5 mph and 10 mph have been used. It is assumed that the flow is acting perpendicular to the face of the barrier to simulate the worst condition. Based on the scenarios, the hydraulic and hydrodynamic forces working on TCTBs are analyzed to determine the factor of safety.

Along with the static water pressure caused by all the scenarios described above, the TCTBs will face a velocity head caused by the upstream energy of the flood water. All of the four types of TCTB have some openings to drain the water from upstream to downstream. These openings allow the upstream flood water to pass through which creates an upstream velocity head acting on the face of the TCTB. The rating curves that were prepared to evaluate the hydraulic performance (shown in Chapter 3) were used to estimate the flow through the openings the upstream velocity and downstream water height for the discharge associated with the upstream water height was determined. Most of the cases, the velocity head was negligible. The downstream water height is considered in calculating the pressure from downstream side and the upward buoyancy acting on the bottom of the barriers.

4.3.3 Calculation of Factor of Safety against Sliding and Overturning

The factor of safety against sliding and overturning has been calculated considering all forces working on a TCTB following the equation in Section 2.4. Details of the calculations (sample calculation) to evaluate the factor of safety for all four TCTBs are shown in Appendix C. For all the cases a cross slope of 0° and a coefficient of friction of 0.62 is considered. An Excel Worksheet is prepared for each of the TCTBs in such a way that by changing the upstream water height, downstream water height, upstream velocity, coefficient of friction, cross slope of the roadway and the geometry of the TCTBs, the factor of safety against sliding and overturning can be calculated for any combination of the above mentioned variables, which was verified by hand calculation for at least two different situations. Then the factor of safety against sliding and overturning is calculated for each of the TCTBs considering the four flood scenarios with variable flooding situation.

The cross-slope is very common in roadways to facilitate drainage or to provide super elevation in horizontal curves. If the road surface has a cross-slope, the factor of safety against sliding and overturning will be affected. A parametric study is performed considering the different cross slopes of the roadway such as 0°, 3°, 5°, and 8°. The cross-slope is always considered outward with respect to water pressure. Parametric study is also performed considering the coefficient of friction for different pavement surfaces.

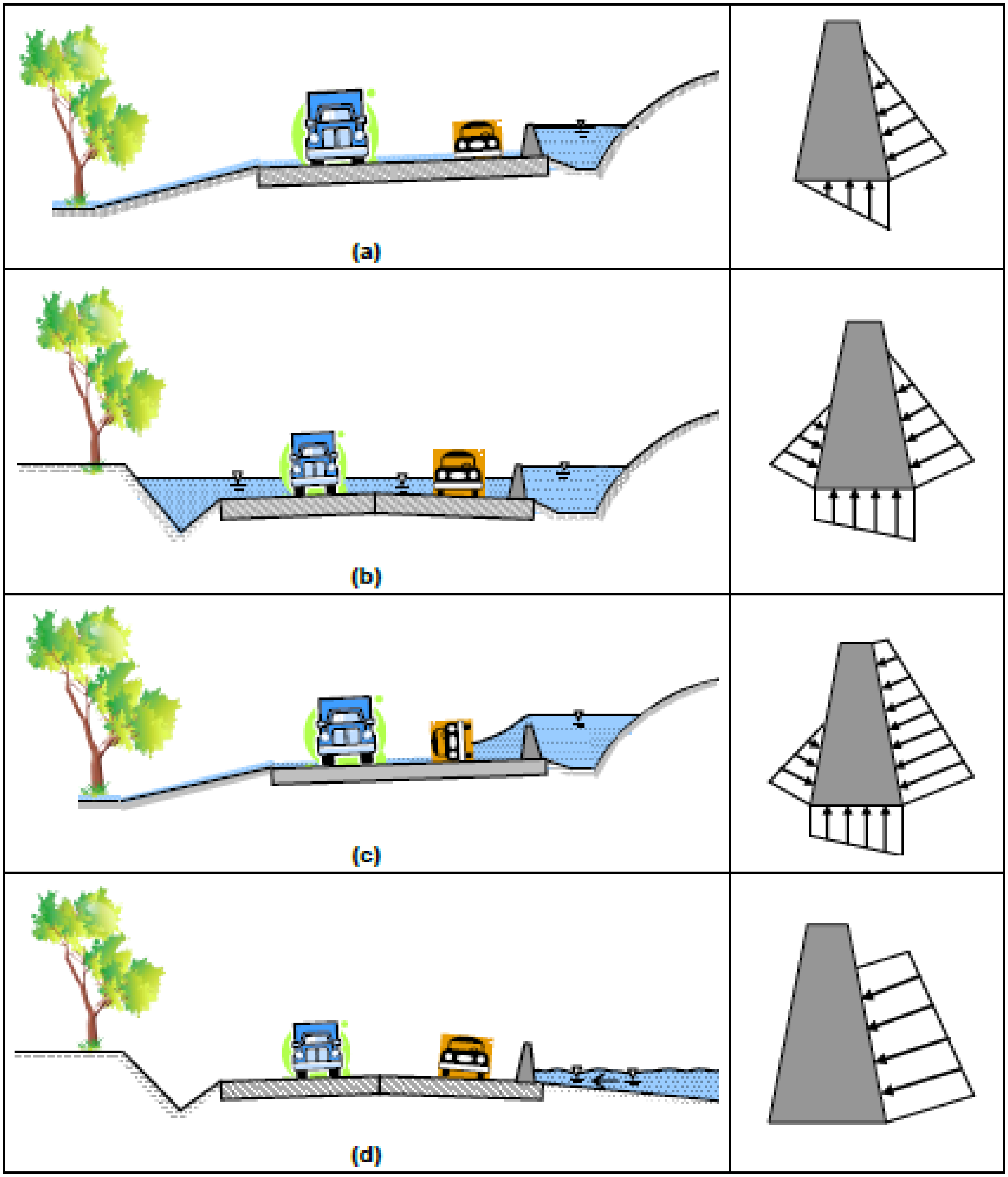

Figure 4.4. Different Scenarios: (a) Scenario 1, (b) Scenario 2, (c) Scenario 3, and (d) Scenario 4.

4.3.4 Results for the Determination of Coefficient of Friction

4.3.4.1 Validation of the Method

To understand the effect of different bearing stresses on coefficient of friction, the coefficient of friction for concrete and asphalt surfaces were measured first with the standard stress level (1 psi) and then with a bearing stress of 2 psi. The coefficient of friction for concrete surface varies from 0.69 to 0.77 (Table 4.2) for the higher stress level and from 0.78 to 0.98 for standard stress level. Similarly, the coefficient of friction for asphalt surface varies from 0.61 to 0.69 for higher stress level and from 0.62 to 0.76 for standard stress level.

At the microscopic level, the surface of any solid, no matter how polished, is quite rough. Two mating surfaces are in contact only on the tips of the asperities (Blau, 1996). When two solid surfaces are brought together the area of contact area is actually extremely small compared to the apparent area of contact. A higher bearing stress level might destroy some of the microstructures and make the surface smoother, which might be the reason for the lower coefficient of friction at higher stress level.

Table 4.2. Coefficient of Friction between Pavement Surfaces and TCTB at Different Bearing Stress.

Pavement Type	Surface Characteristics	Condition (dry/wet)	Coefficient of Friction: Standard Bearing Stress (1 psi)	Coefficient of Friction: Higher Bearing Stress (2 psi)
Concrete Pavement	Rough finish, age > 10 yrs	dry	0.98	0.77
		wet	0.89	0.77
	Semi-Rough finish, age 5-10 yrs	dry	0.90	0.71
		wet	0.87	0.76
	Smooth finish, age 5-10 yrs	dry	0.79	0.75
		wet	0.78	0.75
	Smooth finish, age 2-3 yrs	dry	0.85	0.71
		wet	0.81	0.69
Asphalt Pavement	Rough finish with crack, age 5 yrs	dry	0.76	0.68
		wet	0.72	0.69
	Rough finish without crack, age 5 yrs	dry	0.70	0.61
		wet	0.62	0.66
	Smooth finish with crack, age 1-2 yrs	dry	0.72	0.61
		wet	0.68	0.62
	Smooth finish without crack, age 1-2 yrs	dry	0.73	0.62
		wet	0.70	0.71

Statistical test (pooled t-test with $\alpha = 0.05$) showed that, in our observation, for both concrete and asphalt pavement, there is a significant difference between the mean coefficient of friction determined with standard stress level (1 psi) and with a higher stress level (2 psi) (P = 0.0004 for concrete and P = 0.0293 for asphalt surface).

In order to address the issue of the variation of the coefficient of friction with bearing stress, four different common pavement surfaces are chosen to determine the coefficient of friction at different stress levels. The variation of the coefficient of friction with bearing stress is shown in Figure 4.5. The coefficient of friction decreases approximately 18-22% when the bearing stress increases from 1.0 psi to 2.0 psi and then remains unchanged for the concrete surface. For the asphalt surface, the coefficient of friction decreases approximately 22-23% when the bearing stress increases from 1.0 psi to 2.0 psi and then decreases slowly.

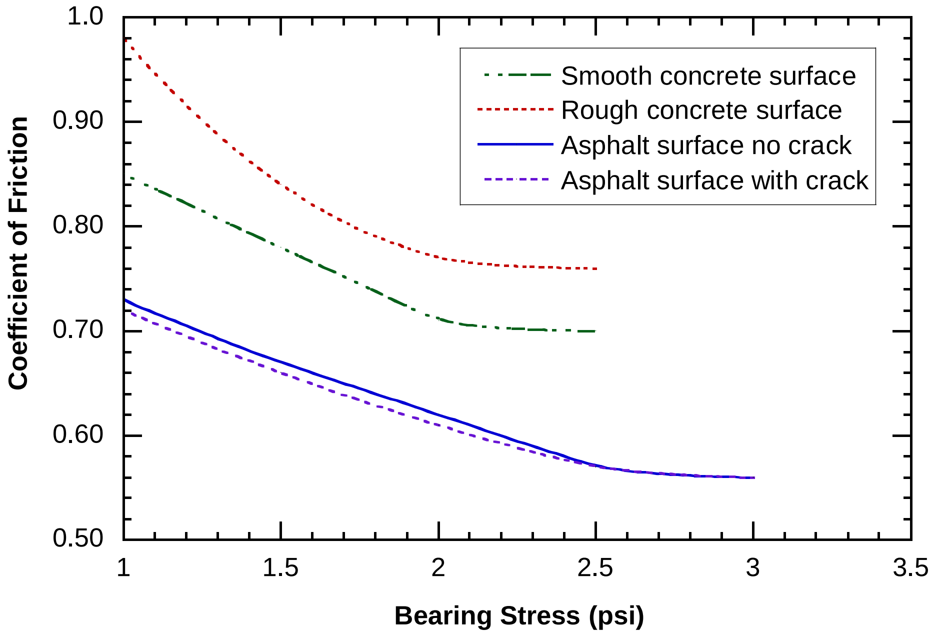

Figure 4.5. Variation of the Coefficient of Friction with Different Bearing Stresses for Concrete and Asphalt Surfaces.

4.3.4.2 Coefficient of Friction for Concrete and Asphalt Surfaces

The coefficient of friction between the pavement surfaces (concrete and asphalt) and the bottom surface of TCTBs are shown in Table 4.3. The coefficient of friction between the concrete surface and the bottom surface of TCTB varies from 0.78 to 0.98. Similarly, the coefficient of friction between the asphalt surface and the bottom surface of TCTB varies from 0.62 to 0.76.

4.3.4.3 Coefficient of Friction for Base, Subbase, and Subgrade Surfaces

The coefficient of friction between the bottom surface of the TCTB and the base, subbase, and sugrade surfaces are shown in Table 4.4. The coefficient of friction between the bottom surface of the TCTB and the base surface varies between 0.54 and 0.75. Similarly, the coefficient of friction between the bottom surfaces of the TCTBs varies between 0.50 and 0.69 for subbase, and between 0.61 and 0.88 for compacted subgrade.

Table 4.3. Coefficient of Friction between Pavement Surfaces and TCTBs.

Pavement Type	Surface Characteristics	Condition (dry/wet)	Coefficient of Friction
Concrete Pavement	Rough finish, age > 10 yrs	dry wet	0.98 0.89
	Semi-Rough finish, age 5-10 yrs	dry wet	0.90 0.87
	Smooth finish, age 5-10 yrs	dry wet	0.79 0.78
	Smooth finish, age 2-3 yrs	dry wet	0.85 0.81
Asphalt Pavement	Rough finish with crack, age 5 yrs	dry wet	0.76 0.72
	Rough finish without crack, age 5 yrs	dry wet	0.70 0.62
	Smooth finish with crack, age 1-2 yrs	dry wet	0.72 0.68
	Smooth finish without crack, age 1-2 yrs	dry wet	0.73 0.70

The coefficient of friction decreases slightly in wet condition for base surfaces, whereas, the coefficient of friction increases in wet condition for both subbase and subgrade perhaps due to the cohesive nature of the materials because the subbase and subgrade have some clayey particles.

4.3.4.4 Effect of Dry or Wet Surface

A statistical (pooled t-test) test was conducted to understand whether the difference between the mean coefficient of friction for dry surface and wet surface is significant for each of the surfaces or not. The pooled t-test was conducted assuming a significance level, α = 0.05. This test requires that the samples should be independent and collected from a population of normal distribution, and the variances of the population should be equal. The results of the pooled t-tests are shown with a P-value for each of the surfaces in Table 4.5. The P-value for each surface with dry and wet conditions is greater than the significance level of 0.05 for all types of surfaces (i.e., concrete, asphalt, base, subbase, and subgrade), which suggests that there is no significant difference between the mean coefficient of friction for dry and wet surfaces for all types of pavement.

Table 4.4. Coefficient of Friction for the Base, Subbase, and Subgrade with the TCTBs.

Pavement Component	Test Location	Condition (dry/wet)	Coefficient of Friction
Base	Location 1	dry	0.75
		wet	0.74
	Location 2	dry	0.68
		wet	0.61
	Location 3	dry	0.66
		wet	0.57
	Location 4	dry	0.65
		wet	0.54
Subbase	Location 1	dry	0.56
		wet	0.62
	Location 2	dry	0.64
		wet	0.69
	Location 3	dry	0.50
		wet	0.56
	Location 4	dry	0.50
		wet	0.56
Subgrade	Location 1	dry	0.70
		wet	0.65
	Location 2	dry	0.61
		wet	0.66
	Location 3	dry	0.68
		wet	0.88
	Location 4	dry	0.67
		wet	0.71

4.3.4.5 Effect of Dirt on Surfaces

The coefficient of friction between the bottom surface of the TCTBs and the pavement surfaces after adding some dirt (sand) at the bottom of testing block are shown in Table 4.6 along with the coefficient of friction without any dirt. It shows that the coefficient of friction decreases significantly due to the presence of dirt in between two frictional surfaces. It was also observed that the decrease of the coefficient of friction is higher in smooth surface compared to that of the rough surface. The coefficient of friction varies from 0.34 to 0.61 for concrete surface and from 0.40 to 0.60 for asphalt surface when dirt was added.

Statistical test (pooled t-test) with a significance level α = 0.05 shows that the decrease in coefficient of friction due to the presence of dirt in between two surfaces is significant for both concrete (P = 0.0001) and asphalt (P = 0.0001) surfaces.

Table 4.5. Statistical Analysis for the Mean Coefficient of Friction (α = 0.05).

Pavement Surface	Mean Coefficient of Friction (standard deviation)		P-value (Pooled t-test)	Significant Difference?
	Dry	**Wet**		
Concrete	0.88 (0.08)	0.84 (0.05)	0.4070	No
Asphalt	0.73 (0.03)	0.68 (0.04)	0.1057	No
Base	0.69 (0.05)	0.62 (0.09)	0.2070	No
Subbase	0.55 (0.07)	0.60 (0.06)	0.2518	No
Subgrade	0.67 (0.04)	0.73 (0.11)	0.3300	No

4.3.5 Stability Analysis of the TCTBs during Extreme Flood

The stability of TCTBs against sliding and overturning during extreme flood is expressed in terms of factor of safety. Factor of safety higher than 1 means the TCTB is stable in that particular situation. Similarly, factor of safety less than 1 means the TCTB is unstable in that particular situation.

Table 4.6. Effect of the Presence of Dirt in between Two Surfaces.

Pavement Type	Surface Characteristics	Condition (dry/wet)	Coefficient of Friction	
			Without Dirt	**With Dirt**
Concrete Pavement	Rough finish, age > 10 yrs	dry	0.98	0.61
		wet	0.89	0.53
	Semi-Rough finish, age 5-10 yrs	dry	0.90	0.47
		wet	0.87	0.43
	Smooth finish, age 5-10 yrs	dry	0.79	0.37
		wet	0.78	0.35
	Smooth finish, age 2-3 yrs	dry	0.85	0.37
		wet	0.81	0.34

Asphalt Pavement	Rough finish with crack, age 5 yrs	dry	0.76	0.60
		wet	0.72	0.48
	Rough finish without crack, age 5 yrs	dry	0.70	0.60
		wet	0.62	0.46
	Smooth finish with crack, age 1-2 yrs	dry	0.72	0.45
		wet	0.68	0.45
	Smooth finish without crack, age 1-2 yrs	dry	0.73	0.50
		wet	0.70	0.40

Factor of safety against sliding and overturning is calculated assuming the cross slope of the highway is 0° and the coefficient of friction is 0.62, which is basically the lowest coefficient of friction between the asphalt pavement surface (mostly used surface for placing TCTBs) and the bottom surface of TCTBs found during our field measurement.

4.3.5.1 Single Slope Concrete Barrier (SSCB)

Stability of SSCB against sliding and overturning during extreme flood is shown in terms of factor of safety against sliding and overturning for flood scenarios 1, 2, 3, and 4 in Figures 4.6, 4.7, 4.8, and 4.9, respectively. Figure 4.6 represents the factor of safety against sliding and overturning for flood scenario 1 and shows that the factor of safety against sliding (Figure 4.6a) becomes less than 1 when the upstream water height is more than 39 in. and the factor of safety against overturning is more than 1 when the upstream water height equals to the barrier height. Thus, the SSCB is stable as long as the upstream water height is less than 39 in. for flood scenario 1.

Figure 4.7 represents the flood scenario 2, which shows that the factor of safety against sliding becomes less than 1 when the downstream water height is less than 23 in. When the downstream water height is more than 23 in. then the pressure from both sides makes it stable. The factor of safety against overturning is always more than 1. Thus, the SSCB is stable when the upstream water height is equal to the height of the barrier and the downstream water height is at least 23 in.

Figure 4.8 shows that the factor of safety against sliding and overturning becomes less than 1 when the barrier is submerged under water with flowing flood water from upstream (flood scenario 3). Thus, the SSCB is unstable with respect to sliding and overturning for flood scenario 3.

Figure 4.9 represents the factor of safety against sliding and overturning for flood scenario 4 when the tidal surge is coming toward the TCTBs in coastal area. The factor of safety against sliding becomes less than 1 when the surge water height is higher than 32 in. and the surge velocity is 5 mph. Similarly, it becomes less than 1 when the surge water height is higher than 19 in. and the surge velocity is 10 mph. The factor of safety against overturning becomes less than 1 when the surge water height is higher than 37 in. and the surge velocity is 5 mph, but it becomes less than 1 when the surge water height is higher than 28 in. and the surge velocity is 10 mph. Thus, the SSCB is stable when the surge water height is less than 32 in. and the surge velocity is 5 mph or when the surge water height is less than 19 in. and the surge velocity is 10 mph.

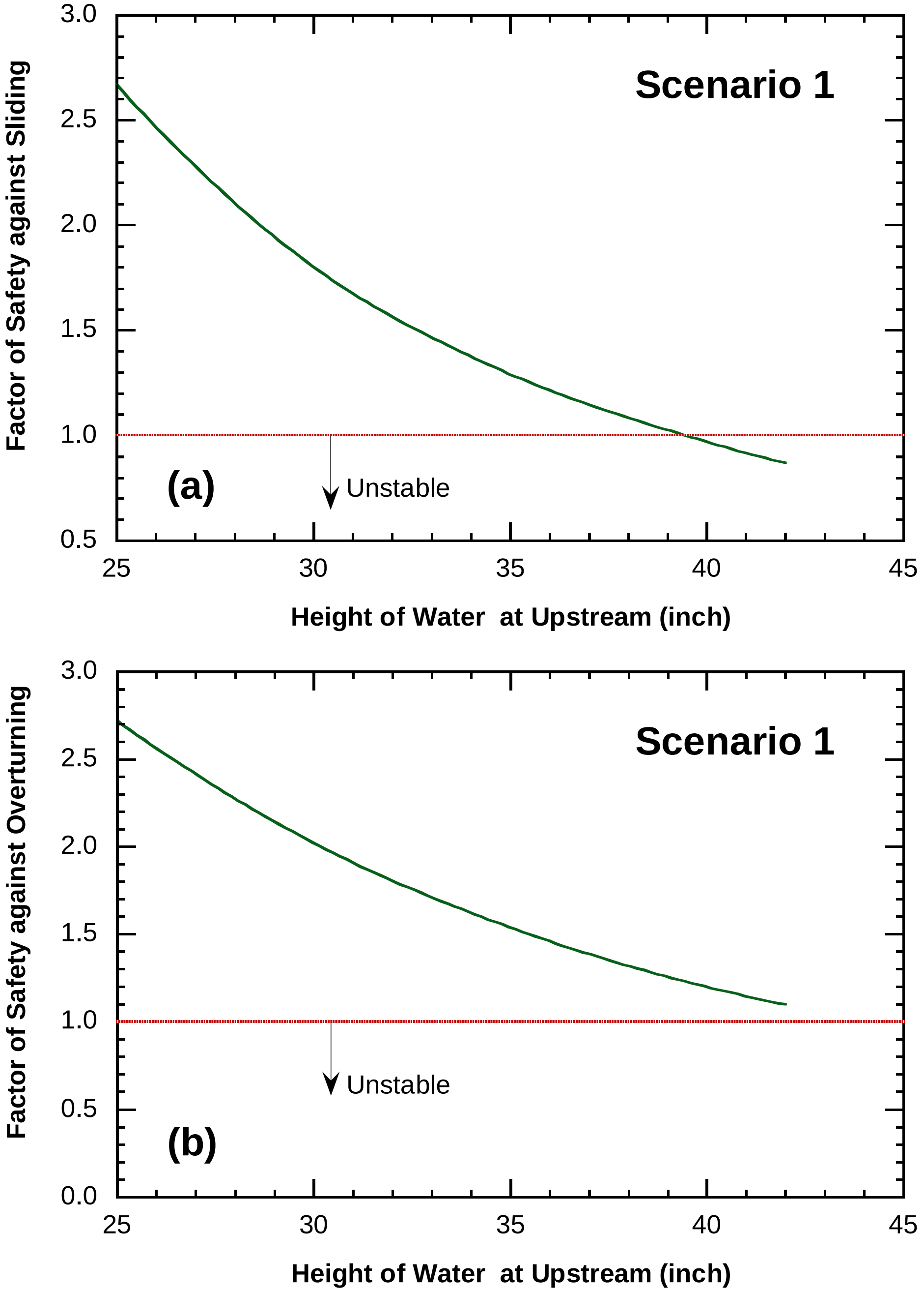

Figure 4.6. Factor of Safety against (a) Sliding and (b) Overturning for the SSCB for Flood Scenario 1.

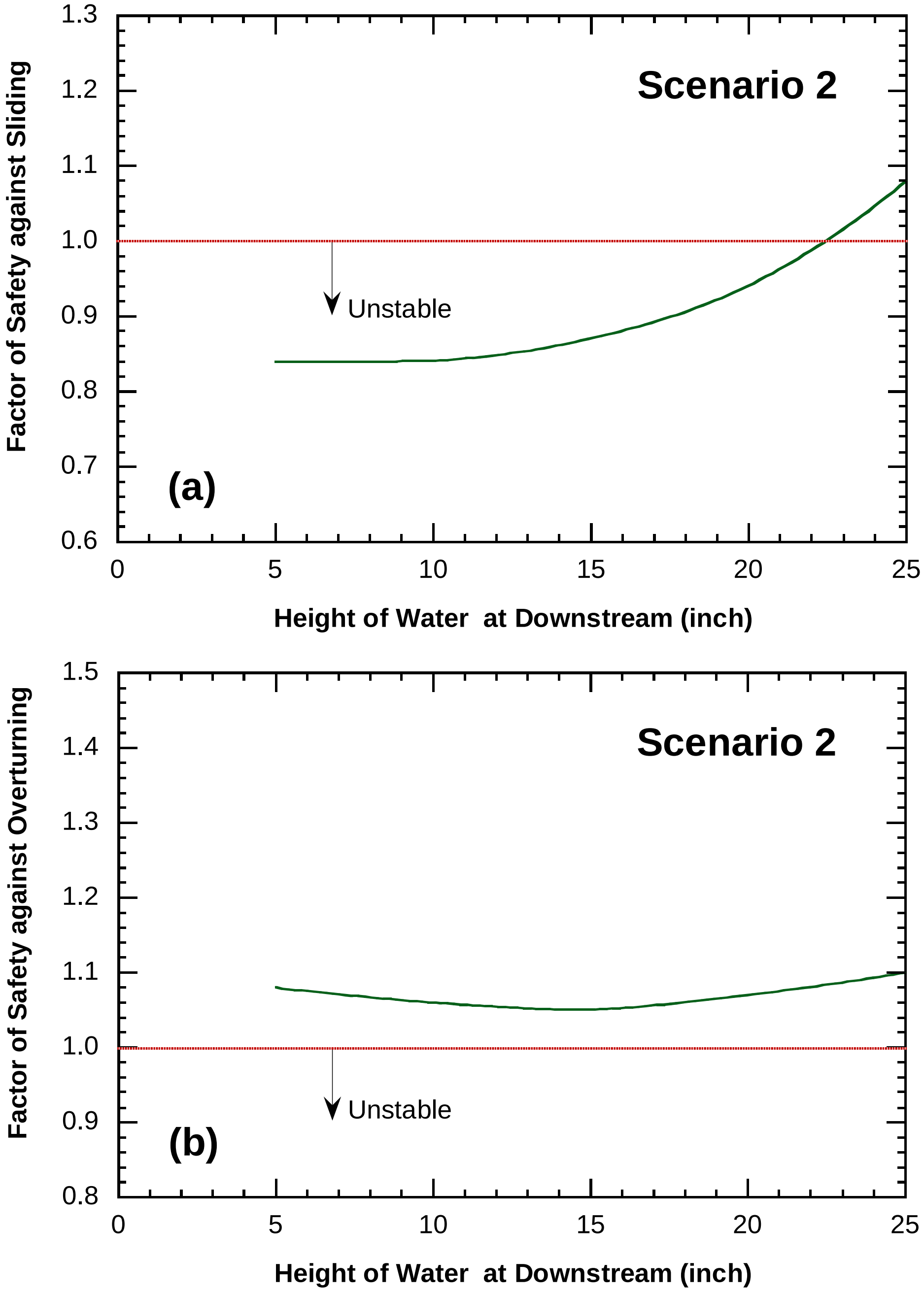

Figure 4.7. Factor of Safety against (a) Sliding and (b) Overturning for the SSCB in Flood Scenario 2.

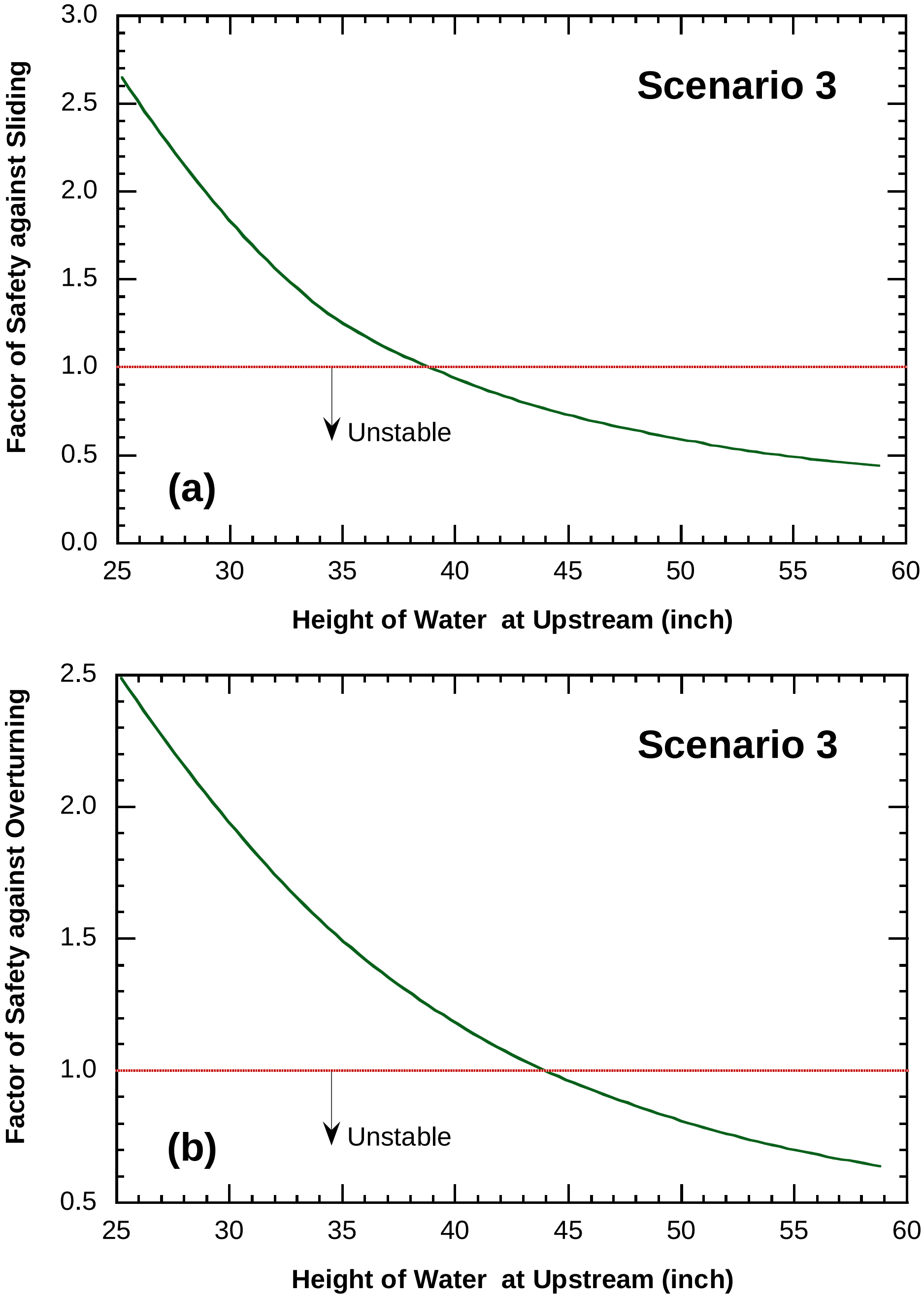

Figure 4.8. Factor of Safety against (a) Sliding and (b) Overturning for the SSCB for Flood Scenario 3.

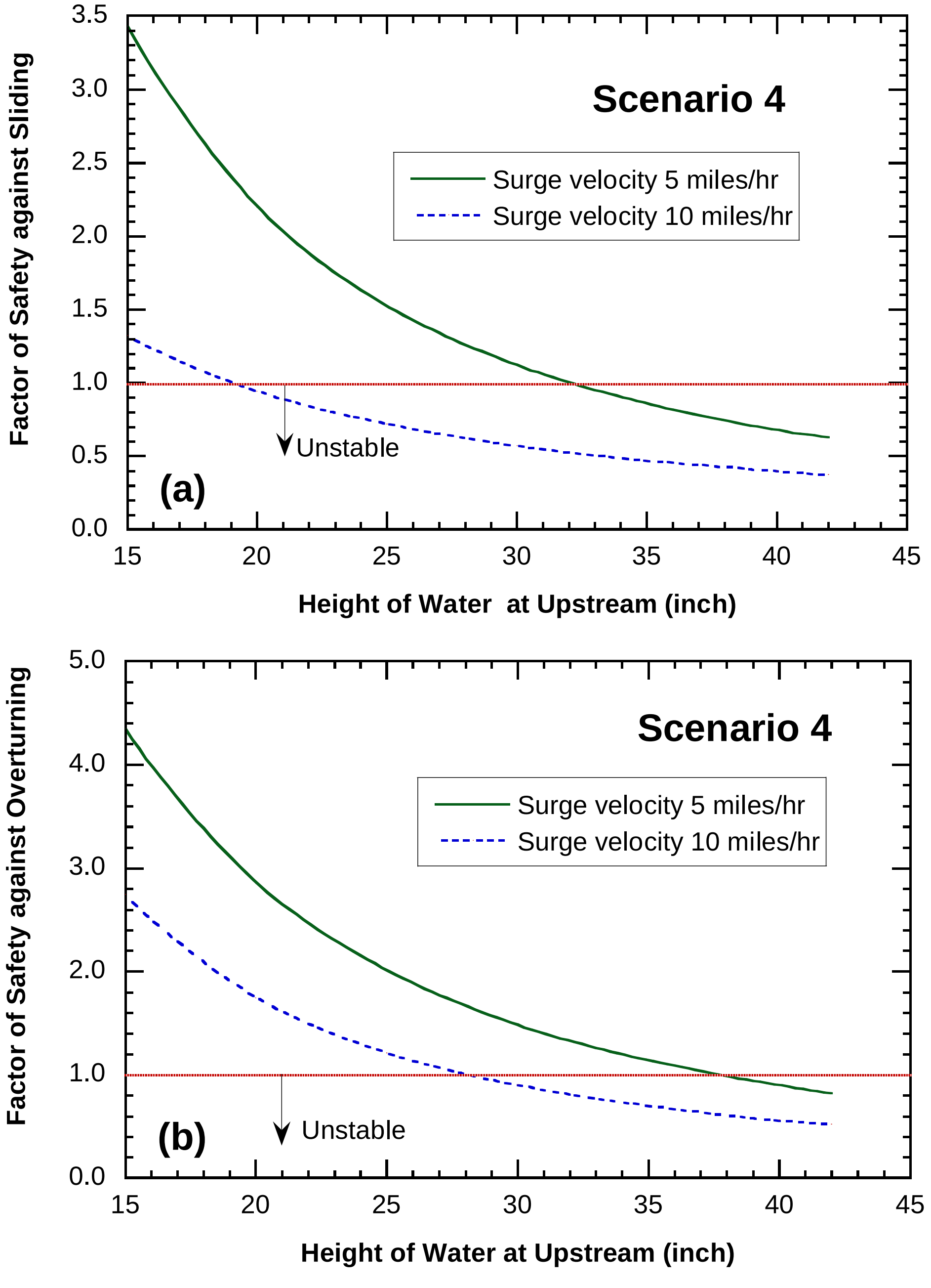

Figure 4.9. Factor of Safety against (a) Sliding and (b) Overturning for the SSCB for Flood Scenario 4.

4.3.5.2 F-Shaped Concrete Safety Barrier (CSB)

The stability of CSB against sliding and overturning during extreme flood is expressed in terms of factor of safety for flood scenarios 1, 2, 3, and 4, and are shown in Figures 4.10, 4.11, 4.12, and 4.13, respectively.

Figure 4.10 represents the factor of safety against sliding and overturning for flood scenario 1 and shows that the factor of safety against sliding (Figure 4.10a) is more than 1 even when the upstream water height is equal to the height of the barrier (33 in.) and the factor of safety against overturning is more than 1 even the upstream water height equals to the barrier height. Thus, the CSB is stable until the upstream water height is greater than 32 in. for flood scenario 1.

Figure 4.11 represents the flood scenario 2, which shows that the factor of safety against sliding becomes less than 1 when the downstream water height is less than 15 in. When the downstream water height is more than 15 in. then the pressure from both sides makes it stable. The factor of safety against overturning decreases as the downstream water increases up to a height of 14 in. where the slope changes for the CSB and then increases as the downstream water height is increased above 14 in. However, the factor of safety against overturning is always more than 1. Thus, the CSB is stable when the upstream water height is equal to the height of the barrier and the downstream water height is at least 15 in.

Figure 4.12 shows that the factor of safety against sliding becomes less than 1 as soon as the CSB is submerged under the flowing flood water from upstream. However, the factor of safety against overturning becomes less than 1 when the barrier is submerged under water with upstream water height at least 40 in. Thus, the CSB is unstable with respect to sliding and overturning for flood scenario 3.

Figure 4.13 represents the factor of safety against sliding and overturning for flood scenario 4 when the tidal surge is coming toward the TCTBs in coastal region. The factor of safety against sliding becomes less than 1 when the surge water height is higher than 24 in. and the surge velocity is 5 mph. Similarly, it becomes less than 1 when the surge water height is higher than 12 in. and the surge velocity is 10 mph. The factor of safety against overturning becomes less than 1 when the surge water height is just equal to the barrier height and the surge velocity is 5 mph or it becomes less than 1 when the surge water height is higher than 23 in. and the surge velocity is 10 mph. Thus, the CSB is stable when the surge water height is less than 24 in. and the surge velocity is 5 mph or when the surge water height is less than 12 in. and the surge velocity is 10 mph.

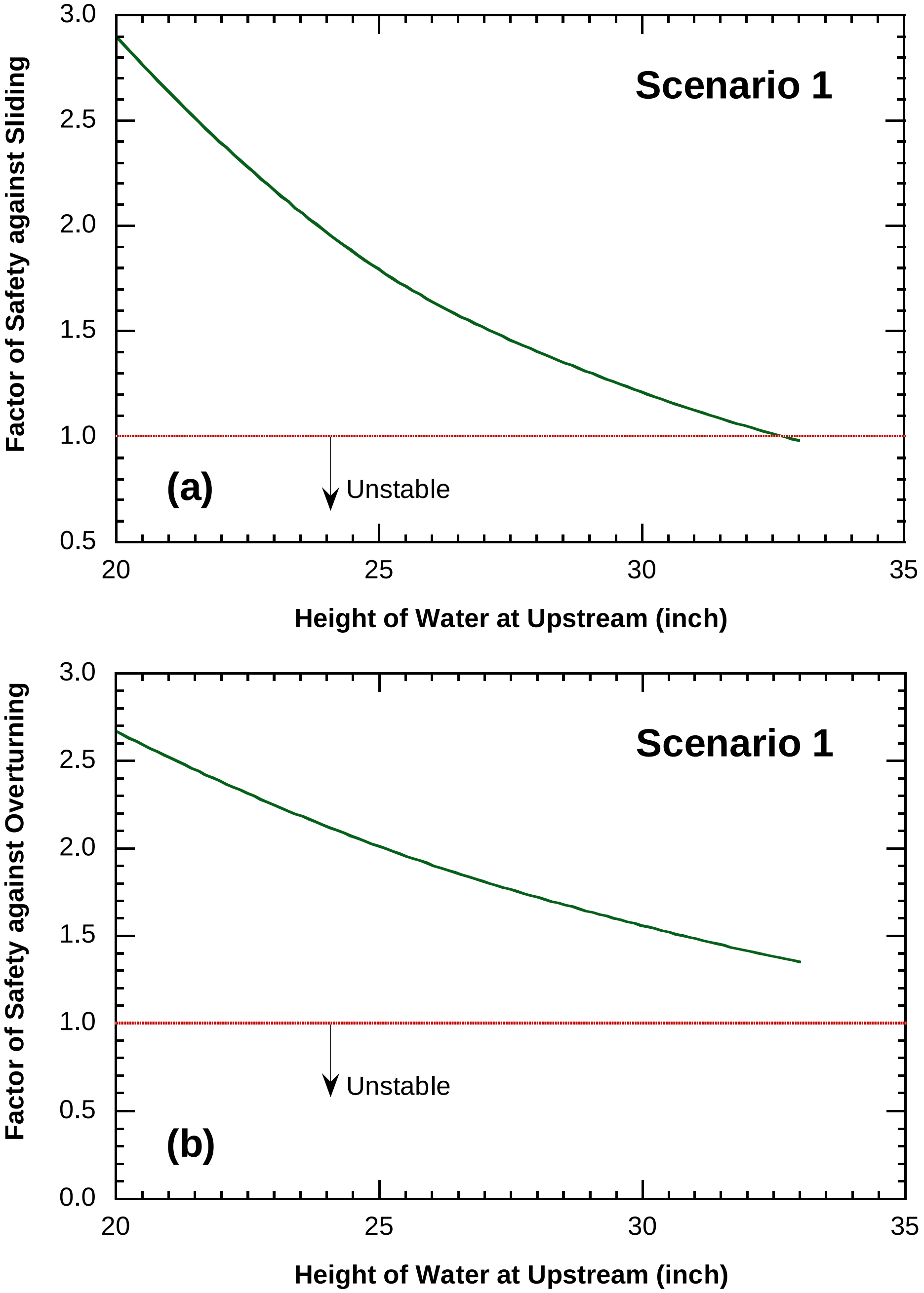

Figure 4.10. Factor of Safety against (a) Sliding and (b) Overturning for the CSB for Flood Scenario 1.

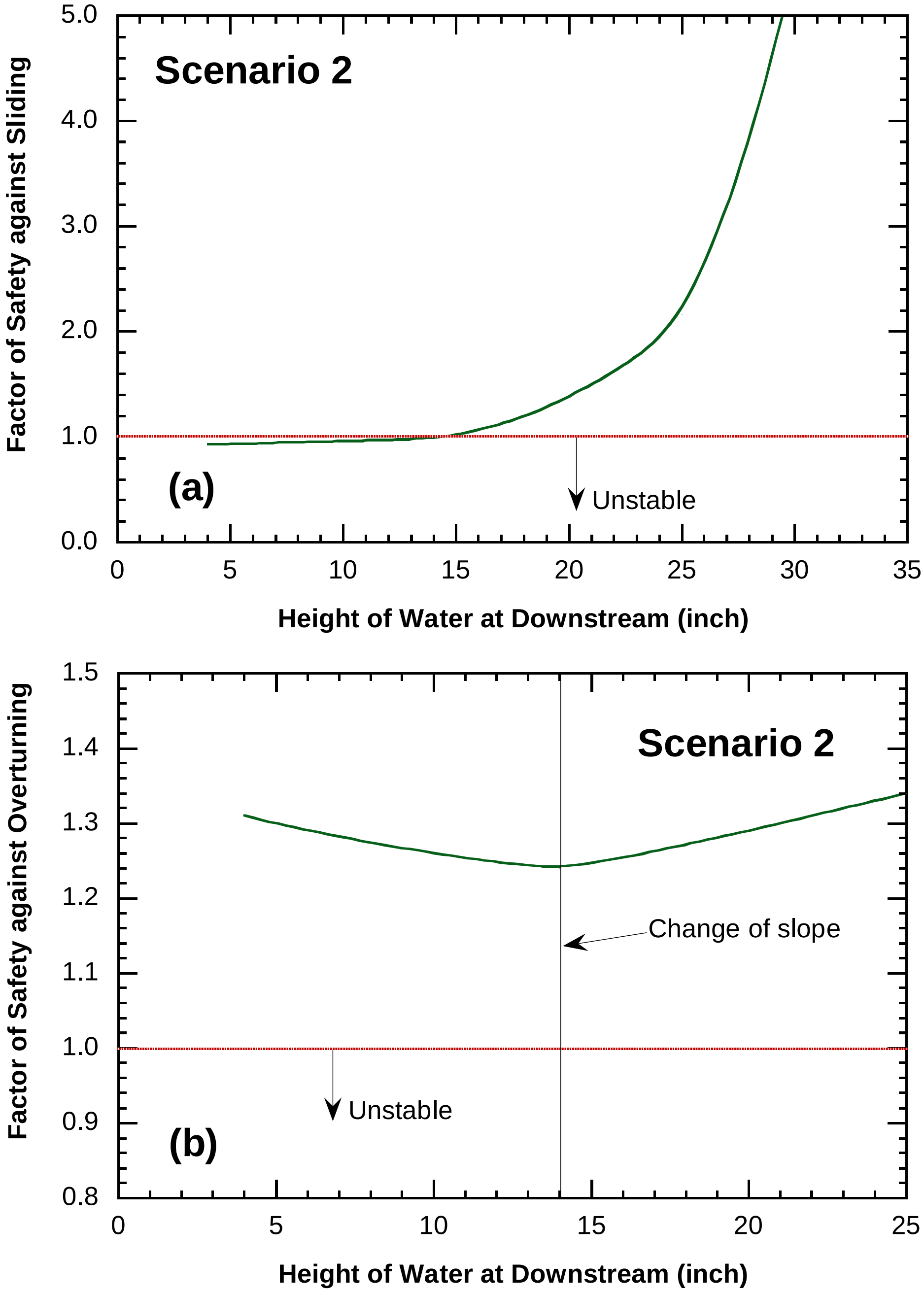

Figure 4.11. Factor of Safety against (a) Sliding and (b) Overturning for the CSB for Flood Scenario 2.

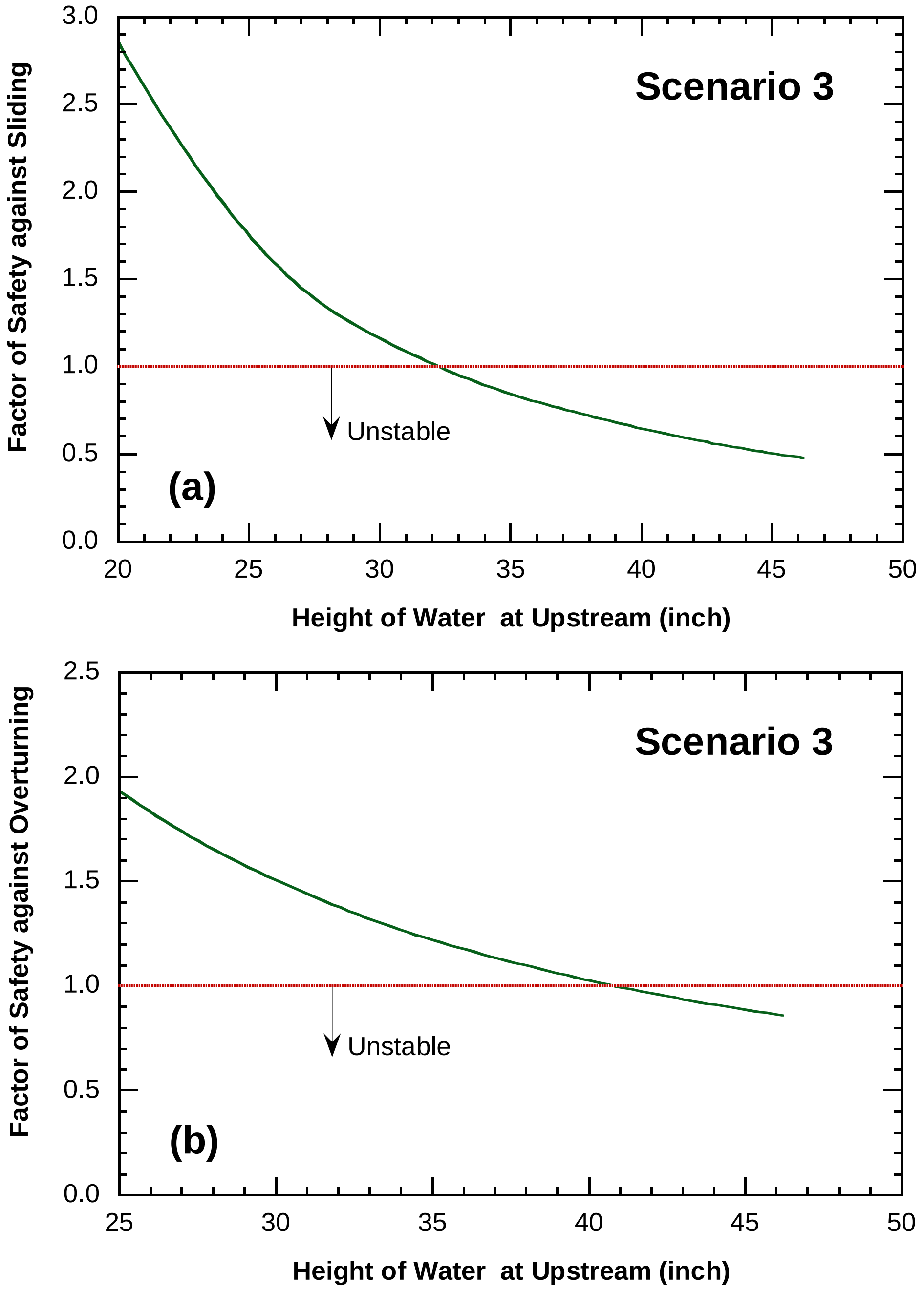

Figure 4.12. Factor of Safety against (a) Sliding and (b) Overturning for the CSB for Flood Scenario 3.

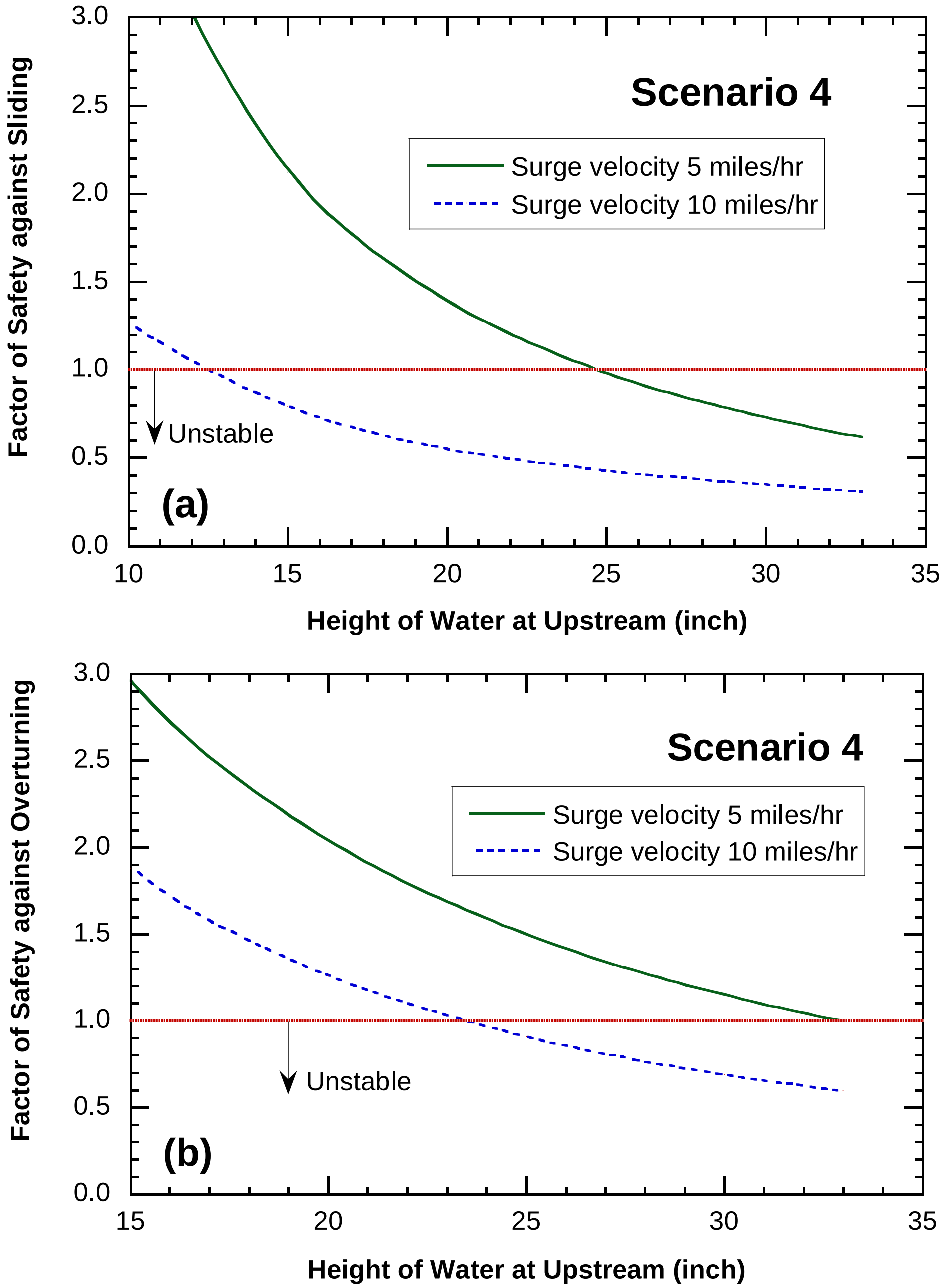

Figure 4.13. Factor of Safety against (a) Sliding and (b) Overturning for the CSB for Flood Scenario 4.

4.3.5.3 Modified Single Slope Concrete Barrier (MSSCB)

The stability of MSSCB against sliding and overturning during extreme flood is expressed in terms of factor of safety for flood scenarios 1, 2, 3, and 4, and are shown in Figures 4.14, 4.15, 4.16, and 4.17, respectively.

Figure 4.14 represents the factor of safety against sliding and overturning for flood scenario 1 and shows that the factor of safety against sliding and overturning are more than 1 up to the upstream water height equal to the barrier height. Thus, the MSSCB is stable for flood scenario 1.

Figure 4.15 represents the flood scenario 2, which shows that the factor of safety against sliding and overturning drops suddenly as soon as the water in downstream touches the top surface of the openings when the buoyancy force starts working. The factor of safety against sliding becomes less than 1 when the downstream water height varies between 5 in. and 9 in. or between 12 in. and 20 in. The factor of safety against overturning is always more than 1 for flood scenario 2. For a practical consideration, the MSSCB is stable when the downstream water height is higher than 20 in. for flood scenario 2.

Figure 4.16 shows that the factor of safety against sliding becomes less than 1 as soon as the CSB is submerged under the flowing flood water from upstream. However, the factor of safety against overturning becomes less than 1 when the barrier is submerged under water with upstream water height at least 40 in.

Figure 4.16 shows that the factor of safety against sliding and overturning are always less than 1 when the MSSCB is submerged under water with flowing flood water from upstream. Thus, the MSSCB is unstable with respect to sliding and overturning for flood scenario 3.

Figure 4.17 represents the factor of safety against sliding and overturning for flood scenario 4 when the tidal surge is coming toward the TCTBs in coastal region. The factor of safety against sliding becomes less than 1 when the surge water height is higher than 34 in. and the surge velocity is 5 mph. Similarly, it becomes less than 1 when the surge water height is higher than 21 in. and the surge velocity is 10 mph. The factor of safety against overturning becomes less than 1 when the surge water height is 37 in. and the surge velocity is 5 mph or it becomes less than 1 when the surge water height is higher than 28 in. and the surge velocity is 10 mph. Thus, the MSSCB is stable when the surge water height is less than 34 in. and the surge velocity is 5 mph or when the surge water height is less than 21 in. and the surge velocity is 10 mph.

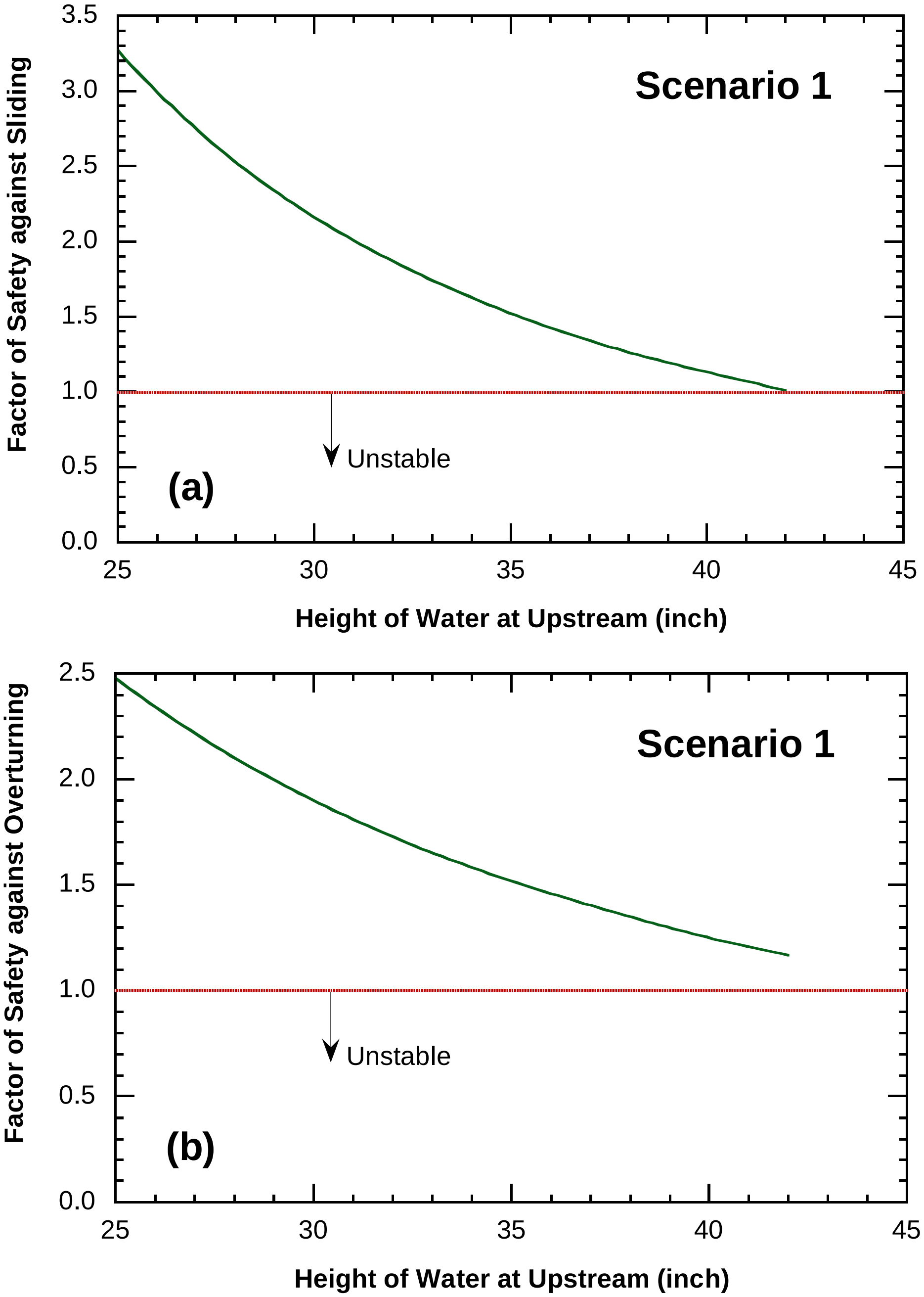

Figure 4.14. Factor of Safety against (a) Sliding and (b) Overturning for the MSSCB for Flood Scenario 1.

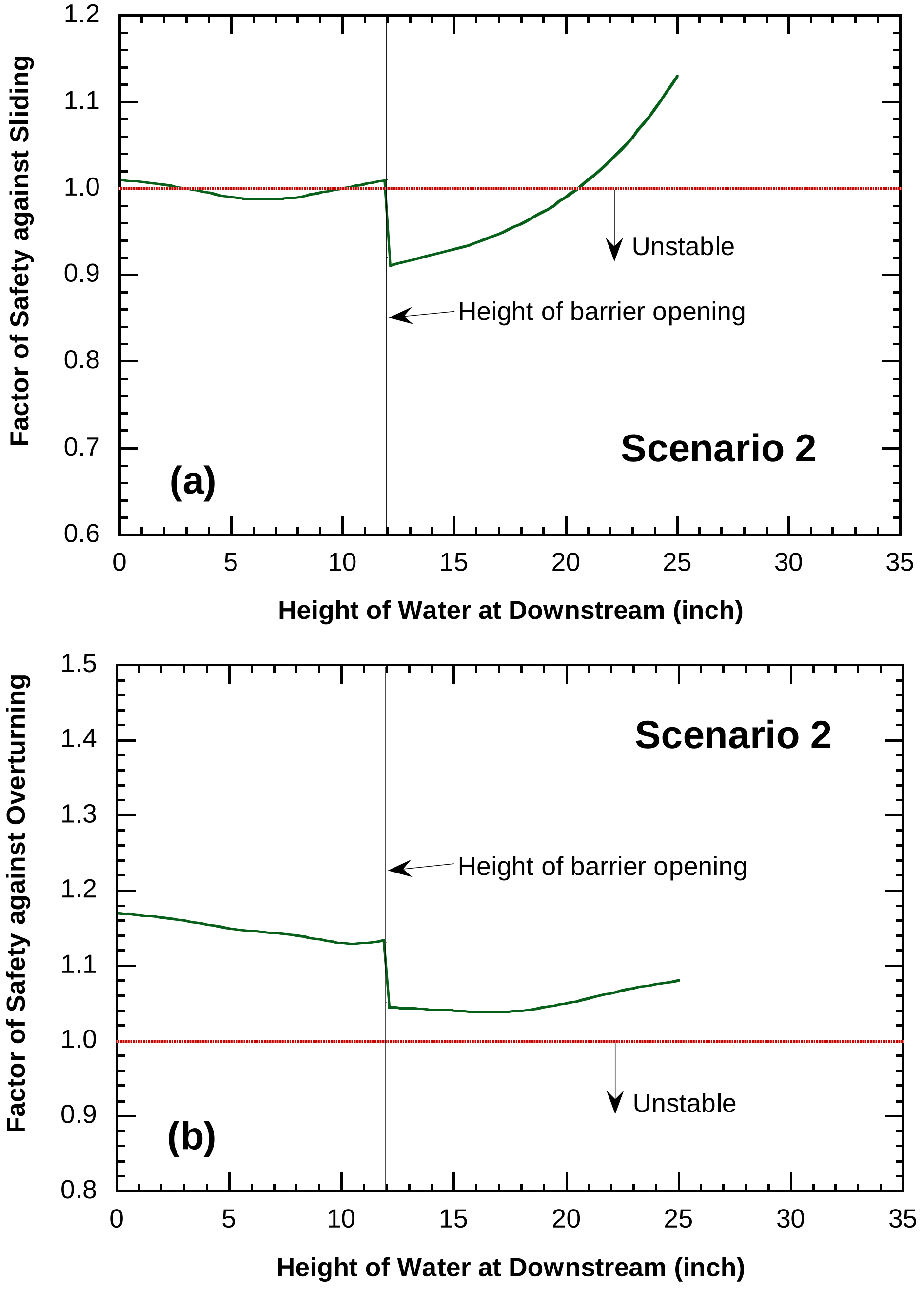

Figure 4.15. Factor of Safety against (a) Sliding and (b) Overturning for the MSSCB for Flood Scenario 2.

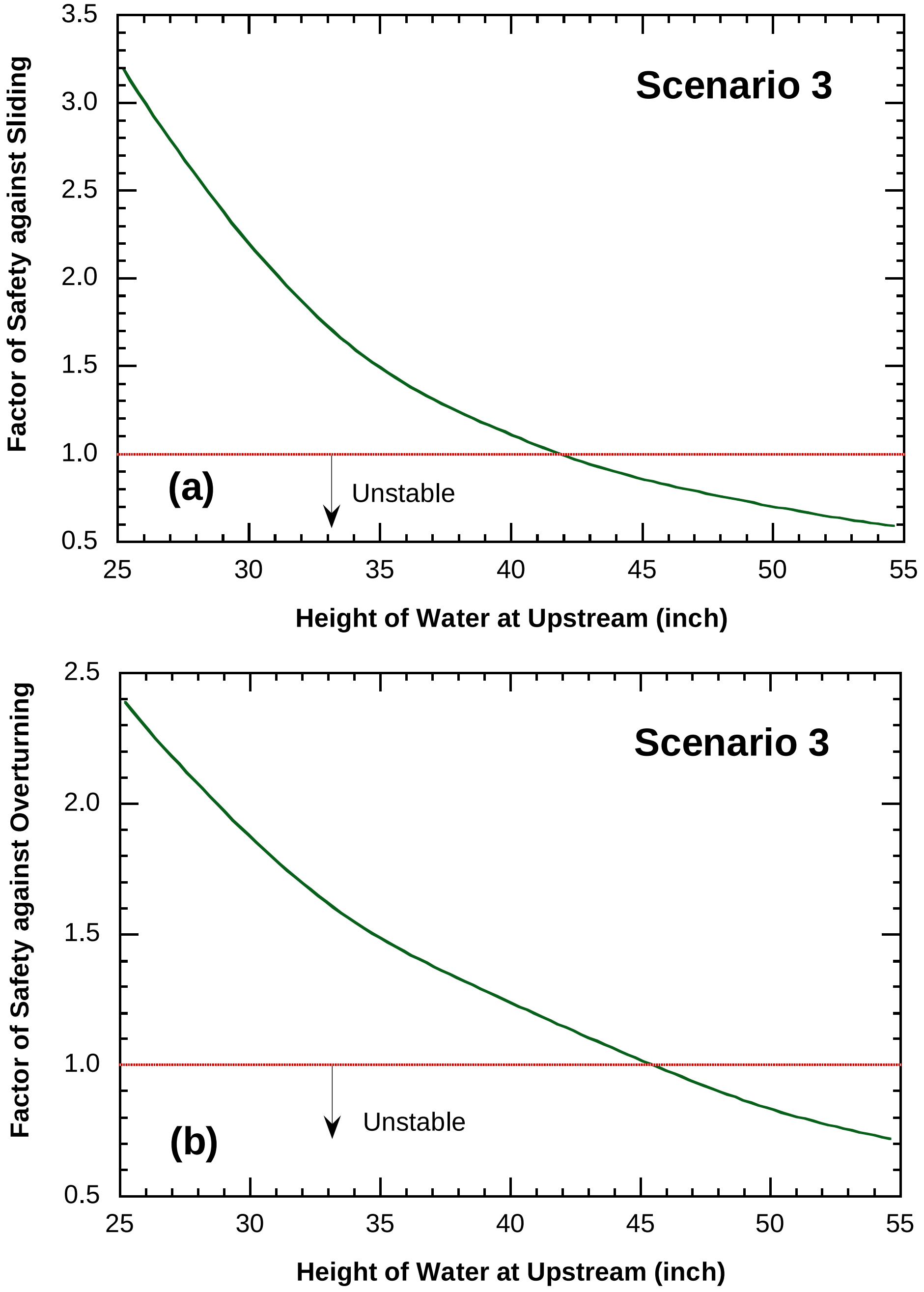

Figure 4.16. Factor of Safety against (a) Sliding and (b) Overturning for the MSSCB for Flood Scenario 3.

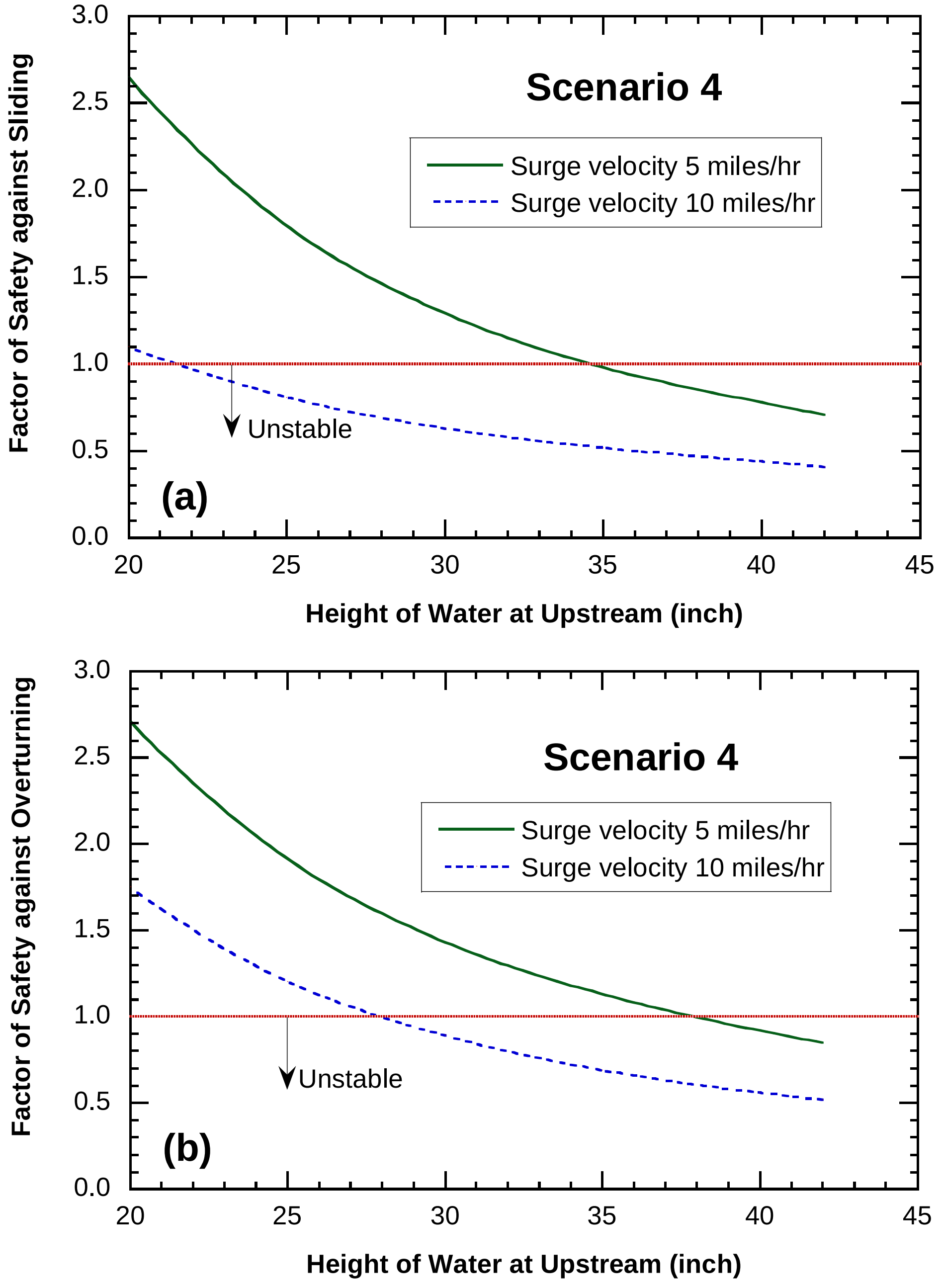

Figure 4.17. Factor of Safety against (a) Sliding and (b) Overturning for the MSSCB for Flood Scenario 4.

4.3.5.4 Low Speed Traffic Barrier

The stability of LPCB against sliding and overturning during extreme flood is expressed in terms of factor of safety for flood scenarios 1, 2, 3, and 4, and are shown in Figures 4.18, 4.19, 4.20, and 4.21, respectively.

Figures 4.18, 4.19, and 4.20 shows that the factor of safety against sliding and overturning are more than 1 for flood scenarios 1, 2, and 3, respectively. Thus, the LPCB is stable for flood scenarios 1, 2, and 3.

Figure 4.21 represents the factor of safety against sliding and overturning for flood scenario 4 when the tidal surge is coming toward the TCTBs in coastal region. The factor of safety against sliding and overturning is always higher than 1 even when the surge water height is equal to the height of the barrier and surge water velocity is 5 mph. However, the factor of safety against sliding becomes less than 1 only when the surge water height is higher than 13 in. and the surge velocity is 10 mph. The factor of safety against overturning is always higher than 1.

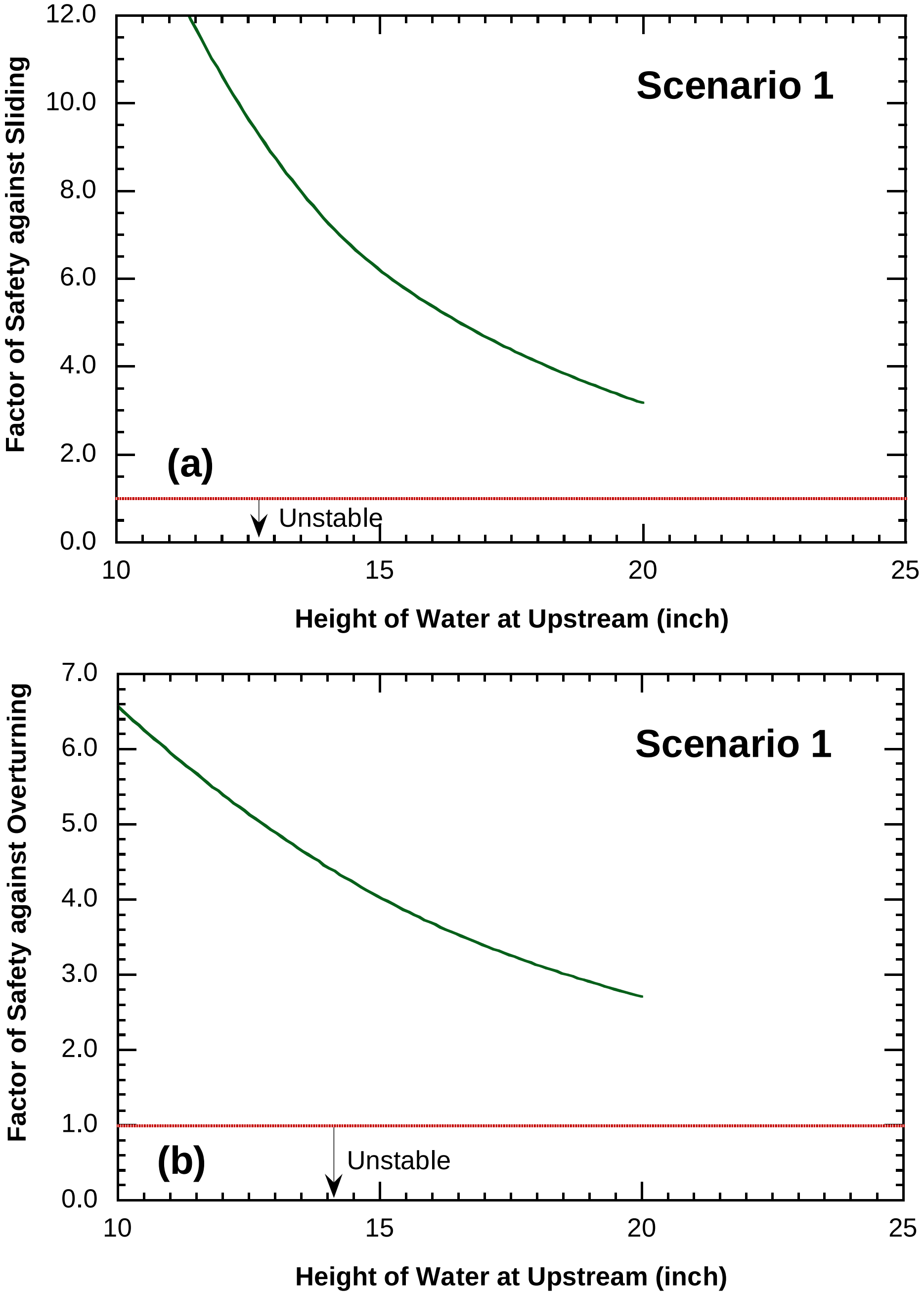

Figure 4.18. Factor of Safety against (a) Sliding and (b) Overturning for the LPCB for Flood Scenario 1.

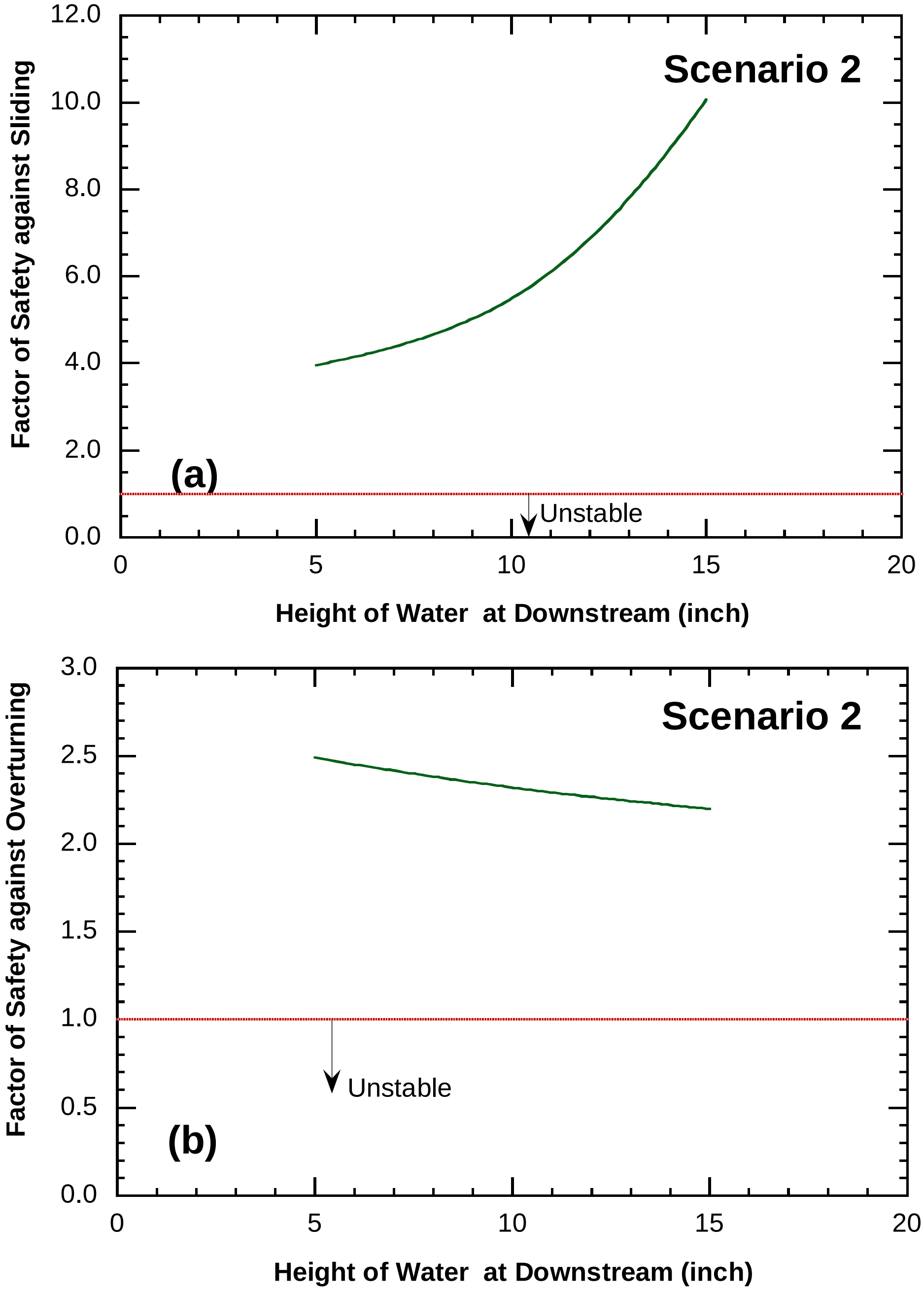

Figure 4.19. Factor of Safety against (a) Sliding and (b) Overturning for the LPCB for Flood Scenario 2.

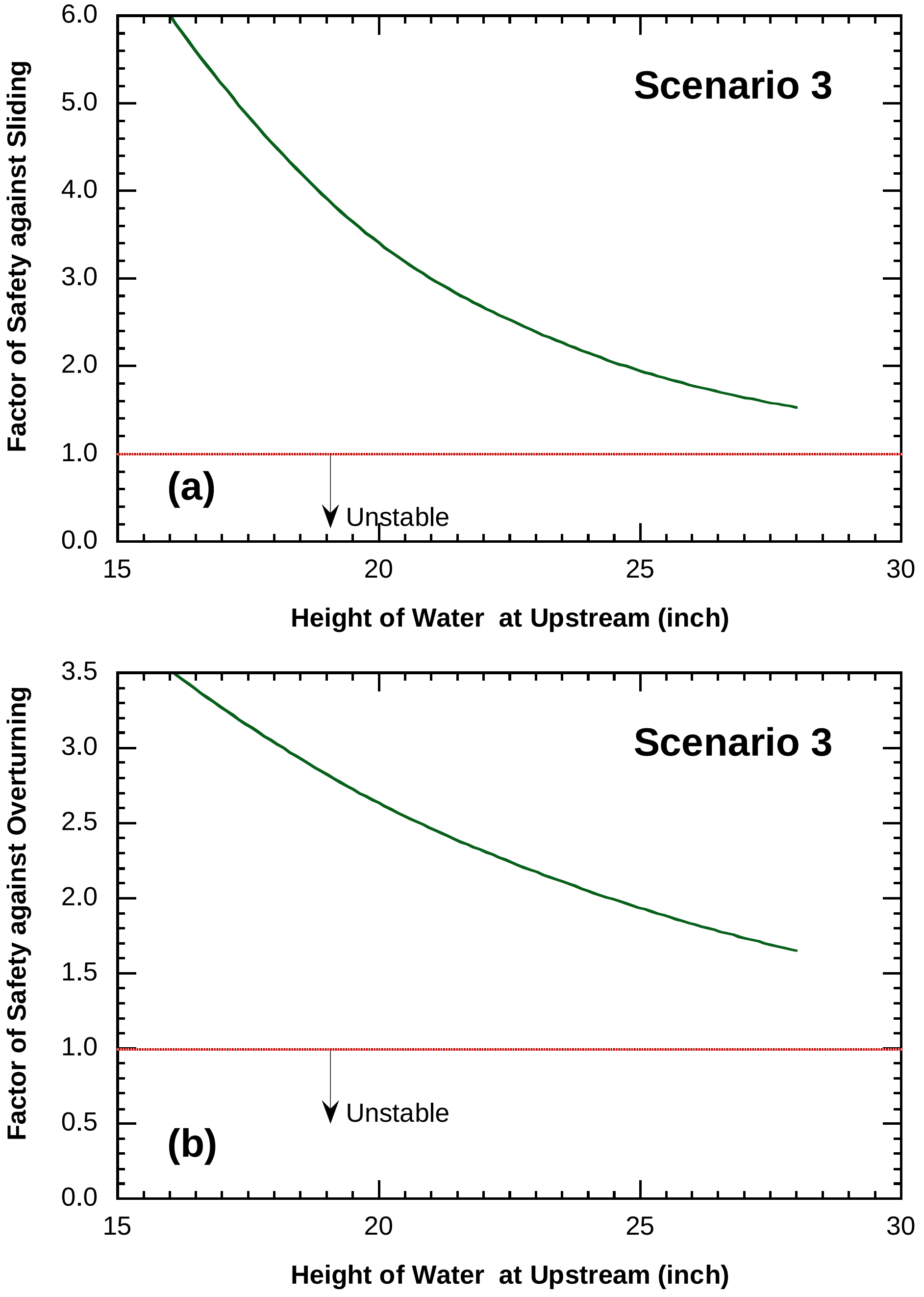

Figure 4.20. Factor of Safety against (a) Sliding and (b) Overturning for the LPCB for Flood Scenario 3.

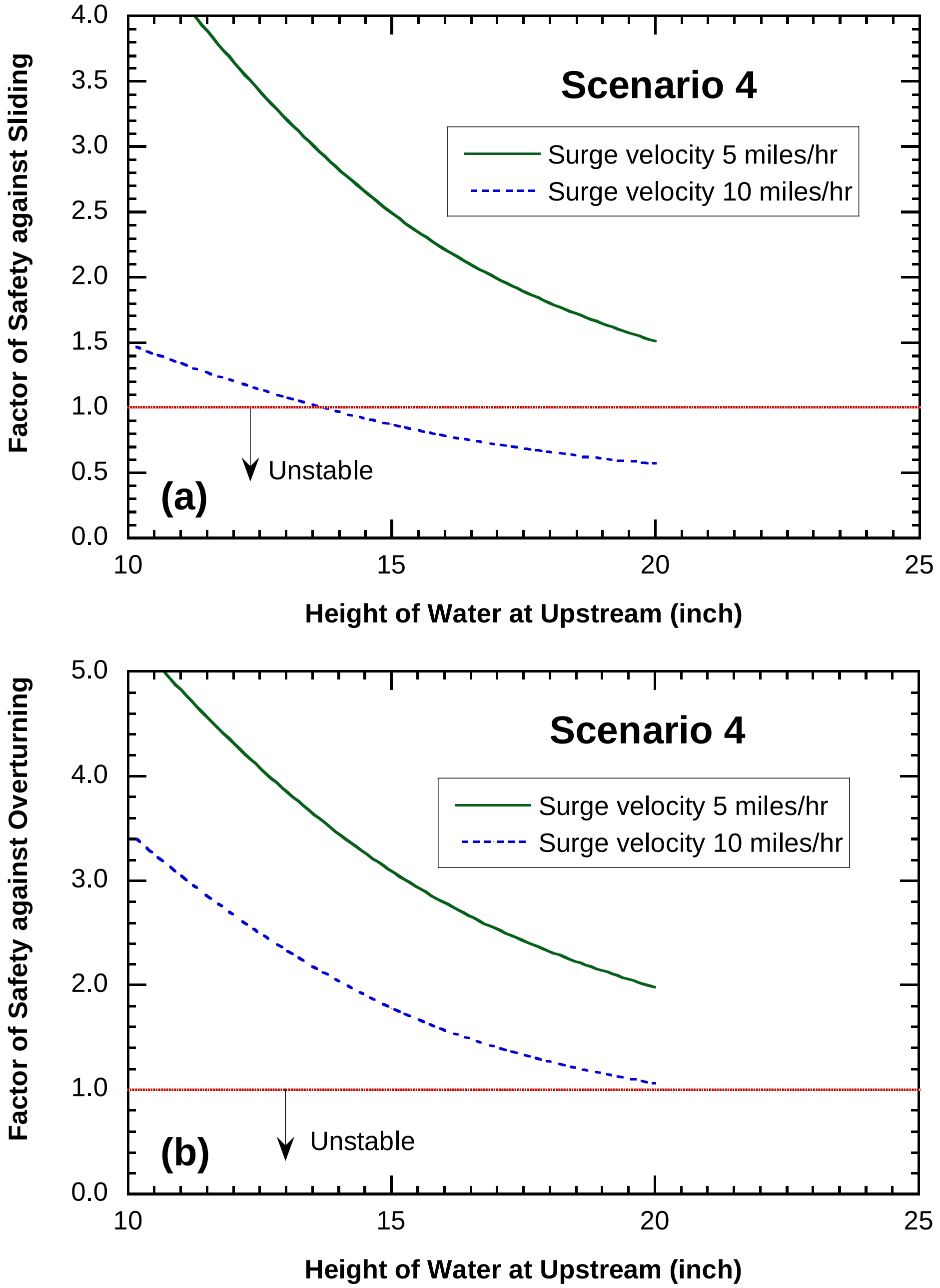

Figure 4.21. Factor of Safety against (a) Sliding and (b) Overturning for the LPCB for Flood Scenario 4.

CHAPTER 5: MODELING OF TCTBS USING HEC-RAS

5.1 INTRODUCTION

When designing highway drainage structures such as culverts and bridges, the hydraulic modeling software HEC-RAS (Hydrologic Engineering Center-River Analysis System) is often used in order to determine the water elevation that will result for various flows. Currently, if the water elevation overtops the roadway, the program can be set to calculate the flow using the pressure/weir method. In this calculation, the standard broad crested weir equation is used with a recommended value of 2.6 for the weir coefficient. However, when an obstruction such as a Temporary Concrete Traffic Barrier (TCTB) is placed on the roadway this coefficient will no longer will be applicable to describe that flow, because the barrier will act as an obstruction and will cause the upstream energy to increase compared to what would be calculated using the suggested weir coefficient. In order to model the effect that placing a barrier on the roadway will have, the weir coefficient can be modified to match an experimentally derived rating curve for the barrier that is going to be used. This section will explore how this can be accomplished by using two steady state example problems in HEC-RAS and the Concrete Safety Barrier (CSB (1)-04).

5.2 HYDRAULIC RATING CURVE

For the examples demonstrated in this chapter the CSB was selected as the barrier to be analyzed. The rating curve for this barrier has been reproduced below in Figure 5.1.

This rating curve is non-dimensional because it was developed using a half scale model of the barrier, and the parameters needed to be non-dimensional in order to relate the model to the actual barrier. This however, is also advantageous for modeling in HEC-RAS, because the non-dimensional form allows for the easy calculation of the flow rate and energy upstream for varying widths of barriers by simply inserting the known values.

5.3 HEC-RAS EXAMPLES

Several example problems are included when HEC-RAS Version 4.0 is downloaded from the United States Army Corps of Engineers website http://www.hec.usace.army.mil/software/hec-ras/. The two examples that this report will be using are the Single Bridge-Example 2 and ConSpan Culvert Example, which may be found by searching the default project folder where HEC-RAS data is stored. In the Single Bridge-Example 2 simulation a simpler procedure by which a flat roadway surface will be evaluated, and in the ConSpan Culvert Example a procedure will be developed by which barrier placement on a sloped roadway can be modeled. A sample screenshot showing the two examples is show below in Figure 5.2.

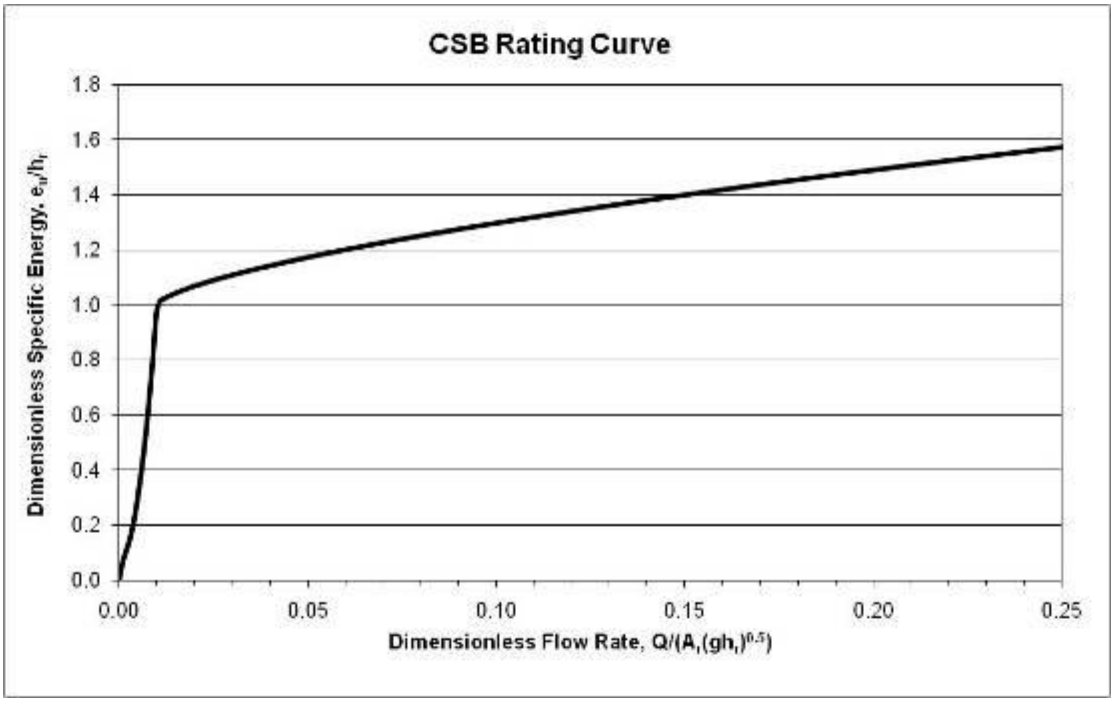

Figure 5.1. Rating Curve for CSB.

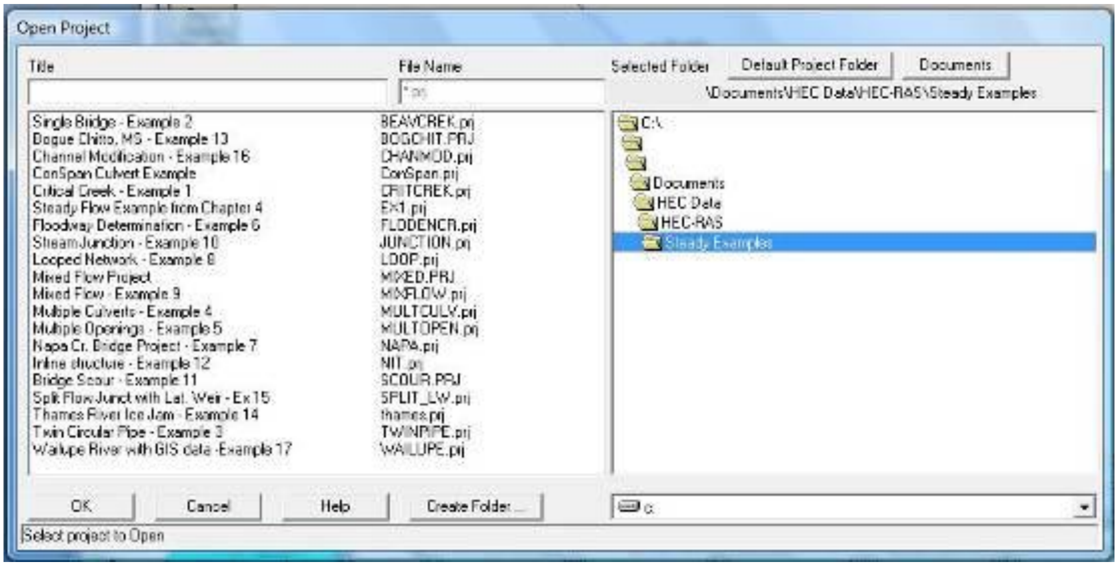

\Documents\HEC Data\HEC-RAS\Steady Examples

Title	File Name
Single Bridge - Example 2	BEAVCREK.prj
Bogue Chitto, MS - Example 13	BOGCHIT.PRJ
Channel Modification - Example 16	CHANMOD.prj
ConSpan Culvert Example	ConSpan.prj
Critical Creek - Example 1	CRITCREK.prj
Steady Flow Example from Chapter 4	EX1.prj
Floodway Determination - Example 6	FLODENCR.prj
Stream Junction - Example 10	JUNCTION.prj
Looped Network - Example 8	LOOP.prj
Mixed Flow Project	MIXED.PRJ
Mixed Flow - Example 9	MIXFLOW.prj
Multiple Culverts - Example 4	MULTCULV.prj
Multiple Openings - Example 5	MULTOPEN.prj
Napa Cr. Bridge Project - Example 7	NAPA.prj
Inline structure - Example 12	NIT.prj
Bridge Scour - Example 11	SCOUR.PRJ
Split Flow Junct with Lat. Weir - Ex 15	SPLIT_LW.prj
Thames River Ice Jam - Example 14	thames.prj
Twin Circular Pipe - Example 3	TWINPIPE.prj
Wailupe River with GIS data -Example 17	WAILUPE.prj

Select project to Open

Figure 5.2. HEC-RAS Open Project Screenshot.

5.4 HEC-RAS SINGLE BRIDGE-EXAMPLE 2

In the HEC-RAS Single Bridge-Example 2, a bridge with a level deck is used to show how a horizontal roadway surface might be modeled. The procedure was developed as part of TxDOT Research Project 0-5492 presented by Charbeneau et al. (2008). The procedure that this report uses for this example, however, can also be used to model the flow through a culvert with a horizontal roadway surface, because when modeling both structures the pressure/weir method is utilized. Furthermore, an iterative approach is necessary to solve this problem because as the weir coefficient changes so will the weir flow rate.

In the procedure developed by Charbeneau et al. (2008) the non-dimensional rating curve will be used to determine the dimensional weir coefficient used in HEC-RAS. In order to do this the general weir equation, Equation 7.1, can be transformed into a non-dimensional form, Equation 7.2. In Equation 7.1 (Q) is the flow rate over the weir, (C) is the dimensional weir coefficient, (L) is the length of the weir and (H) is the height over the weir. In Equation 7.2 the general equation has been algebraically transformed to be in terms of the non-dimensional flow rate and non-dimensional energy used in the rating curve and (C_w) has been given the subscript w to denote that it is the non-dimensional coefficient. Furthermore, the energy upstream of the barrier (e_u), which is the total energy minus the elevation of the deck, has been substituted for (H).

$$Q = CLH^{1.5} \tag{5.1}$$

$$\frac{Q}{L\sqrt{g{h_r}^3}} = C_w \left(\frac{e_u}{h_r}\right)^{1.5} \tag{5.2}$$

Where h_r is the height of the barrier minus the elevation of the deck as shown in Figure 3.2. By comparing the two equations it is possible to see that the relationship between the non-dimensional and dimensional coefficients is the square root of gravity. This relationship is shown below in Equation 7.3.

$$C = C_w\sqrt{g} \tag{5.3}$$

In the report by Charbeneau et al. (2008) the following procedure is outlined to solve the Single Bridge-Example 2 problem:

1. Run HEC-RAS with default weir coefficient C = 2.6 $ft^{0.5}/s$ (1.44 $m^{0.5}/s$), and obtain the flow rate over bridge deck (weir flow, Q_{weir}, provided by RAS).
2. Non-dimensionalize Q_{weir} with length of bridge crest (L provided by RAS as difference between left and right weir stations) and barrier height, h_r, using barrier of interest in the form of $\frac{Q}{L\sqrt{g{h_r}^3}}$.
3. Obtain dimensionless upstream specific energy for given dimensionless weir flow rate using rating curve from Figure 5.1. (Note: This can also be done by using the Enon Visual Basic script included in the Appendix)
4. Determine dimensionless weir coefficient, Cw, using Equation 5.2.
5. Determine dimensional RAS weir coefficient, C, using Equation 5.3.

6. Re-run HEC-RAS with new weir coefficient C.
7. Repeat steps 1 through 6 until RAS weir coefficient converges, typically within one percent relative error from the previous iteration.

The first step in this procedure is to run a steady flow simulation in HEC-RAS using a weir coefficient of 2.6. Once this is accomplished, the Bridge Output screen (Figure 5.3) can be opened and the required values ascertained. For this analysis, the values that are needed are: Q_{weir}, Weir Sta Lt, and Weir Sta Rt.

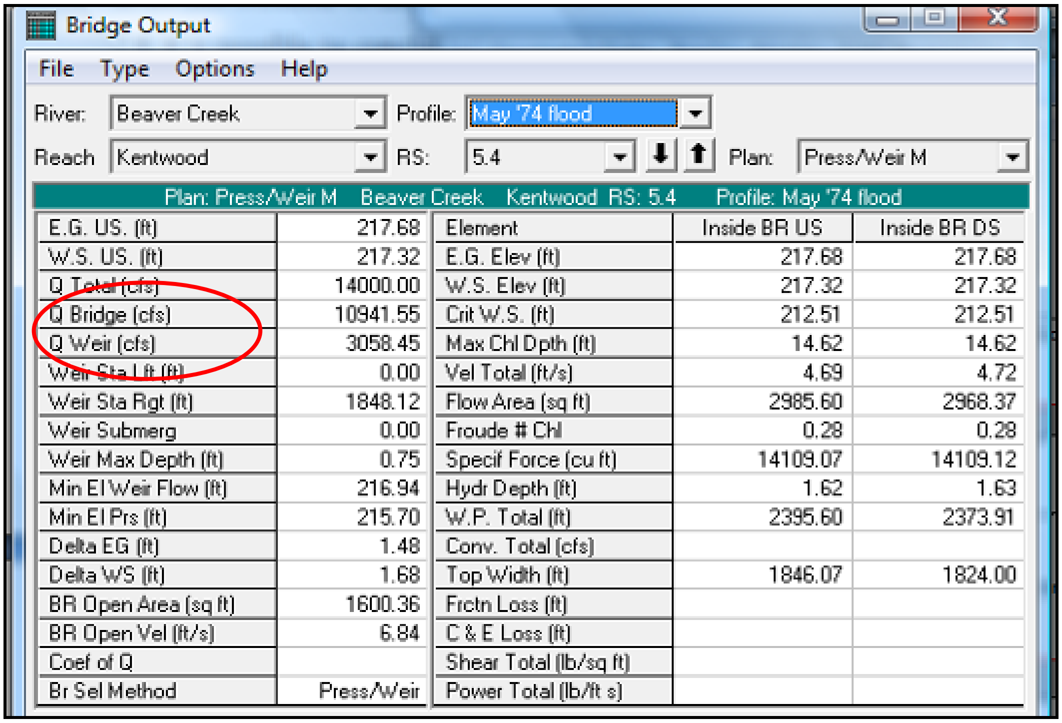

River: Beaver Creek
Profile: May '74 flood
Reach: Kentwood
RS: 5.4
Plan: Press/Weir M

Plan: Press/Weir M Beaver Creek Kentwood RS: 5.4 Profile: May '74 flood

E.G. US. (ft)	217.68	Element	Inside BR US	Inside BR DS
W.S. US. (ft)	217.32	E.G. Elev (ft)	217.68	217.68
Q Total (cfs)	14000.00	W.S. Elev (ft)	217.32	217.32
Q Bridge (cfs)	10941.55	Crit W.S. (ft)	212.51	212.51
Q Weir (cfs)	3058.45	Max Chl Dpth (ft)	14.62	14.62
Weir Sta Lft (ft)	0.00	Vel Total (ft/s)	4.69	4.72
Weir Sta Rgt (ft)	1848.12	Flow Area (sq ft)	2985.60	2968.37
Weir Submerg	0.00	Froude # Chl	0.28	0.28
Weir Max Depth (ft)	0.75	Specif Force (cu ft)	14109.07	14109.12
Min El Weir Flow (ft)	216.94	Hydr Depth (ft)	1.62	1.63
Min El Prs (ft)	215.70	W.P. Total (ft)	2395.60	2373.91
Delta EG (ft)	1.48	Conv. Total (cfs)		
Delta WS (ft)	1.68	Top Width (ft)	1846.07	1824.00
BR Open Area (sq ft)	1600.36	Frctn Loss (ft)		
BR Open Vel (ft/s)	6.84	C & E Loss (ft)		
Coef of Q		Shear Total (lb/sq ft)		
Br Sel Method	Press/Weir	Power Total (lb/ft s)		

Figure 5.3. HEC-RAS Bridge Output.

The critical values for subsequent iterations are shown in Table 5.1. With these values, Steps 1 and 2 can be accomplished. For the example analysis done in this report, Step 3 was then completed by using the Enon function in Excel (as shown in Appendix D) to calculate the non-dimensional energy predicted by the rating curve (value = 1.209). Now that the non-dimensional energy and non-dimensional flow rate have been calculated, Equations 5.2 and 5.3 can be used to calculate a new value for the HEC-RAS weir coefficient of 0.272. Table 5.2 below shows the results of this procedure for the seven iterations necessary in order for the weir coefficient to converge. By comparing the upstream energy (e_u) in the last iteration to that computed in the initial HEC-RAS run with a weir coefficient of 2.6, it is possible to conclude that placing the barrier on the bridge surface will result in an increase of energy of 2.26 ft and a corresponding decrease of 1811.02 cfs in the weir flow rate.

Table 5.1. HEC-RAS Initial Summary.

Parameters	Input Value
C	2.6
High Chord (ft)	216.93
U.S. E_u (ft)	217.68
U.S. e_u (ft)	0.75
Q_{weir} (cfs)	3058.45
h_r (ft)	2.75
L (ft)	1848.12

Table 5.2. Single Bridge-Example 7 Iterations.

Step	Parameters	Iterations						
		1	2	3	4	5	6	7
(Step 1)	**Q_{weir} (cfs)**	3058.5	1767.0	1446.9	1329.5	1283.5	1258.4	1247.4
	L (ft)	1848.1	1849.2	1849.4	1849.5	1849.5	1849.6	1849.6
(Step 2)	**$Q/L(gh_r^3)^{0.5}$**	0.064	0.037	0.030	0.028	0.027	0.026	0.026
(Step 3)	**e_u/h_r**	1.209	1.131	1.108	1.099	1.096	1.093	1.093
	e_u (ft)	3.325	3.111	3.047	3.023	3.013	3.007	3.006
(Step 4)	**C_w**	0.048	0.031	0.026	0.024	0.023	0.023	0.023
(Step 5)	**C ($ft^{0.5}/s$)**	0.272	0.174	0.147	0.137	0.133	0.130	0.129

The final weir coefficient C = 0.129 $ft^{0.5}/s$ will likely appear too small. Typical weir coefficient values for use with Equation 5.1 range from 2.5 to 3.1 (US Customary units), with the HEC-RAS default value C = 2.6. The apparent difficulty lies primarily with choice of datum. Standard application of HEC-RAS would take the top of the rail or barrier as the upper chord of the bridge. For this example with h_r = 2.75 ft, the high chord would be 216.93 + 2.75 = 219.68 ft. The head on this high chord corresponding to the final e_u value is $H = e_u - h_r = 0.256$ ft. With the default weir coefficient, this standard application would give a weir discharge $Q_{weir} = C\,L\,H^{1.5} = 2.6 \times 1850 \times (0.256)^{1.5} = 620$ cfs, which is approximately half the magnitude calculated in this example. In order for a standard application of HEC-RAS to provide the results presented herein, a weir coefficient value $C = Q_{weir}/[L\,H^{1.5}] = 5.21$ would need to be used, which is significantly larger than the expected range of values. Based on this discussion it is concluded that a standard application of HEC-RAS will predict a larger upstream headwater (when typical weir coefficient values are used).

5.5 HEC-RAS CONSPAN CULVERT EXAMPLE

In this section, the procedure for solving the weir coefficient necessary to simulate placement of the CSB (1)-04 TCTB in the Single ConSpan Culvert Example will be presented. The main difference between this and the previous example is that the roadway is not flat and energy over the roadway is used to determine flow rate, rather than using the weir flow rate to determine the energy Similar to the Single Bridge-Example 2 procedure, this example uses an iterative approach in order to balance the flow rate and water elevation calculated in HEC-RAS with the values that are obtained using the data from the rating curve.

5.5.1 HEC-RAS Example Modifications

In the ConSpan Culvert Example a single barrel Conspan arched pipe is used to transmit water from one side of the roadway to the other. One modification is necessary to this example problem to ensure that weir flow is developed. The example problem comes preloaded with flow data corresponding to the 5, 10, 25, and 50 year floods. The greatest flow rate, which is 1000 cfs (50 year flood) does not result in water overtopping the roadway. For the example presented in this report, a value of 2000 cfs was entered to make it more obvious that the water level to rise above the height of the roadway. An example screenshot of the modifications to the steady state flow data is shown in Figure 5.4.

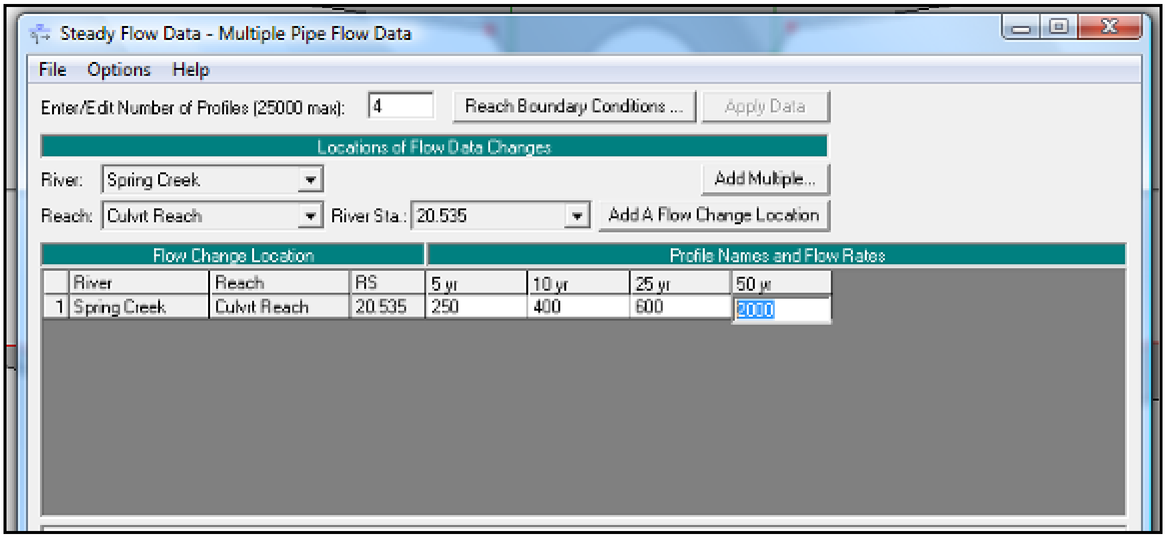

Enter/Edit Number of Profiles (25000 max): 4

River: Spring Creek

Reach: Culvrt Reach

River Sta.: 20.535

	River	Reach	RS	5 yr	10 yr	25 yr	50 yr
1	Spring Creek	Culvrt Reach	20.535	250	400	600	2000

Figure 5.4. HEC-RAS Example Flow Alteration.

5.5.2 ConSpan Culvert Procedure

As stated earlier, in order to solve for the weir coefficient that describes the flow over a roadway with barriers, an iterative procedure must be used. The first step in this procedure is to obtain the flow rate over the roadway as if the barrier were not there. This is done by performing a steady flow simulation in HEC-RAS with the weir coefficient initially set to the recommended value of 2.6 (Note: This should be the default value already entered in the Conspan example). After this analysis is completed, the culvert output table can be opened and the values needed for the subsequent calculations can be garnered. The culvert output for this analysis is presented below as Figure 5.5. The values that are of most importance in this table are: weir flow (Q Weir), the left and right limits of the weir flow (Weir Sta Lft/Rgt), and upstream energy (U.S. E.G.).

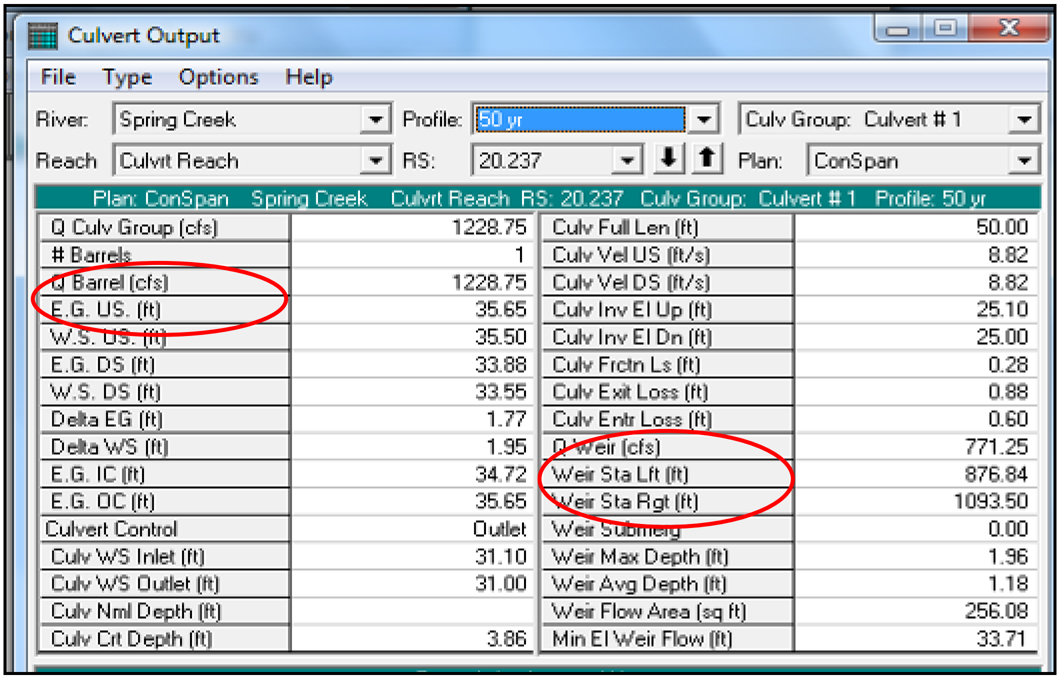

River: Spring Creek
Profile: 50 yr
Culv Group: Culvert # 1
Reach: Culvrt Reach
RS: 20.237
Plan: ConSpan

Plan: ConSpan   Spring Creek   Culvrt Reach RS: 20.237   Culv Group: Culvert # 1   Profile: 50 yr

Q Culv Group (cfs)	1228.75	Culv Full Len (ft)	50.00
# Barrels	1	Culv Vel US (ft/s)	8.82
Q Barrel (cfs)	1228.75	Culv Vel DS (ft/s)	8.82
E.G. US. (ft)	35.65	Culv Inv El Up (ft)	25.10
W.S. US. (ft)	35.50	Culv Inv El Dn (ft)	25.00
E.G. DS (ft)	33.88	Culv Frctn Ls (ft)	0.28
W.S. DS (ft)	33.55	Culv Exit Loss (ft)	0.88
Delta EG (ft)	1.77	Culv Entr Loss (ft)	0.60
Delta WS (ft)	1.95	Q Weir (cfs)	771.25
E.G. IC (ft)	34.72	Weir Sta Lft (ft)	876.84
E.G. OC (ft)	35.65	Weir Sta Rgt (ft)	1093.50
Culvert Control	Outlet	Weir Submerg	0.00
Culv WS Inlet (ft)	31.10	Weir Max Depth (ft)	1.96
Culv WS Outlet (ft)	31.00	Weir Avg Depth (ft)	1.18
Culv Nml Depth (ft)		Weir Flow Area (sq ft)	256.08
Culv Crt Depth (ft)	3.86	Min El Weir Flow (ft)	33.71

Figure 5.5. ConSpan Culvert Output (C=2.6).

With these numbers it is then possible to perform the first iteration. In order to do this we must first approximate the roadway as a series of horizontal crested weirs. This is because the equation that describes the flow over a weir is based on flow over a horizontal surface; however, the roadway is sloped. For this example problem the roadway was broken into 5 equal length weirs, with outside of the outmost left and right weirs placed at the Weir Sta Lft and Weir Sta Rgt locations. Furthermore, the elevation of each weir approximation was taken to be the average of the left and right roadway elevations of each weir segment. Figure 5.6 below, shows the roadway cross-section, the weir approximation and the U.S. E.G. for the first analysis with the Weir Coefficient (C) equal to 2.6. Now that the roadway has been approximated as a set of horizontal weirs.

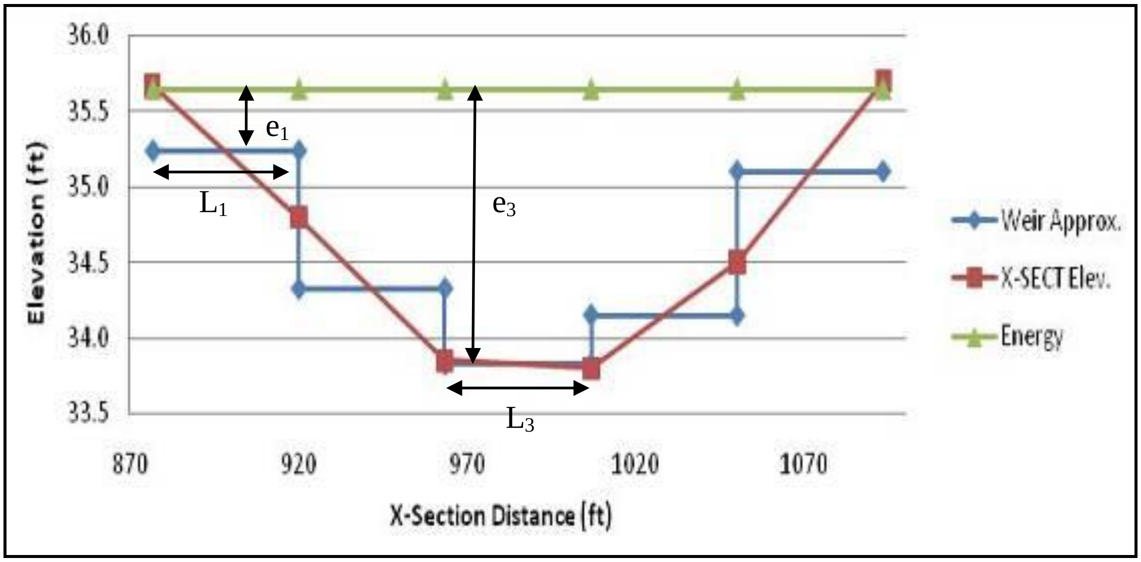

Figure 5.6. Weir Approximations.

An example of this calculation done in Excel is shown below in Table 5.3. The values in Table 5.3 were interpolated from the roadway elevations given below. The reason that they were interpolated was because the weir approximation left and right positions will not line up perfectly with the elevations given. The roadway elevations given in Figure 5.6 are from this interpolation. If the reader wants the elevations all they have to do is look at Table 5.3. The left STA, right STA, X-Sect elev. left, and X-Sect elev. right columns give all the information needed.

The following iterative procedure can be followed in order to determine the weir coefficient value:

1. Calculate the energy (e) over each section by subtracting the i^{th} weir elevation $(W.E.)_i$ from the U.S. E.G (Column 1 Table 5.3).
2. The next calculation (Column 2 Table 5.3) is then to convert this energy to the non-dimensional form used in the rating curve by simply dividing by the height of the barrier (h_r).
3. With the non-dimensional energy over each weir and the rating curve, it is then possible to find the non-dimensional flow (Column 3 Table 5.3) over each weir (Note: This can be done by simply interpolating from Figure 5.1 or by using the visual basic script provided in the Appendix D).
4. Next, the flow rate (Column 4 Table 5.3) over each weir segment can be calculated by simply solving for the actual flow rate (Q) through substituting the height of the barrier (h_r) into the non-dimensional equation. Since Qnon = Q/(L*(gh_r^3).5), it is possible to rearrange this equation to solve for Q.
5. Furthermore, a dimensional weir coefficient (Column 5 Table 5.3) can be calculated for each weir segment by rearranging the weir equation ($Q=CLH^{1.5}$, where H equals the energy (e_i) over the weir).
6. Finally, the value of the weir coefficient for the next iteration can be calculated by taking the average of the coefficients for each weir approximation.

It should be noted that the total weir flow rate (summation of column 4) is equal to 31.78 cfs, and that this value is less than 771.25 cfs, which was reported by HEC-RAS. The purpose of the subsequent iterations will be to determine a weir coefficient that accurately models the flow past the barrier based on the rating curve with a flow rate equal to the weir flow rate calculated in HEC-RAS.

In Table 5.3, the X-SECT Elev. LT is different from the X-SECT Elev. RT because X-SECT Elev. LT is the elevation of the roadway surface at the same x-sect distance as the left side of the ith weir approximation and X-SECT Elev. RT is the roadway surface elevation at the same x-sect distance as the right side of the ith weir approximation. These values were used in order to get the average elevation of each weir approximation.

Table 5.3. ConSpan Calculations in Excel (1st Iteration).

				X-SECT			**(1)**	**(2)**	**(3)**	**(4)**	**(5)**
	Length (ft)	**Left STA** (ft)	**Right STA** (ft)	**Elev. LT** (ft)	**Elev. RT** (ft)	**Avg. Elev.** (ft)	**e_i** (ft)	**e_i/h_r** (ft/ft)	**Qnon**	**Q** (cfs)	**C** ($ft^{0.5}/s$)
L_1	43.3	876.8	920.2	35.67	34.80	35.24	0.41	0.151	0.003	3.18	0.274
L_2	43.3	920.2	963.5	34.80	33.85	34.33	1.33	0.482	0.007	7.47	0.113
L_3	43.3	963.5	1006.8	33.85	33.80	33.83	1.83	0.664	0.008	8.99	0.084
L_4	43.3	1006.8	1050.2	33.80	34.50	34.15	1.50	0.545	0.007	8.04	0.101
L_5	43.3	1050.2	1093.5	34.50	35.70	35.10	0.55	0.200	0.004	4.11	0.232
									Average C =		0.161
									Q Total =		31.78

5.5.3 ConSpan Second Iteration

The procedure for the second iteration is the same as what was done in the first iteration with the exception that the weir coefficient used in HEC-RAS should now be set equal to 0.161. If this value is used, a culvert output similar to Figure 5.7 will be obtained. Using these values and the procedure employed in the first iteration, a new weir coefficient value of 0.265 should then be attained along with a total flow rate of 515.14 cfs. An example of the calculations completed for the second iteration is shown below in Table 5.4.

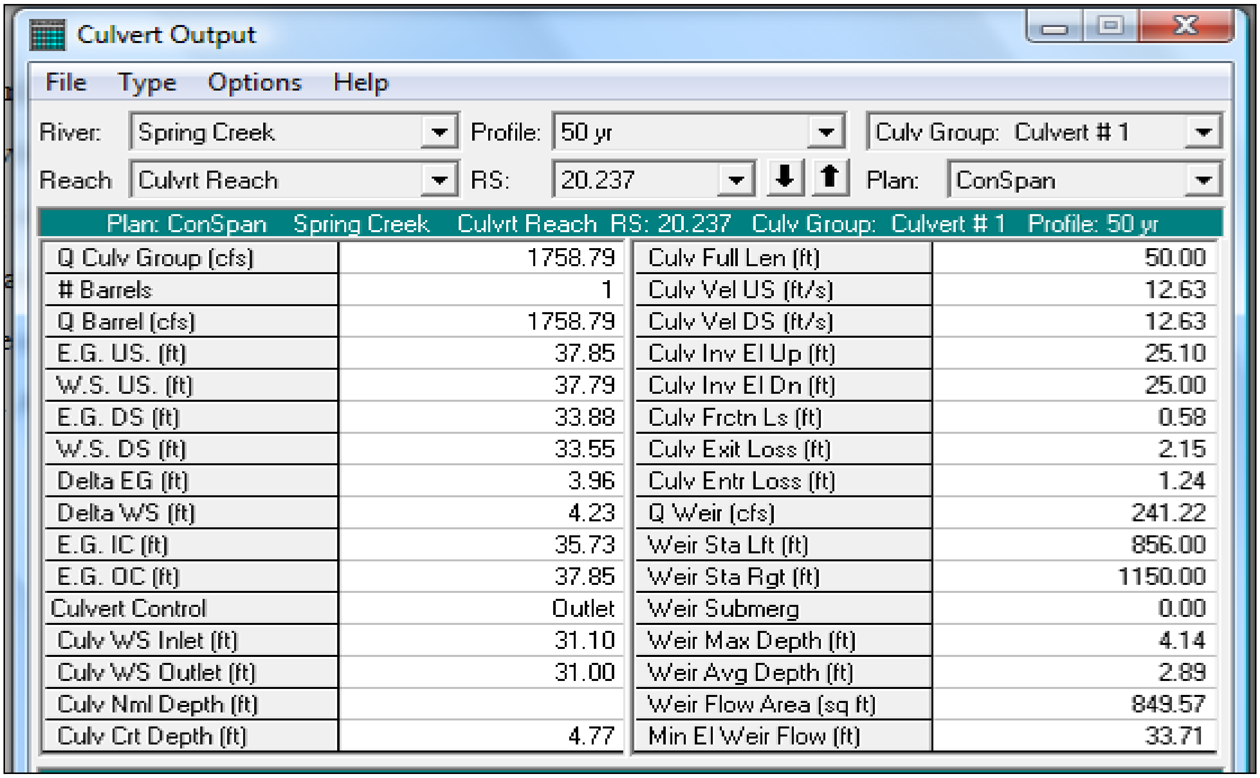

River: Spring Creek
Profile: 50 yr
Culv Group: Culvert # 1
Reach: Culvrt Reach
RS: 20.237
Plan: ConSpan

Plan: ConSpan Spring Creek Culvrt Reach RS: 20.237 Culv Group: Culvert # 1 Profile: 50 yr

Q Culv Group (cfs)	1758.79	Culv Full Len (ft)	50.00
# Barrels	1	Culv Vel US (ft/s)	12.63
Q Barrel (cfs)	1758.79	Culv Vel DS (ft/s)	12.63
E.G. US. (ft)	37.85	Culv Inv El Up (ft)	25.10
W.S. US. (ft)	37.79	Culv Inv El Dn (ft)	25.00
E.G. DS (ft)	33.88	Culv Frctn Ls (ft)	0.58
W.S. DS (ft)	33.55	Culv Exit Loss (ft)	2.15
Delta EG (ft)	3.96	Culv Entr Loss (ft)	1.24
Delta WS (ft)	4.23	Q Weir (cfs)	241.22
E.G. IC (ft)	35.73	Weir Sta Lft (ft)	856.00
E.G. OC (ft)	37.85	Weir Sta Rgt (ft)	1150.00
Culvert Control	Outlet	Weir Submerg	0.00
Culv WS Inlet (ft)	31.10	Weir Max Depth (ft)	4.14
Culv WS Outlet (ft)	31.00	Weir Avg Depth (ft)	2.89
Culv Nml Depth (ft)		Weir Flow Area (sq ft)	849.57
Culv Crt Depth (ft)	4.77	Min El Weir Flow (ft)	33.71

Figure 5.7. ConSpan Culvert Output 2 (C=0.161).

Table 5.4. ConSpan Calculations in Excel (2nd Iteration).

							(1)	**(2)**	**(3)**	**(4)**	**(5)**
	Length (ft)	**Left STA** (ft)	**Right STA** (ft)	**X-SECT Elev. LT** (ft)	**X-SECT Elev. RT** (ft)	**Avg. Elev.** (ft)	**e_i** (ft)	**e_i/h_r** (ft/ft)	**Qnon**	**Q** (cfs)	**C** ($ft^{0.5}/s$)
L_1	58.8	856.0	914.8	36.10	34.80	35.45	2.4	0.87	0.009	14.21	0.065
L_2	58.8	914.8	973.6	34.80	33.90	34.35	3.5	1.27	0.090	136.65	0.355
L_3	58.8	973.6	1032.4	33.90	33.70	33.80	4.1	1.47	0.191	290.89	0.607
L_4	58.8	1032.4	1091.2	33.70	35.70	34.70	3.2	1.15	0.041	62.91	0.191
L_5	58.8	1091.2	1150.0	35.70	37.20	36.45	1.4	0.51	0.007	10.47	0.108
										Average C =	0.265
										Q Total =	515.14

5.5.4 ConSpan Results

A graph of the results of the first four iterations is presented below in Figure 5.8. After four iterations it can be seen that a solution converges around a weir coefficient value of 0.246. At this value the flow rate and water elevations developed in HEC-RAS and by the rating curve produce similar results. The final flow rate over the roadway and the upstream energy can then be calculated by inserting a value of 0.246 for the weir coefficient in HEC-RAS. The result is a flow rate of 311.07 cfs and an upstream energy at the barrier of 37.51 ft. The original flow rate calculated without the barrier placement was 771.25, and the upstream energy was 35.65 ft. By placing the barrier, the flow rate over the roadway will then decrease by 460.18 cfs and the upstream energy will increase by 1.86 ft.

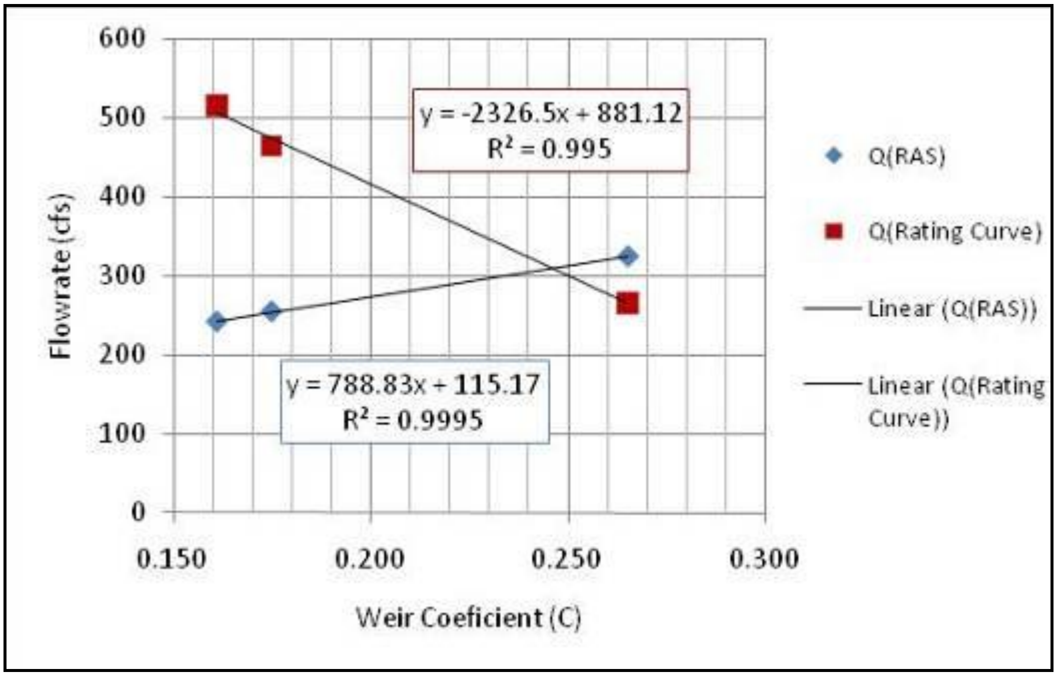

Figure 5.8. Plot of Calculated Flow Rates vs. Weir Coefficients.

5.6 CONCLUSIONS

This chapter has shown that it is possible to modify the weir coefficient value in HEC-RAS in order to hydraulically model the placement of a concrete traffic barrier on the roadway surface. To do this, an iterative procedure must be used. Two example problems, the Single Bridge-Example 2 and ConSpan Culvert have been demonstrated with the Concrete Safety Barrier (CSB(1)-04) in this report. In the Single Bridge-Example 2 procedure an increase in the upstream energy of 2.25 ft and a decrease in the weir flow rate of 1811.02 cfs occurred as a result of barrier placement. Furthermore, through the ConSpan example it can be seen that placing the barrier on the roadway will result in the upstream energy increasing by 1.86 ft and the flow rate decreasing by 460.18 cfs.

CHAPTER 6: PARAMETRIC STUDY

6.1 INTRODUCTION

The stability of TCTBs was calculated for different flood scenarios. Most of the factors that can affect the stability were considered for the calculation for factor of safety. However, the most two important factors that can vary in the field and might have significant effect on stability has been used for parametric study.

6.2 PARAMETRIC STUDY

6.2.1 Parametric Study Considering Cross Slope of the Roadway

A parametric study has been performed to evaluate how the factor of safety against sliding and overturning changes due to change in cross slope of the roadway. Cross slopes of 0°, 3°, 5°, and 8° are considered for the parametric study for flood scenarios 1 and 2 for all of the four TCTBs. Since most of the TCTBs are unstable for flood scenarios 3 and 4 for a cross slope of 0°, it is assumed that they will also be unstable for higher cross slopes.

6.2.1.1 Single Slope Concrete Barrier

The effect of cross slope on factor of safety against sliding and overturning of a SSCB for flood scenarios 1 and 2 is shown in Figures 6.1 and 6.2, respectively. Figures 6.1 and 6.2 show that the factor of safety against sliding and overturning decreases as the cross slope increases for both the flood scenarios. Thus, the SSCBs are more vulnerable against sliding or overturning when the cross slope increases.

Figure 6.1 shows that the factor of safety against sliding becomes less than 1 when the upstream water height is more than 34 in. for a cross slope 8° compared to the upstream water height is more than 39 in. for a cross slope 0°. Thus, the SSCBs can start sliding when the upstream water height is more than 34 in. (instead of 39 in.) when the cross slope changes from 0° to 8°. The factor of safety against overturning decreases as the cross slope increases. However, the factor of safety against overturning always remains more than 1 for flood scenario 1. Thus, the SSCBs are stable when the upstream water height is less than 39 in. for a cross slope 0°, 37.5 in. for a cross slope 3°, 36 in. for a cross slope 5°, and 34 in. for a cross slope 8°.

Figure 6.2 represents the flood scenario 2, which shows that the factor of safety against sliding is always less than 1 when the downstream water height is less than 24 in. for any cross slopes (0°-8°). The factor of safety against overturning is always higher than 1 for a cross slope 0°, but it is only higher than 1 when the downstream water height is more than 24 in. for cross slope of 8°.

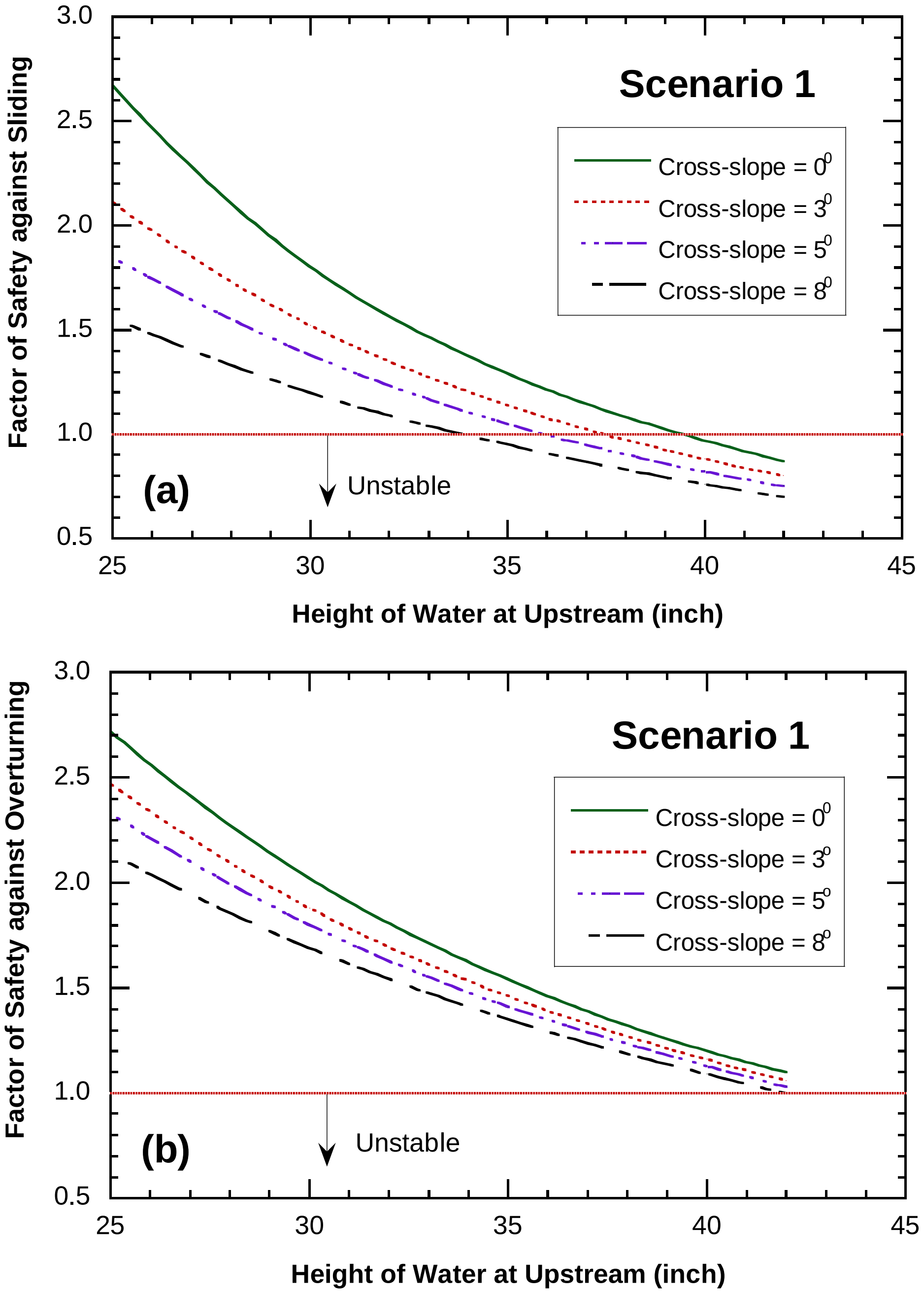

Figure 6.1. Effect of Cross Slope on Factor of Safety against (a) Sliding and (b) Overturning for the SSCB for Flood Scenario 1.

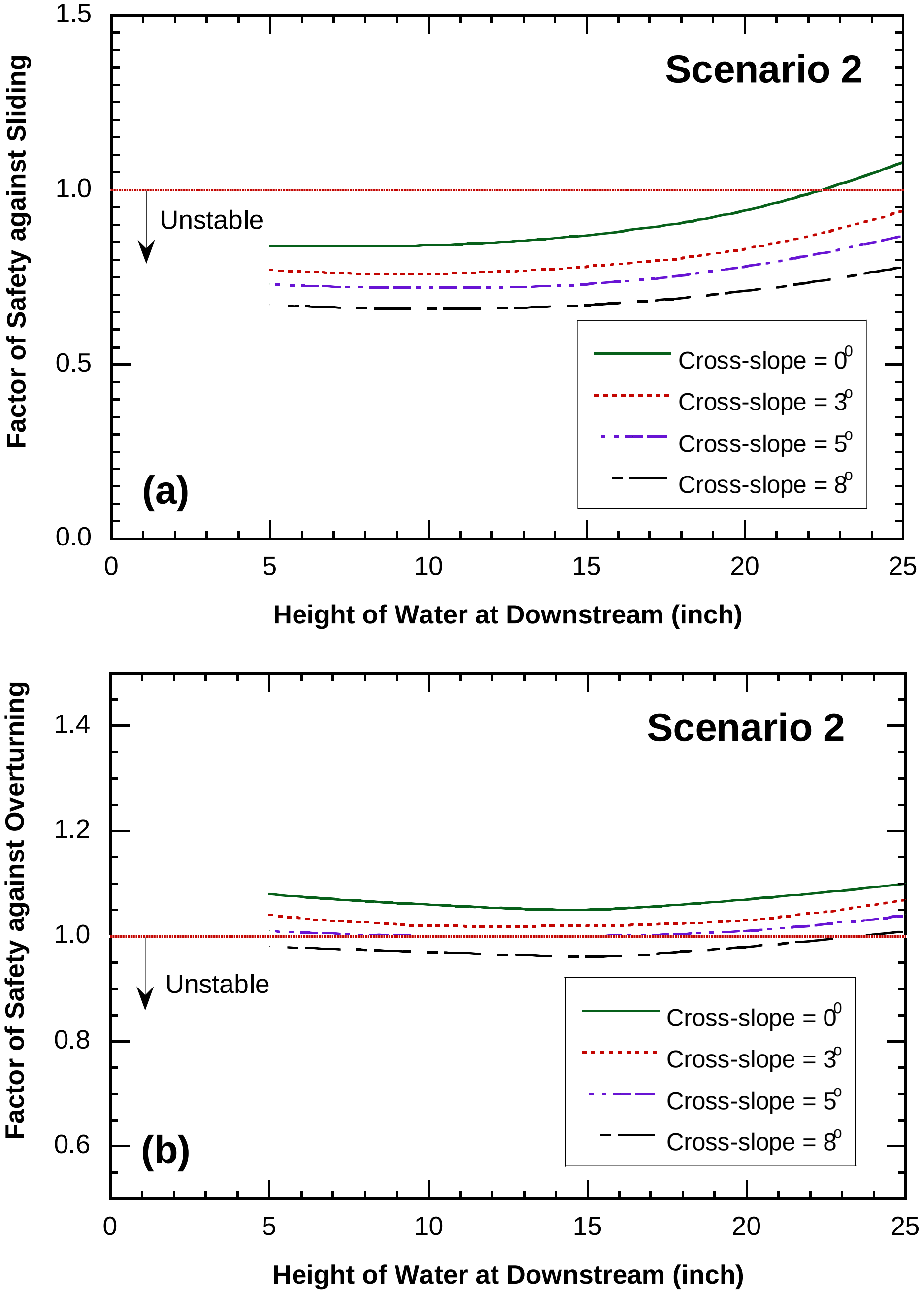

Figure 6.2. Effect of Cross Slope on Factor of Safety against (a) Sliding and (b) Overturning for the SSCB for Flood Scenario 2.

6.2.1.2 F-Shaped Concrete Safety Barrier (CSB)

The effect of cross slope on factor of safety against sliding and overturning of a CSB for flood scenarios 1 and 2 is shown in Figures 6.3 and 6.4, respectively. Similar to SSCB, the factor of safety of CSB against sliding and overturning decreases as the cross slope increases for both the flood scenarios. Thus, the stability of CSB is more vulnerable against sliding or overturning when the cross slope increases.

Figure 6.3 represents the flood scenario 1, which shows that the factor of safety against sliding is always higher than 1 when the cross slope is 0°, but it becomes less than 1 when the upstream water height is more than 28 in. for a cross slope 8°. Thus, the CSBs are stable for a cross slope of 0°, but can be unstable (start sliding) when the upstream water height is more than 28 in. when the cross slope changes from 0° to 8°. The factor of safety against overturning decreases as the cross slope increases. However, the factor of safety against overturning always remains more than 1 for flood scenario 1. Thus, the stability of CSB is controlled by the factor of safety against sliding and the CSB is always stable for flood scenario 1 when the cross slope is 0°, but it can become unstable when the cross slope changes to 8°.

Figure 6.4 represents the flood scenario 2 which shows that the factor of safety against sliding is always less than 1 when the downstream water height is less than 15 in. for a cross slopes of 0°. As the cross slope changes from 0° to 8°, the factor of safety against sliding remains less than 1 until the downstream water height is less than 22 in. The factor of safety against overturning is always higher than 1 for any cross slope (0° to 8°) for flood scenario 2. Similar to the flood scenario 1, the stability of CSB is controlled by the factor of safety against sliding. The CSB is stable when the downstream water height is less than 15 in. for a cross slopes of 0° or the downstream water height is less than 22 in. for a cross slopes of 8°.

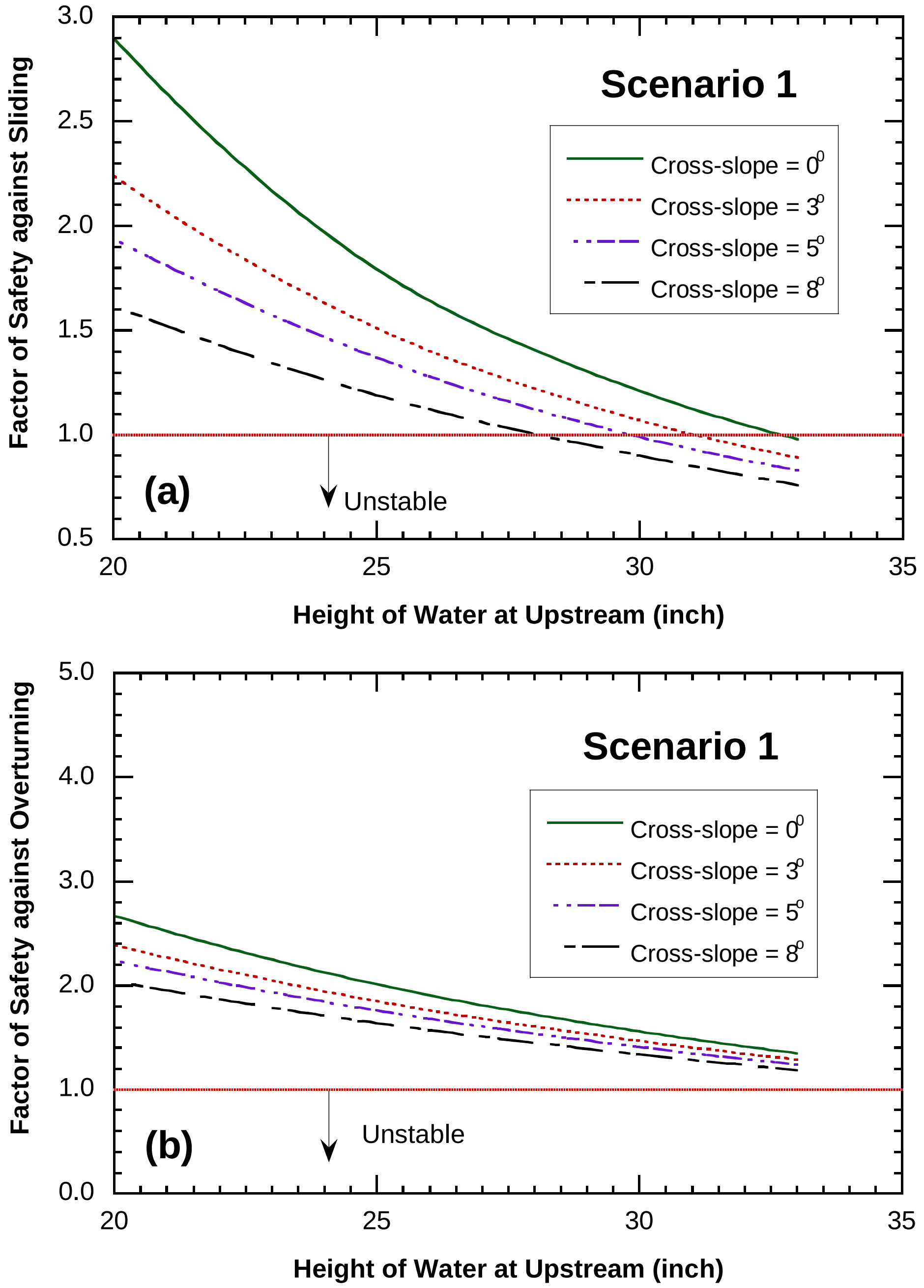

Figure 6.3. Factor of Safety against (a) Sliding and (b) Overturning for the CSB for the Flood Scenario 1.

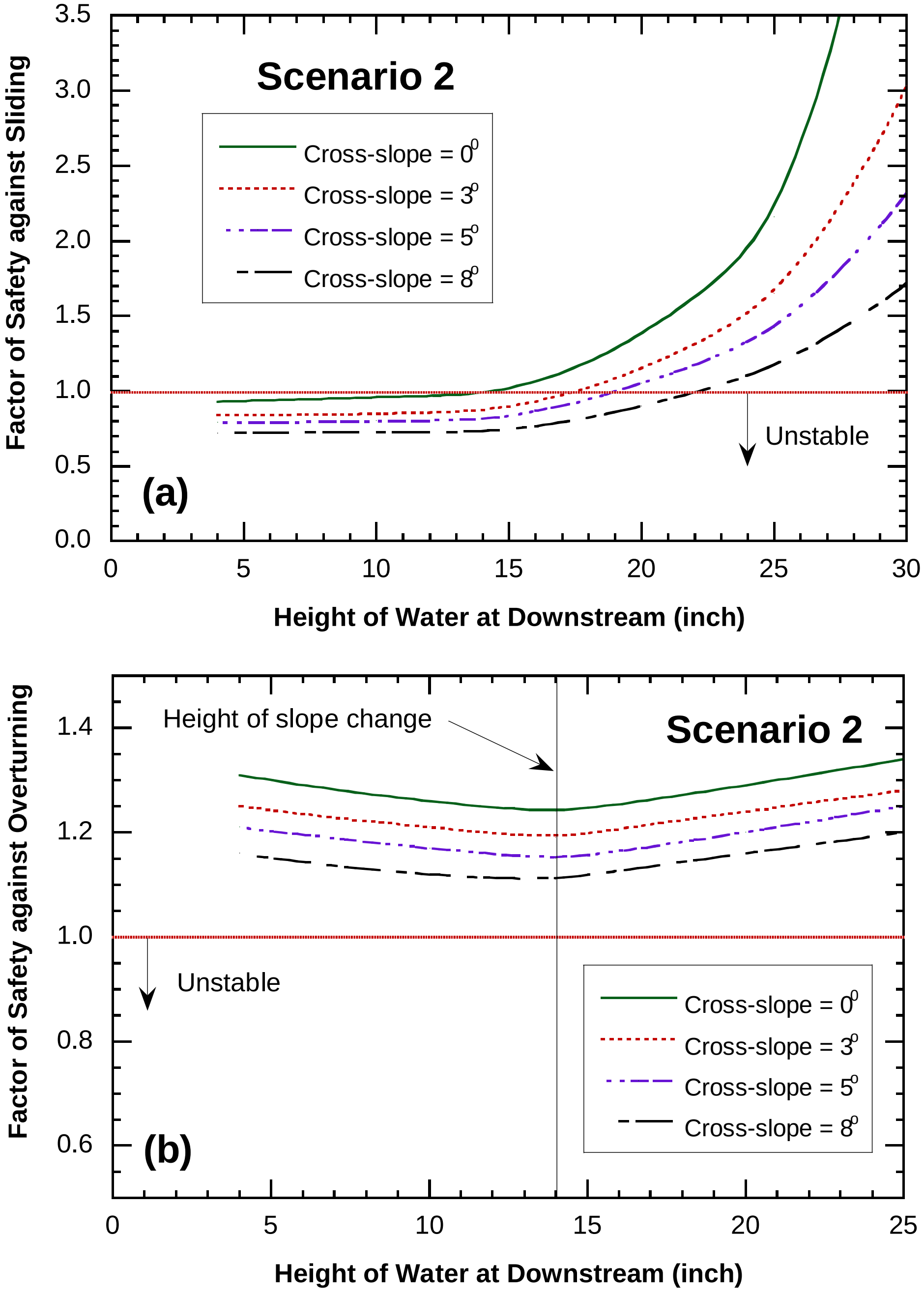

Figure 6.4. Factor of Safety against (a) Sliding and (b) Overturning for the CSB for the Flood Scenario 2.

6.2.1.3 Modified Single Slope Concrete Barrier (MSSCB)

The effect of cross slope on factor of safety against sliding and overturning of a MSSCB for flood scenarios 1 and 2 is shown in Figures 6.5 and 6.6, respectively. Similar to SSCB and CSB, the factor of safety against sliding and overturning of MSSCB decreases as the cross slope increases for both the flood scenarios.

Figure 6.5 represents the flood scenario 1 which shows that the factor of safety against sliding is always higher than 1 when the cross slope is 0°, but it becomes less than 1 when the upstream water height is more than 36 in. for a cross slope of 8°. Thus, the MSSCBs are stable for a cross slope of 0°, but can be unstable (start sliding) when the upstream water height is more than 36 in. when the cross slope changes from 0° to 8°. The factor of safety against overturning decreases as the cross slope increases. However, the factor of safety against overturning always remains more than 1 for flood scenario 1. Thus, the stability of MSSCB is controlled by the factor of safety against sliding and the MSSCB is always stable for flood scenario 1 when the cross slope is 0°, but it can become unstable when the cross slope changes from 0° to 8°.

Figure 6.6 represents the flood scenario 2, which shows that the factor of safety against sliding is always less than 1 when the downstream water height is less than 20 in. for a cross slopes of 0°. As the cross slope changes from 0° to 8°, the factor of safety against sliding remains less than 1 until the downstream water height is less than 32 in. The factor of safety against overturning is always higher than 1 for a cross slope of 0° for flood scenario 2. As the cross slope increases, the factor of safety against overturning becomes less than 1.

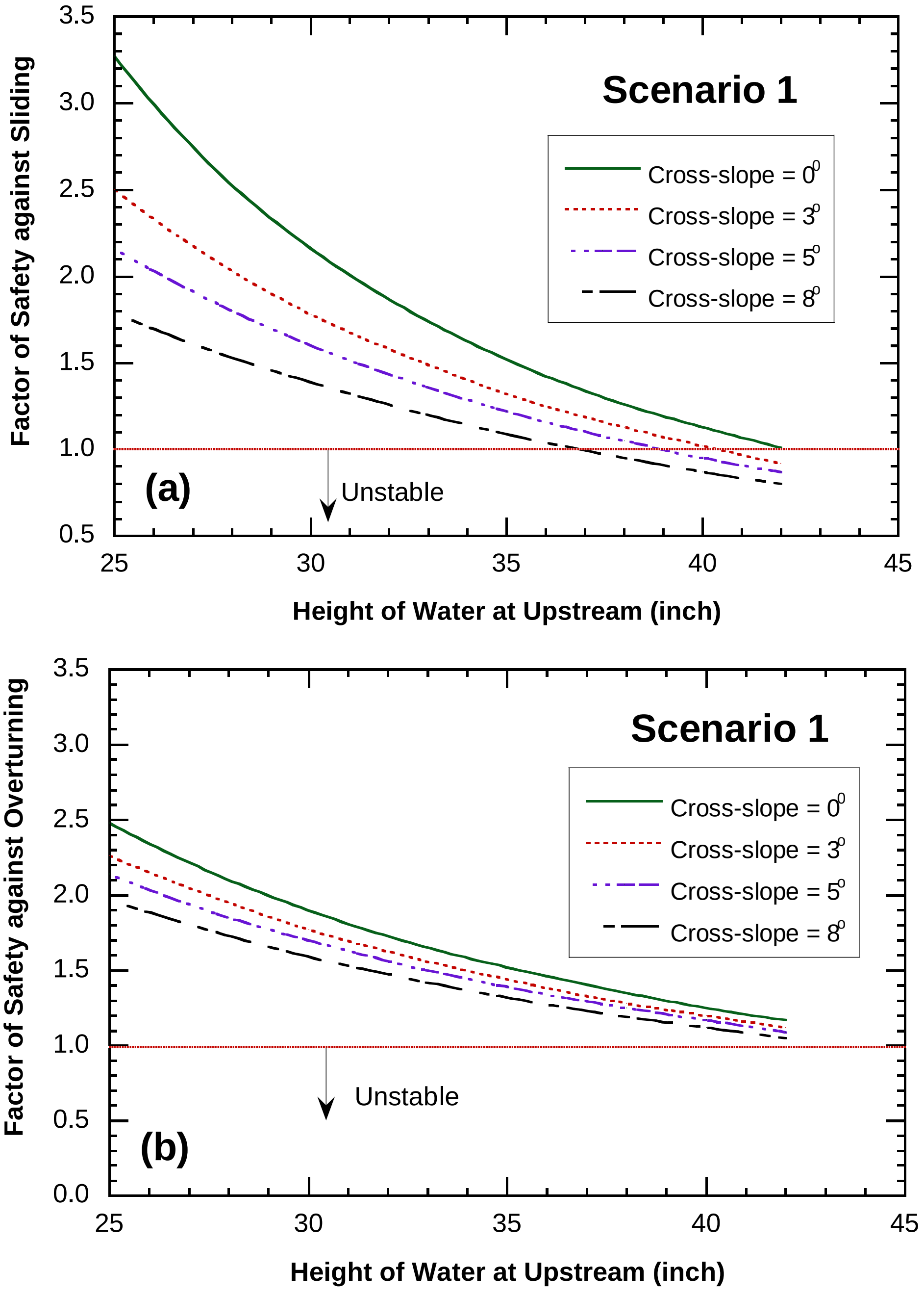

Figure 6.5. Factor of Safety against (a) Sliding and (b) Overturning for the MSSCB for Flood Scenario 1.

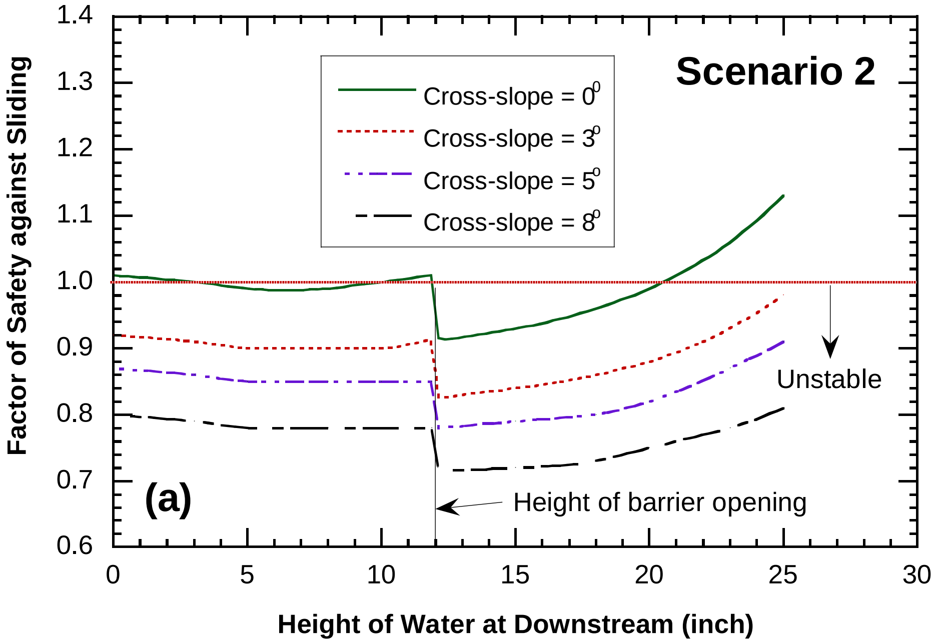

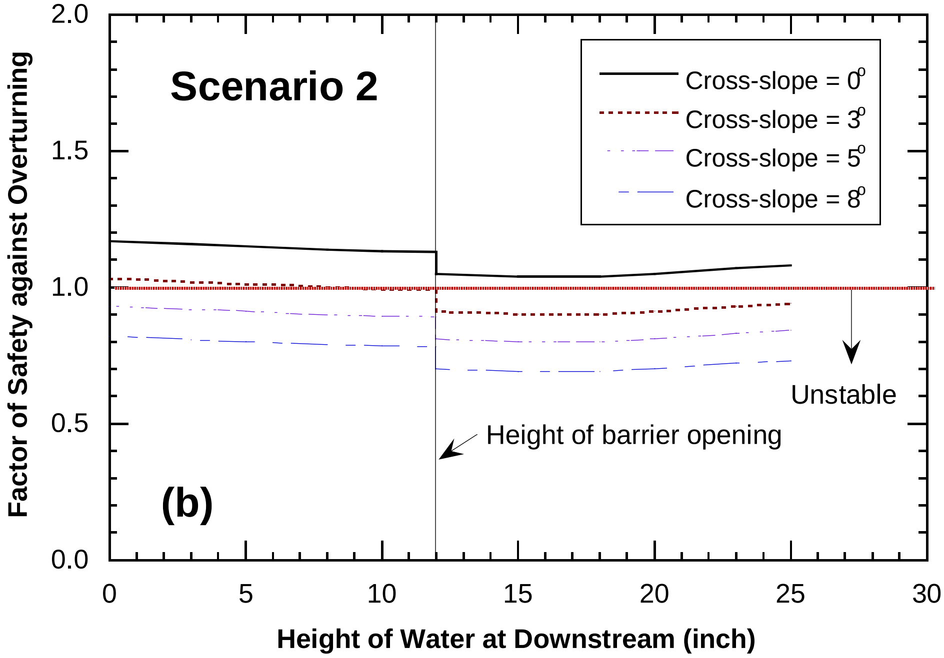

Figure 6.6. Factor of Safety against (a) Sliding and (b) Overturning for the MSSCB for Flood Scenario 2.

6.2.1.4 Low Speed Traffic Barrier (LPCB)

The effect of cross slope on factor of safety against sliding and overturning of a LPCB for flood scenarios 1 and 2 are shown in Figures 6.7 and 6.8, respectively. The factor of safety against sliding and overturning is always more than 1 for all the cross slopes 0°-8°. Thus, the LPCB is stable in all cross slopes for flood scenarios 1 and 2.

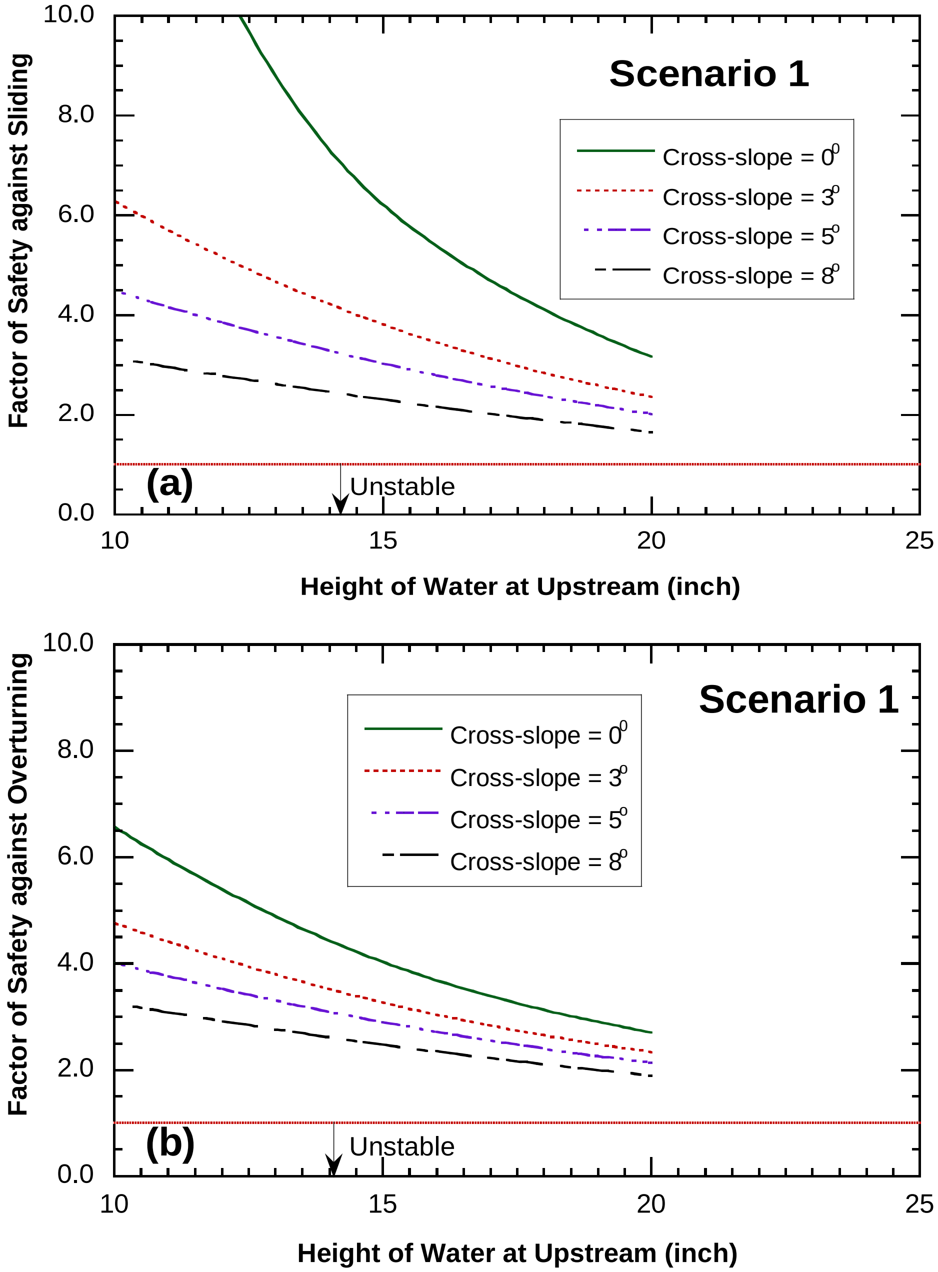

Figure 6.7. Factor of Safety against (a) Sliding and (b) Overturning for LPCB for Flood Scenario 1.

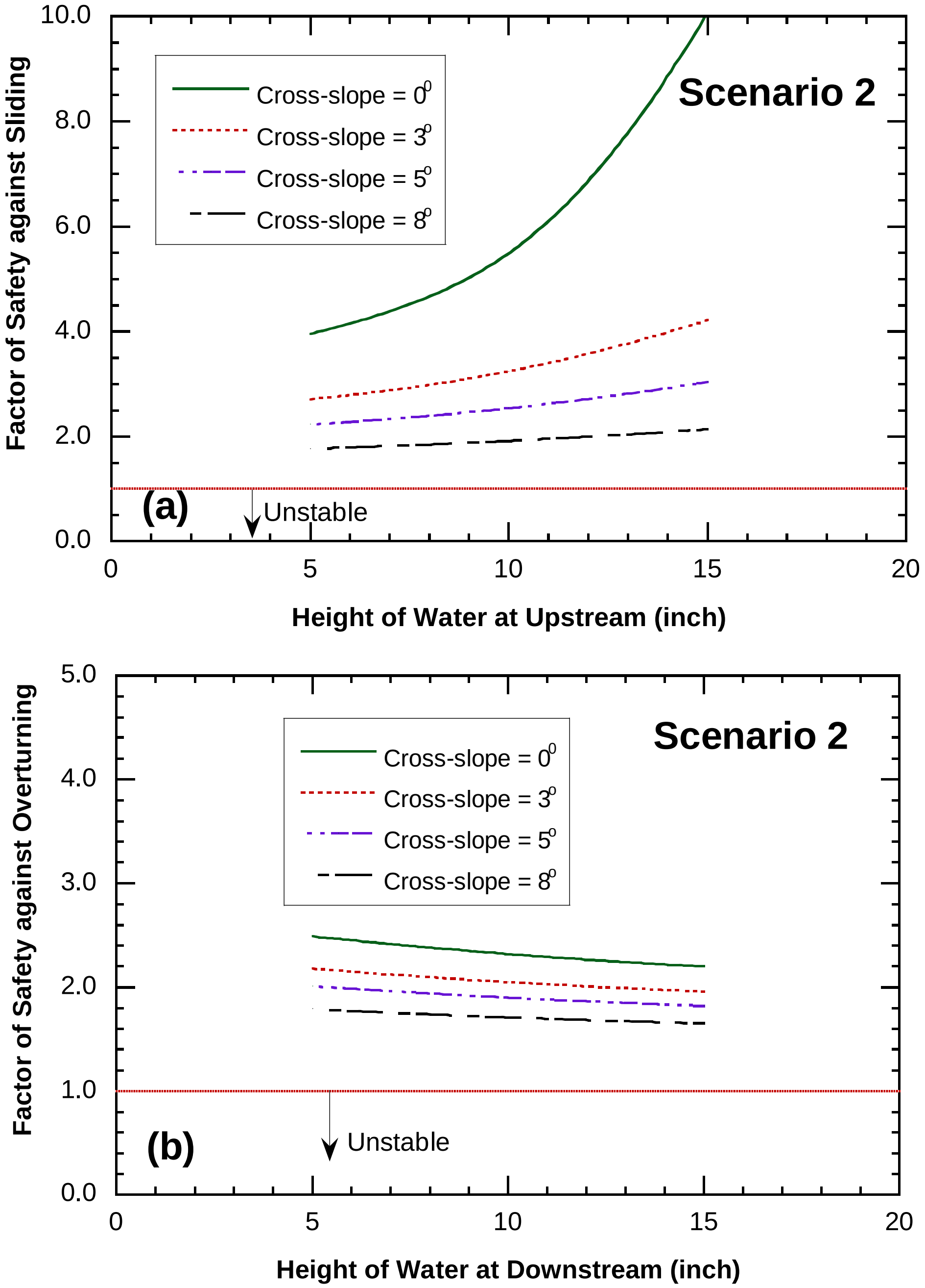

Figure 6.8. Factor of Safety against (a) Sliding and (b) Overturning for LPCB for Flood Scenario 2.

6.2.2 Parametric Study Considering Different Coefficient of Friction

A parametric study has been performed to evaluate how the factor of safety against sliding changes with the changing coefficient of friction for different pavement surfaces. The factor of safety against overturning does not depend on coefficient of friction. Coefficient of friction for different surfaces, such as the asphalt surface (0.62), concrete surface (0.78), base surface (0.54), subbase surface (0.50), and subgrade (0.61) are considered for the parametric study for the flood scenarios 1 and 2 for all four types of TCTBs. Since most of the TCTBs are unstable for flood scenarios 3 and 4, they are not included in the parametric study.

6.2.2.1 Single Slope Concrete Barrier (SSCB)

The effect of coefficient of friction on the factor of safety against sliding of a SSCB for flood scenarios 1 and 2 are shown in Figures 6.9 and 6.10, respectively. The factor of safety against sliding of a SSCB decreases as the coefficient of friction between the road surface and the bottom surface of the TCTB decreases.

Figure 6.9 represents the flood scenario 1, which shows that the factor of safety against sliding for concrete surface ($\mu = 0.78$) is always higher than 1, but the factor of safety against sliding could be less than 1 for base or subbase surfaces since their coefficients of friction are lower compared to concrete.

Figure 6.10 represents the flood scenario 2, which shows that the factor of safety against sliding is always higher than 1. The factor of safety against sliding could be lower than 1 for asphalt, base, subbase, and subgrade surfaces.

6.2.2.2 F-Shaped Concrete Barrier (CSB)

The effect of coefficient of friction on the factor of safety against sliding of a CSB for flood scenarios 1 and 2 are shown in Figures 6.11 and 6.12, respectively. Similar to SSCB, the factor of safety against sliding of a CSB decreases as the coefficient of friction between the road surface and the bottom of the TCTB decreases.

Figure 6.11 represents the flood scenario 1, which shows that the factor of safety against sliding for concrete surface ($\mu = 0.78$) is always higher than 1, but the factor of safety against sliding could be less than 1 for base or subbase surfaces since their coefficients of friction are lower compared to concrete.

Figure 6.12 represents the flood scenario 2 and shows that similar to SSCB, the factor of safety against sliding for CSB always becomes less than 1 for asphalt, base, subbase and subgrade surfaces when the downstream water height is less than 25 in. However, the factor of safety of a CSB on a concrete surface is always stable for flood scenario 2.

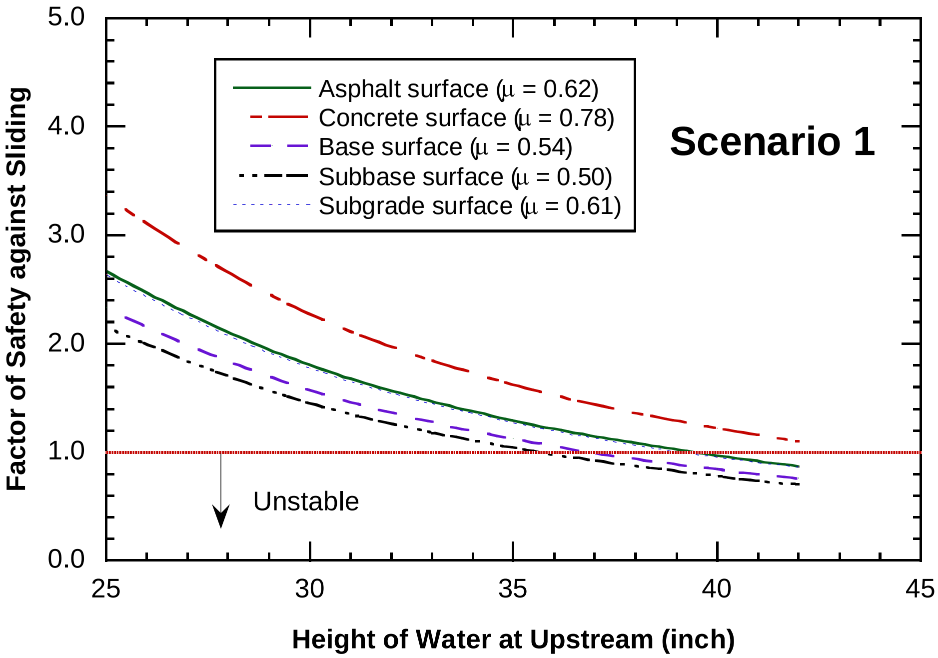

Figure 6.9. Effect of the Coefficient of Friction on the Factor of Safety against Sliding of a SSCB for Flood Scenario 1.

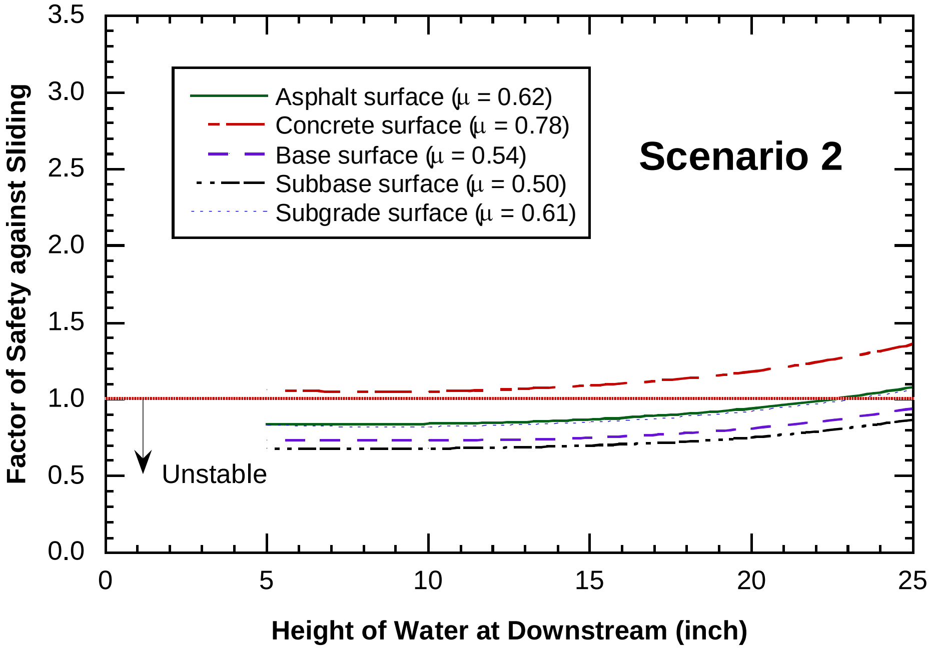

Figure 6.10. Effect of the Coefficient of Friction on the Factor of Safety against Sliding of a SSCB for Flood Scenario 2.

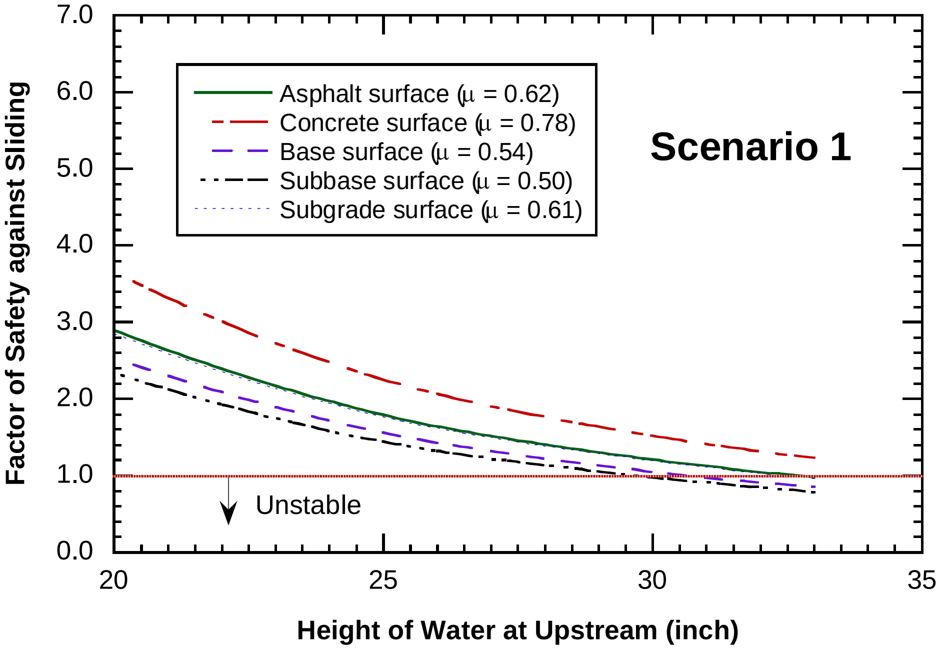

Figure 6.11. Effect of the Coefficient of Friction on the Factor of Safety against Sliding of a CSB for Flood Scenario 1.

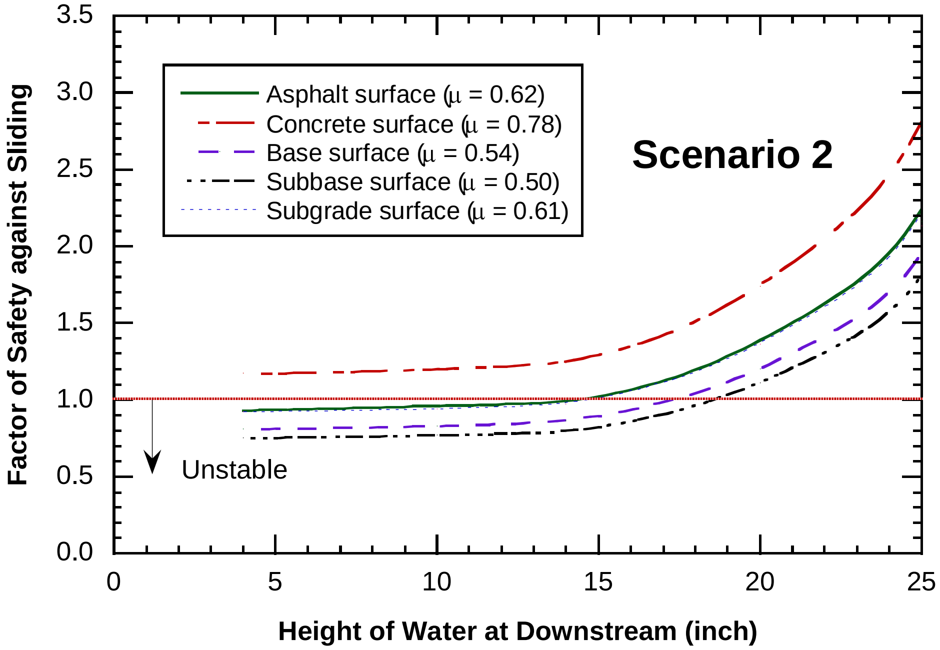

Figure 6.12. Effect of the Coefficient of Friction on the Factor of Safety against Sliding of a CSB for Flood Scenario 1.

6.2.2.3 Modified Traffic Barrier (MSSCB)

The effect of coefficient of friction on the factor of safety against sliding of a MSSCB for flood scenarios 1 and 2 are shown in Figures 6.13 and 6.14, respectively. The factor of safety against sliding of a SSCB decreases as the coefficient of friction between the road surface and the bottom surface of the TCTB decreases.

Figure 6.13 represents the flood scenario 1 which shows that the factor of safety against sliding for concrete surface (μ = 0.78), subgrade surface (μ = 0.61), and asphalt surface (μ = 0.62) is always higher than 1, but the factor of safety against sliding could be less than 1 for base (μ = 0.54) or subbase (μ = 0.50) surfaces since their coefficients of friction are lower compared to other three surfaces.

Figure 6.14 represents the flood scenario 2, which shows that the factor of safety against sliding is always higher than 1. The factor of safety against sliding could be lower than 1 for asphalt, base, subbase, and subgrade surfaces.

6.2.2.4 Low Speed Traffic Barrier (LPCB)

The effect of coefficient of friction on the factor of safety against sliding of a LPCB for flood scenarios 1 and 2 are shown in Figures 6.15 and 6.16, respectively. Similar to all other TCTBs, the factor of safety against sliding of a LPCB decreases as the coefficient of friction between the road surface and the bottom surface of the TCTB decreases. Figure 6.15 and 6.16 shows that the factor of safety against sliding is always more than 1 for all the surfaces for flood scenarios 1 and 2.

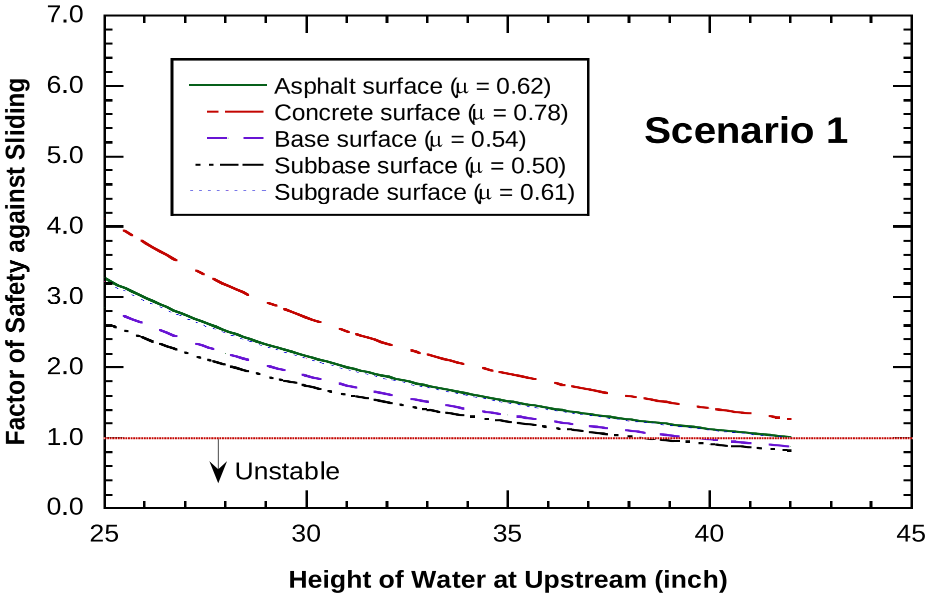

Figure 6.13. Effect of the Coefficient of Friction on the Factor of Safety against Sliding of a MSSCB for Flood Scenario 1.

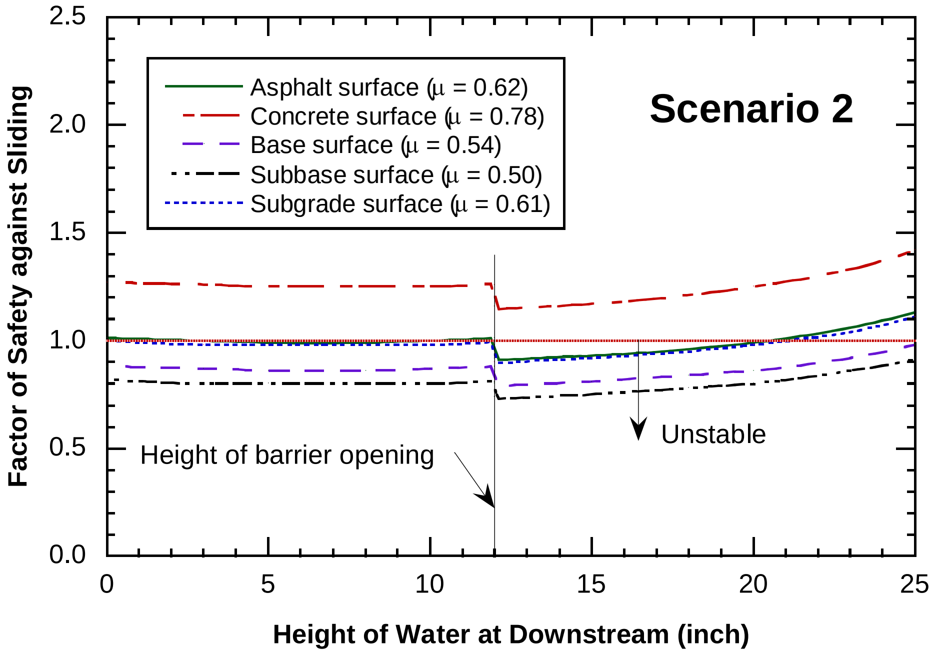

Figure 6.14. Effect of the Coefficient of Friction on the Factor of Safety against Sliding of a MSSCB for Flood Scenario 2.

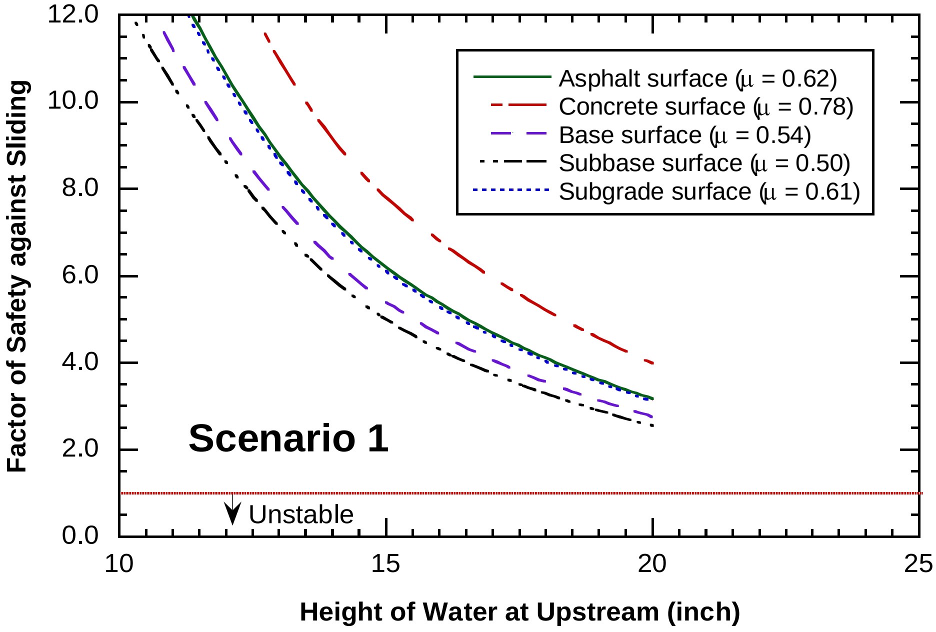

Figure 6.15. Effect of the Coefficient of Friction on the Factor of Safety against Sliding of a LPCB for Flood Scenario 1.

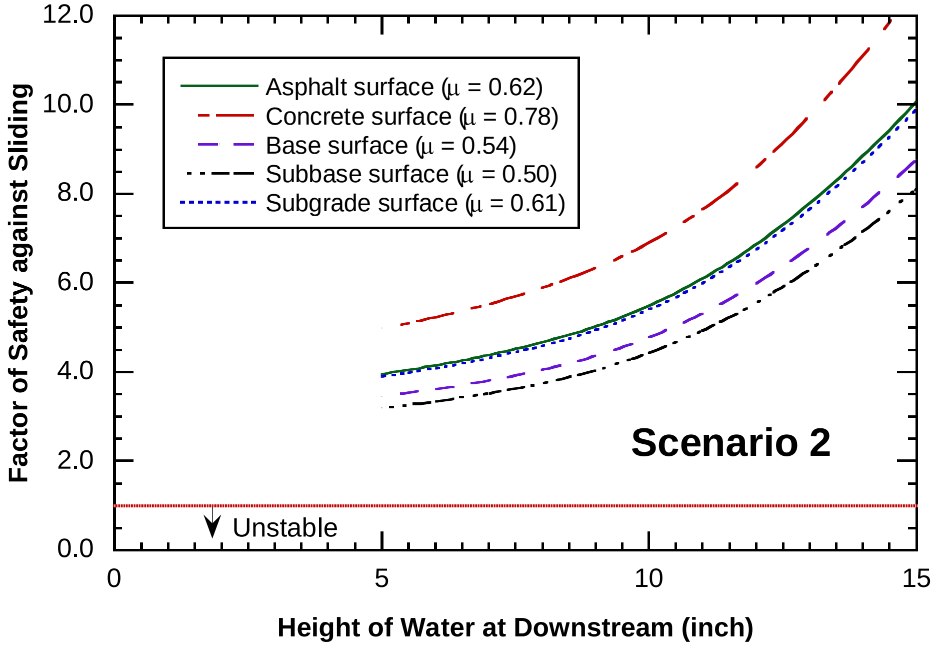

Figure 6.16. Effect of the Coefficient of Friction on the Factor of Safety against Sliding of a LPCB for Flood Scenario 2.

CHAPTER 7: SUMMARY AND CONCLUSIONS

7.1 PERFORMANCE OF THE TCTBS

- The rating curves for four standard TCTBs, such as the SSCB, SSCB-SPL, CSB, and LPCB were developed based on previous research presented by Charbeneau et al. (2008). This model proved to fit the experimentally derived data quite well, but is limited to modeling barriers in which experimental data has been obtained. This is because the model equations contain three coefficients which can only be obtained through fitting the model to the data.
- Villemonte Model and the Empirical Model were used to simulate the submergence condition. Both models require physical modeling in order to derive a single coefficient term. The Villemonte Model, which is an adaptation from earlier research (Villemonte, 1947), is independent of the flow rate. The Empirical Model developed in the paper by Charbeneau et al. (2008), however, is dependent on the flow rate. Both models have similar accuracy, with the Villemonte Model being the easiest and most straightforward to use. Therefore, when modeling the effect of submergence for the four barriers selected in this research, the Villemonte Model is the clear choice to be used.
- A simple change to the fraction of open space (F_o) in the rating curve model equations could be used in the modeling of a barrier with varying degrees of clogging. This is because the F_o describes the area of the drainage opening, and when the drainage opening becomes clogged this number will be reduced. Two scenarios were tested with MSSCB, one with the barrier's drainage opening 75% clogged and the other with it 50% clogged, which showed that when the F_o was adjusted to represent the two clogged conditions the model fit the experimental data quite well. Thus, the performance of a clogged TCTB can be predicted from a rating curve for varying amounts of clogging by simply manipulating the F_o in the model rating curve equations.
- The rating curve of TCTB could be used in the hydraulic modeling software HEC-RAS, in order to model the placement of barrier on a roadway surface. To accomplish this, two example problems were considered. The first consists of a flat roadway surface and the second is a roadway with a vertical curve. In order to solve these problems the weir coefficient that HEC-RAS uses as part of the pressure/weir method can be altered in order simulate the placement of a barrier on the roadway.

7.2 DETERMINATION OF COEFFICIENT OF FRICTION

- The coefficient of friction between the TCTB surface and the pavement surfaces with different ages, textures, and types are determined following the ASTM C1028–07 standard method. The coefficient of friction varies from 0.78 to 0.98 for concrete surface, 0.62 to 0.76 for asphalt surface, 0.54 to 0.75 for base surface, 0.50 to 0.69 for subbase surface, and 0.61 to 0.88 for subgrade surface.
- To understand the effect of bearing stress on coefficient of friction, the coefficient of friction between the bottom surface of TCTBs and the concrete and asphalt surfaces was measured with two different stress levels of 1 psi (standard test) and 2 psi. Statistical test (pooled t-test with $\alpha = 0.05$) showed that there is a significant difference between the mean

coefficient of friction for both concrete and asphalt pavement when the stress changes ($P = 0.0004$ for concrete and $P = 0.0293$ for asphalt surface).

- Since the bearing stress has a pronounced effect on coefficient of friction and the standard TCTBs provide different bearing stresses on road surface, the variation of coefficient of friction between the bottom surface of TCTBs and various other road surfaces with different bearing stresses is determined. The coefficient of friction for the concrete surface decreases approximately 18-22% when the bearing stress increases from 1 psi to 2.0 psi and then remains unchanged. Similarly, the coefficient of friction for the pavement surface decreases approximately 22-23% when the bearing stress increases from 1 psi to 2 psi and then decreases slowly.
- In order to understand the effect of surface condition (dry or moist) on the coefficient of friction, the coefficient of friction was determined for a number of surfaces for both wet and dry condition and a statistical (pooled t-test) test was conducted assuming a significance level, $\alpha = 0.05$. Although the mean coefficient of friction is slightly higher for dry surface, the test results from the statistical analysis suggest that there is no significance difference between the mean coefficient of friction for dry and wet surfaces for all of the surface combinations.
- To understand the effect of the presence of dirt in between the bottom surface of TCTBs and the concrete and asphalt road surfaces, the coefficient of friction was determined with the presence of some sand particles ($d_{50} = 0.62$ mm, $d_{10} = 0.43$ mm). A statistical test (pooled t-test) with a significance level $\alpha = 0.05$ suggests that the coefficient of friction decreases significantly due to the presence of dirt in between two surfaces for both concrete ($P = 0.0001$) and asphalt ($P = 0.0001$) surfaces.

7.3 STABILITY OF TCTBS

- The SSCB is unstable either against sliding or overturning for all surfaces (concrete, asphalt, base, subbase, and subgrade) except concrete surfaces even at 0° cross slope for all of the four flood scenarios. The SSCB is stable on concrete surface if the cross slope is less than 3° for only flood scenario 1.
- The CSB is stable if it is placed on a concrete surface with a cross slope less than 5° for flood scenarios 1 and 2. The CSB is also stable if it is placed on asphalt surface with a cross slope of 0° for flood scenario 1. All other cases, the CSB is unstable.
- The MSSCB is stable if it is placed on a concrete surface with a cross slope less than 5° for flood scenario 1 and a cross slope less than 3° for flood scenario 2. The MSSCB is also stable if it is placed on asphalt surface with a cross slope of 0° for flood scenario 1. All other cases, the MSSCB is unstable.
- The LPCB is stable for all surfaces with a cross slope up to 8° for flood scenarios 1, 2, and 3. It is also stable in flood scenario 4 when the surge water height is equal to the height of the barrier and surge water velocity is 5 mph. However, it becomes unstable when the surge water height is higher than 13 in. and the surge velocity is 10 mph.

7.4 MODELING TCTB EXACERBATED ROADWAY FLOODING WITH HEC-RAS

- It is possible to modify the weir coefficient value in HEC-RAS in order to hydraulically model the placement of a concrete traffic barrier on the roadway surface. To do this, an iterative procedure must be used. Two example problems, the Single Bridge-Example 2 and ConSpan Culvert have been demonstrated with the Concrete Safety Barrier (CSB(1)-04) in this study. In the Single Bridge-Example 2 procedure, an increase in the upstream energy of 2.25 ft and a decrease in the weir flow rate of 1811.02 cfs occurred as a result of barrier placement. Furthermore, through the ConSpan example it can be seen that placing the barrier on the roadway will result in the upstream energy increasing by 1.86 ft and the flow rate decreasing by 460.18 cfs.

7.5 PARAMETRIC STUDY

- To understand the effect of cross slope (one of the most important variable in the field) on stability of TCTBs, the factor of safety against sliding and overturning is determined for flood scenarios 1 and 2 for a wide range of cross slopes. The factor of safety against sliding and overturning decreases as the cross slopes of the roadway (outward direction of flow) increases. The rate and the pattern at which the factor of safety varies with the variation of cross slope depend on the types of TCTBs and the flood scenarios.
- The factor of safety against sliding depends on the coefficient of friction. Thus, the factor of safety against sliding for different TCTBs was analyzed considering different road surfaces. The factor of safety against sliding increases with the increasing coefficient of friction. Thus, the factor of safety against sliding is highest for concrete ($\mu = 0.78$) and lowest for subbases surface ($\mu = 0.50$) among all surfaces considered. The rate and the pattern at which the factor of safety varies with the variation of roadway surfaces depend on the types of TCTBs and the flood scenarios.

REFERENCES

ASTM-C1028-07 Standard Test Method for Determining the Static Coefficient of Friction of Ceramic Tile and Other Like Surfaces by the Horizontal Dynamometer Pull-Meter Method.

Benson, K. (2004). *Hydraulic Effects of Safety End Treatments on Culvert Performance.* M.S. Thesis in Engineering, The University of Texas at Austin.

Blau, P. J. (1996). *Friction Science and Technology.* New York: Dekker.

Bos, M. (1989). Discharge Measurements Structures. *Publication 20*. Wageningen, The Netherlands: International Institute for Land Reclamation and Improvement.

Bowden, F. P. and Tabor, D. (1986). *The Friction and Lubrication of Solids.* Oxford, England: Oxford University Press.

Bradley, J.N. (1978). *Hydraulics of Bridge Waterways,* Hydraulic Design Series No. 1, Federal Highway Administration, U.S. Government Printing Office, Washington, D.C., FHWA-EPD86-101, NTIS PB86-181708, second edition 1970, 111 pages.

Brater, E.F., H.W. King, J.E. Lindell, and C. Y. Wei. (1996). *Handbook of Hydraulics,* 7th edition.

Charbeneau, R.J., Henderson, A.D., and Sherman, L.C. (2006): "Hydraulic Performance Curves for Highway Culverts," *Journal of Hydraulic Engineering*, Vol. 132, No. 5, p. 474-481.

Charbeneau, Randall J., Brandon Klenzendorf, Michael E. Barrett (2008): "Hydraulic Performance of Bridge Rails," *Report No. FHWA/TX-08/0-5492-1*, Texas Department of Transportation

Coduto, D. P. (2001): *Foundation Design: Principles and practices*, second edition, Prentice Hall, New York.

Cody Hudson, Brandon Klenzendorf, Randall Charbeneau, and Michael Barrett (2009): Evaluation of Hydraulic Performances of Standard and Modified TCTB,
Project No. 0-6094 Task 2.

Das, B. M. (2006): Principles of Geotechnical Engineering, sixth edition, Thomson publishers. Engineers, Davis CA.

Division, http://www.dot.state.tx.us/insdtdot/ orgchart/cmd/cserve/standard/bridge-e.htm.

FHWA (2007): *FHWA Caltrans Bridge Rail Guide 2005*, 15 March 2007, U.S. Department of Transportation, Federal Highway Administration, Bridge Technology, http://www.fhwa.dot.gov/bridge/bridgerail/index.cfm.

HEC (Hydrologic Engineering Center). (2001). *HEC-RAS, River Analysis System, User's Manual, Hydraulic Reference Manual, and Applications Guide,* U.S. Army Corps of Engineers, Washington D.C.

Henderson, F.M. (1966): *Open Channel Flow*, Macmillan Publishing Co., Inc., New York.

Henry, J.J.; ABE, H; Kameyama, S; Tamai, A; Kasahara, A; Saito, K. (2000). Determination of International Friction Index (IFI) Using the Circular Texture Meter (CTM) and the Dynamic Friction Tester (DFT), Fourth International Symposium on Pavement Surface Characteristics of Roads and Airfields, PIARC, pp. 109-121.

Hibbeler, R. C. (2008): *Mechanics of Materials,* seventh edition, Prentice Hall publishers.

Jackson, N. M. (2008). Harmonization of Texture and Skid-Resistance Measurements**,** *Report No. FL/DOT/SMO/08-BDH-23*, Florida Department of Transportation.

King, H., & Brater, E. (1963). *Handbook of Hydraulics*, fifth edition. New York: McGraw-Hill Book Company.

Klenzendorf, J. B., Michael E. Barrett, and Randall J. Charbeneau (in press): **"**Incorporating Bridge Rail Hydraulics for Floodplain Mapping." *Journal of Hydraulic Engineering*.

Klenzendorf, J.B. (2007): *Hydraulic Performance of Bridge Rails based on Rating Curves and Submergence Effects,* M.S. Thesis in Engineering, The University of Texas at Austin.

Konieczki, M. V. (2007). Effect of Bridge Deck Submergence on Backwater, MS thesis, The University of Texas at Austin.

Kranc, S. C. (1997). "Hydraulic Performance of Structures for Bridge Drainage," *Report No. 747*, Florida Department of Transportation.

Kranc, S. C., Cristopher J. Cromwell, Clayton J. Rabens, Nathan Collier and Bryan Fast (2005): "Experimental Investigation and Analysis of Flow Under Barrier Walls," *Report No. BC-353-27*, Florida Department of Transportation.

Mott, R. (2000). *Applied Fluid Mechanics.* Upper Saddle River, New Jersey: Prentice-Hall, Inc.

Robinson, D. I., and McGhee, T. J. (1993): "Computer Modeling of Side-Flow Weirs," *Journal of Irrigation and Drainage Engineering*, Vol. 119, No. 6.

Ross, H.E., Sicking, D.L., Zimmer, R.A., and Michie, J.D. (1993): *National Cooperative Highway Research Program Report 350: Recommended Procedures for the Safety Performance Evaluation of Highway Features,* Transportation Research Board, National Research Council, National Academy Press, Washington, D.C.

Rouse, H. (1950). *Engineering Hydraulics, Proceedings of the Fourth Hydraulics Conference, Iowa Institute of Hydraulic Research, June 12-15, 1949.* New York: John Wiley & Sons, Inc.

Singh, R. and Satyanarayana, T. (1994): "Automated Field Irrigation System Using Side Weirs," *Journal of Irrigation and Drainage Engineering*, Vol. 120, No. 1.

Stinson, K W; Roberts, C P; Gray, B E; Rhodes, E O; Fleming, E M; Martin, G E; Schlesinger, G. F; Moyer, RA, (1934). Coefficient of Friction Between Tires And Road Surfaces, Highway Research Board Proceedings, Vol. 13(1), pp. 169-188.

Tullis, B.P., Young, J.C., and Chandler, M.A. (2007): "Head-Discharge Relationships for Submerged Labyrinth Weirs," *Journal of Hydraulic Engineering*, Vol. 133, No. 3, pp. 248-254.

TxDOT (2004). *Hydraulic Design Manual*, Texas Department of Transportation, Austin, TX.

TxDOT (2005). *Bridge Railing Manual*, Texas Department of Transportation, Austin, TX.

TxDOT (2007). *Bridge Standards*, Texas Department of Transportation, Bridge Division, http://www.dot.state.tx.us/insdtdot/orgchart/cmd/cserve/standard/bridge-e.htm

TxDOT. (2009). *Roadway Standards.* Retrieved 2009, from Texas Department of Transportation Homepage: http://www.dot.state.tx.us/insdtdot/orgchart/cmd/cserve/standard/rdwylse.htm University Press, 1986.

Villemonte, J. (1947). Submerged-Weir Discharge Studies. *Engineering News-Record*, pp. 866-869.

APPENDIX A: GUIDELINES FOR USING TCTB IN FLOOD PRONE ZONE

A.1 GUIDELINES FOR USING TCTBs IN FLOOD PRONE ZONE

The following guidelines for the use of TCTBs is applicable only for in flood prone zone and whether the construction (for which the TCTBs will be placed) is expected to continue in a season when extreme flood can be expected. Thus, the location at which the TCTBs will be placed and the period of construction must be identified. If the construction period is not known clearly, it is always recommended to consider a flood season.

- Every TCTB must be washed and cleaned before placement so that there will not be any loose dirt at the bottom surface of the TCTB.
- The bed on which the TCTBs will be placed must be cleaned so that there will not be any loose dirt on the surface.
- The cross slope (outward to the flow) of the bed on which the TCTBs will be placed must be measured accurately.
- The surface materials of the bed must be identified to understand the coefficient of friction. Coefficient of friction for five common bed surfaces is included in this report. If the bed surface materials cannot be identified clearly, a conservative assumption is recommended.
- From the landscape of the location, and the geometry and drainage pattern of the roadway, the possible flood scenario(s) must be identified based on the Fig. 4.4. If the location is not in the coastal region, flood scenario 4 should be cancelled from consideration.
- Once the possible flood scenarios are identified, the type of TCTBs that can be used in that particular location could be identified from the Table A.1. If more than one type of barriers can be used for the particular location, other factors such as, availability, speed restriction, special needs (i.e., crossing Ocelots) etc. could be considered.
- If the construction location is close to coastal area, flood scenario 4 must be considered along with other possible flood scenarios.
- LPCB is the only barrier that could be used all possible scenarios that have been considered in this study. However, LPCB is only applicable for low speed area.
- Any special situation when it is necessary to use any TCTB that does not qualify according to Table A.1, the TCTBs must be anchored to avoid any failure against sliding or overturning.
- The type or size of the anchors that could be used was not studied, because it is beyond the scope of this research project.

Table A.1. Guideline for Using TCTBs at Different Field Conditions and Flood Scenario.

Pavement Surface	Cross Slope (deg)	Type of TCTB															
		SSCB				CSB				MSSCB				LPCB			
		F. S.-1	F. S.-2	F. S.-3	F. S.-4	F. S.-1	F. S.-2	F. S.-3	F. S.-4	F. S.-1	F. S.-2	F. S.-3	F. S.-4	F. S.-1	F. S.-2	F. S.-3	F. S.-4
Concrete	0	Yes	No	No	No	Yes	Yes	No	No	Yes	Yes	No	No	Yes	Yes	Yes	Yes
	3	Yes	No	No	No	Yes	Yes	No	No	Yes	Yes	No	No	Yes	Yes	Yes	Yes
	5	No	No	No	No	Yes	Yes	No	No	Yes	No	No	No	Yes	Yes	Yes	Yes
	8	No	No	No	No	No	No	No	No	No	No	No	No	Yes	Yes	Yes	Yes
Asphalt	0	No	No	No	No	Yes	No	No	No	Yes	No	No	No	Yes	Yes	Yes	Yes
	3	No	No	No	No	No	No	No	No	No	No	No	No	Yes	Yes	Yes	Yes
	5	No	No	No	No	No	No	No	No	No	No	No	No	Yes	Yes	Yes	Yes
	8	No	No	No	No	No	No	No	No	No	No	No	No	Yes	Yes	Yes	Yes
Base	0	No	No	No	No	No	No	No	No	No	No	No	No	Yes	Yes	Yes	Yes
	3	No	No	No	No	No	No	No	No	No	No	No	No	Yes	Yes	Yes	Yes
	5	No	No	No	No	No	No	No	No	No	No	No	No	Yes	Yes	Yes	Yes
	8	No	No	No	No	No	No	No	No	No	No	No	No	Yes	Yes	Yes	Yes
Subbase	0	No	No	No	No	No	No	No	No	No	No	No	No	Yes	Yes	Yes	Yes
	3	No	No	No	No	No	No	No	No	No	No	No	No	Yes	Yes	Yes	Yes
	5	No	No	No	No	No	No	No	No	No	No	No	No	Yes	Yes	Yes	Yes
	8	No	No	No	No	No	No	No	No	No	No	No	No	Yes	Yes	Yes	Yes
Subgrade	0	No	No	No	No	No	No	No	No	No	No	No	No	Yes	Yes	Yes	Yes
	3	No	No	No	No	No	No	No	No	No	No	No	No	Yes	Yes	Yes	Yes
	5	No	No	No	No	No	No	No	No	No	No	No	No	Yes	Yes	Yes	Yes
	8	No	No	No	No	No	No	No	No	No	No	No	No	Yes	Yes	Yes	Yes

Note: SSCB = Single slope concrete barrier, CSB = Concrete safety barrier, MSSCB = Modified single slope concrete barrier, LPCB =Low profile concrete barrier, and F. S. = Flood Scenario.

A.2. MOST EFFICIENT TCTB FROM THE PERSPECTIVE OF HYDRAULIC PERFORMANCE

The rating curves for different TCTBs are shown in Fig. A.1. It can be seen from Fig. A.1 that the SSCB(SPL) is the most efficient TxDOT TCTB. The photo of SSCB (SPL) is shown in Fig. A.2. The standard drawing of the SSCB (SPL) is shown in Appendix B.

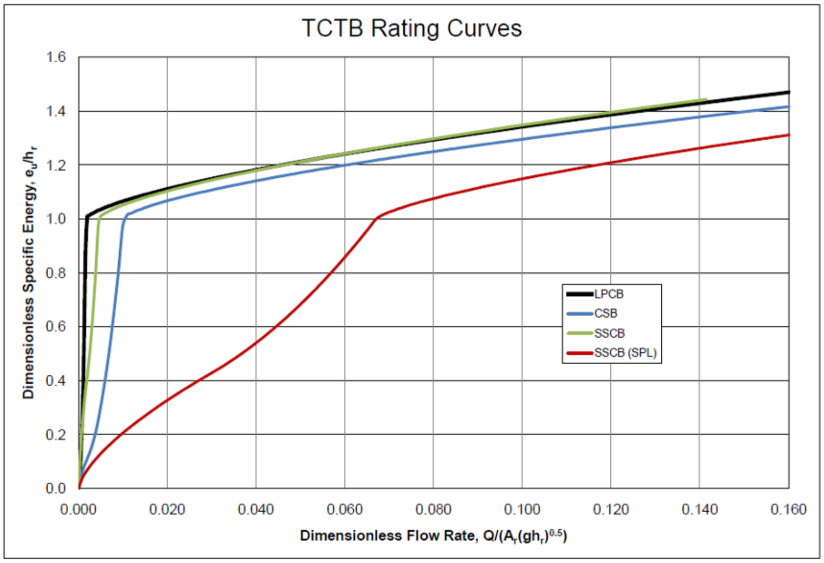

Figure A.1. Rating Curve for Different TCTBs.

Figure A.2. The SSCB (SPL).

A.3. MOST EFFICIENT TCTB FROM THE PERSPECTIVE OF STABILITY

It can be seen from Table A.1 that the LPCB is the most efficient TCTB. The LPCB can be used for all the scenarios considered for this study. The standard drawing of the LPCB is shown in Appendix B.

APPENDIX B: STANDARD DRAWINGS FOR TCTB (TXDOT, 2009)

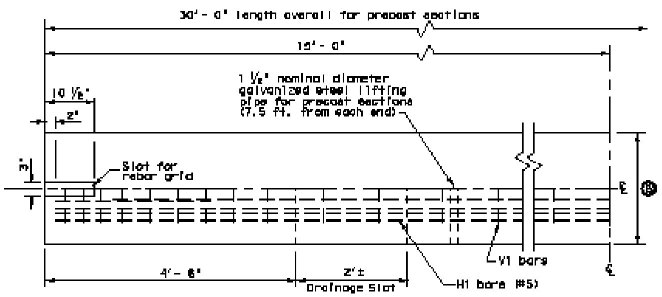

PLAN VIEW

(SYMMETRICAL ABOUTCENTER LINE)

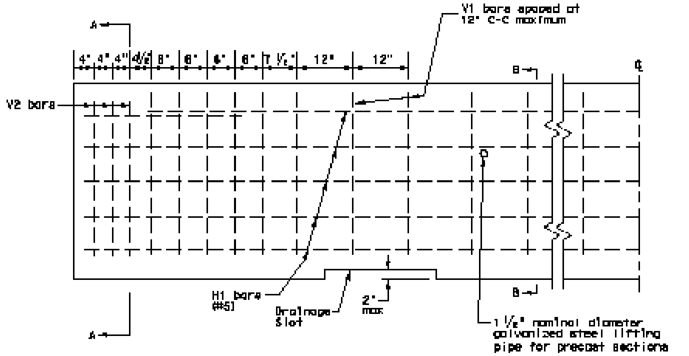

ELEVATION

(SYMMETRICAL ABOUT CENTERLINE)

GENERAL NOTES

1. Precast barrier length shall be 30 feet (± 1") unless otherwise specified in the plans. Cast-in-place or slip-formed barrier shall have an intermediate barrier joint at a maximum spacing of 100 feet unless otherwise directed by the Engineer. Refer to the intermediate barrier joint detail. Cast-in-place or slip-formed barrier will have the vertical V1 bars placed at 12" C-C maximum except near joints. The narrower vertical bar spacing at the ends of each barrier segment, as shown in the elevation view, will be required at the joints. The V2 bars shown in the elevation view will be replaced by V1 bars for cast-in-place or slip-form construction.
2. The usual temporary installation will require the placement of the rebar grid in the ungrouted slot. The usual permanent installation using precast barrier will connect the barrier segments with the rebar grid placed in the slot and grouted in place.
3. When installed in a permanent roadway location, the end connections of the precast barrier shall be grouted with a mixture of two parts sand and one part cement with enough water to make the mixture plastic. Grouting shall be done in a manner that will assure a smooth surface at the joint.
4. All concrete shall be class C or H, unless otherwise specified.
5. All reinforcing steel shall be Grade 60, unless otherwise specified.
6. Each precast barrier to be installed in a temporary location shall be delivered with a rebar grid.
7. Chamfer top and end edges 3/4 inch.
8. Unless otherwise shown in the plans, the Contractor has the option of placing either precast or cast-in-place permanent concrete barrier. Cast-in-place barrier may be slip-formed. Additional reinforcement may be tack welded to the upper two-thirds of the reinforcing cage to provide bracing. Lifting pipe, rebar grid and slot shall be omitted for cast-in-place or slip-form construction.
9. Bar splices for roadway barrier shall be a minimum of 24 times the nominal diameter of the bar.
10. Welded wire fabric may be used as an option to conventional reinforcement for precast or cast-in-place barrier. Welded wire fabric shall be made in accordance with ASTM A 497.
11. Conduit will be provided only when called for elsewhere in the plans. The position of the conduit or conduit passageway may be adjusted to facilitate construction, subject to approval of the Engineer.
12. Transitions to barrier height, as needed, shall be determined by the Engineer. Changes in barrier height should not normally exceed 2 inches per 30 foot. Vertical steel shall be uniformly transitioned throughout the variation in barrier height as directed by the Engineer.
13. A 36 inch minimum height differential between top of barrier and top of ACP shall be required at placement in order to allow for up to 6 inches of future overlays while maintaining a 30 inch minimum future effective height of barrier. Total minimal barrier height for design is therefore dictated by allowance for future overlays plus existing stairstep dimension "5". Minimums typically rounded to 42", 48" or 54" to facilitate precasting.

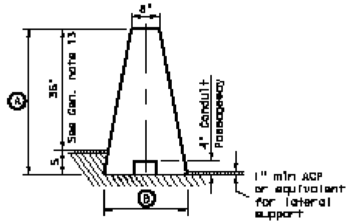

TYPICAL SECTION

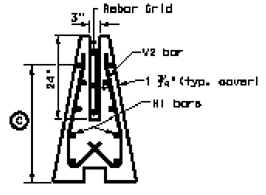

SECTION A-A

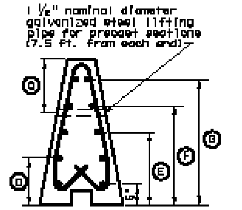

SECTION B-B

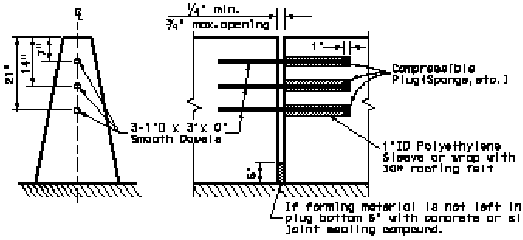

INTERMEDIATE BARRIER JOINT DETAIL (cast-in-place or slip-formed sections)

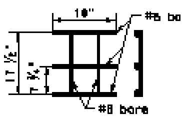

REBAR GRID

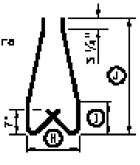

V2 BAR (#4)

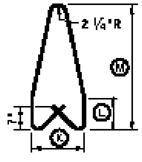

V1 BAR (#4)

REINFORCING DETAILS

R = Radius
D = Diameter

When precast barrier is to be used with the welded wire fabric option, conventional bar reinforcement will be required within 2 ft., plus a development length of 18", from the ends of each barrier segment.

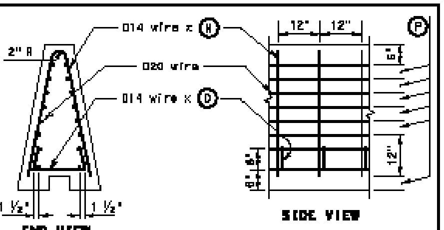

END VIEW

SIDE VIEW

Welded wire fabric
P x 12 - D20 x D14
60 ksi minimum yield strength

WELDED WIRE FABRIC OPTIONAL REINFORCING

Barrier Height	DIMENSIONS (Inches)															
Ⓐ	Ⓑ	Ⓒ	Ⓓ	Ⓔ	Ⓕ	Ⓖ	Ⓗ	Ⓘ	Ⓙ	Ⓚ	Ⓛ	Ⓜ	Ⓝ	Ⓞ	Ⓟ	Ⓠ
42	24	33 1/2	13 1/2	21	28 1/2	36	15	9 1/4	33 1/4	15	9 1/4	36	72	28	4	15 1/2
48	26 5/32	39 1/2	15	24	33	42	17 1/4	10 3/4	39 1/4	17 1/4	10 3/4	42	84	31 1/2	5	17
54	28 7/16	45 1/2	16 1/2	27	37 1/2	48	19 1/2	12 1/4	45 1/4	19 1/2	12 1/4	48	96	34 3/4	6	18 1/2

Texas Department of Transportation
Design Division (Roadway)

SINGLE SLOPE CONCRETE BARRIER
TYPE 2

SSCB(2)-00A

FILE: sscb200a.dgn	DN: GTH	CK: GTB	DW: BRD	CK: TRW
© TxDOT MAY 1992	CONT	FEDERAL AID PROJECT		SHEET
REVISIONS	COUNTY	CONTROL	SECT	JOB	HIGHWAY

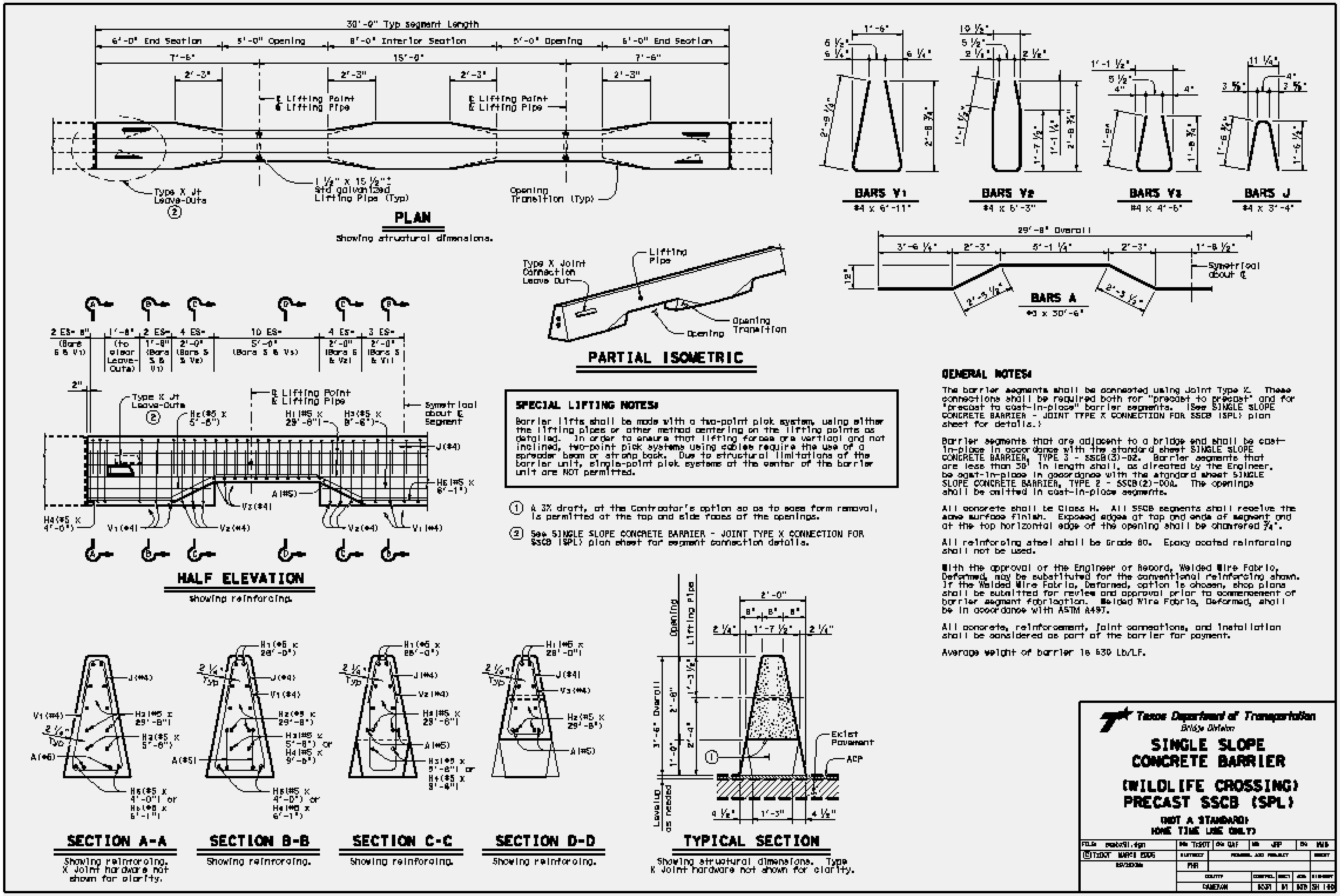

SPECIAL LIFTING NOTES:

Barrier lifts shall be made with a two-point pick system, using either the lifting pipes or other method centering on the lifting points as detailed. In order to ensure that lifting forces are vertical and not inclined, two-point pick systems using cables require the use of a spreader beam or strong back. Due to structural limitations of the barrier unit, single-point pick systems at the center of the barrier unit are NOT permitted.

① A 3% draft, at the Contractor's option so as to ease form removal, is permitted at the top and side faces of the openings.

② See SINGLE SLOPE CONCRETE BARRIER - JOINT TYPE X CONNECTION FOR SSCB (SPL) plan sheet for segment connection details.

GENERAL NOTES:

The barrier segments shall be connected using Joint Type X. These connections shall be required both for "precast to precast" and for "precast to cast-in-place" barrier segments. (See SINGLE SLOPE CONCRETE BARRIER - JOINT TYPE X CONNECTION FOR SSCB (SPL) plan sheet for details.)

Barrier segments that are adjacent to a bridge end shall be cast-in-place in accordance with the standard sheet SINGLE SLOPE CONCRETE BARRIER, TYPE 3 - SSCB(3)-02. Barrier segments that are less than 30' in length shall, as directed by the Engineer, be cast-in-place in accordance with the standard sheet SINGLE SLOPE CONCRETE BARRIER, TYPE 2 - SSCB(2)-00A. The openings shall be omitted in cast-in-place segments.

All concrete shall be Class H. All SSCB segments shall receive the same surface finish. Exposed edges at top and ends of segment and at the top horizontal edge of the opening shall be chamfered ¾".

All reinforcing steel shall be Grade 60. Epoxy coated reinforcing shall not be used.

With the approval of the Engineer of Record, Welded Wire Fabric, Deformed, may be substituted for the conventional reinforcing shown. If the Welded Wire Fabric, Deformed, option is chosen, shop plans shall be submitted for review and approval prior to commencement of barrier segment fabrication. Welded Wire Fabric, Deformed, shall be in accordance with ASTM A497.

All concrete, reinforcement, joint connections, and installation shall be considered as part of the barrier for payment.

Average weight of barrier is 630 Lb/LF.

Texas Department of Transportation
Bridge Division

SINGLE SLOPE CONCRETE BARRIER

(WILDLIFE CROSSING) PRECAST SSCB (SPL)

(NOT A STANDARD)
(ONE TIME USE ONLY)

FILE:	DN: TxDOT	CK:	DW: JRP	CK:
©TxDOT MARCH 2005	DISTRICT	FEDERAL AID PROJECT		SHEET
	PHR			
	COUNTY	CONTROL	SECT	JOB	HIGHWAY
	CAMERON				SH

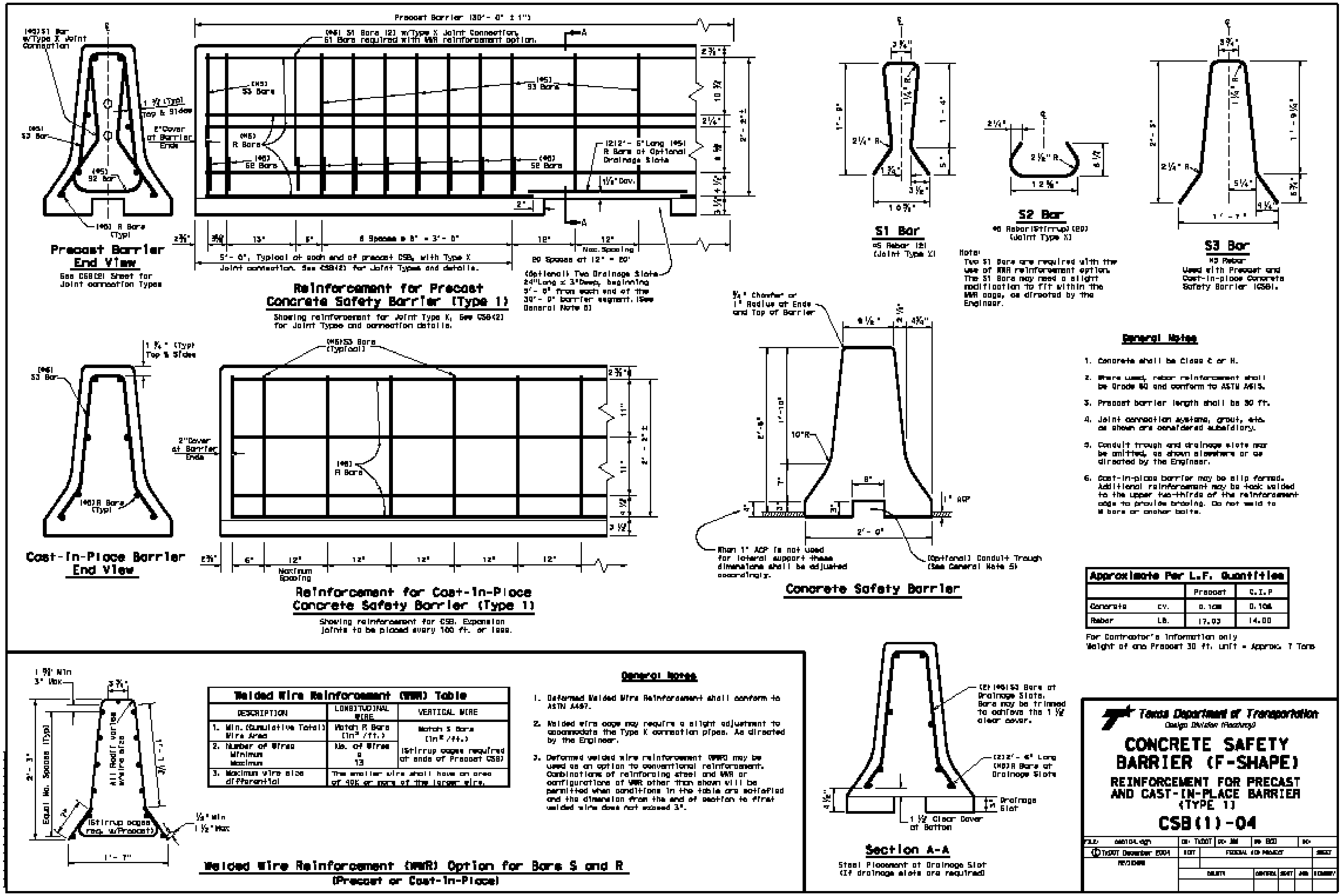

Precast Barrier End View

See CSB(2) Sheet for Joint connection Types

Reinforcement for Precast Concrete Safety Barrier (Type 1)

Showing reinforcement for Joint Type X. See CSB(2) for Joint Types and connection details.

Cast-In-Place Barrier End View

Reinforcement for Cast-In-Place Concrete Safety Barrier (Type 1)

Showing reinforcement for CSB. Expansion joints to be placed every 100 ft. or less.

S1 Bar

#5 Rebar (2)
(Joint Type X)

S2 Bar

#5 Rebar(Stirrup)(20)
(Joint Type X)

Note:
Two S1 Bars are required with the use of WWR reinforcement option. The S1 Bars may need a slight modification to fit within the WWR cage, as directed by the Engineer.

S3 Bar

#5 Rebar
Used with Precast and Cast-in-place Concrete Safety Barrier (CSB).

Concrete Safety Barrier

General Notes

1. Concrete shall be Class C or H.
2. Where used, rebar reinforcement shall be Grade 60 and conform to ASTM A615.
3. Precast barrier length shall be 30 ft.
4. Joint connection systems, grout, etc. as shown are considered subsidiary.
5. Conduit trough and drainage slots may be omitted, as shown elsewhere or as directed by the Engineer.
6. Cast-in-place barrier may be slip formed. Additional reinforcement may be tack welded to the upper two-thirds of the reinforcement cage to provide bracing. Do not weld to R bars or anchor bolts.

Approximate Per L.F. Quantities		Precast	C.I.P
Concrete	CY.	0.108	0.106
Rebar	LB.	17.03	14.00

For Contractor's Information only
Weight of one Precast 30 ft. unit = Approx. 7 Tons

Section A-A

Steel Placement at Drainage Slot
(If drainage slots are required)

Welded Wire Reinforcement (WWR) Table		
DESCRIPTION	LONGITUDINAL WIRE	VERTICAL WIRE
1. Min. (Cumulative Total) Wire Area	Match R Bars (In² /ft.)	Match S Bars (In² /ft.) (Stirrup cages required at ends of Precast CSB)
2. Number of Wires Minimum Maximum	No. of Wires 8 13	
3. Maximum wire size differential	The smaller wire shall have an area of 40% or more of the larger wire.	

General Notes

1. Deformed Welded Wire Reinforcement shall conform to ASTN A497.
2. Welded wire cage may require a slight adjustment to accommodate the Type X connection pipes. As directed by the Engineer.
3. Deformed welded wire reinforcement (WWR) may be used as an option to conventional reinforcement. Combinations of reinforcing steel and WWR or configurations of WWR other than shown will be permitted when conditions in the table are satisfied and the dimension from the end of section to first welded wire does not exceed 3".

Welded Wire Reinforcement (WWR) Option for Bars S and R
(Precast or Cast-In-Place)

Texas Department of Transportation
Design Division Standard

CONCRETE SAFETY BARRIER (F-SHAPE)

REINFORCEMENT FOR PRECAST AND CAST-IN-PLACE BARRIER (TYPE 1)

CSB(1)-04

FILE: csb104.dgn	DN: TxDOT	CK:	DW:	CK:
© TxDOT December 2004	DIST	FEDERAL AID PROJECT		SHEET
REVISIONS	COUNTY	CONTROL	SECT	JOB	HIGHWAY

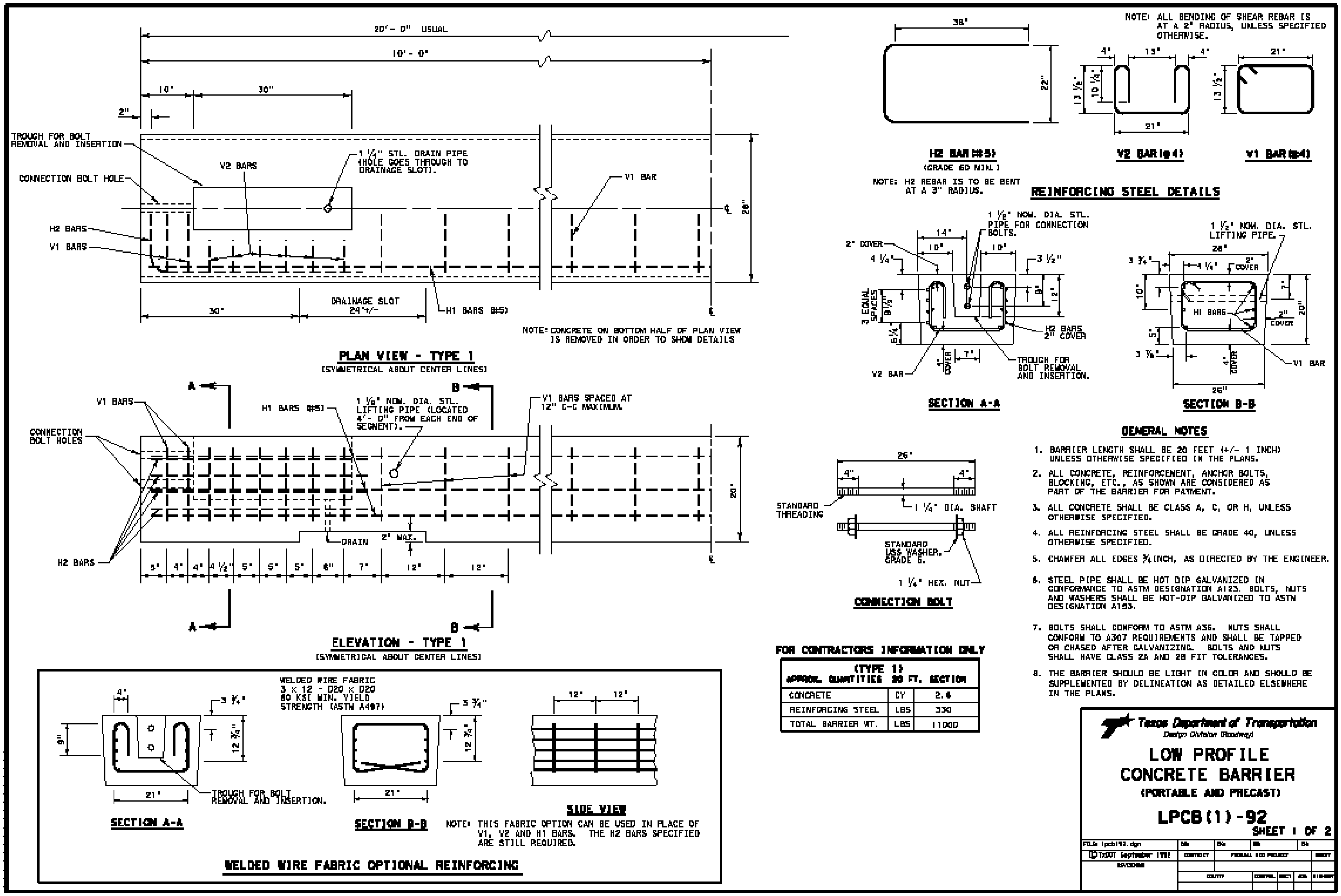

GENERAL NOTES

1. BARRIER LENGTH SHALL BE 20 FEET (+/- 1 INCH) UNLESS OTHERWISE SPECIFIED IN THE PLANS.
2. ALL CONCRETE, REINFORCEMENT, ANCHOR BOLTS, BLOCKING, ETC., AS SHOWN ARE CONSIDERED AS PART OF THE BARRIER FOR PAYMENT.
3. ALL CONCRETE SHALL BE CLASS A, C, OR H, UNLESS OTHERWISE SPECIFIED.
4. ALL REINFORCING STEEL SHALL BE GRADE 40, UNLESS OTHERWISE SPECIFIED.
5. CHAMFER ALL EDGES 3/4 INCH, AS DIRECTED BY THE ENGINEER.
6. STEEL PIPE SHALL BE HOT DIP GALVANIZED IN CONFORMANCE TO ASTM DESIGNATION A123. BOLTS, NUTS AND WASHERS SHALL BE HOT-DIP GALVANIZED TO ASTM DESIGNATION A153.
7. BOLTS SHALL CONFORM TO ASTM A36. NUTS SHALL CONFORM TO A307 REQUIREMENTS AND SHALL BE TAPPED OR CHASED AFTER GALVANIZING. BOLTS AND NUTS SHALL HAVE CLASS 2A AND 2B FIT TOLERANCES.
8. THE BARRIER SHOULD BE LIGHT IN COLOR AND SHOULD BE SUPPLEMENTED BY DELINEATION AS DETAILED ELSEWHERE IN THE PLANS.

FOR CONTRACTORS INFORMATION ONLY

(TYPE 1) APPROX. QUANTITIES 20 FT. SECTION		
CONCRETE	CY	2.4
REINFORCING STEEL	LBS	330
TOTAL BARRIER WT.	LBS	11000

Texas Department of Transportation
Design Division (Roadway)

LOW PROFILE CONCRETE BARRIER

(PORTABLE AND PRECAST)

LPCB(1)-92

SHEET 1 OF 2

FILE: lpcb192.dgn
©TxDOT September 1992

APPENDIX C: SAMPLE CALCULATIONS

C.1 Sample Calculation of Single Slope Traffic Barrier for Scenario 3 with upstream water height 58.8 in.:

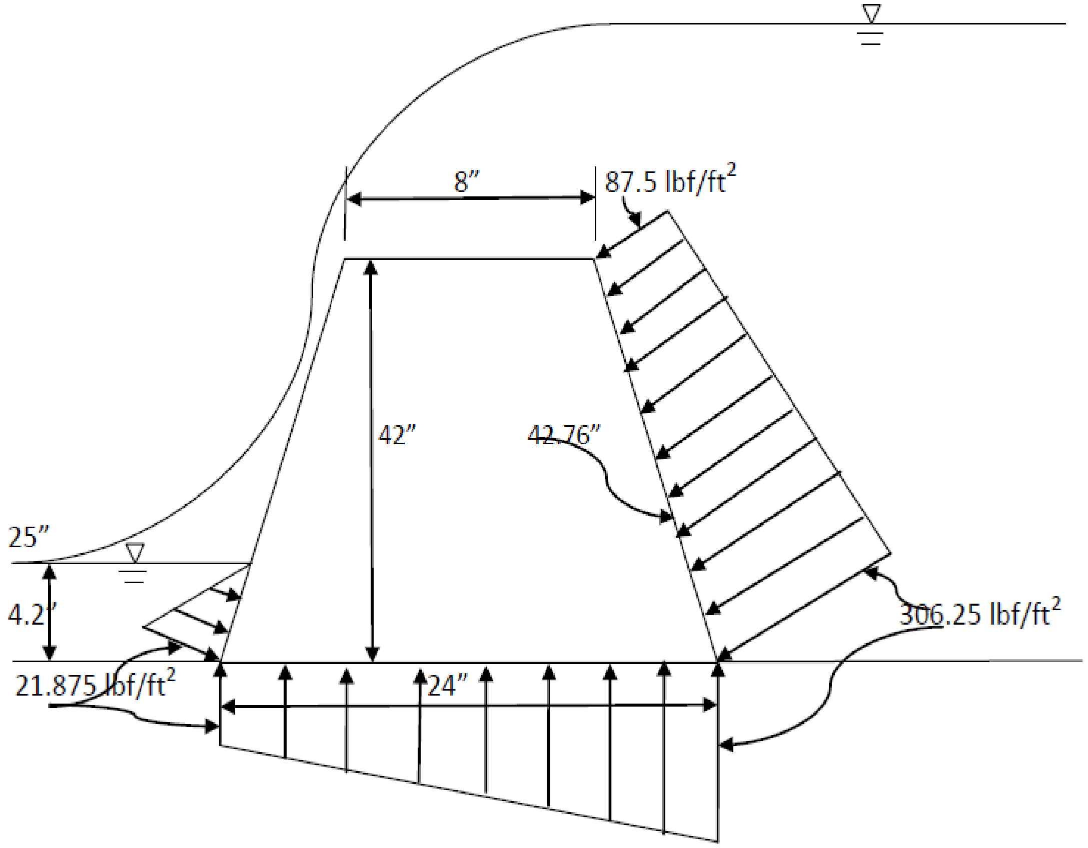

Figure C.1-1. A Single Slope Traffic Barrier Facing Water Pressure under Scenario 3 with Upstream Water Height of 58.8 in.

<u>Geometry and self weight of barrier:</u>

Cross-sectional area = $\frac{(8"+24")}{2} \times 42" = 672\ in^2$

Area of conduit opening = $4'' \times 4"$ = 16 in^2

Net cross-sectional area = (672 – 16) = 656 in^2

Gross volume of the barrier = $\frac{656\,\text{in}^2}{144} \times 30' = 136.66\ \text{ft}^3$

Volume of longitudinal opening = $(\frac{24"}{12}) \times (\frac{2"}{12}) \times (\frac{24"}{12}) \times 2\ \text{no.} = 1.33\ \text{ft}^3$

Net volume of the barrier = 136.66 – 1.33 = 135.33 ft^3

Weight of the barrier = 135.33 $ft^3 \times$ 150 lbf/ft^3 = 20299.5 lbf

Upstream water effect (assuming 58.8″ of water):

Pressure of water at the bottom level of the barrier = 62.5 lbf/ft$^3 \times \frac{58.8''}{12}$ = 306.25 lbf/ft^2

Pressure at the top level of opening of the barrier = 62.5 lbf/ft$^3 \times \frac{56.8''}{12}$ = 295.83 lbf/ft^2

Pressure of water at the top level of the barrier = 62.5 lbf/ft$^3 \times \frac{16.8''}{12}$ = 87.5 lbf/ft^2

Gross force on the upstream face of the barrier =

$$\frac{(306.25\ \text{lbf/ft}^2 + 87.5\ \text{lbf/ft}^2)}{2} \times \left(\frac{42.76''}{12}\right) \times 30' = 21046\ \text{lbf}$$

Force on the opening = $\frac{(306.25\ \text{lbf/ft}^2 + 295.83\ \text{lbf/ft}^2)}{2} \times \left(\frac{42.76}{42} \times \frac{2''}{12}\right) \times 2' \times 2\ \text{no.} = 204\ \text{lbf}$

Net force on the upstream face of the barrier = 21046 – 204 = 20842 lbf

Upstream velocity effect:

Using the rating curve for single slope traffic barrier, we get, for $e_u/h_r = \frac{58.8''}{42''}$ =1.4, dimensionless flow rate, $Q/(A_r(gh_r)^{0.5})$ = 0.125

Here,

Height of barrier, h_r = 42″ = 3.5 ft

Height of upstream water = 58.8″ = 4.9 ft

Area through which water is passing, A_r = (4.9′-3.5′)$\times$ 30 + (2″/12)$\times$ 4′= 42.67 ft^2

g = 32.2 ft/sec^2

So, the discharge,

$$Q = 0.125 \times A_r \times (gh_r)^{0.5})$$

$$= 0.125\times 42.67\ \mathrm{ft}^2\ \times(32.2\ \mathrm{ft}/\ \mathrm{sec}^2 \times 3.5\ \mathrm{ft})^{0.5}$$

$$= 56.62\ \mathrm{ft}^3/\mathrm{sec}$$

And the velocity of upstream flow, $v = Q/A = 56.62\ \mathrm{ft}^3/\mathrm{sec} \times 42.67\ \mathrm{ft}^2 = 1.33\ \mathrm{ft/sec}$

Velocity head = $\frac{v^2}{2g} = \frac{(1.33\ \mathrm{ft/sec})^2}{2\times 32.2\ \mathrm{ft/sec}^2} = 0.027\ \mathrm{ft}$

Force for velocity head = $0.027\times 62.5\ \mathrm{lbf/ft}^3 \times(\frac{42.76"}{12}) \times 30' = 180.4\ \mathrm{lbf}$

Downstream water effect:

Calculation of downstream water height:

From the above calculation, the total upstream energy, E = 4.9′ + 0.027′ = 4.927′

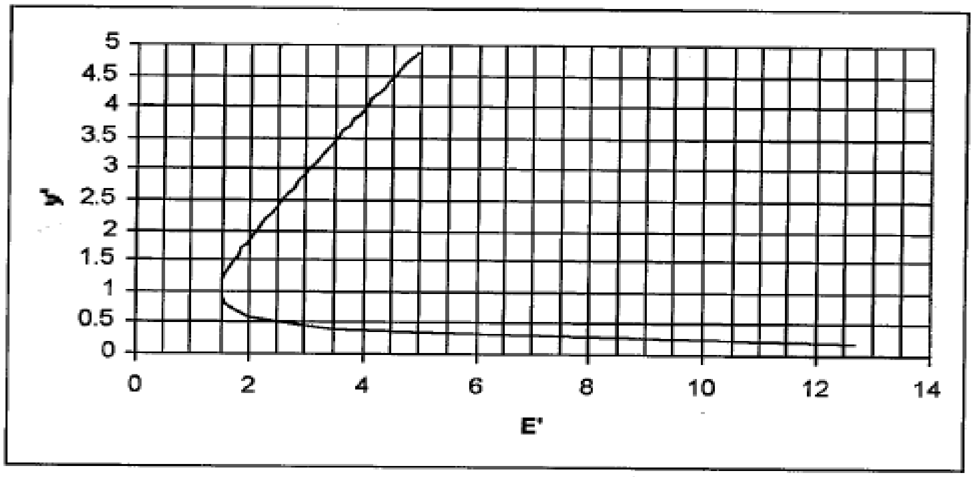

Figure C.1-2. Dimensionless E-y Curve.
Source: Open Channel Hydraulics by Richards H. French

Using the dimensionless E-y curve we find that for upstream energy of 4.927′, the downstream water height will be 0.35′ = 4.2 in.

Pressure of water at the bottom level of the barrier = $62.5\ \mathrm{lbf/ft}^3 \times \frac{4.2"}{12} = 21.875\ \mathrm{lbf}/ft^2$

Force on the downstream face of the barrier = $(1/2)\times 21.875\ \mathrm{lbf/ft}^2 \times(\frac{42.76}{42} \times \frac{4.2"}{12})\times 30' = 117\ \mathrm{lbf}$

Effect of upward buoyancy:

Buoyant force acting on the bottom of the barrier

= 21.875 lbf× (24"/12) × 30′ + (1/2) × (306.25 – 21.875) *lbf* ×(24″/12)× 30′

= 1313 lbf + 8531 lbf = 9844 lbf

We can say, of the 9844 lbf, 1313 lbf is acting at 12″ from downstream edge and 8531 lbf is acting at 16″ from downstream edge.

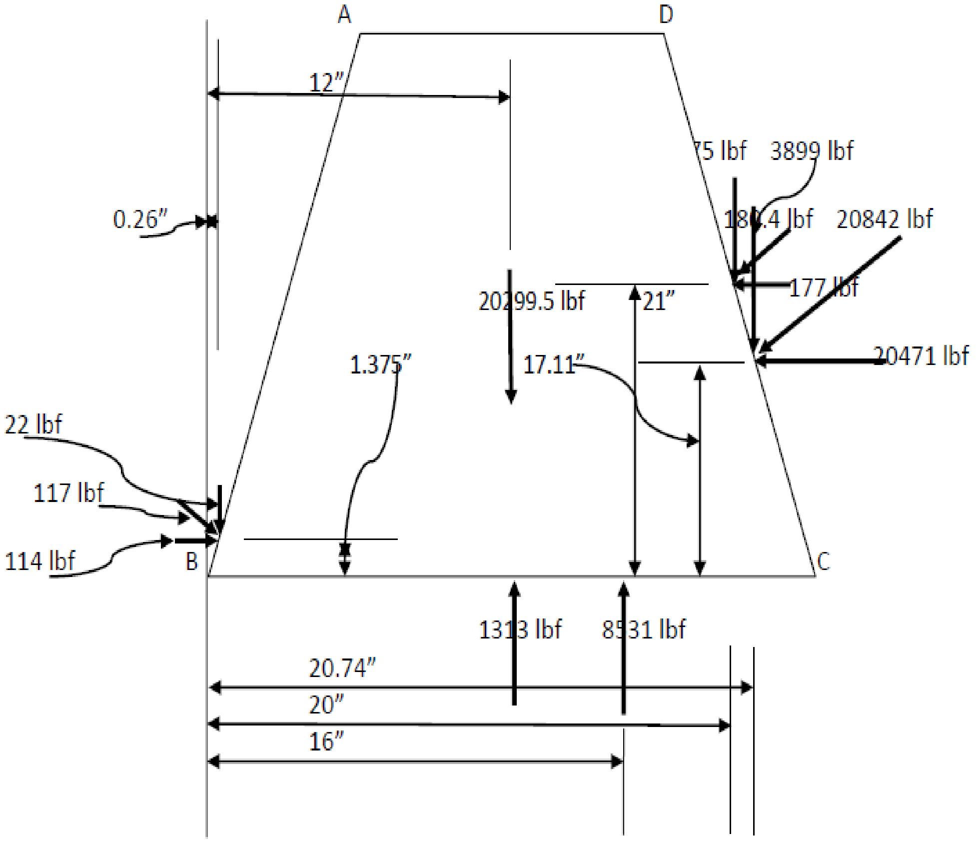

Figure C.1-3. Free Body Diagram of the Single Slope Traffic Barrier under Acting Forces.

Calculation of factor of safety against sliding:

From the free body diagram, the total downward force = (20299.5 + 22 + 3899 + 33.75 – 1313 – 8531) lbf = 14410.25 lbf

So, the factor of safety against sliding = $\frac{\text{Resisting frictional force}}{\text{Horizontal sliding force}}$

$$= \frac{\text{Coefficient of friction} \times \text{total downward force}}{\text{Horizontal sliding force}}$$

$$= \frac{0.62 \times 14410.25 \text{ lbf}}{(20471 + 177 - 114)\text{lbf}}$$

$$= \frac{8934 \text{ lbf}}{20534 \text{ lbf}}$$

= 0.435 ≈ **0.44** (according to Excel worksheet calculation)

Calculation of factor of safety against overturning:

Centroid of pressure trapezoid for upstream water pressure = $\frac{h(2a+b)}{3(a+b)}$

$$= \frac{42.76\,(2*87.5+306.75)}{3\,(87.5+306.75)}$$

$$= \frac{20599.63}{1182.75}$$

= 17.42″

Centroid of pressure triangle for downstream water pressure = $\frac{h}{3} = \frac{4.2}{3}$ = 1.4″

Factor of safety against overturning = $\frac{\text{Summation of resisting moments against point B}}{\text{Summation of overturning moments against point B}}$

$$= \frac{114 \text{ lbf} \times 1.375'' + 22 \text{ lbf} \times 0.26'' + 20299.5 \text{ lbf} \times 12'' + 33.75 \text{ lbf} \times 20'' + 3899 \text{ lbf} \times 20.74''}{177 \text{ lbf} \times 21'' + 20471 \text{ lbf} \times 17.11'' + 8531 \text{ lbf} \times 16'' + 1313 \text{ lbf} \times 12''}$$

$$= \frac{325296.73 \text{ lbf-in}}{506227.81 \text{ lbf-in}}$$

= 0.642 ≈ $\mathbf{0.64}$ (according to Excel worksheet calculation)

C.2. Sample Calculation of F-Shaped Traffic Barrier for Scenario 1 with upstream water height 33″:

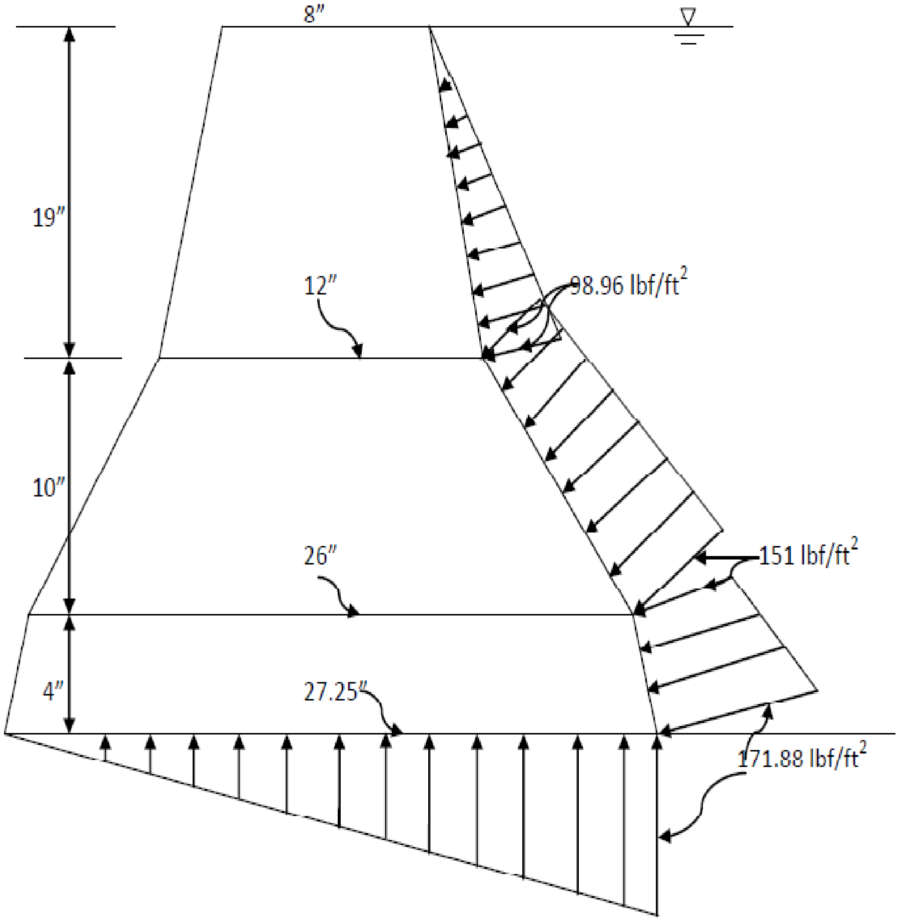

Figure C.2-1. An F-Shaped Traffic Barrier Facing Water Pressure under Scenario 1 with Upstream Water Height 33 in.

<u>Geometry and self weight of barrier:</u>

Gross cross-sectional area =

$$\frac{(27.25"+26")}{2} \times 4"+ \frac{(26"+12")}{2} \times 10" + \frac{(12+8)}{2} \times 19" = 486.5 \text{ in}^2$$

Area of conduit opening = $4'' \times 6'' = 24\ in^2$

Net cross-sectional area = $(486.5 - 24) = 462.5\ in^2$

Gross volume of the barrier = $\frac{462.5 \text{in}^2}{144} \times 30' = 96.35 \text{ ft}^3$

Volume of longitudinal opening = $(\frac{24''}{12}) \times (\frac{2''}{12}) \times (\frac{27.25}{12}) \times 2 \text{ no.} = 1.51 \text{ ft}^3$

Net volume of the barrier = 96.35 – 1.51 = 94.84 ft^3

Weight of the barrier = 94.84 $\text{ft}^3 \times$ 150 lbf/ft^3 = 14226 lbf

<u>Upstream water effect (assuming 33″ of water):</u>

Pressure of water at the bottom level of the barrier = 62.5 lbf/$\text{ft}^3 \times \frac{33''}{12}$ = 171.88 lbf/ft^2

Pressure of water at the top level of opening of the barrier = 62.5 lbf/$\text{ft}^3 \times \frac{31''}{12}$ = 161.5 lbf/ft^2

Pressure of water at the top level of first slope of the barrier = 62.5 lbf/$\text{ft}^3 \times \frac{29''}{12}$ = 151 lbf/ft^2

Pressure of water at the top level of second slope of the barrier= 62.5 lbf/$\text{ft}^3 \frac{19''}{12}$ = 98.96 lbf/ft^2

Gross force on the face of first slope of the barrier = $\frac{(171.88 \text{ lbf/ft}^2 + 151 \text{ lbf/ft}^2)}{2} \times \left(\frac{4.05''}{12}\right) \times 30'$
= 1634 lbf

Force on the opening = $\frac{(171.88 \text{ lbf/ft}^2 + 161.5 \text{ lbf/ ft}^2)}{2} \times \left(\frac{2.025''}{12}\right) \times 2' \times 2 \text{ no.} = 113 \text{ lbf}$

Net force on the face of first slope of the barrier = 1634 – 113 = 1521 lbf

Force on the face of second slope of the barrier = $\frac{(151 \text{ lbf/ft}^2 + 98.96 \text{ lbf/ ft}^2)}{2} \times \left(\frac{12.21''}{12}\right) \times 30'$
= 3815 lbf

Force on the face of third slope of the barrier = $\frac{98.96 \text{ lbf/ ft}^2}{2} \times \left(\frac{19.10''}{12}\right) \times 30'$
= 2362 lbf

Total force on the upstream face of the barrier = (1521 + 3815 + 2362) = 7698 lbf

<u>Effect of upward buoyancy:</u>

Buoyant force acting on the bottom of the barrier = $(1/2) \times (171.88 \text{ lbf}) \times (27.25''/12) \times 30'$
= 5854 lbf

Here, the effect of opening is neglected.

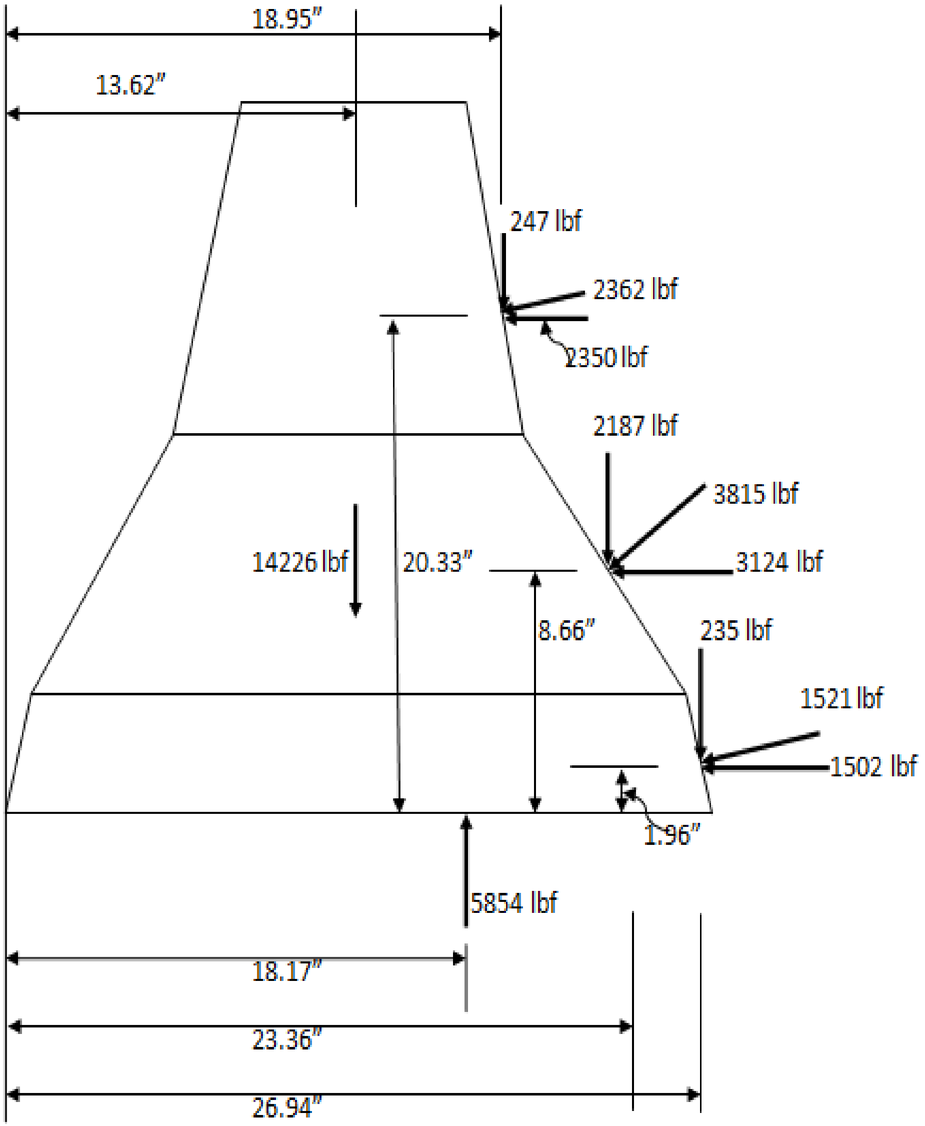

Figure C.2-2. Free Body Diagram of the F-Shaped Traffic Barrier under Acting Forces.

<u>Calculation of factor of safety against sliding:</u>

From the free body diagram, the total downward force = (14226 + 235 + 2187 + 247 – 5854) lbf
= 11041 lbf

Horizontal sliding force = (1502 + 3124 + 2350) lbf = 6976 lbf

So, the factor of safety against sliding = $\frac{\text{Resisting frictional force}}{\text{Horizontal sliding force}}$

$$= \frac{\text{Coefficient of friction} \times \text{total downward force}}{\text{Horizontal sliding force}}$$

$$= \frac{0.62 \times 11041 \text{ lbf}}{6976 \text{ lbf}}$$

$= \frac{6845 \text{ lbf}}{6976 \text{ lbf}}$

$= 0.98 \approx \mathbf{0.98}$ (according to Excel worksheet calculation)

<u>Calculation of factor of safety against overturning:</u>

Centroid of pressure trapezoid for first slope $= \frac{h(2a+b)}{3(a+b)}$

$= \frac{4.05(2*151+171.88)}{3(151+171.88)}$

$= \frac{1919}{968.64}$

$= 1.98''$

Centroid of pressure trapezoid for second slope $= \frac{h(2a+b)}{3(a+b)}$

$= \frac{12.21(2*98.96+151)}{3(98.96+151)}$

$= \frac{4260.31}{750}$

$= 5.68''$

Centroid of pressure triangle for third slope $= \frac{h}{3} = \frac{19.1}{3} = 6.367''$

Centroid of pressure triangle for upward buoyancy $= \frac{2h}{3} = \frac{2*27.25}{3} = 18.167''$

Factor of safety against overturning $= \frac{\text{Summation of resisting moments against point D}}{\text{Summation of overturning moments against point D}}$

$= \frac{14226 \text{ lbf}\times 13.625'' + 247 \text{ lbf}\times 18.955'' + 2187 \text{ lbf}\times 23.365'' + 235 \text{ lbf}\times 26.944''}{2350 \text{ lbf}\times 20.33'' + 3124 \text{ lbf}\times 8.65'' + 1502 \text{ lbf}\times 1.955'' + 5854 \text{ lbf}\times 18.167''}$

$= \frac{255726 \text{ lbf-in}}{184147 \text{ lbf-in}}$

$= 1.38 \approx \mathbf{1.35}$ (according to Excel worksheet calculation)

This variation may be happened due to approximation and negligence of decimal places in hand calculation shown here.

C.3 Sample Calculation of Modified Traffic Barrier for Scenario 2 with upstream water height of 42″ and downstream water height of 25″.

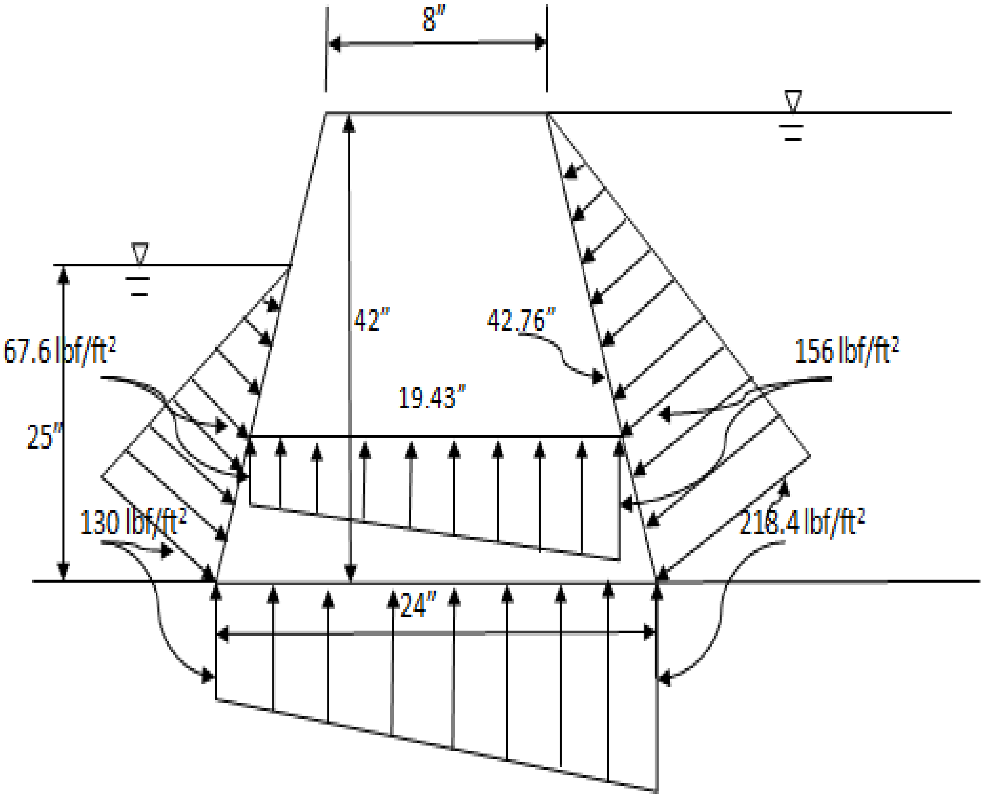

Figure C.3-1. A Modified Traffic Barrier Facing Water Pressure under Scenario 2 with Upstream Water Height of 42 in. and Downstream Water Height of 25 in.

<u>Geometry and self weight of barrier:</u>

Cross-sectional area = $\frac{(8"+24")}{2} \times 42" = 672 \text{ in}^2$

Gross volume of the barrier = $\frac{672 \text{ in}^2}{144} \times 30' = 140 \text{ ft}^3$

Volume of opening = $\frac{(19.43"+24")}{2\times12} \times 1' \times 5' \times 2 \text{ no.} = 18.09 \text{ ft}^3$

Net volume of the barrier = 140 – 18.09 = 121.9 ft^3

Weight of the barrier = 121.9 ft^3 × 150 lbf/ft^3 = 18285 lbf

Upstream water effect (assuming 42” of water):

Pressure of water at the bottom level of the barrier = 62.5 lbf/ft^3 × $\frac{42''}{12}$ = 218.4 lbf/ft^2

Pressure of water at the top level of opening of the barrier = 62.5 lbf/ft^3 × $\frac{32''}{12}$ = 156 lbf/ft^2

Gross force on the upstream face of the barrier = (1/2)×218.4 lbf/ft^2 ×(42.76″/12)×30’ = 11673 lbf

Force on the opening = $\frac{(156\ \text{lbf/ft}^2+218.4\text{lbf/ ft}^2)}{2}\times\left(\frac{42.76}{42}\times\frac{12''}{12}\right)\times 10' = 1905\ \text{lbf}$

Net force on the upstream face of the barrier = 11673 – 1905 = 9768 lbf

Calculation of force for velocity:

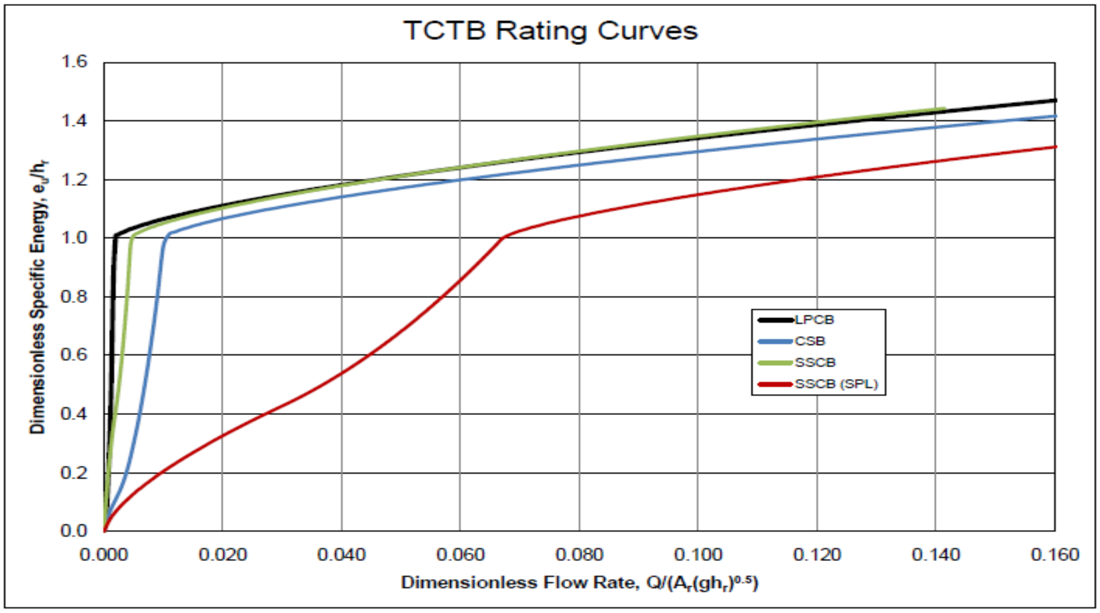

Figure C.3-2. TCTB Rating Curves (Source Hudson et al. 2009).

Using the rating curve for modified traffic barrier SSCB (SPL), we get, for e_u/h_r=1, dimensionless flow rate, $Q/(A_r(gh_r\ )^{0.5})$ = 0.0672

Here,

Height of barrier, h_r = 42″ = 3.5 ft
Area through which water is passing, A_r = 2×5′×1′ = 10 ft^2
g = 32.2 ft/sec^2

So, the discharge, $Q = 0.0672 \times A_r \times (gh_r)^{0.5})$

$= 0.0672 \times 10\ \text{ft}^2 \times (32.2\ \text{ft/sec}^2 \times 3.5\ \text{ft})^{0.5}$

$= 7.13\ \text{ft}^3/\text{sec}$

And the velocity of upstream flow, $v = Q/A = 7.13\ \text{ft}^3/\text{sec} \times 10\ \text{ft}^2 = 0.71\ \text{ft/sec}$

Velocity head $= \frac{v^2}{2g} = \frac{(0.71\ \text{ft/sec})^2}{2 \times 32.2\ \text{ft/sec}^2} = 0.00783\ \text{ft}$

Force for velocity head $= 0.00783 \times 62.5\ \text{lbf/ft}^3 \times (\frac{42.76''}{12} \times 30' - 10' \times 1') = 47.3\ \text{lbf}$

Downstream water effect (assuming 25” of water):

Pressure of water at the bottom level of the barrier $= 62.5\ \text{lbf/ft}^3 \times \frac{25''}{12} = 130\ \text{lbf/ft}^2$

Pressure of water at the top level of opening of the barrier $= 62.5\ \text{lbf/ft}^3 \times \frac{13''}{12} = 67.6\ \text{lbf/ft}^2$

Gross force on the downstream face of the barrier $= (1/2) \times 130\ \text{lbf/ft}^2 \times (\frac{42.76}{42} \times \frac{25''}{12}) \times 30' = 4136$ lbf

Force on the opening $= \frac{(130\ \text{lbf} + 67.6\text{lbf})}{2} \times \left(\frac{42.76}{42} \times \frac{12''}{12}\right) \times 10' = 1006\ \text{lbf}$

Net force on the downstream face of the barrier = 4136 – 1006 = 3130 lbf

Effect of upward buoyancy:

Buoyant force acting on the bottom of the barrier

$= 130\ \text{lbf} \times (24''/12) \times 20' + (1/2) \times (218.4 - 130)\ \text{lbf} \times (24''/12) \times 20'$

= 5200 lbf + 1768 lbf = 6968 lbf

We can say, of the 6968 lbf, 5200 lbf is acting at 12″ from downstream edge and 1768 lbf is acting at 16″ from downstream edge.

Buoyant force acting on the top of the opening of the barrier

$= 67.6\ \text{lbf} \times (19.43''/12) \times 10' + (1/2) \times (156 - 67.6)\ \text{lbf} \times (19.43''/12) \times 10'$

= 1095 lbf + 715 lbf = 1810 lbf

We can say, of the 1810 lbf, 1095 lbf is acting at 12″ from downstream edge and 1768 lbf is acting at 15.24″ from downstream edge.

Total upward buoyant force = 6968 + 1810 = 8778 lbf

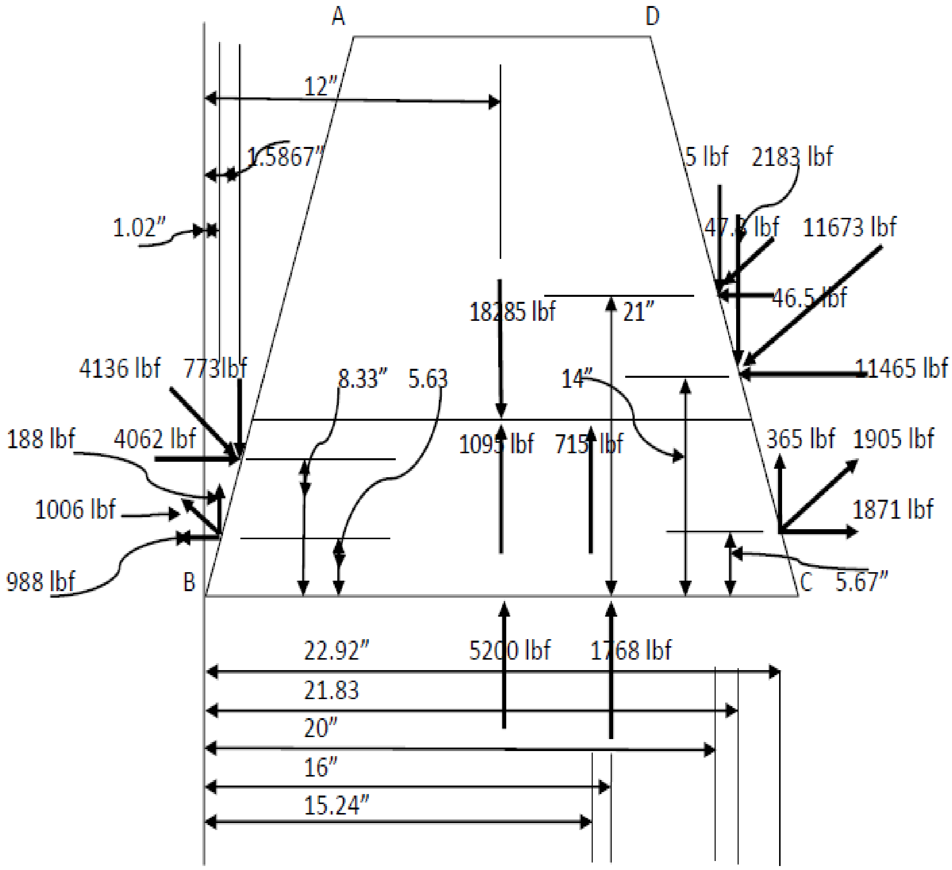

Figure C.3-3. Free Body Diagram of the Modified Traffic Barrier under Acting Forces.

Calculation of factor of safety against sliding:

From the free body diagram, the total downward force = (18285 + 2183 − 365 + 8.85 + 773 − 188 – 5200 – 1768 – 1095 − 715) lbf = 11918 lbf

So, the factor of safety against sliding = $\frac{\text{Resisting frictional force}}{\text{Horizontal sliding force}}$

$$= \frac{\text{Coefficient of friction} \times \text{total downward force}}{\text{Horizontal sliding force}}$$

$$= \frac{0.62 \times 11918 \text{ lbf}}{(11465 + 46.46 - 1871 - 4062 + 988)\text{lbf}}$$

$= \frac{7389 \text{ lbf}}{6566 \text{ lbf}}$

= 1.125 ≈ **1.13** (according to Excel worksheet calculation)

<u>Calculation of factor of safety against overturning:</u>

Centroid of pressure triangle for upstream water (gross) pressure $= \frac{h}{3} = \frac{42''}{3}$ = 14”

Centroid of pressure trapezoid for opening area of upstream water pressure = $\frac{h(2a+b)}{3(a+b)}$

$= \frac{12.21\,(2*156+218.4)}{3\,(156+218.4)}$

$= \frac{6476}{1123}$

= 5.76″

Centroid of pressure triangle for downstream water (gross) pressure $= \frac{h}{3} = \frac{25''}{3}$ = 8.33″

Centroid of pressure trapezoid for opening area of downstream water pressure = $\frac{h(2a+b)}{3(a+b)}$

$= \frac{12.21\,(2*67.6+130)}{3\,(67.6+130)}$

$= \frac{3238}{593}$

= 5.46″

Factor of safety against overturning = $\frac{\text{Summation of resisting moments against point B}}{\text{Summation of overturning moments against point B}}$

$$= \frac{4062 \text{ lbf}\times 8.33''+773 \text{ lbf}\times 1.5867''+18258 \text{ lbf}\times 12''+8.5 \text{ lbf}\times 20''+2183 \text{ lbf}\times 21.83''+1871 \text{ lbf}\times 5.67''}{988 \text{ lbf}\times 5.36''+188 \text{ lbf}\times 1.02''+5200 \text{ lbf}\times 12''+1768 \text{ lbf}\times 16''+1095 \text{ lbf}\times 12''+715 \text{ lbf}\times 15.24''+356 \text{ lbf}\times 22.92''+11465 \text{ lbf}\times 14''+46.5 \text{ lbf}\times 21''}$$

$= \frac{312916.44 \text{ lbf-in}}{289858 \text{ lbf-in}}$

=1.079 ≈ **1.08** (according to Excel worksheet calculation)

C.4 Sample Calculation of Low Speed Traffic Barrier for Scenario 4 with upstream water velocity 10 mph:

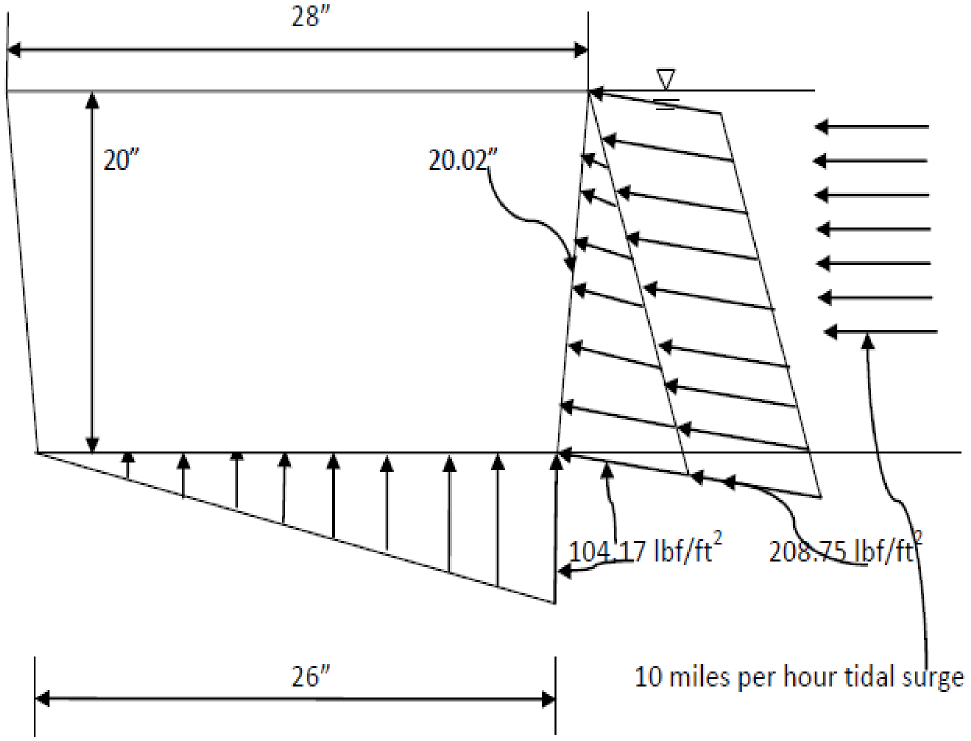

Figure C.4-1. A Low Speed Traffic Barrier Facing Water Pressure under Scenario 4 with Upstream Water Height of 20 in. and Surge Velocity of 10 mph.

Geometry and self weight of barrier:

Cross-sectional area = $\frac{(28"+26")}{2} \times 20" = 540 \text{ in}^2$

Area of conduit opening = 16 in^2 (assuming)

Net cross-sectional area = (540 – 12) = 528 in^2

Gross volume of the barrier = $\frac{528 \text{ in}^2}{144} \times 20' = 73.33 \text{ ft}^3$

Volume of longitudinal opening = $(\frac{26"}{12}) \times (\frac{3"}{12}) \times (\frac{30"}{12}) \times 2 \text{ no.} = 2.71 \text{ ft}^3$

Net volume of the barrier = 73.33 – 2.71 = 70.63 ft^3

Weight of the barrier = 70.63 $\text{ft}^3 \times 150\ \text{lbf/ft}^3$ = 10593 lbf

Upstream water effect (assuming 20″ of water):

Pressure of water at the bottom level of the barrier = 62.5 $\text{lbf/ft}^3 \times \frac{20''}{12}$ = 104.17 lbf/ft^2

Pressure at the top level of opening of the barrier = 62.5 $\text{lbf/ft}^3 \times \frac{17''}{12}$ = 88.54 lbf/ft^2

Gross force on the upstream face of the barrier = $\frac{104.17\ \text{lbf/ft}^2}{2} \times \left(\frac{20.02''}{12}\right) \times 20' = 1738\ \text{lbf}$

Force on the opening = $\frac{(104.17\ \text{lbf/ft}^2 + 88.54\ \text{lbf/ft}^2)}{2} \times \left(\frac{20.02}{20} \times \frac{3''}{12}\right) \times 2.5' \times 2\ \text{no.} = 120\ \text{lbf}$

Net force on the upstream face of the barrier = 1738 – 120 = 1618 lbf

Upstream velocity effect:

Velocity of upstream water, v = 10 mph

$= \frac{10 \times 1760 \times 3\ \text{ft}}{60 \times 60\ \text{sec}}$

= 14.67 ft/sec

Velocity head = $\frac{v^2}{2g} = \frac{(14.67\ \text{ft/sec})^2}{2 \times 32.2\ \text{ft/sec}^2}$ = 3.34 ft

Force for vel. head = 3.34 $\text{ft} \times 62.5\ \text{lbf/ft}^3 \times (\frac{20.02''}{12}) \times 20'$ = 208.75 $\text{lbf/ft}^2 \times 33.37\ \text{ft}^2$ = 6965 lbf

Effect of upward buoyancy:

Buoyant force acting on the bottom of the barrier

$= (1/2) \times (104.17\ \text{lbf}) \times (26''/12) \times 20'$

= 2257 lbf

Here the effect of opening is neglected.

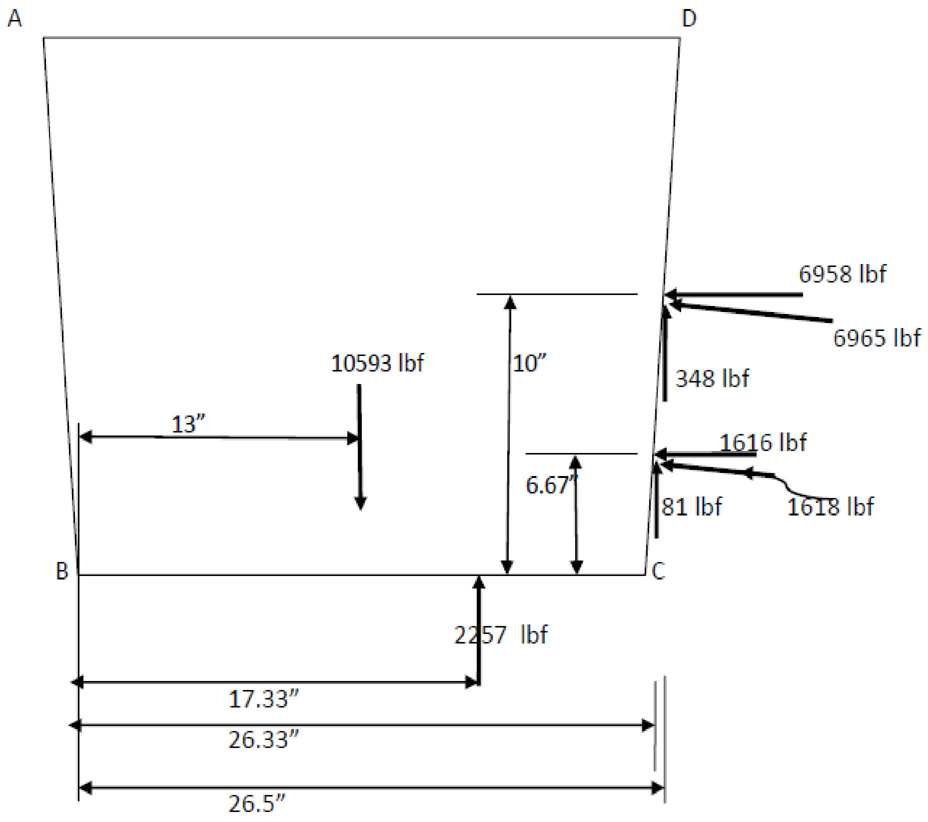

Figure C.4-2. Free Body Diagram of the Low Speed Traffic Barrier under Acting Forces.

<u>Calculation of factor of safety against sliding:</u>

From the free body diagram, the total downward force = (10593 − 348 − 81 − 2257) lbf = 7907 lbf

So, the factor of safety against sliding = $\frac{\text{Resisting frictional force}}{\text{Horizontal sliding force}}$

$= \frac{\text{Coefficient of friction} \times \text{total downward force}}{\text{Horizontal sliding force}}$

$= \frac{0.62 \times 7907 \text{ lbf}}{(6958 + 1616)\text{lbf}}$

$= \frac{4902 \text{ lbf}}{8574 \text{ lbf}}$

= 0.57 ≈ **0.57** (according to Excel worksheet calculation)

Calculation of factor of safety against overturning:

Factor of safety against overturning = $\frac{\text{Summation of resisting moments against point B}}{\text{Summation of overturning moments against point B}}$

$$= \frac{10593 \text{ lbf}\times 13''}{6958 \text{ lbf}\times 10''+348 \text{ lbf}\times 26.5''+1616 \text{ lbf}\times 6.67''+81 \text{ lbf}\times 26.33''+2257 \text{ lbf}\times 17.33''}$$

$$= \frac{137709 \text{ lbf}-\text{in}}{130827 \text{ lbf}-\text{in}}$$

= 1.053 $\approx \mathbf{1.06}$ (according to Excel worksheet calculation)

APPENDIX D: MICROSOFT EXCEL FUNCTIONS

D.1 Qnon (non-dimensional flow rate) Visual Basic Script

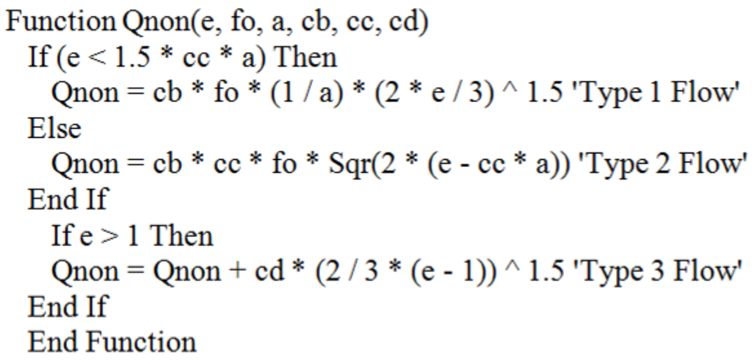

```
Function Qnon(e, fo, a, cb, cc, cd)
  If (e < 1.5 * cc * a) Then
    Qnon = cb * fo * (1 / a) * (2 * e / 3) ^ 1.5 'Type 1 Flow'
  Else
    Qnon = cb * cc * fo * Sqr(2 * (e - cc * a)) 'Type 2 Flow'
  End If
    If e > 1 Then
    Qnon = Qnon + cd * (2 / 3 * (e - 1)) ^ 1.5 'Type 3 Flow'
  End If
  End Function
```

where,

$e = e_l/h_r$
fo = fraction of open space
$a = h_{rl}/h_r$
cb = horizontal contraction coefficient
cc = vertical contraction coefficient
cd = weir flow coefficient

D.2 Enon (non-dimensional energy) Visual Basic Script

```
Function Eguess(Q, fo, a, cb, cc, cd)
    If Q < cb * cc ^ 1.5 * fo * Sqr(a) Then
        Eguess = 1.5 * (Q * a / (cb * fo)) ^ (2 / 3)
    Else
        Eguess = ((Q / (cb * cc * fo)) ^ 2) / 2 + cc * a
    End If

End Function


Function Enon(Q, fo, a, cb, cc, cd)
   Eps = 0.0001
   Q_t = 0#

   Emax = Eguess(Q, fo, a, cb, cc, cd)
   emin = 0#

   Do While Abs(Q − Q_t) > Eps
      etest = (Emax + emin) / 2
      Q_t = Qnon(etest, fo, a, cb, cc, cd)
      If Q_t < Q Then
         emin = etest
      Else
         Emax = etest
      End If
   Loop

   Enon = etest
End Function
```

Q = non-dimensional flow rate, $\frac{q}{\sqrt{gh_r^3}}$